On the Function of Variable Regions in the F-BAR Proteins SrGAP3 and Syndapin1

Dissertation

der Mathematisch-Naturwissenschaftlichen Fakultät

der Eberhard Karls Universität Tübingen

zur Erlangung des Grades eines

Doktors der Naturwissenschaften

(Dr. rer. nat.)

vorgelegt von

Silvia Würtenberger

aus Friedrichroda

Tübingen

2014

Gedruckt mit Genehmigung der Mathematisch-Naturwissenschaftlichen Fakultät der Eberhard Karls Universität Tübingen.

Tag der mündlichen Qualifikation:	16.03.2015
Dekan:	Prof. Dr. Wolfgang Rosenstiel
1. Berichterstatter:	Prof. Dr. Andrei Lupas
2. Berichterstatter:	Prof. Dr. Boris Maček

Für meine Familie

"Others have seen what is and asked why. I have seen what could be and asked why not."

Pablo Picasso
in *Metamorphoses of the Human Form : Graphic Works, 1895-1972*

Danksagung

Zuerst möchte ich mich bei Yvonne Groemping für die Möglichkeit diese Arbeit in ihrer Gruppe durchführen zu können bedanken. Ihre Unterstützung, ihr Vertrauen, sowie unzählige fachliche und ermutigende Diskussionen waren wesentlich für das Gelingen dieser Arbeit.

Ich bedanke mich weiterhin bei Andrei Lupas für seine großzügige Unterstützung und die Möglichkeit, unsere Arbeit in Anbindung an seine Abteilung durchführen zu können. Ich danke ihm außerdem für die Betreuung und die Begutachtung dieser Arbeit, sowie für fachlichen Rat im Rahmen des *Thesis Advisory Committee*.

Bei Boris Maček möchte ich mich für die Begutachtung dieser Arbeit als Vertreter des Fachbereichs Biologie der Mathematisch-Naturwissenschaftlichen Fakultät der Universität Tübingen bedanken. Weiterhin danke ich ihm für seine fachliche Unterstützung im Rahmen des *Thesis Advisory Committee*. Darüberhinaus danke ich Volkmar Braun und Gerd Jürgens, die an der Disputation dieser Arbeit teilgenommen haben.

Dagmar Sigurdardottir danke ich recht herzlich für ihre Unterstützung im finalen Jahr dieser Arbeit und für hilfreiche und motivierende Diskussionen in Bezug auf die Struktur und Präsentation dieser Arbeit.

Wolram Antonin danke ich ebenfalls für seine fachliche Unterstützung als Mitglied des *Thesis Advisory Committee*.

Bei Jason Kerr bedanke ich mich für die großzügige Unterstützung über die vergangenen Jahre und motivierende Tritte in die richtige Richtung.

Mein Dank gilt außerdem den aktuellen und früheren Mitglieder der AG Groemping für die freundschaftliche Zusammenarbeit und viele helfende Hände; im einzelnen Martin "The Technician" Schückel, Beatrice Laudenbach, Julia Rumpf, Anitha Jeganantham, Carsten Kintscher, Roy Eylenstein, Arne Rufer, Theresia Niese und Rebecca Dölker.

Heinz Schwarz und Matthias Flötenmeyer haben mich in die Welt der Elektronenmikroskopie eingewiesen und mit unermüdlichem Arbeitseifer nach Lösungen bei technischen Problemen gesucht. Dafür bedanke ich mich recht herz-

lich. Weiterhin bedanke ich mich bei Johannes Madlung für die freundliche Zusammenarbeit bei der Analyse von Massenspektrometrie-Daten. Mein Dank gilt weiterhin unserem Kollaborationspartner Aleksander Czogalla von der TU Dresden für eine lehrreiche Zusammenarbeit im Bereich der Membraninteraktionen. Bei Bijàn Mir-Montazeri möchte ich mich für seine Unterstützung zu Beginn dieser Arbeit und gewinnbringende Brainstorming-Sessions bedanken. Außerdem danke ich Murray Coles für die freundliche und lehrreiche Zusammenarbeit in Fragen der NMR-Spektroskopie bedanken. Bei Moritz Ammelburg bedanke ich mich für die freundschaftliche und lehrreiche Zusammenarbeit bei der bioinformatischen Sequenzanalyse, sowie das kritische Lesen des Manuskripts. Bei Carolin Ewers und Vikram Alva bedanke ich mich ebenfalls für die kritische Korrektur dieses Manuskripts.

Ein besonderer Dank geht an Moritz Ammelburg, Dara Forouzan und Martin Schückel, die mein Leben innerhalb und außerhalb des Labors auf viele verschiedene Weisen bereichert haben.

Abschließend möchte ich mich bei allen aktuellen und früheren Mitgliedern der Abteilung für Proteinevolution für ihre stete Hilfsbereitschaft und die freundschaftliche Arbeitsatmosphäre bedanken.

Abstract

Cellular signalling and membrane trafficking critically depend on the assembly of proteins into large complexes via transient protein-protein and protein-lipid interactions. For this purpose, involved proteins possess different adaptor domains, which are combined based on a modular principle in a single polypeptide chain. A prevalent interaction mode constitutes binding of adaptor domains to linear motifs, which are frequently located in intrinsically disordered regions. The typically low affinity and promiscuous nature, with which linear motifs bind their targets, establishes reversibility and flexibility within the system. Additional membrane-interaction modules, such as F-BAR (Fes-Cip4-homology Bin-Amphiphysin-Rvs) domains, assist not only in the localisation of these multi-protein complexes, but can also affect membrane shape, which is a prerequisite for membrane trafficking. In this thesis, I have investigated linear motifs in the variable regions of two F-BAR domain-containing proteins, srGAP3 (Slit-Robo GTPase-activating protein 3) and Syndapin1 (synaptic Dynamin-associated protein 1), with respect to binding partners and functional implications of the formed complexes.

SrGAP proteins have been implicated in different aspects of neuronal development and were identified as downstream effectors in the Slit-Robo pathway, in which they transmit the signal to the actin cytoskeleton, thereby affecting targeting of axons and neuronal migration. These findings were mainly based on the characterisation of their highly conserved globular domains, while the function of the variable C-terminal region (CTR) remained elusive. My bioinformatic analysis predicts that this region of srGAP proteins is intrinsically disordered and contains linear motifs for the interaction with 14-3-3 proteins as well as Src-homology 3 (SH3) domains. 14-3-3 proteins typically engage in phospho-dependent interactions, while SH3 domains recognise proline-rich motifs. Employing different biochemical and biophysical methods, I show that the CTR of the family member srGAP3 confers binding to the SH3 domains of the endocytic proteins Endophilin-A1, Endophilin-A2, and Amphiphysin, as well as the Ras signalling adaptor Grb2 under *in vivo* conditions and *in vitro*. Moreover, a single proline-rich motif in the CTR is sufficient for all of these interactions. Furthermore, I provide evidence that the CTR binds the 14-3-3 isoforms γ and θ/τ *in vivo* and I identify two phosphorylated positions involved in the formation of these complexes. These results therefore not only uncover a potential function of srGAP3 in endocytosis and Ras signalling, but also sug-

gest that the CTR is subject to phosphoregulation and may act as an adaptor platform connecting srGAP3 with different protein networks.

Syndapins have likewise been implicated in endocytic processes, in which they function as auxiliary factors during vesicle formation. Vesicle trafficking requires the separation and fusion of membranes through a concerted action of membrane-bending proteins, the lipid composition, and the actin cytoskeleton, which have to be precisely regulated in time and space. The F-BAR domain of Syndapin1 exhibits potent membrane sculpting activity, which is regulated through an autoinhibitory clamp between the C-terminal SH3 domain and the N-terminal F-BAR domain and is activated upon binding of ligands to the SH3 domain. I show that binding of the Eps15-homology domain-containing protein 1 (EHD1) to two Asn-Pro-Phe motifs located in the central variable region of Syndapin1 constitutes an alternative route for release of the autoinhibition. The Syndapin1-EHD1 complex plays a role in endocytic receptor recycling and, therefore, I propose that activation of Syndapin1 by EHD1 is a crucial step in the molecular mechanism underlying membrane trafficking processes governed by this protein complex.

Contents

List of Tables

List of Figures

Abbreviations

Å	*Å*ngström, 100 pm
α-Centractin	centrosome-associated actin homolog
α-Cop	coatomer subunit α
3′	end of DNA strand with free hydroxy group
5′	end of DNA strand with free phosphate group
E. coli	*Escherichia coli*
H. sapiens	*Homo sapiens*
aa	amino acid
AMPA	α-amino-3-hydroxy-5-methyl-4-isoxazolepropionic acid
AP2α2	adaptor protein 2 subunit α2
APS	ammonium persulfate
ARHGAP4	Rho GTPase-activating protein 4
ATP	adenosine-5-triphosphate
AU	arbitrary unit
AxxA	mutated PxxP peptide motif with proline replaced by alanine
Bin	Myc box-dependent-interacting protein
BLAST	basic local alignment search tool
C-terminus	carboxy terminus
CC	coiled coil
CD	circular dichroism
Cdc42	cell division cycle 42 protein, GTP-binding protein
Cip4	Cdc42-interacting protein 4
Co-IP	co-immunoprecipitation
CTR	C-terminal region
DMEM	Dulbecco's modified Eagle's medium
DMSO	dimethyl sulfoxide
DnaK	heat shock protein 70
dNTP	deoxyribonucleotide triphosphate
Drebrin	developmentally-regulated brain protein
DTE	dithioerythritol
DTT	dithiothreitol

Dynamin	GTPase mediating vesicle scission in endocytosis
EB1	microtubule-associated End-binding protein 1
EDTA	ethylene diamine tetraacetic acid
eGFP	enhanced green fluorescent protein
EH	Eps15 homology domain
Em	emission wavelength
Eps15	epidermal growth factor receptor substrate 15
Ex	excitation wavelength
F-BAR	Fes-Cip4-homology Bin-Amphiphysin-Rvs domain
FBP17	Formin-binding protein 17
Fes	feline sarcoma oncogene
Gab1	Grb2-associated-binding protein 1
GAP	GTPase-activating protein
GI	sequence identifier from http://www.ncbi.nlm.nih.gov/
Grb2	growth factor receptor-bound protein 2
GSH	glutathione, γ-L-Glutamyl-L-cysteinylglycine
GST	glutathione S-transferase
GTP	guanosine-5-triphosphate
GTPase	GTP-binding and hydrolysing protein
H	enthalpy
HEK293T	human embryonic kidney 293 cells containing the SV40 large T-antigen
Hepes	4-(2-hydroxyethyl)-1-piperazineethanesulfonic acid
His_6	tag composed of 6 consecutive His residues
HRP	horseradish peroxidase
IPTG	isopropyl-β-D-thiogalactopyranoside
ITC	isothermal titration calorimetry
K_d	dissociation constant
kDa	kilo-Dalton
LB	Luria Bertani
LC	liquid chromatography
M	mol/l
mCherry	monomeric variant of red fluorescent protein
MES	2-(N-morpholino)ethanesulfonic acid
mol%	molar percentage
MS	mass spectrometry
MW	molecular weight
Myc	myelocytomatosis oncogene

N	stoichiometry
N-BAR	Bin-Amphiphysin-Rvs domain with additional N-terminal helix
N-terminus	amino terminus
n.d.	non detectable
Neuro2A	mouse neuroblastoma cell line
NMR	nuclear magnetic resonance
Nonidet P-40	octyl phenoxypolyethoxylethanol
NP-40	nonyl phenoxypolyethoxylethanol
NPF	peptide motif comprising asparagine-proline-phenylalanine
NPF1	NPF motif closer to N-terminus
NPF2	NPF motif closer to C-terminus
OD_x	optical density at x nm
P-value	probability of obtaining test statistics given that null hypothesis is true
PAGE	polyacrylamide gel electrophoresis
PBS	phosphate-buffered saline
PBS-T	phosphate-buffered saline supplemented with Tween-20
PDB ID	identifier of protein structure in the protein data bank, http://www.pdb.org
PE	phosphatidylethanolamine
PEI	polyethylenimine
PKx	protein kinase x
PMSF	phenylmethylsulphonyl fluorid
Protein G	bacterial immunoglobulin-binding protein G
PS	phosphatidylserine
PSI	position-specific iterative
PtdIns(x)P_y	phosphatidylinositol phosphorylated at position(s) x, leading to y phospho-groups
Px	postnatal day x
PxxP	peptide motif comprising two prolines enclosing any two other amino acids
Ras	rat sarcoma GTPase
RFP	red fluorescent protein
Rho	Ras homologous GTPase
Robo	roundabout receptor
RTK	receptor tyrosine kinase
Rvs	reduced viability upon starvation protein from *Saccharomyces cerevisiae*

S-tag	protein tag derived from Ribonuclease A
SDS	sodium dodecyl sulfate
SH	Src homology domain
SH3C	C-terminal SH3 domain
SH3N	N-terminal SH3 domain
Sos1	son of sevenless 1
srGAP	Slit-Robo GTPase-activating protein
Strap	serine-threonine kinase receptor-associated protein
SUMO	small ubiquitin-like modifier protein
T_M	melting temperature
TEMED	N,N,N′,N′-tetramethylethylenediamine
Tris	tris(hydroxymethyl)-amino-methane
U	units (enzyme activity)
Vps26A	vacuolar protein sorting-associated protein 26A
Vps35	vacuolar protein sorting-associated protein 35
w/v	weight per volume
w/w	weight per weight
WD40 domain	domain composed of tandem copies of structural motif of approximately 40 residues usually ending with tryptophan-aspartic acid dipeptides
WRC	WAVE-regulatory complex, multi-protein complex involved in actin polymerisation

1. GENERAL INTRODUCTION

Brain function relies on the activity of highly interconnected networks of neurons, which communicate with each other via electrochemical signals. To perform this task, neurons possess a highly polarised morphology with branched dendrites, which mainly serve the signal reception, and axons, which form long projections and transmit the signal via synapses to downstream cells. Specialised molecular features, such as voltage-gated ion channels for the formation of action potentials of axons [1] or Golgi outpost in dendrites [2] encode the functional differentiation of the compartments and are characteristic for this cell type [2]. Furthermore, the positioning of these cells and their connection pattern as well as the network maintenance critically depend on complex signalling and membrane trafficking processes [2, 3].

Synaptic transmission at chemical synapses relies on the release of neurotransmitters into the synaptic cleft through fusion of synaptic vesicles with the presynaptic membrane [4–7] and binding of these transmitters to specific receptors in the postsynaptic membrane [1]. To date, four different pathways for compensatory re-uptake of synaptic vesicle membranes have been described: clathrin-mediated endocytosis [8], kiss-and-run endocytosis [9], activity-dependent bulk endocytosis [10, 11], and an ultrafast clathrin-independent pathway [12]. In neurons, endocytosis and endocytic recycling are not only fundamental to the synaptic vesicle cycle, but also required for correct positioning of neuronal membrane proteins and receptors, which will eventually determine, how a neuron responds to incoming signals or guidance molecules [3, 13]. Selective removal of axonal proteins from somatodentritic compartments, for example, is known to enable axonal targeting of proteins that initially were subject to non-specific sorting into both, the somatodentritic and axonal compartments [3, 14, 15]. Neurons can also adjust the sensitivity, with which they react to external guidance molecules, through desensitization via endocytic uptake of the respective receptors [16, 17].

The endosomal system (Fig. 1.1) serves as a sorting station for endocytosed cargo as well as for newly arriving transport vesicles from the trans-Golgi network [3]. However, neuronal endosomes are not well described, but expected to be much more diverse and adjusted to fulfil neuron-specific functions, such as long-distance retrograde axonal transport (see above) [3, 18]. Each endosomal compartment is characterised by the presence of specific phospholipids and proteins, which establish its identity by promoting compartment-

specific protein complex assembly and signalling [18, 19]. EH-domain containing (EHD) proteins (see chapter 8 for specific introduction) and the GTPases of the ADP-ribosylation factor (Arf) and the Ras-related in brain (Rab) families are key players in these membrane trafficking processes [20–22].

Endocytosed vesicles fuse with the early endosome (Fig. 1.1), which is characterised by a mildly acidic lumen that facilitates release of ligands from endocytosed receptors [19, 23]. Cargo sorted into the tubular fraction of the early endosome can either enter the fast recycling route back to the plasma membrane, the slow recycling pathway via the endocytic recycling compartment (ERC), or retrograde transport to the trans-Golgi network. Cargo tagged for degradation is sorted into the lumen of the early endosome, which will subsequently - via multivesicular bodies - fuse with lysosomes (Fig. 1.1, reviewed in [18, 19, 23, 24]). Surface levels of α-amino-3-hydroxy-5-methyl-4-isoxazolepropionic acid (AMPA) receptors at the postsynaptic membrane, for example, are regulated via endocytosis and either subsequent recycling, when the uptake is triggered through N-methyl-D-aspartate (NMDA) receptor activation, or subsequent degradation, when bound to external ligands (reviewed in [25]).

Vesicle trafficking processes are energetically expensive and require active membrane-bending into, for example, tubular structures, which can subsequently be separated from the source compartment through constriction and fission of the stalk [27]. Fusion of vesicles with target membranes represents the reverse process [28]. For these purposes, membrane-interacting proteins act in concert with specific lipids and the actin cytoskeleton to drive such complex membrane rearrangements in response to specific cellular signals [29, 30].

1.1. Modular Architecture of Signalling Proteins

Efficient signalling critically depends on the assembly of higher-order complexes [31], which not only form at the site of signal reception, but also during the transmission process in the cytosol or nucleus [32]. For this purpose, many signalling proteins possess a modular architecture employing different adaptor domains for the interaction with other proteins, nucleic acids, or phospholipids [33]. In fact, the cell regulates a large variety of processes using a limited set of these domains in a combinatorial manner [33]. Combinations of these independently folded units in a single polypeptide chain enables linking of downstream targets as well as cross-talk between different pathways and ensures a modulated response to various incoming signals through signal integration [32, 33]. Another feature of signalling proteins, especially of regulatory hubs, is their enrichment in intrinsically disordered regions that are characterised by the absence of a stable 3D structure in isolation [34–36], but the presence of alternative functional modules, such as linear motifs [37]. In the following

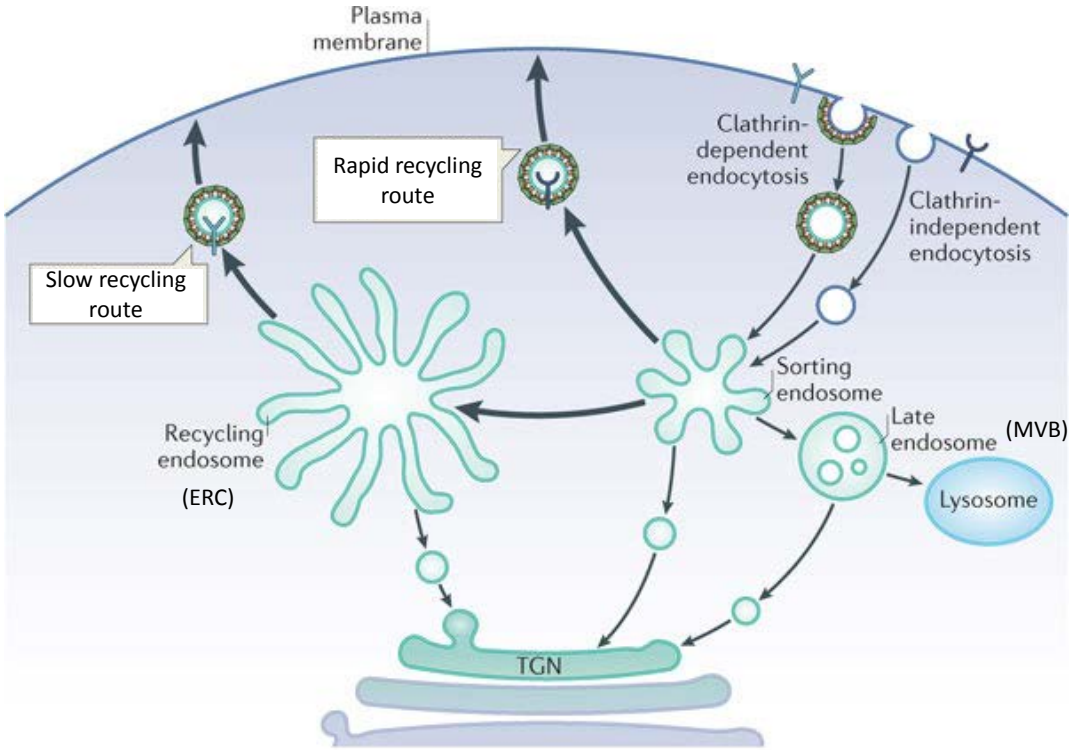

Figure 1.1.: Pathways of endocytic recycling. Cargo can be recycled after endocytosis via clathrin-dependent or clathrin-independent mechanisms. The major sorting compartments as well as trafficking routes are indicated. A detailed description of the recycling pathway can be found in the text. MVB, multi-vesicular body; TGN, trans-Golgi network; ERC, endocytic recycling compartment. The figure was adapted from Hsu, Bai and Li [26].

subsections, I will therefore introduce the concept of intrinsic disorder as well as linear motifs and outline the structure and function of adaptor domains that are relevant to this work.

1.1.1. Intrinsic Disorder and Linear Motifs

The structure-function paradigm was first challenged in the 1970s, when protein regions were discovered, which lacked recognisable structural elements, albeit being functional [38–40]. Such so called "intrinsically disordered" [41] or "natively unfolded" [42] regions can be as short as a few residues or even span full proteins [37, 40, 43]. Although "intrinsic disorder" describes a set of various conformational states [37], they share the absence of hydrophobic residues to form an ordered hydrophobic core [37] as well as the presence of charged and polar residues [44]. The absence of any structural element can, for example, be instrumental to the function of flexible linkers connecting two globular domains [37]. Other functions of intrinsically disordered regions usually involve binding to proteins or small molecules, which is often accompanied by different degrees of disorder-to-order transitions [37]: Intrinsically disordered regions have been associated with chaperone activities, allosteric modulation, or complex assembly [37]. Binding either involves larger regions undergoing disorder-to-order transitions, called molecular recognition features (MoRF), or smaller entities, called linear motifs [37].

Short linear motifs are between 3 to 11 residues long and usually bind to globular domains, such as proline-rich motifs to Src-homology 3 domains or phosphorylated motifs to 14-3-3 proteins (see below) [45, 46]. The interactions serve a number of different purposes: They either affect the localisation as well as the stability of the protein or mediate the recruitment of binding partners and the formation of multi-protein complexes [37, 45]. Linear motifs mostly reside in intrinsically disordered regions [47], in which multiple motifs often occur close in space, even in overlapping segments [37, 45]. This opens up the opportunity for switch-like regulation of complex formation [48, 49] through mutually exclusive binding to neighbouring motifs and/or post-translational modifications [36, 45]. The interface of protein-peptide complexes is generally smaller compared to structured interfaces [47, 50], which often results in weaker affinities [45], but multiple motifs in one polypeptide chain can be used in a cooperative fashion to increase the affinity and/or specificity [45].

1.1.2. Protein-Protein Interaction Domains

The Src-Homology 3 Domain

Src-homology 3 (SH3) domains confer binding to proline-rich sequences and play a role in numerous cellular processes in eukaryotes, such as signal transduction, actin cytoskeletal dynamics, cellular movement, or membrane trafficking [51]. They are 60 to 70 residues long and fold into five anti-parallel β-strands that form two β-sheets, which are linked by the RT-loop, the n-Src-loop, a distal loop and a 3_{10}-helix (Fig. 1.2A, p. 7) [52–54]. The binding surface consists of two shallow grooves for accommodation of the canonical PxxP ligand sequence, which adopts a left-handed type II polyproline helix conformation [52, 54–56]. An additional specificity pocket determines the binding orientation of the ligand by recognising positively charged residues preceding (type I, consensus *[RK]xxPxxP*) or following (type II, consensus *PxxPx[KR]*) the PxxP core (Fig. 1.2A, p. 7) [57–59]. In addition to these canonical SH3 domain-ligands, which mostly bind with low affinities in the micromolar range [51], an increasing number of non-PxxP peptides (such as RxxK motifs [60]) and even structured domains (such as ubiquitin-like domains [61] or Dbl-homology domains [62]) have been reported to bind SH3 domains [63]. These atypical ligands often exploit different and more extensive contacts with the specificity pocket [63, 64], which can result in unusual high binding affinities in the nanomolar range [63]. However, high affinity SH3-mediated interactions are not always correlated with high specificity and SH3 domains employ a panel of different mechanisms, such as sterical hindrance through flanking regions [65] or multivalent interactions [45, 66], to selectively bind their targets [51, 63]

The Eps15-Homology Domain

The Eps15-homology domain [67, 68] is present in metazoans, plants, and certain fungi [69] and usually found in proteins involved in membrane trafficking and endocytosis [69–71]. Its fold consists of two helix-loop-helix (EF hand) motifs connected by a short antiparallel β-sheet (Fig. 1.2B, p. 7) [69, 72]. Moreover, EF hand motifs are known to bind calcium [73] and some, but not all EH domains share this ability [69]. Most ligand peptides follow the sequence Asn-Pro-Phe (NPF), which adopts a type I β-turn and deeply inserts into the binding pocket (Fig. 1.2B, p. 7) [69, 72, 74]. Alternative ligand sequences, such as Asp-Pro-Phe motifs [75], have also been described [69]. Like SH3 domains, EH domains usually engage in low affinity interactions in the micromolar range [69, 72, 76], in which specificity might be ensured by flanking regions [76] as well as unconventional binding modes [77]. Stonin2, for example, carries two NPF motifs that simultaneously bind the second EH domain of Eps15 in a high affinity complex by engaging an additional hydrophobic pocket [77].

14-3-3 Proteins

14-3-3 proteins play an important role in many cellular pathways, such as apoptosis, metabolism, cell cycle progression, or transcription and are conserved among eukaryotes [78]. In mammals, this protein family comprises seven isoforms (β, γ, ϵ, η, σ, θ/τ, and ζ) [79], which bind to their targets as rigid, saddle-shaped homo- or heterodimers (Fig. 1.2C, p. 7) [79–81]. Their property to function as independent protein interaction modules sets them apart from other adaptor domains, although a structurally similar domain in the protein Smg7 with potentially similar function has been identified [79, 82]. Binding motifs typically contain a phosphorylated serine or threonine residue and follow the consensus *RSx[pS]xP* in mode I or *Rx[F/Y]x[pS]xP* in mode II [80, 83–85]. *In vivo* ligands can, however, contain sequence motifs that substantially diverge from this consensus [79, 81]. The target motifs are mainly phosphorylated by basophilic kinases, such as cAMP-dependent protein kinase (PKA) or protein kinase B (PKB) [78, 81, 86], and often occur in multiple copies in a single polypeptide chain, thereby allowing simultaneous docking of the two binding sites in the 14-3-3 dimer [87].

1.1.3. Lipid Interaction Domains

Correct positioning and activation of signalling complexes relies - in addition to protein-protein and protein-nucleic acid interactions - on tethering of the complexes on specific membranes [30]. For this purpose, many signalling proteins are equipped with phospholipid interaction domains [33]. Pleckstrin-homology (PH) domains [89] and Phox (PX) domains [90], for example, recognise specific phosphoinositides (PtdIns), which allow targeting to specific membrane types [30]. The PX domain of yeast Vam7 (vacuolar morphogenesis protein 7), for example, specifically binds PtdIns(3)P, which is important for its localisation at vacuolar membranes [90].

BAR domains (initially identified in the proteins **B**IN, **A**mphiphysin, **R**vs [91]) constitute another class of membrane interaction modules, which have not only been associated with membrane binding, but also membrane reshaping (compare general introduction on vesicle trafficking, p. 2) [92]. Domains of this superfamily [92, 93] fold into rigid, crescent-shaped dimers [92–94], which consist of a six-helical bundle with three helices in each monomer and helical tips protruding from this central core [92, 95] (Fig. 1.3). The membrane interaction surface is mostly located on the concave site [95–99] and composed of positively charged amino acid patches, which enable binding to the negatively charged headgroups of phospholipids [95, 99–101]. The degree of intrinsic curvature is a distinguishing feature of individual BAR domain subfamilies (Fig. 1.3) and

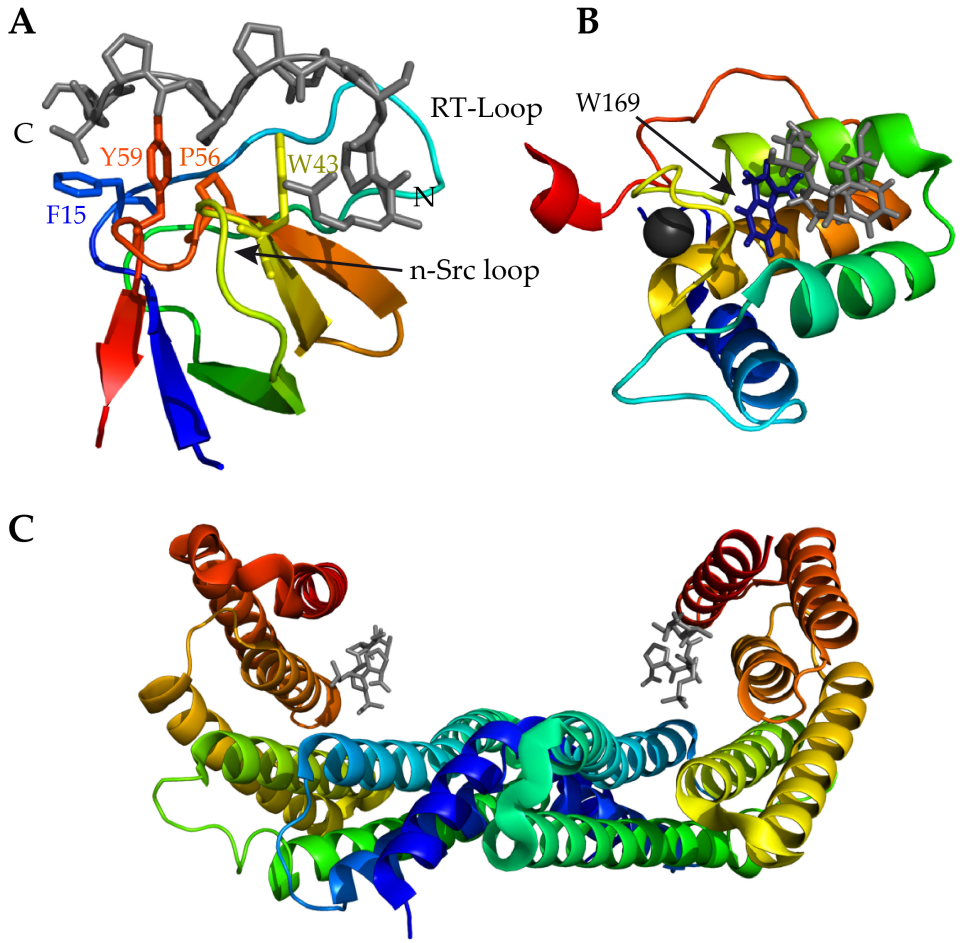

Figure 1.2.: Structures of different adaptor domains and adaptor proteins in complex with ligands. Domains are shown in cartoon representation and in rainbow coloring from blue (N-terminus) to red (C-terminus). The peptides are illustrated as grey sticks. **A:** Src-homology 3 (SH3) domain of rat beta-PIX in complex with a peptide derived from AIP-4 (RPSRPPPPTP) in class I orientation. The N- and C-termini of the peptide as well as the RT-loop and the n-Src loop of the SH3 are labelled. SH3 domain residues important for binding are shown as colored sticks. PDB code: 2P4R [88]. **B:** The second Eps15-homology domain of human Eps15 in complex with an NPF peptide derived from Hrb. The conserved Trp at the bottom of the binding pocket is shown in colored stick representation and the Ca^{2+} ion as dark grey sphere. PDB code: 1FF1 [72]. **C:** The human 14-3-3γ homodimer in complex with the RAIpSLP peptide (pS denotes a phosphorylated serine), PDB code: 2B05. Structures were visualised with PyMOL, Version 1.4.1., Schrödinger, LLC.

BAR domains have been suggested to induce or stabilise bent membrane topologies by imposing this inherent curvature in a scaffolding mechanism onto the underlying lipid bilayer [92, 95]. This largely results in stabilised membrane curvatures that correspond to their own intrinsic shape (Fig. 1.3) and has been used to classify BAR modules in the following subcategories [27, 92]:

BAR and N-BAR (for BAR domains carrying an N-terminal amphiphatic helix) domains, such as in Arfaptin, Endophilin, or Amphiphysin, are strongly curved and support highly bent invaginations, which are, for example, found at the constricted neck of endocytic pits (compare introduction on endocytosis, 1.2.1, p. 10) [95, 96].

F-BAR (Fes-Cip4-homology BAR) domains, such as in Fes-Cip4-homology domain only (FCHo), are more shallowly curved and mainly stabilise weakly bent membrane topologies, such as in nascent endocytic pits [98].

I-BAR (for inverse BAR) domains constitute a special subgroup, as their mainly flat structure with the membrane-interaction surface located on the convex side allows them to support flat membrane sheets [102] or protrusions [103, 104].

Furthermore, the morphogenic activity of BAR domains can be modulated by additional features, such as hydrophobic helices of N-BAR domains or wedge loops in the F-BAR domains of Syndapins (Fig. 1.3, indicated by black triangles), which insert into one leaflet of the lipid bilayer [95, 96, 99]. Neighbouring phosphoinositide-binding domains, such as the PX domain in sorting nexin (SNX) 9 [105] or the PH domain in amyloid precursor protein-like (APPL) [106]) assist in targeting to specific compartments (see above) [30].

What could be the mechanism underlying BAR domain-mediated membrane deformation? Lipid bilayers are continuous structures that tend to adopt a circular shape and deviations from this morphology can only be achieved by active processes that are able to overcome the membrane bending rigidity [107]. Asymmetrically distributed lipids between the inner and outer leaflet can, for example, exert considerable membrane stress on the bilayer, as large, negatively charged headgroups will occupy more space, which eventually leads to bulging [29, 30, 107, 108]. Therefore, locally confined attraction of negatively charged phospholipids by BAR domains could contribute to the deformation process [29]. Furthermore, BAR domains have been reported to assemble in spiral- or chain-like lattices around lipid tubes [97, 109, 110] and cooperation among many dimers in a rigid scaffold could provide sufficient stability to resist relaxation of the lipid bilayer [29, 92, 107]. The most effective mechanism for membrane deformation, however, constitutes the insertion of hydrophobic helices, such as those found in N-BAR domains [96, 98], into one leaflet of the bilayer [107]. The insertion will cause local membrane asymmetry and membrane stress [107], which can even promote separation of a single continuous

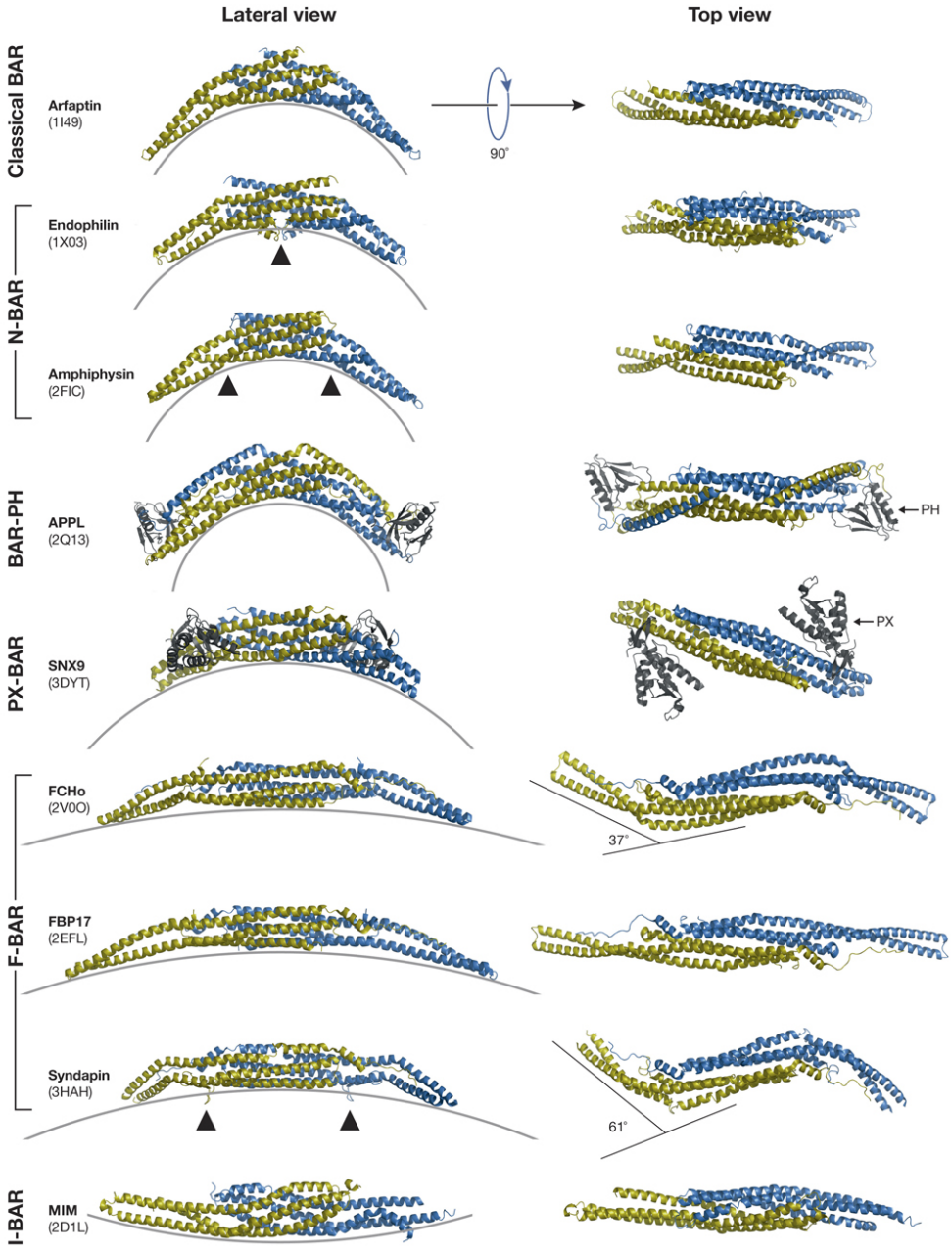

Figure 1.3.: Overview of different BAR domain modules. BAR modules adopt folds with different degrees of curvature. BAR modules (one monomer in yellow and the other in blue) from different subfamilies viewed from the side (left) and from top (right). N-BAR, BAR domain with N-terminal amphipatic helix; F-BAR, Fes-Cip4-homology BAR domain, I-BAR, inverse BAR. Additional domains, such as Pleckstrin-homology (PH) and Phox (PX) are in grey. The membrane is depicted as a grey line. PDB ID are given in brackets. Arrowheads mark positions within the BAR modules for hydrophobic insertion into membranes. This figure and the figure legend were adopted from Qualmann, Koch and Kessels [92].

lipid bilayer into two separate entities ("fission" or "vesiculation", compare p. 2) [107, 111, 112].

Furthermore, curvature formation can be facilitated through a concerted action of membrane bending proteins and oriented actin polymerisation [107]. On the one hand, coupling of membrane deformation with actin polymerisation is established indirectly through recruitment of actin regulators via additional adaptor domains, such as the SH3 domains of Syndapins, which will be discussed in chapter 8. On the other hand, actin regulation can be an inherent feature of certain BAR modules. The I-BAR domains of the IRSp53/MIM family (Fig. 1.3), for example, carry F-actin-bundling activity and bind the Rho GTPase Rac1, which is involved in actin polymerisation (see section 1.2.2 for introduction on Rho GTPases) [104, 113].

1.2. Multi-Protein Complexes in Membrane Trafficking and Signal Transduction

The organisation of signalling proteins in multi-protein complexes through multiple transient and low-affinity interactions allows cooperative decision making [48]. The longer assembly time of a large complex and its dependence on the presence of all binding partners might not only account for reported threshold responses in certain signalling pathways [31], but could also provide an efficient "noise filter" for stochastic signal fluctuations [31, 48]. In the following subsections, I will outline two exemplary pathways to describe the basic concepts of (1) directionality through cooperativity and (2) facilitated assembly of signalling complexes through scaffolds [48].

1.2.1. Example 1: Clathrin-Mediated Endocytosis

Among membrane trafficking pathways, clathrin-mediated endocytosis is the best studied example [27]. It relies on a complex machinery (Fig. 1.4, p. 12), which is sequentially recruited via transient protein interactions to the nascent endocytic pit dependent on the presence of specific phosphoinositides and membrane curvatures [27].

Recruitment of the shallow curved F-BAR proteins, such as FCHo1 [114] (see introduction on BAR modules, Fig. 1.3, p. 9), and adaptor proteins like AP-2 and clathrin nucleate the invagination process and promote formation of PtdIns(4,5)P_2 by phosphatidylinositol 4-phosphate 5-kinase type I [27, 115]. During maturation of the clathrin-coated pit through assembly of the clathrin lattice, additional F-BAR proteins, such as Formin-binding protein 17 [109], and

the highly curved N-BAR proteins Endophilin and Amphiphysin [95, 96] are sequentially added [27, 116], which further constrict the neck through a concerted action of scaffolding and wedging towards fission (compare section 1.1.3 for BAR domain-mediated membrane deformation) [27, 92, 116]. Subsequent recruitment of the 5-phosphatase Synaptojanin by Endophilin to the late stage of pit formation leads to conversion of PtdIns(4,5)P_2 to PtdIns(4)P [27, 117], which is then phosphorylated to PtdIns(3,4)P_2 by phosphatidylinositol 3-kinase C2α [27, 118]. This phosphoinositide conversion is believed to render the pathway irreversible [27] and triggers recruitment of the BAR-domain proteins SNX 9 and SNX 18 via their PX domain (compare introduction on lipid interaction domains, 1.1.3, p. 6) [27, 118]. SNX9 and SNX18 connect the late endocytic pit with the actin machinery [118] and might assist Endophilin and Amphiphysin in the recruitment of the GTPase Dynamin [27, 116, 119]. Finally, Dynamin assembles in helices around the neck and GTP-hydrolysis then promotes conformational changes in these Dynamin oligomers that lead to scission of the vesicle in a sling-like mechanism (reviewed in [27]).

1.2.2. Example 2: Rho GTPase-Regulated Actin Dynamics

Rho GTPases constitute important regulators of actin cytoskeletal dynamics and comprise a family of 20 proteins in mammals, of which RhoA, Rac, and Cdc42 are the best studied examples [120]. Most Rho GTPases cycle between an active GTP-bound state, which allows them to activate numerous downstream effectors, and an inactive GDP-bound state (Fig. 1.5, p. 13) [120]. The transition to the active form is promoted by guanine nucleotide exchange factors (GEF), while GTPase-activating proteins (GAP) facilitate GTP hydrolysis and therefore inactivation (Fig. 1.5, p. 13).

Active Rac, which serves as an example here, transmits the signal to the actin machinery through three pathways (Fig. 1.5, p. 13) [120]: Firstly, it can activate Formins, such as mDia2 (mammalian diaphanous 2) [120, 121], which promote actin polymerisation at the fast-growing (barbed) end of actin filaments [120]. Secondly, it can activate the WAVE-regulatory complex (WRC) [120, 122], which is a multi-protein complex [123] mediating formation of branched filaments through the Arp2/3 (actin-related protein) complex [124, 125]. Through binding of active Rac and the Arp2/3 complex, the WRC acts as a signalling scaffold, which brings together up- and downstream effectors in a single complex [126]. Moreover, the WRC component WAVE also binds to Slit-Robo-GAP3 (srGAP3), which was found to attenuate Rac-mediated actin polymerisation [127] (compare specific introduction chapter 4 for srGAP proteins). Finally, GTP-bound Rac can activate the p21-activated kinase (PAK), which leads to phosphorylation and therefore inactivation of Cofilin by the LIM domain kinase (LIMK), thereby preventing Cofilin-mediated actin depolymerisation [120, 128].

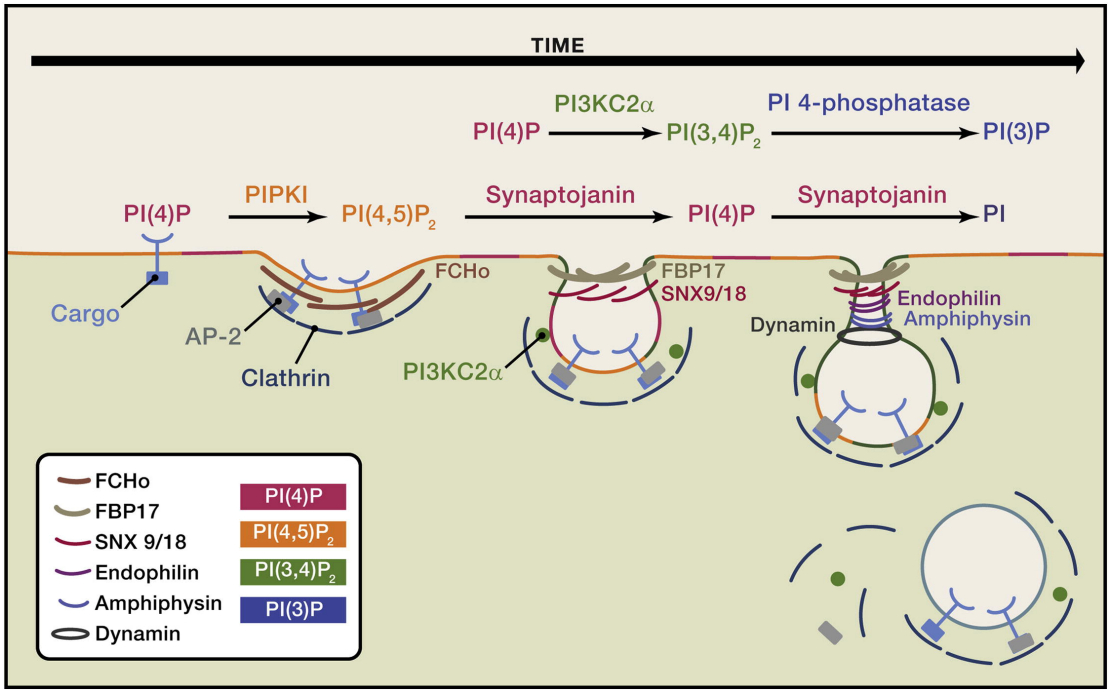

Figure 1.4.: Clathrin-mediated endocytosis. Illustrated are the scission-promoting GTPase Dynamin, the BAR module-containing proteins Fes-Cip4-homology domain only (FCHo), Formin-binding protein 17 (FBP17), sorting nexin (SNX) 9 and 18, Endophilin, and Amphiphysin, the adaptor proteins AP-2 and clathrin as well as the phosphatase Synaptojanin and the lipid-specific kinases phosphatidylinositol 4-phosphate 5-kinase type I (PIPKI) and phosphatidylinositol 3-kinase C2α (PI3KC2α). The phosphoinositide-conversion pathway is indicated. Further information can be found in the text. The figure was adopted from Daumke, Roux and Haucke [27].

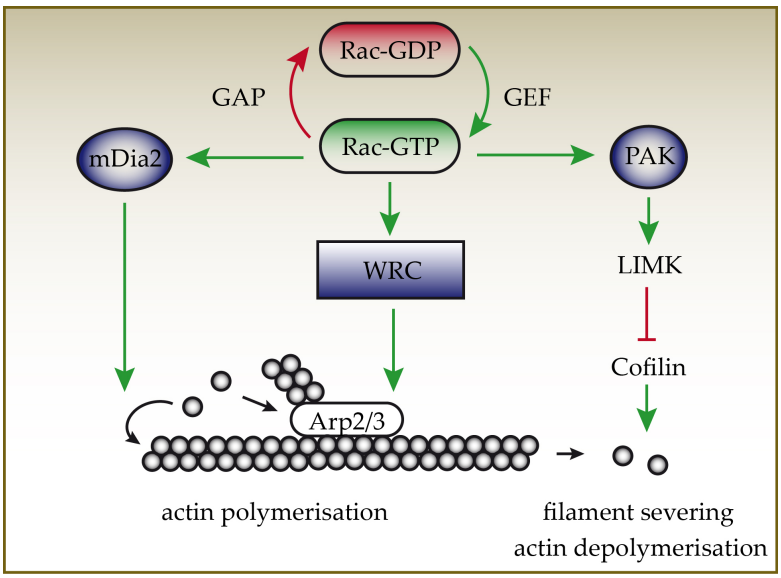

Figure 1.5.: Rho GTPase-mediated actin reorganisation. Illustrated is a model for regulation of actin dynamics by the Rho GTPase Rac. Activation is indicated by green arrows, whereas red arrows depict deactivating or inhibiting signals. GTPase-activating proteins (GAP) promote inactivation (GDP-bound state), whereas guanine nucleotide exchange factors (GEF) promote activation (GTP-bound state) of Rac. GTP-bound Rac can activate actin polymerisation either via formins, such as mDia2 (diaphanous homolog 3), or the WAVE-regulatory complex (WRC), which activates the Arp2/3 (actin-related protein) complex. Note that formins attach actin monomers at the barbed end, whereas Arp2/3 promotes formation of branched filaments. Active Rac might likewise stabilise formed filaments via activation of the PAK kinase/LIM domain Kinase (LIMK) cascade, which leads to phosphorylation and therefore inactivation of Cofilin.

1.3. Aims and Scope

The general goal of this thesis is the characterisation of protein-peptide interactions mediated by variable regions in two F-BAR protein families (see introduction on F-BAR domains, 1.1.3, p. 6): Slit-Robo GAPs (srGAP) and Syndapins. In particular, I focussed on the brain-specific isoforms of the respective families, srGAP3 and Syndapin1. The first project aims at the characterisation of the C-terminal region of srGAP3, which is presumably natively unfolded. As such regions often engage in protein-protein interactions (see introduction on intrinsic disorder, 1.1.1, p. 4), I attempted to identify binding partners as well as to biochemically characterise the formed complexes with respect to binding surfaces and biophysical parameters. This work should provide a basis for subsequent studies on the functional implications of these protein complexes in the framework of neurodevelopmental processes regulated by srGAP3. The second project aims at elucidating the mechanistic implication of a known interaction between the NPF motifs of Syndapin1 and the EH domain of EHD1 [129] (see introduction on EH domains, 1.1.2, p. 5) with respect to the membrane deforming potential of the F-BAR domain of Syndapin1 [99, 130, 131] (see introduction on F-BAR domains, 1.1.3, p. 6). Complex formation between Syndapin1 and EHD1 is involved in endocytic receptor recycling [129] (see introduction on endosomal recycling, Fig. 1.1, p. 3) and this work intends to deliver first insight into the underlying molecular mechanism, though does not aim at fully describing it.

2. CONTRIBUTIONS

This thesis covers two projects, which were both initiated by Yvonne Groemping, who supervised the experimental process and with whom I developed the main working hypotheses.

Characterisation of the C-terminal region of srGAP3
The basic concept for this project was provided by Yvonne Groemping, who suggested that the C-terminal regions of srGAP proteins could act as adaptor platform, which integrates the individual isoforms in different pathways. I cloned, expressed, and purified the C-terminal region of srGAP3. The initial pulldown experiment was carried out together with Anitha Jeganantham, who analysed srGAP1 and therefore provided the respective C-terminal construct of this protein. The mass spectrometric analysis was carried out by the Proteome Center Tübingen. Yvonne Groemping, Anitha Jeganantham and I evaluated the data and chose the set of candidate proteins for validation. Bijàn Mir-Montazeri suggested to use a GFP-nanobody for the validation experiment and drew my attention to the Chromotek GmbH. I designed our fluorescence-based co-immunoprecipitation assay in analogy to Chromotek's GFP-multiTrap assay. I devised the nanobody construct, developed the employed vector series, and established the assay. Purified GFP and mCherry were provided by Martin Schückel. I also established the cell culture experiments and the transfection protocols for our group in collaboration with Daniela Lazzaretti. Yvonne Groemping, Martin Schückel, Beatrice Laudenbach, and I prepared the DNA constructs required for this sub-project. I carried out the fluorescence-based CoIP-assay and therefore identified the binding partners for the subsequent in-depth characterisation. Martin Schückel assisted in several mammalian cell culture experiments. The biological sequence analysis of srGAP proteins and their C-terminal regions was my work, but the strategy was provided by Moritz Ammelburg. This analysis served as basis for the detailed investigation of the identified protein complexes. Together with Yvonne Groemping, I developed the experimental set-up for the identification of linear motifs mediating complex formation with SH3 domains. I cloned, expressed, and purified the proteins and carried out the isothermal titration experiments. Martin Schückel assisted in the repeated purification of several constructs. Furthermore, I prepared the samples for the phosphorylation analysis of srGAP3, while the mass spectrometry experiments were carried out by the Proteome Center Tübingen. I evaluated the provided data set with regard to potential 14-3-3-binding sites, gen-

erated the respective DNA constructs to test relevant motifs for 14-3-3-binding, and carried out the interaction assays. Parts of this project are included in a publication written by me and Yvonne Groemping. Parts exclusively written by me were adopted from the manuscript. Dagmar Sigurdardottir provided advice for structuring and writing of the manuscript.

Regulation of Syndapin1 by EHD1
The second project was initiated by Yvonne Groemping and Julia Rumpf. Yvonne Groemping proposed the idea that the variable linker region of Syndapin1 is involved in the autoinhibition. Julia Rumpf established the electron microscopy assay in collaboration with Heinz Schwarz and made the initial observation that complex formation between Syndapin1 and EHD1 leads to tubule formation on liposomes. The crystal structures of the Syndapin1 F-BAR domain in isolation and in the autoinhibited state, which were published by other groups during this time, immediately suggested that EHD1 might activate Syndapin1. I adjusted the electron microscopy assay in collaboration with Matthias Flötenmeyer and Heinz Schwarz and recorded and analysed the electron microscopic data set included in this thesis. The investigation of the effect of a single EH domain of EHD1, as well as truncated forms of Syndapin1, and the liposome co-pelleting assay were my work. The interpretation of the data as well as the improvement of lipid biochemistry protocols was a collaborative effort of Yvonne Groemping, Aleksander Czogalla, and me. The DNA constructs for these experiments were mainly generated by Julia Rumpf, Yvonne Groemping, and Theresia Niese. Julia Rumpf, Martin Schückel and I expressed and purified the proteins. Julia Rumpf and Martin Schückel carried out isothermal titration experiments for the analysis of complex formation with the full-length proteins as well as fragments thereof, while I carried out the control experiments. Dagmar Sigurdardottir provided advice for structuring of this thesis.

3. GENERAL MATERIALS AND METHODS

This chapter covers general methods of molecular biology, cell biology, biochemistry, and biophysics that were applied in both projects. Basic procedures are outlined, whereas specific adjustments of these protocols are explained in detail in the individual materials and methods sections. Methods that were only relevant to either of the two projects are also described in the respective materials and methods sections.

3.1. Molecular Biology Methods

3.1.1. General Cloning Procedures

Polymerase Chain Reaction (PCR)

DNA, which coded for target genes, was amplified from a plasmid template by polymerase chain reaction (PCR) [132] (see Tab. 3.1 for standard conditions). Specific oligonucleotides for the amplification of the target DNA are given in the appendix (Tab. B.3, p. 167). If the amplification was unsuccessful with standard conditions, a Touchdown PCR protocol [133] was applied instead.

Restriction Digest

Fragments and vectors were processed by restriction digest with type II restriction endonucleases (enzymes from NEB and Thermo Scientific) using the restriction sites that were either introduced via oligonucleotides or already present in the template DNA. The digestion of vectors and PCR fragments was performed according to the manufacturer's protocol and the 5'-phosphate of the digested vector was removed with alkaline phosphatase (FastAP, Thermo Scientific). Digested products were subsequently purified with a PCR purification kit (Qiagen) or via gel electrophoresis (see below) and subsequent gel extraction with a gel extraction kit (Qiagen).

Table 3.1.: Standard PCR conditions.

REACTION MIXTURE			PCR PROGRAMME		
Component	**Amount**	**c_{end}**	**Step**	**Temperature**	**Time**
Forward Primer (40 µM)	1.25 µl	1 µM			
Reverse Primer (40 µM)	1.25 µl	1 µM	1. Initial Melting	98 °C	3 min
GC Buffer (5x)[a]	10 µl	1x	2. Melting	98 °C	10 sec
dNTPs (10 mM)[a]	2.5 µl	0.5 mM	3. Annealing	55 °C	30 sec
Phusion Polymerase (2 U/µl)[a]	0.5 µl	1 U	4. Elongation	72 °C	15-30 sec/kb[b]
Formamide (100 %)	1 µl	3 %	5. Final Elongation	72 °C	10 min
DMSO (100 %)	1 µl	3 %			
$MgSO_4$ (50 mM)[a]	1 µl	1 mM			
Template DNA	200 ng	-	repeat steps 2 to 4 29x		
H_2O	ad 50 µl	-			

[a] from Thermo Scientific
[b] kb: kilobase

Ligation

Inserts were ligated into vectors at 21 °C for 3 to 16 h with the following conditions:

Vector	20 fmol
Insert	60-100 fmol
T4 DNA Ligase Buffer (10x, Thermo Scientific)	1 µl
T4 DNA-Ligase (Thermo Scientific)	1 µl
H_2O	ad 10 µl

Isolation and Analysis of Plasmid DNA

A single colony of transformed bacteria was grown in 4 ml of LB medium containing selective antibiotics (see 3.2.1). Plasmid DNA was isolated using the QIAprep Spin Miniprep Kit (Qiagen).

The correct insertion of the respective PCR fragment was verified by digesting the isolated plasmid DNA with the same restriction enzymes used for cloning or by colony PCR with the original amplification primers (standard PCR conditions: Tab. 3.1). The resulting fragments were analysed by gel electrophoresis. For that purpose, 5 µl of sample were mixed with 1 µl of sample buffer (Thermo Scientific) containing 10 mM Tris/HCl (pH 7.6), 0.03 % bromphenol blue, 0.03 % xylene cyanol FF, 60 % gylcerol and 60 mM EDTA. Agarose gel (1 % w/v) electrophoresis was performed with a constant voltage of 90 V in 1x TAE

buffer (40 mM Tris-acetate, 1 mM EDTA, pH 8.0). Gels were stained with Stain G (Serva).

3.1.2. Site-directed Mutagenesis

Point mutations were either introduced with the QuickChange Site-directed Mutagenesis Kit (Agilent Technologies) according to the manufacturer's protocol or with the method of Edelheit, Hanukoglu and Hanukoglu [134] employing two single-primer amplification reactions. Mutation-containing oligonucleotides were designed with PrimerX:
http://www.bioinformatics.org/primerx/.

3.1.3. Sequencing

All DNA constructs were verified through direct sequencing by the in-house sequencing facility.

3.2. Cell Culture Techniques

3.2.1. Microbiological Cell Culture Techniques

All cloning procedures were carried out with the *E. coli* strain TOP10, whereas protein expressions were performed with the strains BL21 Gold (DE3) and Rosetta 2 (DE3). The genotypes of the strains can be found in the appendix, Tab. A.1, p. 161. Bacteria were rendered chemically competent with $CaCl_2$ as described by Seidman *et al.* [135].

For transformations, 10 µl of a ligation reaction or 1 µl of conventional plasmid DNA were added to 50 µl of competent cells and incubated for 30 min on ice. The cells were exposed to 42 °C for 45 to 70 sec to induce the DNA uptake and subsequently cooled down. After the addition of 400 µl LB medium (10 g/l bactotryptone, 10 g/l NaCl, 5 g/l yeast extract, pH 7.5), the cells were incubated for 1 h at 37 °C. Subsequently, 100 - 450 µl were plated onto LB agar plates containing appropriate selective antibiotics (ampicillin, c_{end} = 100 µg/ml; kanamycin, c_{end} = 50 µg/ml; chloramphenicol, c_{end} = 34 µg/ml).

3.2.2. Mammalian Cell Culture Techniques

Adherent HEK293T cells [136] were cultured in Dulbecco's modified Eagle's medium (DMEM) supplemented with 10 % fetal bovine serum, 100 U/ml penicillin, 100 µg/ml streptomycin, and 2 mM L-Glutamine (all from Invitrogen) at 37 °C in a humidified atmosphere with 5 % CO_2. The HEK293T cells were a gift from Bijàn Mir-Montazeri (LMU München).

Transient transfections were performed with polyethylenimine (PEI, linear, 25 kDa, Sigma) [137]. HEK293T cells were seeded in medium without antibiotics in 100 mm dishes (Greiner Bio-One) and cultured till 90 % confluency. 20 µg of DNA was mixed with PEI in a DNA/PEI ratio of 1:5 (w/w) in DMEM, incubated for 15 min at room temperature, and added dropwise to the cells. The DNA/PEI ratio was optimised according to Ehrhardt *et al.* [138]. The medium was exchanged after 6 h. For smaller dishes, the amount of DNA was adjusted accordingly. The transfection agent was kindly provided by C. Söllner (MPI für Entwicklungsbiologie, Tübingen).

For fluorescence microscopy, HEK293T cells were grown on round coverslips, which were coated with Poly-L-Lysine (P1274, Sigma) according to the manufacturer's protocol. The cells were washed with phosphate-buffered saline (PBS), fixed with 2 % paraformaldehyde, and mounted in Fluoromount-G (SouthernBiotech).

3.3. Protein Biochemistry Methods

3.3.1. SDS Polyacrylamide Gel Electrophoresis (SDS-PAGE)

Protein samples were analysed by discontinuous SDS gel electrophoresis [139] mainly using a 10 % separating gel (375 mM Tris/HCl (pH 8.8), 0.1 % (w/v) SDS, 15 % (w/v) acrylamide, 0.4 % (w/v) bisacrylamide, 0.08 % (w/v) APS, 4 mM TEMED) and a 4.5 % stacking gel (125 mM Tris/HCl (pH 6.8), 4.5 % (w/v) acrylamide, 0.12 % (w/v) bisacrylamide, 0.06 % (w/v) SDS, 0.1 % (w/v) APS and 4.8 mM TEMED). Samples were mixed with sample buffer (32.5 mM Tris/HCl (pH 6.8), 50 mM DTT, 1 % SDS, 5 % glycerol, 0.02 % bromphenol blue) and denatured at 95 °C for 5 min. Proteins were separated at a constant current of 50 mA in SDS running buffer composed of 25 mM Tris/HCl (pH 8.9), 200 mM Glycine and 0.1 % (w/v) SDS and stained with Coomassie Brilliant Blue.

3.3.2. Protein Expression and Purification

For heterologous expression of proteins the *E. coli* strains BL21 Gold (DE3) and Rosetta 2 (DE3) were used. Cultures were grown at 37 °C in LB medium containing selective antibiotics to an OD_{600} of 0.6 to 0.8, at which protein expression was induced with 0.1 to 0.5 mM isopropyl-β-D-thiogalactopyranoside (IPTG). Proteins were expressed at 21 to 28 °C for 5 or 16 h, depending on the respective protein construct (see below). After cell harvest, cell pellets were resuspended in lysis buffer and stored at -80 °C.

Bacteria were lysed with a sonifier (Branson 250, BRANSON Ultraschall) and the soluble fraction separated from cell debris by ultracentrifugation. All proteins were purified by affinity chromatography, an optional ion exchange chromatography step, and subsequent size exclusion chromatography using ÄKTA liquid chromatography systems (GE Healthcare). The purification scheme and buffer conditions were adjusted for each protein according to the parameters from the ProtParam tool (Expert Protein Analysis System (ExPASy) proteomics server, http://www.expasy.org/). All steps were monitored by SDS-PAGE and the folding status of protein domains evaluated by CD spectroscopy (see 3.4.1). Proteins were concentrated in AMICON Ultra centrifugal filters (Millipore), snap frozen, and stored at -80 °C. The protein concentration was determined at 280 nm in an UV/vis spectrophotometer (Nanodrop 1000, Peqlab) using the extinction coefficient obtained from the ProtParam tool.

3.4. Biophysical Methods

3.4.1. Circular Dichroism

Circular dichroism spectroscopy can be applied to estimate the overall composition of secondary structure and the folding status of a protein, since each secondary structure element gives rise to a distinct spectrum (reviewed in [140]).

CD spectra were recorded with a spectropolarimeter (Jasco J-810, Jasco) in the far-UV region (195-250 nm), where the peptide bond depicts the main absorbing entity (reviewed in [140]). Proteins were diluted to a final concentration of 0.2 mg/ml in potassium phosphate buffer (10 mM, pH 7.4) containing 200 mM Na_2SO_4. Measurements were carried out at 20 °C in a cuvette with a cell length of 0.1 cm. The band width was set to 1 nm, the response time to 0.5 sec, and the scanning speed to 100 nm/min. The data of five consecutive measurements was averaged and the resulting spectra, which were corrected for buffer contributions, were analysed with the Spectra Manager II software (Jasco).

Temperature stability and folding state of proteins were assessed by following the denaturation of proteins with increasing temperature. Sigmoidal melting curves indicate cooperative unfolding, which is a characteristic of folded proteins. For this purpose, the change in ellipticity from 20 to 90 °C was measured at a wavelength associated with the largest difference between native and unfolded state (compare [140]). The response time was set to 2 sec, the band width to 3 nm, and the temperature slope to 1 °C/min. The melting temperature was calculated from the inflection point of the melting curve. Curves were plotted with SigmaPlot (version 12.3, Systat Software Inc.).

3.4.2. Isothermal Titration Calorimetry

Isothermal titration calorimetry (ITC) depicts a label-free technique for the investigation of the thermodynamic properties of binding reactions [141] or enzyme kinetics [142]. It measures the heat change upon complex formation when one component is titrated into the other, thereby providing information about the affinity, the binding enthalpy, and the stoichiometry of the reaction [141].

Measurements were carried out in a VP-ITC calorimeter (GE Healthcare) at 20 °C. Prior to measurements, all proteins were extensively dialysed against measurement buffer using Slide-A-Lyzer Cassettes (Thermo Fisher Scientific). Protein concentrations were determined as described under 3.3.2. The ligand was titrated under constant stirring at 300 rpm into the cell in 28 steps of 10 µl, and a spacing between titration steps of 240 sec. Data analysis was performed with MicroCal Origin for ITC (Version 7) assuming a single-site binding model. The integrated heat signal was corrected for the heat of dilution (obtained from reference titrations of syringe component into buffer or GST) and fitted to the following quadratic equation, thus creating the binding isotherm (reviewed in [143]):

$$\Delta Q(i) = Q(i)\frac{dV_i}{V_0}\left[\frac{Q(i)+Q(i-1)}{2}\right] - Q(i-1)$$

with V_i being the volume of ligand titrated at step i and Q the heat content. In a one-site binding model this is:

$$Q = \frac{nM_t\Delta HV_0}{2}\left[1+\frac{X_{t,i}}{nM_t}+\frac{1}{nKM_t}-\sqrt{\left(1+\frac{X_{t,i}}{nM_t}+\frac{1}{nKM_t}\right)^2-\frac{4X_{t,i}}{nM_t}}\right]$$

with X_t being the bulk concentration of titrant at the titration step i, M_t the bulk concentration of analyte, n the number of available binding sites for the titrant in one analyte molecule, V_0 the cell volume at the beginning of the titration, ΔH the molar enthalpy and K the association constant.

Part I.

Characterisation of the C-Terminal Region of SrGAP3

4. INTRODUCTION

Parts of this chapter are included in publication: Wuertenberger and Groemping. "A single PXXP motif in the C-terminal region of srGAP3 mediates binding to multiple SH3 domains." in *FEBS Letters* (2015).

Neuronal migration and axonal targeting are important processes that establish a certain brain architecture and are driven - among other factors - by guidance cues formed by secreted or transmembrane proteins [17, 144]. Slit-Robo signalling is involved in several neurodevelopmental processes and was identified as crucial pathway in mediating the repulsion of commissural axons that have crossed the midline (an imaginary line, which separates the left from the right hemisphere) [145]. Robo (*roundabout* [146]) receptors bind to the secreted Slit protein and mediate its repulsive effects [147–150] by affecting actin cytoskeletal dynamics [17, 144].

The Slit-Robo GTPase-activating proteins (srGAP) act downstream of Robo receptors [151–153] and transmit the signal via Rho GTPases to the actin cytoskeleton [151] (compare introduction on Rho GTPases, section 1.2.2, p. 11). This family comprises the proteins srGAP1, srGAP2, srGAP3, and the more distantly related ARHGAP4, which share a common domain architecture comprising an N-terminal F-BAR domain followed by a GAP domain, and an SH3 domain (Fig. 4.1) [151].

Despite the high degree of sequence conservation in these globular domains [151, 154], srGAP proteins seem to be involved in different aspects of neuronal development [145, 151, 152, 155–158]. This observation might partially be related to non-overlapping expression patterns in the developing and adult brain [159, 160], but was also suggested to depend on different functional associations on a molecular level [145]. SrGAP3, which is also termed “mental disorder GAP” (MEGAP) [161] or “WAVE-associated RacGAP protein” (WRP)

Figure 4.1.: Domain architecture of srGAP proteins. F-BAR, Fes-Cip4-homology-BAR (Bin-Amphiphysin-Rvs) domain; GAP, GTPase-activating domain; SH3, Src-homology 3 domain. The domain boundaries of srGAP3 (*H. sapiens*, isoform 1) are indicated.

[127], was, for example, found to regulate commissural axon pathfinding (see above, [152]) and the migration of neuronal progenitors out of the subventricular zone [157]. However, the functions of srGAP3 are likely to be more complex, since knockout mice present various neurological defects ranging from impairments in cognitive function and development of hydrocephalus to changed synaptic activity [145, 157, 161–163]. Most notably, disruption of the srGAP3 gene has been associated with a severe form of mental retardation [161]. Moreover, srGAP3 is mainly expressed in brain tissue and to a lower extent in kidney [161], whereas srGAP1 and srGAP2 show a broader tissue distribution [151].

On a molecular level, srGAP3 employs its unique domain composition to regulate actin cytoskeletal as well as microtubule dynamics and the formation of cellular protrusions [127, 145, 164, 165]: Via its F-BAR domain it is targeted to membranes [165] and facilitates filopodia formation, which was found to be crucial for dendritic spine initiation [163]. In fact, all F-BAR domains of the srGAP family seem to promote the formation of protrusions rather than invaginations [154, 156], which sets them apart from conventional F-BAR modules (compare introduction on BAR domains, section 1.1.3, p. 6), although the molecular details underlying these findings remain to be elucidated. The SH3 domain mediates complex formation with Robo1 and Robo2 [152, 166], WAVE1 [127], or Lamellipodin [165], thereby enabling signal transmission (see above) and - together with the GAP domain - negative regulation of Rac1-dependent actin polymerisation [127, 151, 161, 164, 165] (compare introduction on Rho GTPases, section 1.2.2, p. 11).

While all of these studies mainly focussed on the N-terminal domains, the function of the less conserved C-terminal region (CTR) [151] remained elusive. In this research project, I therefore attempted to characterise the C-terminal region of srGAP3.

5. MATERIALS AND METHODS

5.1. Bioinformatics

Amino acid sequences of the srGAP family of proteins (srGAP1, 2, and 3, ARHGAP4) were gathered with PSI-BLAST [167] employing searches against the non-redundant protein database (nr) or retrieved from the Reference Sequences Database provided by the National Centre for Biotechnology Information (NCBI) and from the KEGG Orthology Database (group K07526). Remote homologs were identified through transitive sequence profile searches with HHsenser [168]. An overview of the employed databases and bioinformatic tools and the corresponding web links are listed in Tab. 5.1, p. 29. The longest isoform was selected - if applicable - and duplicate sequences were removed, thus leading to a curated set of 247 sequences. The Bioinformatics Toolkit of the MPI for Developmental Biology [169] provided the platform for the integrative sequence analysis outlined below.

Domain boundaries were determined with HHpred [170] searches for homologous proteins of human srGAP3 in three different databases: the Protein Data Bank clustered to a maximum pairwise sequence identity of 70 %, the Structural Classification of Proteins database clustered to a pairwise sequence identity of 95 %, and the protein families (Pfam) database [169, 170]. Sequences were realigned using the implemented maximum accuracy algorithm of HHpred [170] and the derived domain boundaries locally refined through secondary structure prediction with PSIPRED [171] and JPRED [172]. Pairwise sequence comparisons of the srGAP sequences from *H. sapiens* were performed with a global alignment employing the Needleman-Wunsch algorithm provided by the European Molecular Biology Open Software Suite (EMBOSS, EMBOSS Needle tool for protein alignment) [173–175].

In order to delineate sequence relationships between the C-terminal regions of srGAP proteins, amino acid sequences were compared through clustering and visualisation with CLANS [176] employing BLAST [177] with a BLOSUM80 matrix for all-against-all comparisons, and a variable P-value cut-off. Multiple sequence alignments of subclusters and selected sequence sets were produced with MSAProbs [178], MUSCLE [179, 180], T-Coffee [181], or the implemented maximum accuracy algorithm of HHpred [170]. Interactive processing of these alignments based on secondary structure and linear motif predictions

(see below) helped to improve their accuracy when comparing highly divergent sequences. Secondary structure and disorder in the C-terminal region of srGAP proteins were predicted by incorporating the results of a panel of different prediction servers: D2P2 [182], DisProt [183], MoRFpred [184], PredictProtein [185], and Quick2D [169]. The amino acid sequence of human srGAP3 or alignments of respective subclusters from the CLANS map served as input. Coiled-coils were predicted using the consensus of COILS/PCOILS [186] and MARCOIL [187] and heptad repeats were assigned manually.

Candidate linear motifs located in the C-terminal region of srGAP were retrieved from the Eukaryotic Linear Motif (ELM) resource, which searches for functional sites in proteins using regular expressions [188, 189], and Scansite [190, 191], which uses a matrix of selectivity values derived from oriented peptide library screens to predict optimal binding sites for a variety of adaptor domains [80, 192, 193]. Both methods thus depend on datasets of well-characterised domain/motif-interaction types, which precludes the *de novo* identification of motifs. As *de novo* predictor, I employed SLiMPred [194], which uses machine learning on known ELM instances and additional physico-chemical features of the amino acid sequence to predict linear motifs in disordered regions and folded domains [194]. Experimentally verified phosphorylation sites in srGAP3 were collected from the PhosphoSite database [195].

5.2. Molecular Biology Methods

5.2.1. Cloning Strategies and DNA Constructs

For expressions in mammalian cells, a modified pEGFPC2 (Clontech) vector series comprising six constructs was generated, which are termed pEGFPC23C and pmCherryC23C (see Tab. B.2, p. 164): Each vector contained one of three frames, a PreScission Protease (GE Healthcare, here "3C") cleavage site upstream of the multiple cloning site, and eGFP or mCherry, which resulted in the N-terminal tagging of proteins (Fig. 5.1).

The srGAP3 plasmid (isoform 1, *H. sapiens*) was a kind gift from G. Rappold (Universität Heidelberg). Full-length srGAP3 (amino acids (aa) 1-1099) was subcloned into pEGFPC23C and pmCherryC23C. The candidate interaction partners for the fluorescence-based co-immunoprecipitation assay (see 5.3.5) were solely cloned into the pmCherryC23C vectors. DNA templates used for subcloning of target genes were obtained from Addgene, from BioCat GmbH, or kindly provided by other research groups (as enlisted in Tab. B.1, p. 163). The respective PCR primers, gene identifiers (http://www.ncbi.nlm.nih.gov/), and restriction sites can be similarly found in the appendix (Tab. B.3, p. 167).

Table 5.1.: Bioinformatic tools and databases.

Bioinformatic Tool [a]	URL
MPI Bioinformatics Toolkit	http://toolkit.tuebingen.mpg.de/
COILS/PCOILS	http://toolkit.tuebingen.mpg.de/pcoils
CLANS	http://toolkit.tuebingen.mpg.de/clans
D2P2 database	http://d2p2.pro/
DisProt database	http://www.disprot.org/
ELM resource	http://elm.eu.org/
EMBOSS Needle tool	http://www.ebi.ac.uk/Tools/psa/emboss_needle/
HHpred	http://toolkit.tuebingen.mpg.de/hhpred
HHsenser	http://toolkit.tuebingen.mpg.de/hhsenser
JPRED	http://www.compbio.dundee.ac.uk/www-jpred/
KEGG Orthology database	http://www.genome.jp/kegg/ko.html
MARCOIL	http://toolkit.tuebingen.mpg.de/marcoil
MoRFpred	http://biomine-ws.ece.ualberta.ca/MoRFpred/index.html
MSAProbs	http://toolkit.tuebingen.mpg.de/msaprobs
MUSCLE	http://toolkit.tuebingen.mpg.de/muscle
NCBI	http://www.ncbi.nlm.nih.gov/
PhosphoSite	http://www.phosphosite.org/homeAction.do
PredictProtein	http://ppopen.informatik.tu-muenchen.de/
PSIPRED	http://bioinf.cs.ucl.ac.uk/psipred/
Quick2D	http://toolkit.tuebingen.mpg.de/quick2_d
Scansite3	http://scansite3.mit.edu/#home
SLiMPred	http://bioware.ucd.ie/~compass/biowareweb/Server_pages/slimpred.php
T-Coffee	http://tcoffee.crg.cat/

[a] Detailed information on abbreviations can be found in the text.

For expression in *E. coli*, the C-terminal region of srGAP3 (aa 810-1099) was cloned into the pETGST1c vector (provided by Gunter Stier, Heidelberg). Smaller srGAP3 fragments (PxxP-fragment: aa 1047-1079, Linker: aa 470-508), and the SH3 domains of Amphiphysin, Endophilin-A1, Endophilin-A2, and Grb2 were cloned into pGEX6P1 (GE Healthcare). The DNA sequence for the anti-GFP-nanobody (subsequently abbreviated as GFP-nanobody, [compare 196]) was derived from the protein sequence published in Saerens *et al.* [197] and Kubala *et al.* [198]. A codon-optimized DNA construct for expression in *E. coli* cloned into pET29a was ordered from Genscript. It contained an additional Thrombin cleavage site, which enabled the removal of the C-terminal His_6-tag.

The srGAP3 mutant, which is deficient in SH3 domain-binding (srGAP3 AxxA-fragment, compare Tab. B.3, p. 167), was constructed through cassette mutagenesis: Oligonucleotides were phosphorylated with T4 Polynucleotidekinase (NEB) and ligated to produce a fragment that could be incorporated via the BamHI/AgeI sites into the digested pGEX6P1_srGAP3_PxxP-fragment construct (Tab. B.3, p. 167).

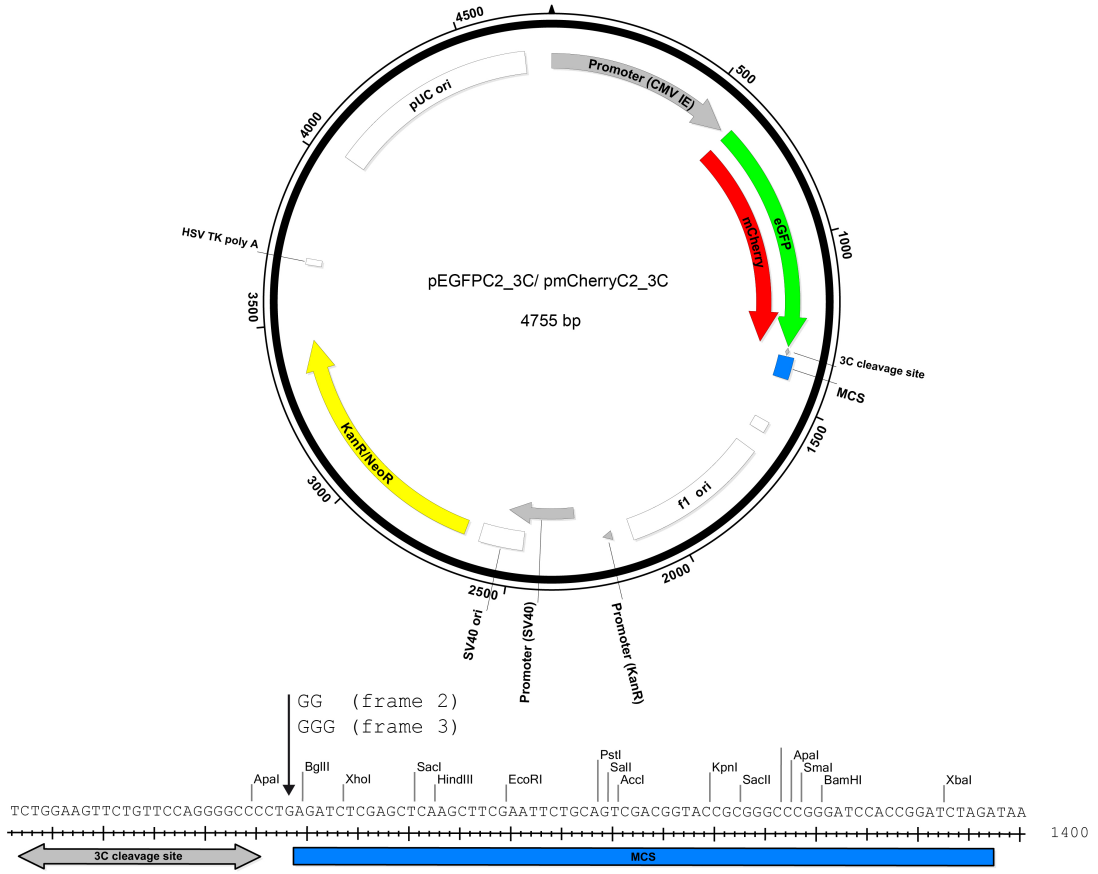

Figure 5.1.: Vector map of the pEGFPC23C/pmCherryC23C vector series. Modified from pEGFPC2 (Clontech), containing either the enhanced green fluorescent protein (eGFP) gene or a gene coding for the monomeric red fluorescent protein variant mCherry. Their expression is under control of human cytomegalovirus immediate early (CMV IE) promoter. The multiple cloning site (MCS) is positioned between a Precission Protease (GE Healthcare) cleavage site ("3C") and the SV40 polyadenylation signal (SV40 poly A). Three different frames were obtained via the introduction of "G" and "GG" at position 1328 (illustrated in the sequence below). The SV40 origin enables the replication in mammalian cells, the pUC origin the replication in *E. coli*, and f1 origin the single-stranded DNA production. A kanamycin resistance gene (KanR) and a corresponding upstream promoter allow for selection in *E. coli*, and a neomycin-resistance cassette consisting of the SV40 early promoter, the neomycin resistance gene (NeoR), and the polyadenylation signal from Herpes simplex virus thymidine kinase (HSV TK poly A) for selection in eukaryotic cells. The figure was adapted from the Clontech vector map.

5.3. Protein Biochemistry Methods

5.3.1. Protein Expression and Purification

The **GFP-nanobody** was expressed in *E. coli* BL21 Gold (DE3) cells. Protein expression was induced with 0.1 mM IPTG and the cells harvested after 16 h at 21 °C. The cells were lysed in 30 mM Hepes (pH 6.8), 300 mM NaCl, 3 mM β-Mercaptoethanol, 10 mM imidazole, 1 mM phenymethylsulfonyl fluoride (PMSF) , and cOmplete Protease Inhibitor Cocktail (Roche) and the crude extract applied to a Ni Sepharose (GE Healthcare) column. After washing with a high salt buffer (1 M NaCl) and removal of DnaK, which is frequently co-purified with unfolded peptides, according to Thain *et al.* [199], bound protein was eluted in a linear imidazole gradient and the S-tag and His_6-tag cleaved off with Thrombin (Sigma). Uncleaved fusion protein was removed with a second Ni Sepharose column and the flow-through, which contained the free nanobody, subjected to a Superdex 75 column (GE Healthcare). The pure protein was concentrated in 20 mM Hepes (pH 7.0), 150 mM NaCl, and 3 mM β-Mercaptoethanol to 13 - 23 mg/ml.

GST-srGAP3-CTR was expressed in *E. coli* Rosetta 2 (DE3) with the same protocol as employed for the GFP-nanobody. The cells were lysed in 30 mM Hepes (pH 6.8), 300 mM NaCl, 4 mM DTE, 4 mM Benzamidine, 2 mM EDTA, and cOmplete Protease Inhibitor Cocktail and the cleared lysate subjected to a Glutathione Sepharose 4B column (GE Healthcare). After washing with a high salt buffer (1 M NaCl) and removal of DnaK according to Thain *et al.* [199], the column was washed with 50 mM MES (pH 6.0), 50 mM NaCl, and 2 mM DTE and bound protein eluted in a step gradient with 60 mM GSH. The protein was further purified with cation exchange chromatography (Source S, GE Healthcare) using MES buffer and eluted in a linear salt gradient. The eluate was subjected to a Superdex 200 column (GE Healthcare) in 20 mM Hepes (pH 6.8), 150 mM NaCl, and 2 mM DTE and the combined srGAP3-containing fractions concentrated to 2 - 11 mg/ml.

The **srGAP3 PxxP-fragment** and **srGAP3 AxxA-fragment** were expressed as GST-fusion proteins in *E. coli* BL21 Gold (DE3) cells with the same protocol as employed for the GFP-nanobody. The cleared lysates were applied to a Glutathione Sepharose 4B column in 50 mM Tris/HCl (pH 8.0), 300 mM NaCl, 4 mM DTE, 4 mM Benzamidine, and cOmplete Protease Inhibitor Cocktail, washed with a high salt buffer (1 M NaCl), and eluted in a linear GSH gradient. The eluate was subjected to size exclusion chromatography (Superdex 75) and the GST-tag cleaved off afterwards using PreScission Protease (GE Healthcare). GST was removed with a second GSH column and a final heat denaturation step (70 °C for 15 min, removal of precipitates by centrifugation for 10 min at 30000 rpm and 4 °C). The gel filtration eluate of the srGAP3 AxxA-fragment contained

a non-proteinaceous contaminant (as assessed by UV spectrometry), presumably including metal ions, which resulted in a brown color of the protein solution. This contaminant could be removed by addition of 10 mM EDTA during heat denaturation and subsequent dialysis against EDTA-free buffer. The proteins were concentrated in 50 mM Tris/HCl (pH 8.0), 200 mM NaCl, and 3 mM β-Mercaptoethanol to a final concentration of 13 - 51 mg/ml.

GST-fusion proteins of **SH3 domains** were expressed in *E. coli* BL21 Gold (DE3) cells. Protein expression was induced with 0.2 to 0.5 mM IPTG and continued for 5 h at 21 - 25 °C. After harvest, the cells were lysed in 20 mM Hepes (pH 7.0), 300 mM NaCl, 4 mM DTE, 4 mM Benzamidine, 2 mM EDTA, and cOmplete Protease Inhibitor Cocktail. The crude extracts were subjected to a Glutathione Sepharose 4B column and eluted after a high salt wash (1 M NaCl) in a linear GSH gradient. The free SH3 domains were produced by incubation with PreScission Protease and separated from the GST-tag via gel filtration (Superdex 75). The SH3 domains were concentrated in 20 mM Hepes (pH 7.0), 150 mM NaCl, and 3 β-Mercaptoethanol to 7 - 43 mg/ml. **GST** was obtained as a byproduct of these SH3 domain purifications.

5.3.2. Western Blotting

Proteins were separated by SDS-PAGE with 10 % polyacrylamide gels and transferred onto a nitrocellulose membrane (pore size 0.45 µm, Whatman) in 25 mM Tris, 150 mM Glycine, and 10 % isopropanol for 1.5 h at 25 V using an XCell II Blot Module (Invitrogen). Effectual protein transfer was monitored with Ponceau S (Sigma) staining and the membrane subsequently blocked with blocking buffer (PBS with 0.1 % Tween 20 (Sigma), 3 % nonfat dry milk powder) for 16 h at 4 °C. Proteins were detected by incubation of the membrane for 2 h at room temperature with primary antibodies (mouse anti-RFP (3F5), rat anti-GFP (3H9), ChromoTek GmbH, rabbit anti-srGAP3 (S1575), Sigma) diluted 1:1000 in blocking buffer. Membranes were washed three times with PBS-T and incubated for 1 h at room temperature with HRP-conjugated secondary antibodies (goat anti-mouse (115-035-146), goat anti-rat (112-035-143), goat anti-rabbit (111-035-144), Jackson ImmuoResearch) diluted 1:3000 in blocking buffer. After washing with PBS-T, bands were developed with Clarity Western ECL substrate (Bio-Rad) and images acquired with a Fusion Sl Imaging System (Peqlab).

For the consecutive detection of two antigens, the membranes were stripped with 60 mM Tris/HCl (pH 6.8), 2 % SDS, 100 mM β-Mercaptoethanol for 30 min at 50 °C, washed extensively with PBS-T, and reprobed with the second primary antibody after blocking.

5.3.3. GST Pull-Down and Mass Spectrometric Analysis

The GST pull-down with rat brain lysate from a rat of stage P14 was performed as described by Rufer *et al.* [200] with the modification that bound proteins were analysed by mass spectrometry instead of Western blotting. The assay was carried out together with Anitha Jeganantham (MPI für Entwicklungsbiologie, Tübingen). We utilised GST-srGAP3-CTR, GST-srGAP1-CTR (*H. sapiens*, residues 799-1085), and GST for these experiments in order to dissect binding partners that were specifically associated with either srGAP family member. GST-srGAP1-CTR was provided by A. Jeganantham. Pull-down fractions were separated by SDS-PAGE and gel sections processed with in-gel tryptic digest and subsequent NanoLC-MS/MS analysis by the Proteome Center Tübingen (Easy-nLC coupled to an LTQ Orbitrap XL, Thermo Fisher Scientific). Data analysis was performed by Johannes Madlung (Proteome Center Tübingen) with the MaxQuant software suite (version 1.0.14.3) [201] and the Mascot search engine (version v.2.2, Matrix Science). We then estimated the general confidence for the identification of true binding partners based on peptide counts and intensity. Proteins were counted as srGAP-positive if the number of peptides was at least twice as high as in the GST-control experiment. The identified candidates were further classified as srGAP3- or srGAP1-specific based on an analogous discrimination criterion.

5.3.4. Phosphorylation Analysis of srGAP3

We analysed the phosphorylation state of endogenous srGAP3 from rat brain (stage P14) and of transiently expressed eGFP-srGAP3 from HEK293T cells using mass spectrometry.

For immunoprecipitations of endogenous srGAP3, the brain tissue was homogenized in lysis buffer containing phosphatase and protease inhibitors (20 mM Tris/HCl (pH 7.5), 150 mM NaCl, 1 % Nonidet P-40 (Roche), 2 mM EDTA, 1 mM Na_3PO_4, 5 mM NaF, 3 mM $Na_4P_2O_7$, 1 mM Na_3VO_4, 2 µl/ml diisopropyl fluorophosphate, and one tablet of cOmplete Protease Inhibitor Cocktail). Cell debris was removed by centrifugation and the lysate pre-cleared with G-protein-coupled beads for 30 min at 4 °C. After removal of the beads, srGAP3 was precipitated by addition of 5 µg of anti-srGAP3 (rabbit) antibody (S1575, Sigma) to 750 µl lysate and the immune complexes allowed to form for 16 h at 4 °C. The complexes were captured by incubation of the lysate with G-protein-coupled beads for 2 h at 4 °C. Beads were pelleted by centrifugation, washed eight times with lysis buffer, and the bound proteins isolated by heat denaturation in SDS sample buffer.

EGFP-srGAP3 was transiently expressed in HEK293T cells (see 3.2.2) and isolated from the lysate in lysis buffer using GFP-binding protein-coupled beads (GFP-Trap_A, ChromoTek GmbH) according to the manufacturer's protocol.

Proteins were separated by SDS-PAGE and gel sections processed as described for the GST pull-down samples (see 5.3.3) by the Proteome Center Tübingen. Phosphopeptides were analysed in an LTQ Orbitrap XL with multistage activation. The data analysis was carried out by Johannes Madlung (Proteome Center Tübingen) with the MaxQuant software suite (version v.1.2.2.9) [201] and the Andromeda search engine [202]. Phosphorylation sites were assigned to a specific amino acid, if the localisation probability of this phosphorylation event was above a threshold of 0.75.

5.3.5. Fluorescence-Based Co-Immunoprecipitation Assay

For interaction studies between srGAP3 and the identified candidate binding partners, I established a fluorescence-based co-immunoprecipitation (Co-IP)-assay in a 96-well format. It relies on the Co-IP of mCherry-tagged candidate proteins with eGFP-tagged srGAP3 from HEK293T lysates and is similar to the commercially available GFP-multiTrap (ChromoTek GmbH; compare [203]).

Lysate preparation

MCherry-tagged candidate proteins were co-transfected with either eGFP-srGAP3 full-length or eGFP into HEK293T cells as described under general materials and methods, section 3.2.2 and harvested after 30 h. About 10^7 cells per sample were lysed in lysis buffer containing phosphatase and protease inhibitors: 10 mM Tris/HCl (pH 7.5), 150 mM NaCl, 0.5 % Nonidet P-40 (Roche), 1 mM EDTA, 5 mM NaF, 3 mM $Na_4P_2O_7$, 1 mM Na_3VO_4, 1 mM PMSF, and one tablet of cOmplete Protease Inhibitor Cocktail. Lysates were cleared by centrifugation for 30 min at 13300 rpm at 4 °C and the volume between the sample containing eGFP-srGAP3 and the eGFP-control adjusted to yield equal mCherry fluorescence (measured with BioTek H4 microplate reader, excitation (Ex) at 590 nm, emission (Em) at 610 nm). To test whether the two constructs were co-expressed in the majority of cells, I monitored their expression with fluorescence microscopy (see 3.2.2 for sample preparation). The images were acquired with a Zeiss LSM 510 Meta and a 63x oil objective. Images were processed with Fiji [204]: The channels were spectrally unmixed [205], a composite image generated and an unsharp mask with a radius of 1.0 and a mask weight of 0.3 applied to the individual pictures. The expression of the proteins was further analysed by Western blotting as described under 5.3.2.

Co-Immunoprecipitation

The GFP-nanobody was immobilised in amino-reactive 96-well plates (Nunc Immobilizer Amino Black, Thermo Scientific) according to the supplier's protocol. A detailed description of the optimisation of the coupling reaction and the assay set-up can be found in the results section (see 6.3.1, p. 48). The purified eGFP and mCherry, used for establishing the assay, was generously provided by Martin Schückel (MPI für Entwicklungsbiologie, Tübingen). Nanobody-containing plates were incubated for 2 h at 4 °C with HEK293T lysates (4 replicates per sample on each plate) and washed twice with PBS-T (0.2 % Tween 20). Subsequently, the fluorescence signals were recorded in PBS in a Mx microplate reader (BioTek) with the following settings: Ex 488 nm (9 nm slit width)/ Em 509 nm (9 nm slit width) for eGFP, Ex 580 nm (9 nm slit width)/ Em 610 nm (13.5 nm slit width) for mCherry, Gain 150, read height 6 mm, and 10 reads with 40 data points. For evaluation of the data, I compared the mCherry-fluorescence of Co-IPs containing eGFP-srGAP3 to the eGFP-control. The statistical analysis of two (α-Cop) to four independent experiments was performed with SigmaPlot (version 12.3, Systat Software Inc.).

5.4. Biophysical Methods

5.4.1. Isothermal Titration Calorimetry

All measurements were carried out at 20 °C and the ligand was titrated under constant stirring at 300 rpm into the cell (cell volume 1.4295 ml) in 28 steps of 10 µl, and a spacing between titration steps of 240 sec. 200 to 1000 µM ligand were titrated into 20 to 100 µM protein solution. Prior to measurements, all proteins were extensively dialysed against 20 mM Hepes (pH 6.8 in titrations with GST-srGAP3-CTR or pH 7.3 intitrations with shorter srGAP3 fragments), 150 mM NaCl, and 5 mM β-Mercaptoethanol.

6. RESULTS

6.1. Bioinformatic Analysis of SrGAP Proteins

6.1.1. Phylogenetic Distribution of SrGAP Proteins

SrGAP proteins have been identified and studied in mammals as well as *Caenorhabditis elegans* [151], but the phylogenetic distribution of this protein family has so far not been analysed in detail. My sequence analysis revealed that srGAPs occur in metazoans, in which Bilateria represent the largest group, but single sequences are also found in Cnidaria and Placozoa. Most sequences in the bilaterian lineage belong to chordates, but they are also present in Echinodermata, Arthropoda, Nematoda, Annelida, Mollusca, and Platyhelminthes. With searches for remote homologs using HHsenser [168], I further detected srGAP genes in the genomes of two unicellular eukaryotes: the choanoflagellate *Salpingoeca rosetta* and the filasterean *Capsaspora owczarzaki* [206]. The srGAP family is therefore conserved over large evolutionary distances, but does not seem to be present ubiquitously. *Drosophila species*, for instance, lack srGAP proteins and only contain representatives of the closest homologous family: Nwk (Nervous Wreck) and FCHSD (FCH and double SH3 domains) proteins (sequence analysis by Anitha Jeganantham, personal communication). The two protein families share the F-BAR domain, but FCHSD and Nwk possess two SH3 domains instead of a GAP and a SH3 domain.

While the three N-terminal domains in srGAP proteins (Fig. 4.1, p. 25) are well conserved, comparison of sequences of the human paralogs showed that the C-terminal region (CTR, see Fig. 4.1, 25 for srGAP architecture) is most divergent within the family, in which ARHGAP4 lacks any detectable similarity (Tab. 6.1, similarly shown in [154, 207]). In order to analyse the amino acid sequence relationships between the C-terminal regions, I clustered and visualised the C-terminal sequences using CLANS (Fig. 6.1) [176]. Three sequences from arthropods and a single mollusc sequence are devoid of C-terminal regions and were thus excluded from further analyses. Chordate srGAP1, 2, and 3 formed the main cluster, in which the vertebrates composed the core (Fig. 6.1). Cephalochordata (*Branchiostoma floridae*) and Tunicata (*Ciona intestinalis*) were positioned at the edge, but remained tightly associated with this cluster at lower P-value cut-offs ($P < 10^{-6}$). ARHGAP4 sequences clustered - as expected from calculated sequence identities (Tab. 6.1) - separately and were only

Table 6.1.: Amino acid sequence identities of the human srGAP family. Sequence identities in percent of srGAP1, 2, 3 and ARHGAP4 from *H. sapiens* were calculated from pairwise alignments using the EMBOSS Needle tool (http://www.ebi.ac.uk/Tools/psa/emboss_needle/).

	Full Sequence%				F-BAR%[a]				GAP%[a]				SH3%[a]				CTR%[a]			
	srGAP1	srGAP2	srGAP3	ARHGAP4	srGAP1	srGAP2	srGAP3	ARHGAP4	srGAP1	srGAP2	srGAP3	ARHGAP4	srGAP1	srGAP2	srGAP3	ARHGAP4	srGAP1	srGAP2	srGAP3	ARHGAP4
srGAP1[b]	–	66	68	37	–	79	77	46	–	74	74	59	–	92	90	53	–	43	44	8
srGAP2[b]		–	58	39		–	70	46		–	51	56		–	85	56		–	35	12
srGAP3[b]			–	39			–	50			–	58			–	52			–	9
ARHGAP4[b]				–				–				–				–				–

[a] F-BAR, Fes-Cip4-homology-BAR (Bin-Amphiphysin-Rvs) domain; GAP, GTPase-activating domain; SH3, Src-homology 3 domain; CTR, C-terminal region.

[b] Uniprot identifier (http://www.uniprot.org/): srGAP1, Q7Z6B7; srGAP2, O75044; srGAP3, O43295; ARHGAP4, P98171.

weakly connected to other vertebrate sequences. Furthermore, Lophotrophozoa and Arthropoda formed a Protostomia super-cluster, which weakly associated with chordate srGAP proteins, while Nematodes remained isolated (Fig. 6.1). Nematode srGAP proteins form a unique subgroup within the set of analysed sequences, as they were the only representatives within the bilaterian clade that are devoid of the SH3 domain.

In summary, these results demonstrated that the degree of similarity between C-terminal sequences mainly reflects the degree of the phylogenetic relationship, which points towards little evolutionary constraints. In the available set of sequences, paralogous srGAP proteins were restricted to the vertebrate clade (Fig. 6.1, inset), which might support the idea that gene amplification events during the emergence of this lineage potentially led to the expansion of paralogous sequences. In contrast, the alternative scenario featuring early secondary loss of paralogous sequences in the protostomian clade lacks evidence from the available data set.

6.1.2. Structural Predictions of the C-terminal Region

The following analyses focused on protein structure predictions for the C-terminal regions of human srGAPs and only partially included data on srGAPs from different origins. My secondary structure and disorder predictions (see Materials and Methods, 5.1, p. 27) revealed that the C-terminal region of srGAP proteins likely lacks a defined 3D structure in isolation (Fig. 6.2, p. 42): Firstly, pre-

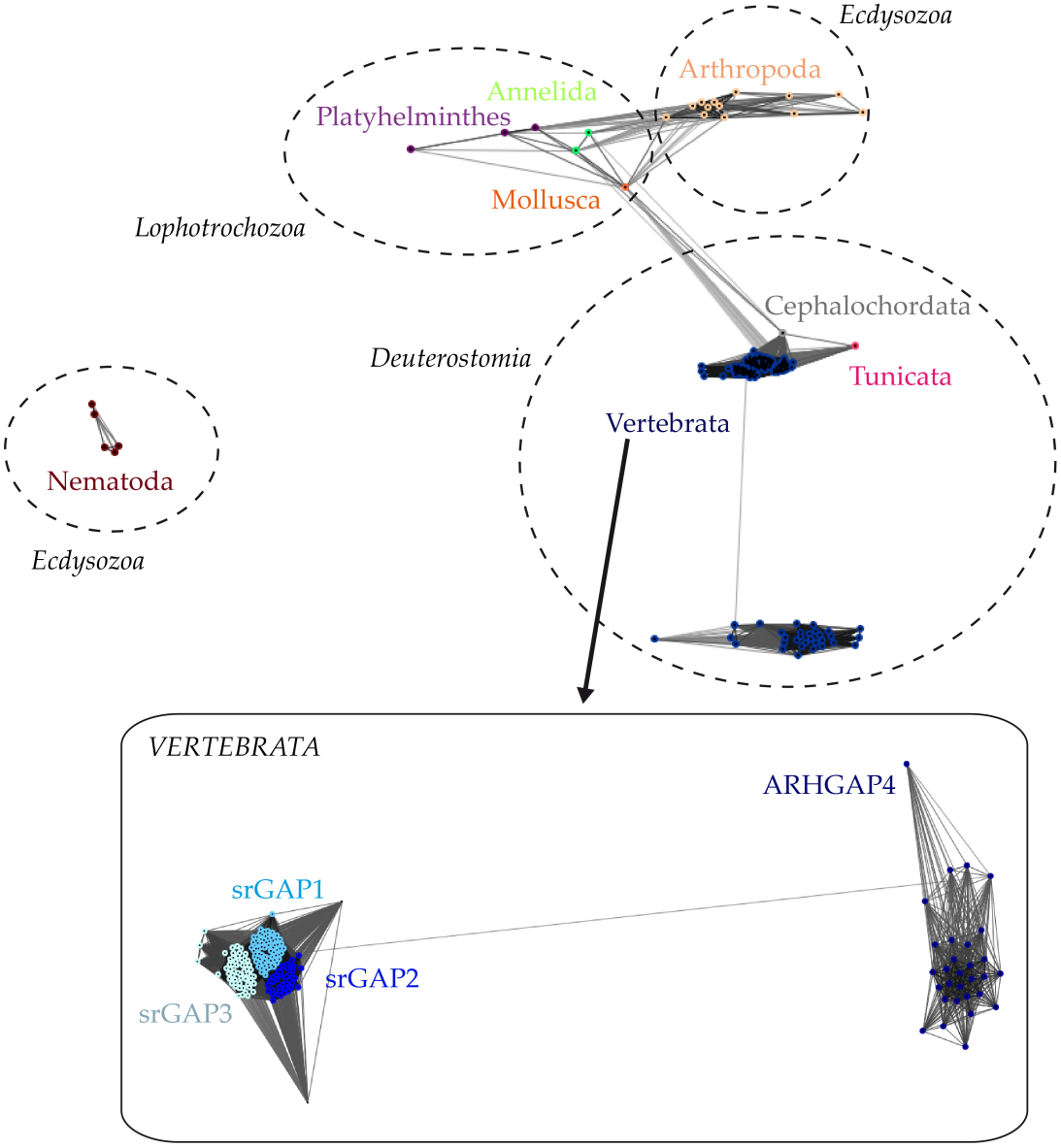

Figure 6.1.: Sequence relationships between C-terminal sequences of srGAP proteins. Amino acid sequences were clustered with CLANS [176] at a P-value < 0.05. Each dot represents an amino acid sequence and grey lines denote similarities between two sequences better than the cut-off. Darker lines correspond to lower P-values. Colors indicate the phylogenetic origin and the main phyla were assigned according to Aguinaldo *et al.* [208], Halanych *et al.* [209] and Dunn *et al.* [210]. The map contains 224 sequences (singletons were excluded). The inset shows paralogous srGAP sequences in shades of blue.

dicted secondary structure elements are α-helical and mainly located in a short conserved region, which also incorporates a predicted coiled-coil segment (Fig. 6.2). Secondly, homology searches employing HHpred [170] failed to detect any similarities to known folded protein domains. Moreover, positively and negatively charged amino acids are evenly distributed, which renders folding into a collapsed globule structure through polar tracts [37] likewise improbable. It is, on the other hand, known that such disordered segments can contain linear interaction motifs [211], which can direct proteins to different pathways through specific protein interactions (see introduction on intrinsic disorder, 1.1.1, p. 4) [45]. Indeed, motif searches predicted numerous short linear interaction motifs for binding of 14-3-3 proteins and SH3 domains within the C-terminal region (Fig. 6.2, p. 42).

SH3 domains (see introduction on SH3 domains, 1.1.2, p. 5) were reported to bind to proline-rich sequences that possess a type II polyproline helix conformation [55, 212] and the orientation of the peptide mainly depends on the location of a positively charged amino acid [58, 59]: According to the ELM resource [188, 189] classification scheme, class I SH3-binding motifs can be described by the regular expression *[RKY]xxPxxP*, while class II peptides are expressed as *PxxPx[KR]*. Non-canonical class I motifs (class III in ELM scheme), in contrast, follow the rather generic consensus *xxx[PV]xxP*, which is associated with lower predictive power. The bioinformatic analysis revealed that all three motif classes are predicted within the C-terminal regions of human srGAP proteins, whereby only two motifs are conserved between different paralogs (Fig. 6.2, p. 42).

The second group of predicted linear motifs constitute 14-3-3-binding sites. 14-3-3 proteins (see introduction on 14-3-3s, 1.1.2, p. 6) form cradle-shaped homo- or heterodimers and engage in phospho-dependent interactions, mainly involving phosphorylated serines and threonines ([79, 84], while atypical non-phosphorylated motifs have also been described [213–216]. The ELM resource classifies motifs complying with the regular expression *RxxSxP* as type 1 and *RxxxS#p* as type 2, in which # represents a hydrophobic amino acid and *p* a semi-conserved proline. The serine residue in the center depicts the phosphorylated position. Type 3 motifs are the least specific with the consensus *[RHK][STALV]x([ST])x[PESRDFTQ]*. I found that motifs of all three classes are predicted within the CTR of human srGAP proteins, of which type 3 motifs formed the largest group (Fig. 6.2, p. 42).

In fact, binding of 14-3-3 proteins is the only function assigned to the C-terminal region of srGAPs so far [207]. In srGAP2, the motif surrounding the phosphorylated residue S930 mediated the interaction with 14-3-3s in HEK293T cells, whereas the corresponding motif in srGAP3 involving the residues S947 and S948 failed to act likewise [207] (Fig. 6.2, p. 42). Which 14-3-3 isoforms or which motifs in srGAP3 were involved in these interactions remained elusive.

Unstructured regions are furthermore exceptionally rich in phosphorylation sites [217], which provide a means of allosteric regulation of protein-protein interactions or are involved in autoinhibitory mechanisms [48]. It is therefore not surprising, that the C-terminal region of srGAP3 contains many phosphorylation sites and a subset of those is even located within predicted 14-3-3-interaction motifs (Fig. 6.2, p. 42).

In summary, these results support the idea that the C-terminal region of srGAP proteins is intrinsically disordered. Furthermore, mammalian srGAP1, 2, and 3 contain potential linear motifs, which could serve as interaction surface for yet to be identified adaptor proteins. This concept provided the basis for the experimental characterisation of the C-terminal region of srGAP3 outlined in the following sections.

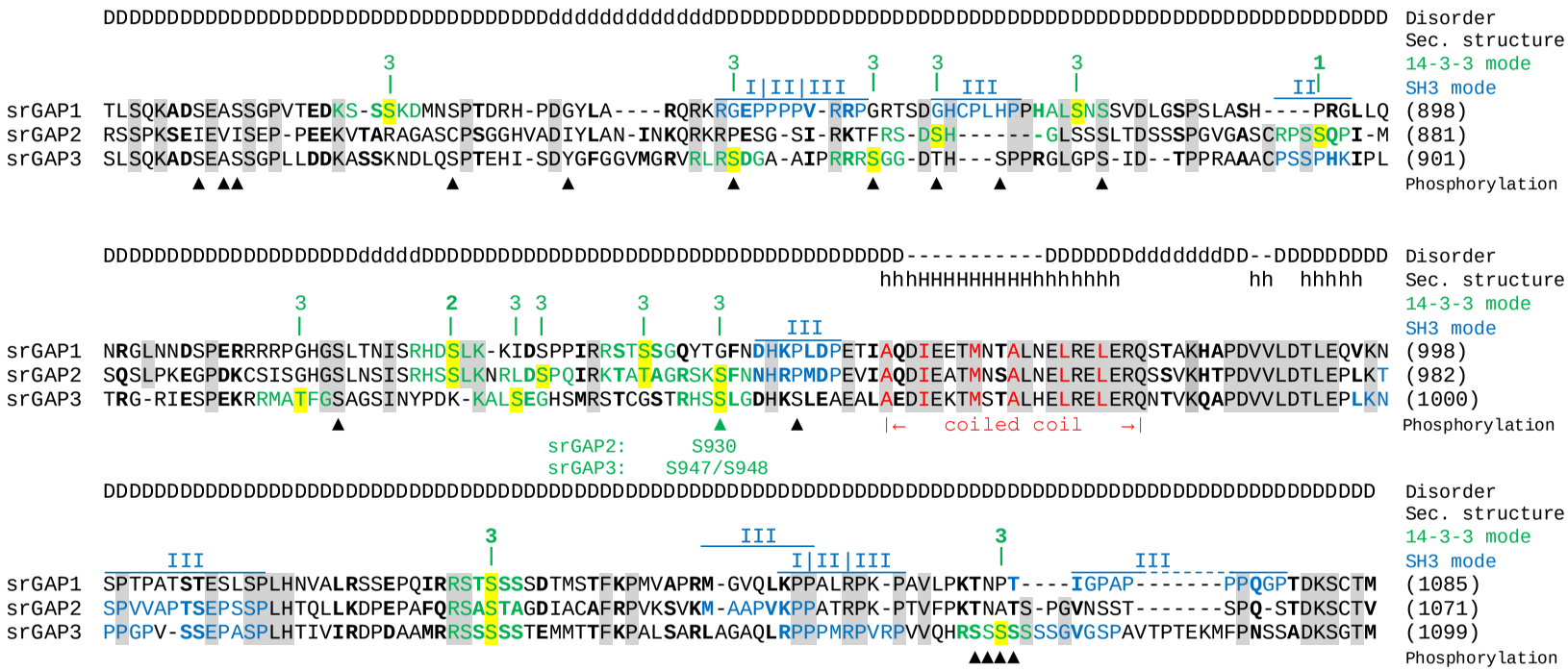

Figure 6.2.: The C-terminal region of srGAP proteins is predicted to be disordered and contains possible linear interaction motifs. MSAProbs [178] alignment of the C-terminal regions (CTR) of srGAP1-3 from *H. sapiens*. Conserved positions are highlighted in grey and similar residues are printed in bold. Disordered residues are represented by D or d, if more than half or exactly half of the predictors reported disorder at this position, respectively. Secondary structure was assigned using Quick2D: H and h illustrate high and low helix probability, respectively. Further indicated are predicted 14-3-3-binding sites (green) and SH3-binding sites (blue) with the respective motif class of the ELM classification scheme (see http://elm.eu.org/) depicted above. Predicted phosphorylated residues within these motifs are highlighted in yellow. The coiled-coil region is marked in red (highlighted are the a and d positions in the heptad repeat). Phosphorylation sites of srGAP3 enlisted in the PhosphoSite database are marked by ▲. The green triangle indicates the identified 14-3-3-binding site in srGAP2 and the corresponding non-interacting motif in srGAP3 [207]. Details on employed databases and bioinformatic tools can be found in the methods chapter (see 5.1, p. 27).

6.2. Identification of Potential C-terminal Binding Partners in the Rat Brain

Paralogous srGAP proteins in mammals were reported to regulate different aspects of neural development [155, 157, 158, 163, 218], which is at least partially attributed to dissimilar spatio-temporal regulation patterns [159, 160, 219], but could also depend on the differential recognition of binding partners. In this way, individual paralogs could be targeted to different cellular networks, where they could exert specific functions that set them apart from cognate srGAPs. My bioinformatic analysis revealed that the C-terminal region might function as a protein-interaction surface that has the potential to drive the formation of distinct complexes for paralogous srGAP proteins. Nevertheless, binding capabilities and specificities of this segment are far from being understood and I therefore aimed at the identification of C-terminal binding partners of srGAP3.

The human srGAP proteins 1, 2, and 3, but not ARHGAP4, were reported to bind 14-3-3 proteins in HEK293T cells and complex formation was found to be mediated by the C-terminal region [207]. Since other attempts to identify interaction partners for the C-terminal region of srGAP3 using yeast-two-hybrid screens were unsuccessful [220], I pursued a different, non-library-based strategy: A candidate approach, in which potential binding partners were identified from pull-down experiments with rat brain lysate and further validated *in vivo* and *in vitro*.

The expression of srGAP3 is developmentally regulated and the highest expression levels in the rat brain occur between stage P1 and P14 [221]. On a cellular level, srGAP3 is distributed between the nucleus and the cytoplasm in the developing brain, but mostly relocates to the nucleus in adult rats [159]. As we intended to identify cytosolic srGAP3-binding proteins, we performed GST pull-down experiments with brain lysate from a rat of stage P14. The GST-tagged C-terminal regions of human srGAP3 and srGAP1 were tested in parallel in order to detect specific proteins for either family member (see Materials and Methods, 5.3.3, for information on data analysis). GST-srGAP3-CTR (construct architecture is displayed in Fig. 6.3) was purified to homogeneity as assessed by SDS-PAGE (Fig. 6.4). Since the analysis of srGAP1 is the focus of the PhD thesis of A. Jeganantham, I only display data for srGAP1-CTR, if it is necessary for the interpretation of the results concerning srGAP3. SrGAP2 was not under investigation in the research group at the time of this experiment and therefore not included in the analysis.

Using mass spectrometry, we found numerous proteins specifically pulled down by GST-srGAP3-CTR (see Tab. 6.2, p. 47 for exemplary results). In accordance with earlier studies [207], we identified six of the seven mammalian

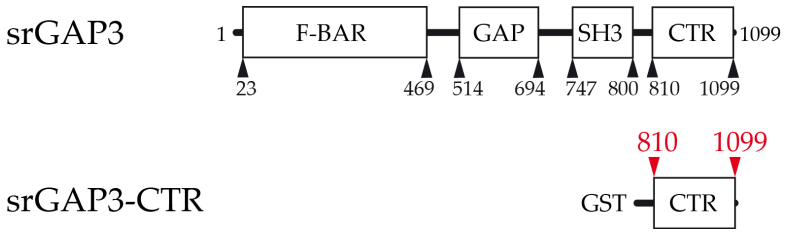

Figure 6.3.: Domain architecture of srGAP3 full-length and the C-terminal region (CTR) fused to GST. F-BAR, Fes-Cip4-homology-BAR (Bin-Amphiphysin-Rvs) domain; GAP, GTPase-activating domain; SH3, Src-homology 3 domain. The domain boundaries of srGAP3 (*H. sapiens*, isoform 1) and the construct boundaries of GST-srGAP3-CTR are indicated in black and red, respectively.

Figure 6.4.: GST pull-down with rat brain lysate. **A:** GST-srGAP3-CTR (residues 810-1099, 57.8 kDa) was purified to homogeneity as assessed by SDS-PAGE. Double bands originated from mixed dimer formation via GST with a GST-CTR-degradation product. **B:** SDS gel of GST pull-down of rat brain lysate with GST (negative control), GST-srGAP1-CTR (residues 799-1085), and GST-srGAP3-CTR. Marked gel sections were analysed by mass spectrometry. Bands containing bait proteins (black triangles) were excluded from the analysis. GST-srGAP1-CTR was provided by A. Jeganantham.

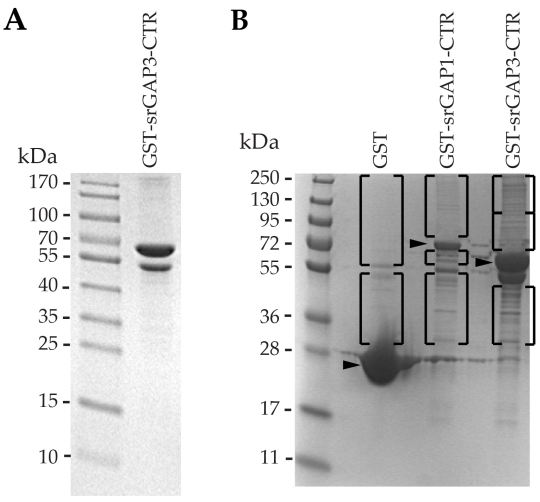

14-3-3 proteins (β, γ, ϵ, η, θ/τ, and ζ [79]), but not the isoform σ, which provided evidence that srGAP3 also interacts with this protein family in the rat brain. In addition, several SH3 domain-containing proteins (Amphiphysin, Endophilin-A1, Endophilin-A2, Grb2) specifically associated with GST-srGAP3-CTR (Tab. 6.2, p. 47), which supported the bioinformatical predictions (compare Fig. 6.2, p. 42).

As my bioinformatical analysis was biased towards the prediction of known motifs (compare Materials and Methods, p. 28) and the binding specificities of many proteins that specifically associated with srGAP3 had not been characterised extensively, we decided not to restrict subsequent validation experiments to 14-3-3s and SH3 domain-containing proteins. Instead, we selected candidate proteins based on a panel of different criteria: the confidence, with which they were identified in pull-downs with GST-srGAP3-CTR (at least ten peptides or two orders of magnitude higher intensity compared to the control experiment), reported protein-binding capabilities, reported cytosolic localisation, and the availability of clones. This approach yielded a set of 19 proteins (marked with arrows in Tab. 6.2, p. 47), which were mainly specific for srGAP3. The candidates either carried typical adaptor modules such as WD40 domains (α-Cop, Strap) [222], SH3 domains (see above), the α-appendage of AP2 [223, 224], and the C-terminal domain of EB1 [225], or had been shown to engage in protein-protein interactions (14-3-3 [79], Vps26A [226], Vps35 [227, 228], Neurochondrin [229, 230], α-Centractin [231, 232]).

Since pull-down experiments employing tissue lysates will result in the isolation of large multi-protein complexes, in which many proteins only indirectly bind to the bait protein [233], I combined this initial analysis with a fluorescence-based co-immunoprecipitation approach in order to dissect direct binding partners (compare Discussion, 7.1, p. 73).

Table 6.2.: Exemplary results of mass spectrometric analysis of the GST pull-down experiment with srGAPs using rat brain lysate. For clarity, only a representative subset of all identified proteins is listed. Arrows mark proteins that were included in subsequent interaction studies. Proteins containing SH3 domains are highlighted in blue and 14-3-3 proteins in green.

Protein Names	Uniprot[a]	**GST-srGAP3-CTR**[a]		**GST-srGAP1-CTR**[a]		**GST**	
		Peptides[b]	Intensity[b]	Peptides	Intensity	Peptides	Intensity
srGAP3-specific proteins							
⇒ 14-3-3 protein β/α	P35213	10	$1.16 \cdot 10^7$	3	0[c]	2	0
⇒ 14-3-3 protein γ	P61983	13	$5.50 \cdot 10^7$	3	0	2	$1.70 \cdot 10^5$
⇒ 14-3-3 protein ϵ	P62260	18	$1.73 \cdot 10^8$	8	$1.22 \cdot 10^7$	8	$5.15 \cdot 10^6$
⇒ 14-3-3 protein ζ/δ	P63102	16	$9.42 \cdot 10^7$	3	0	1	0
⇒ 14-3-3 protein η	P68511	11	$2.42 \cdot 10^7$	3	0	2	0
⇒ 14-3-3 protein θ/τ	P68255	10	$1.00 \cdot 10^7$	3	0	2	0
⇒ α-Centractin	P85515	14	$1.68 \cdot 10^8$	3	$3.12 \cdot 10^6$	1	$1.93 \cdot 10^5$
⇒ α-Cop protein	B5DFK1	24	$3.73 \cdot 10^7$	0	0	0	0
⇒ Amphiphysin	O08838	14	$1.90 \cdot 10^7$	2	$3.43 \cdot 10^5$	2	$3.02 \cdot 10^5$
Clathrin heavy chain 1	P11442	23	$3.96 \cdot 10^7$	4	$1.08 \cdot 10^6$	6	$1.48 \cdot 10^6$
⇒ Drebrin	Q07266	11	$1.45 \cdot 10^7$	0	0	0	0
Dynamin-1-like protein	O35303	29	$8.63 \cdot 10^7$	16	$1.29 \cdot 10^7$	9	$3.10 \cdot 10^6$
Dynamin-3	Q08877	22	$4.82 \cdot 10^7$	9	$9.55 \cdot 10^6$	5	$2.20 \cdot 10^6$
⇒ Microtubule-associated protein RP/EB1	Q66HR2	7	$1.49 \cdot 10^7$	1	$3.34 \cdot 10^5$	2	$3.86 \cdot 10^5$
⇒ Endophilin-A1	O35179	17	$2.33 \cdot 10^8$	7	$9.27 \cdot 10^6$	2	$9.21 \cdot 10^5$
⇒ Endophilin-A2	O35964	13	$8.97 \cdot 10^7$	4	$5.64 \cdot 10^7$	2	0
F-actin-capping protein subunit α-2	Q3T1K5	6	$4.27 \cdot 10^7$	3	$4.91 \cdot 10^6$	0	0
G-protein-signaling modulator 1	Q9R080	10	$1.11 \cdot 10^7$	2	$5.87 \cdot 10^5$	1	$1.17 \cdot 10^5$
⇒ Growth factor receptor-bound protein 2; GRB2	P62994	3	$3.52 \cdot 10^6$	0	0	0	0
Kinesin-like protein KIF3A	Q9WV62	9	$1.31 \cdot 10^7$	0	0	0	0
⇒ Neurochondrin	O35095	14	$4.08 \cdot 10^7$	7	$7.95 \cdot 10^6$	5	$2.01 \cdot 10^6$
Ubiquitin-conjugating enzyme E2 Z	Q3B7D1	4	$3.96 \cdot 10^6$	1	$4.75 \cdot 10^5$	1	$2.24 \cdot 10^5$
⇒ Vacuolar protein sorting-associated protein 26A, Vps26A	Q6AY86	4	$5.08 \cdot 10^6$	0	0	0	0
VPS26 protein homolog; Vps26b	B1WBS4	12	$3.85 \cdot 10^7$	2	$7.06 \cdot 10^5$	0	0
⇒ Vps35 protein	B5DFC1	25	$9.77 \cdot 10^7$	3	$2.93 \cdot 10^6$	1	$1.55 \cdot 10^5$

continued on next page

(continued)

Protein Names	Uniprot	GST-srGAP3-CTR		GST-srGAP1-CTR		GST	
		Peptides	Intensity	Peptides	Intensity	Peptides	Intensity
srGAP3- and srGAP1-specific proteins							
⇒ AP-2 complex subunit α-2	P18484	37	$8.65 \cdot 10^7$	27	$3.86 \cdot 10^7$	8	$3.09 \cdot 10^6$
ARF GTPase-activating protein GIT1	Q9Z272	13	$1.62 \cdot 10^7$	7	$3.60 \cdot 10^6$	0	0
Cyclin-dependent kinase 5	Q03114	8	$3.91 \cdot 10^7$	5	$2.91 \cdot 10^6$	3	$6.72 \cdot 10^5$
Neuronal migration protein doublecortin	Q9ESI7	11	$1.03 \cdot 10^7$	5	$1.45 \cdot 10^6$	1	$1.23 \cdot 10^5$
Dynactin subunit 1;p150-glued	P28023	39	$1.54 \cdot 10^8$	12	$4.50 \cdot 10^6$	1	$3.50 \cdot 10^4$
F-actin-capping protein subunit β	Q5XI32	8	$2.71 \cdot 10^7$	5	$2.42 \cdot 10^6$	0	0
FERM, RhoGEF and pleckstrin domain-containing protein 1	F1LYQ8	13	$1.48 \cdot 10^7$	14	$1.30 \cdot 10^7$	0	0
Hook3	F1MA65	7	$1.34 \cdot 10^7$	5	$1.61 \cdot 10^6$	1	$9.47 \cdot 10^4$
Kinesin-like protein KIF2A	Q9WV63	13	$1.61 \cdot 10^7$	15	$1.52 \cdot 10^7$	0	0
Nck-associated protein 1	P55161	43	$2.91 \cdot 10^8$	23	$2.27 \cdot 10^7$	1	$7.23 \cdot 10^4$
Rho guanine nucleotide exchange factor 2	Q5FVC2	7	$6.42 \cdot 10^6$	12	$8.20 \cdot 10^6$	0	0
Protein transport protein Sec31A	Q9Z2Q1	12	$1.89 \cdot 10^7$	6	$2.44 \cdot 10^6$	1	$1.70 \cdot 10^5$
⇒ Serine-threonine kinase receptor-associated protein, Strap	Q5XIG8	8	$1.45 \cdot 10^7$	10	$1.14 \cdot 10^7$	0	0
SH3 domain-containing kinase-binding protein 1, SH3KBP1	Q925Q9	7	$8.02 \cdot 10^6$	11	$1.11 \cdot 10^7$	0	0
Tripartite motif-containing protein 3	O70277	8	$1.18 \cdot 10^7$	9	$1.10 \cdot 10^7$	0	0
Vesicle-fusing ATPase	Q9QUL6	26	$6.66 \cdot 10^7$	15	$1.41 \cdot 10^7$	8	$3.03 \cdot 10^6$

[a] Identifier in Uniprot database: http://www.uniprot.org; CTR, C-terminal region (residues 810-1099 of srGAP3 and residues 799-1085 of srGAP1).

[b] Number of identified peptides and intensity in arbitrary units.

[c] Value is set to 0, if the MaxQuant software is unable to interpret the isotope pattern of the respective peptides. In this case, peptide intensities cannot be quantified, but the fragmentation pattern of the peptides is used for their identification (see [201] for further details).

6.3. Validation of the Interaction With SrGAP3 *In Vivo*

6.3.1. Establishment of a Fluorescence-Based Co-IP Assay

To confirm the interaction of srGAP3 with the 19 full-length mammalian proteins *in vivo* (marked by arrows in Tab. 6.2), I established a fluorescence-based Co-IP assay in a 96-well format using eGFP-tagged srGAP3 and mCherry-tagged candidate proteins (Fig. 6.5, see method description in section 5.3.5, p. 34 for more information).

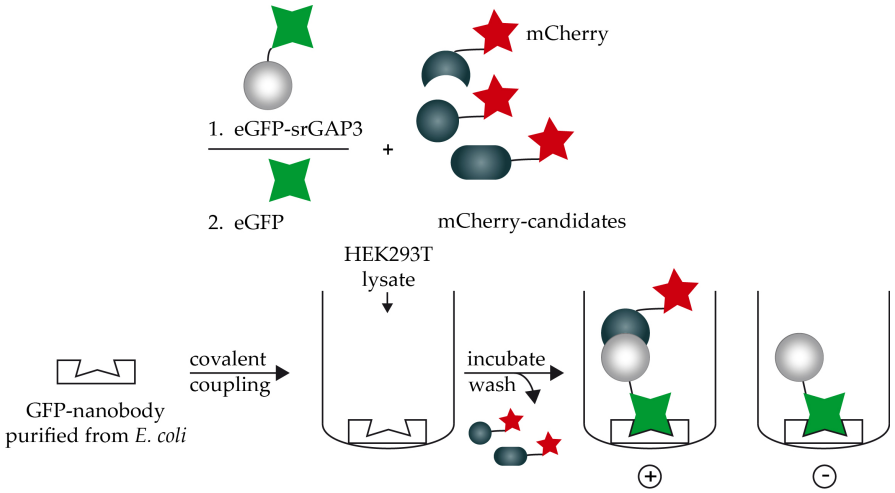

Figure 6.5.: Set-up of the fluorescence-based Co-IP assay. MCherry-tagged candidate binding partners are co-transfected with either eGFP-srGAP3 (1) or eGFP (2) into HEK293T cells and subsequently a co-immunoprecipitation with the lysate is performed in a 96-well format with an immobilised GFP-nanobody. The mCherry-fluorescence signal serves as read-out.

Production of the GFP-Nanobody

Nanobodies have emerged as valuable tools in research and diagnostics (reviewed in [234]) and are derived from the antigen binding site of camelid heavy-chain antibodies [235, 236]. The term "nanobody" - originally coined by the company Ablynx - relates to their small size (around 15 kDa) and to the fact that they only comprise a single polypeptide chain [235]. Several milligrams of antibody can therefore easily be purified from *E. coli* and tailored to specific requirements through the attachment of protein tags (reviewed in [234]). Rothbauer *et al.* [196] developed a nanobody directed against GFP, which was applied in this study (sequence information from [198]). Fusing srGAP3 to

eGFP via a short linker sequence permitted the oriented, yet flexible immobilisation of srGAP3 via this GFP-nanobody on a solid support (Fig. 6.5).

The GFP-nanobody was expressed in *E. coli* BL21 Gold (DE3) and purified to homogeneity as assessed by SDS-PAGE (Fig. 6.6). To test whether the purified GFP-nanobody correctly discriminated between eGFP and mCherry, I compared binding of the nanobody to purified eGFP and mCherry using ITC. The GFP-nanobody bound eGFP with a K_d of approximately 0.5 nM in a 1:1 stoichiometry (data not shown), which is in accordance with the findings of Saerens *et al.* [197] and Kubala *et al.* [198]. Binding to mCherry was undetectable in the employed concentration range and was therefore at least five orders of magnitude weaker. For the purposes of this study, I concluded that the GFP-nanobody specifically recognised eGFP in solution.

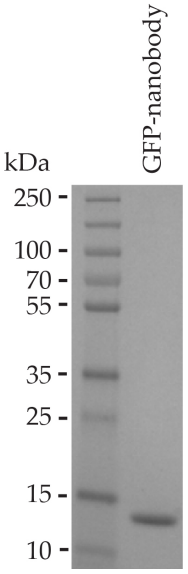

Figure 6.6.: Purity control of the GFP-nanobody. SDS-PAGE of the final protein pool of the GFP-nanobody (13.6 kDa) purification.

Immobilisation of the GFP-Nanobody

The GFP-nanobody was covalently coupled to 96-well plates with an amino-reactive surface (Nunc Immobilizer Amino Black, Thermo Scientific). I optimised the immobilisation conditions according to the supplier's recommendations in two different buffers: Na_2CO_3 and PBS (Fig. 6.7). The highest amount of coupled protein was obtained at 1000 µg/ml nanobody in 100 mM Na_2CO_3 (pH 9.7) incubated for 1.5 h at 25 °C (Fig. 6.7). From these results, it can be concluded that the nanobody was mainly coupled via primary amines, which is supported by the Na_2CO_3 buffer, and only weakly via thiols, which is supported by both, Na_2CO_3 and PBS. Increased nanobody concentrations resulted in similar eGFP fluorescence signals after incubation with purified eGFP (data

not shown), which suggested that 1000 µg/ml nanobody saturated the surface. Unreacted sites were inactivated with ethanolamine.

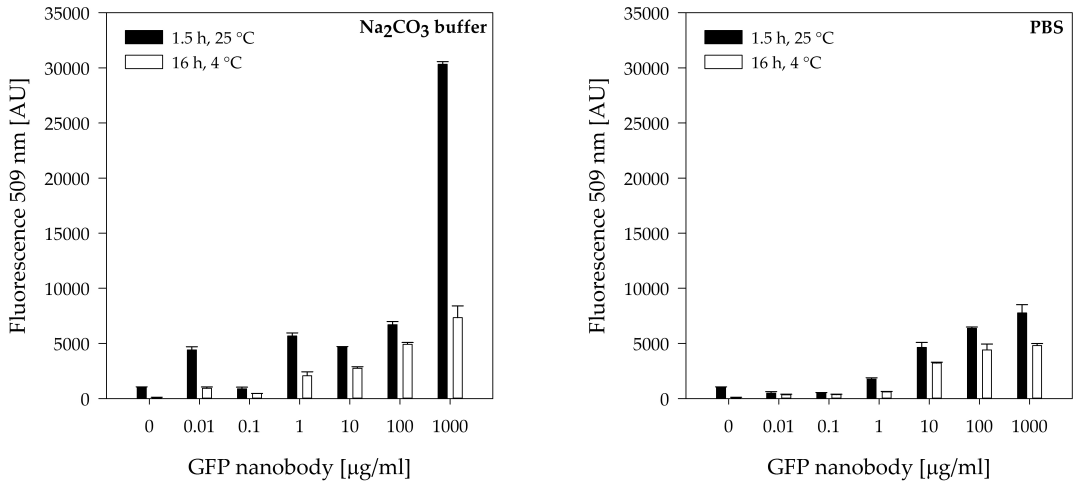

Figure 6.7.: Optimising GFP-nanobody immobilisation conditions. The GFP-nanobody was immobilised on Nunc Immobilizer Amino plates (Thermo Scientific) in either Na_2CO_3 buffer (left) or PBS (right). Different protein concentrations, two incubation times, and two different temperatures were tested. After washing, coupled nanobody was detected by incubation of the wells with purified eGFP (20 µg/ml). The residual eGFP-fluorescence was measured with a BioTek Mx Reader (Ex 488 nm/ Em 509 nm; AU, arbitrary units) is plotted. The standard deviation between three technical replicates is shown. The statistical analysis was performed with SigmaPlot (version 12.3, Systat Software Inc.).

Sensitivity of the Assay

I then determined the detection limit for eGFP expressed in mammalian cells. For this purpose, I transfected HEK293T cells with an pEGFPC23C expression vector, incubated the immobilised GFP-nanobody with the cleared lysate (for transfection conditions and sample processing see Materials and Methods, 3.2.2 and 5.3.5), and recorded the eGFP- and mCherry-fluorescence signal after washing.

The immobilised GFP-nanobody successfully precipitated eGFP from HEK293T cells (Tab. 6.3) and the resulting fluorescence signals were comparable to those of purified eGFP (compare Fig. 6.7, left panel). Wells not coated with nanobody, but inactivated with ethanolamine served as negative controls. They were subjected to the same washing protocol as nanobody-containing wells and then incubated with eGFP-containing lysate. The fluorescence intensities of these wells were close to instrument background levels in the eGFP channel (compare negative controls of eGFP- and mCherry-containing lysates at

Table 6.3.: Immobilised GFP-nanobody specifically recognises eGFP transiently expressed in HEK293T cells. HEK293T cell lysates containing either eGFP or mCherry were applied to wells with (+) and without (–) GFP-nanobody. The fluorescence signals are given in arbitrary units.

	HEK293T lysate			
GFP-nanobody	eGFP		mCherry	
	Ex/Em[a]			
	488 nm/509 nm	*586 nm/610 nm*	*488 nm/509 nm*	*586 nm/610 nm*
+	27402 ± 119[b]	49 ± 5	455 ± 22	119 ± 5
–	514 ± 70	47 ± 19	520 ± 70	81 ± 19

[a] Ex, excitation wavelength; Em, emission wavelength.
[b] Indicated is the standard deviation of three independent experiments.

Ex 488 nm/Em 509 nm, Tab. 6.3), which demonstrated the absence of unspecific eGFP-binding to the plates. I then determined the sensitivity of the assay experimentally: Employing a dilution series of eGFP-containing lysates, I measured the minimal amount of eGFP required to achieve at least 90 % saturation of binding sites per well (≥ 10000 arbitrary units with Ex 488 nm/ Em 509 nm, data not shown). Only lysates fulfilling this criterion were included in subsequent experiments to ensure that the amount of bound mCherry-tagged binding partner was independent of the eGFP-concentration.

To test whether the blocking and washing protocol sufficiently inhibited unspecific binding of the hydrophobic mCherry, I carried out the assay with mCherry expressed in HEK293T cells. The mCherry-fluorescence intensities were similar in presence and absence of GFP-nanobody, indicating that eGFP, but not mCherry was specifically precipitated from cell lysates (Tab. 6.3). I noticed, however, weak unspecific binding of mCherry to the plate (Tab. 6.3), which could be eliminated by increasing the ethanolamine concentration from 10 nM to 10 mM in subsequent experiments.

Expression Analysis of Candidates and SrGAP3 Transiently Transfected into HEK293T

SrGAP3 served as bait and was cloned into the vector pEGFPC23C (Tab. 6.4, p. 52). The full-length sequence of srGAP3 was chosen, since the protein dimerises via its N-terminal F-BAR domain [163], which increases local binding site concentration and could thus strengthen otherwise weak monomeric interactions. Prey constructs (candidates, srGAP3, and GST) were cloned into the vector pmCherryC23C resulting in N-terminally mCherry-tagged proteins

Table 6.4.: Protein constructs for the analysis of srGAP3-binding *in vivo*. Candidate and control proteins were N-terminally tagged with mCherry. SrGAP3 was produced as eGFP-fusion as well as mCherry-fusion protein.

Protein Name	Species[a]	MW[a] [kDa]	mCherry/eGFP-Fusion MW [kDa]	Conservation % similarity/ % identity[a]
Microtubule-associtated transport				
α-Centractin	Hs	42.6	71.3	–
EB1	Hs	30.0	57.4	–
Drebrin	Hs	71.4	99.6	–
Signal transduction				
Grb2	Hs	25.2	53.6	–
Neurochondrin	Hs	78.9	107.0	–
RNA transport/processing				
Strap	Hs	38.4	66.6	–
Phosphoregulation				
14-3-3β	Hs	28.1	56.1	–
14-3-3γ	Rn	28.3	57.2	100 %
14-3-3ϵ	Rn	29.2	57.4	100 %
14-3-3ζ	Hs	27.8	57.0	–
14-3-3η	Hs	28.2	56.2	–
14-3-3θ/τ	Hs	27.8	56.0	–
Endocytosis				
Endophilin-A2	Hs	41.5	70.4	–
AP2α2 (701-938)	Mm	27.0	55.1	98.7/96.2 %
Endophilin-A1	Hs	40.0	68.9	–
Amphiphysin	Rn	74.9	103.8	88.9/86.4 %
Vesicle transport				
α-Cop	Mm	138.4	167.3	99.2/98.4 %
Vps26A	Hs	38.2	67.5	–
Vps35	Hs	91.7	120.1	–
Controls/bait proteins				
GST	from pGEX6P1[a]	25.8	52.2	–
srGAP3	Hs	124.5	154.1	–
eGFP	from pEGFPC23C[a]	30.3	–	–

[a] Hs, *Homo sapiens*; Rn, *Rattus norvegicus*; Mm, *Mus musculus*; pGEX6P1, vector (GE Healthcare); pEGFPC23C, vector; MW, expected molecular weight; Amino acid sequence conservation to human ortholog calculated from pairwise alignment with Needleman-Wunsch algorithm: http://www.ebi.ac.uk/Tools/psa/emboss_needle/.

(Tab. 6.4). In case of AP2α2, I only used the appendage domain (residues 701-938), which carries the adaptor function [223].

For five constructs, we could only obtain DNA of either rat or mouse origin, but sequence alignments revealed that the amino acid conservation was - apart from Amphiphysin - close to 100 % (see Tab. 6.4, p. 52). However, the SH3 domain of Amphiphysin, which depicts a possible interaction region, shares 97.3 % sequence identity with its human ortholog (compare 6.4.1, p. 57). The outcome of the experiments is therefore expected to be independent of the genetic origin of these constructs.

Western blot analyses confirmed the expression of all proteins in full length (Fig. 6.8). In accordance with reported data [237], the band of tagged Drebrin appeared at 130 kDa instead of 100 kDa. Furthermore, almost all mCherry-tagged proteins produced double bands, whose origin remained elusive. A mass spectrometric analsis of the bands revealed that they both contained the repective construct in full length, while post-translational modifications, such as phosphorylation, acetylation, ubiquitilation, or SUMOylation were undetectable. Furthermore, all candidate constructs were co-expressed with eGFP or eGFP-srGAP3 in 70 - 90 % of cells as assessed by fluorescence microscopy (exemplary image in Fig. 6.9, p. 54). As srGAP3 was reported to be expressed in kidney [161], I tested whether HEK293T cells contain endogenous srGAP3 using Western blotting. I was unable to detect this protein with conventional antibodies (data not shown) and thus concluded that endogenous background levels of srGAP3 are sufficiently low to exclude interference with my assay.

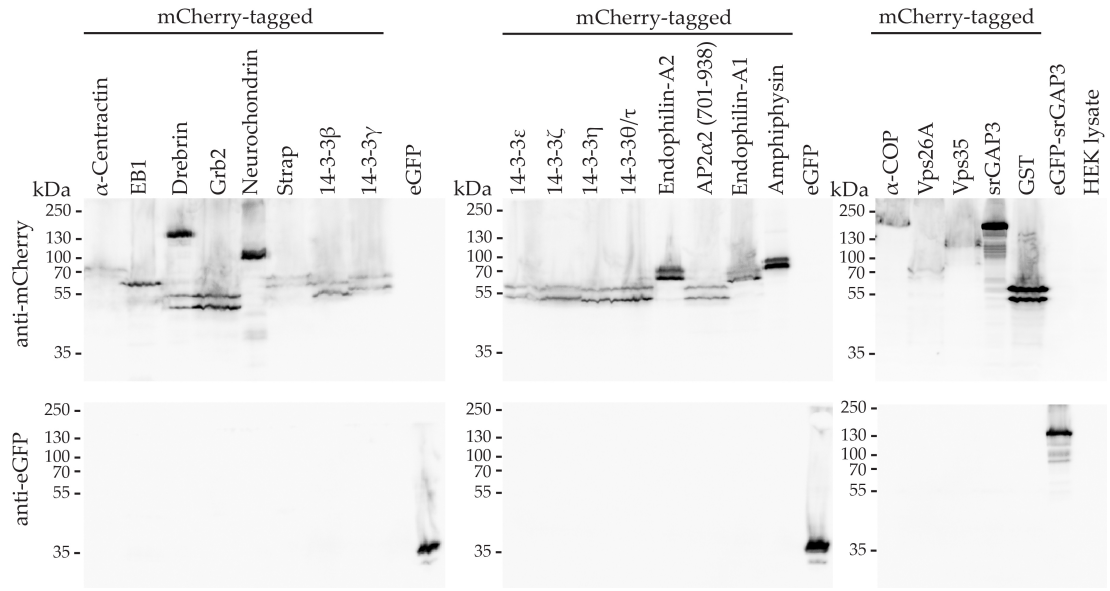

Figure 6.8.: Prey and bait proteins are expressed in HEK293T cells. Constructs of mCherry-tagged candidate proteins ("prey"), eGFP-tagged srGAP3 ("bait"), or eGFP alone were transfected into HEK293T cells and the expression was analysed by Western blots of cell lysates using anti-mCherry (upper panel) and anti-GFP (lower panel) antibodies. The expected molecular weight of the fusion proteins are listed in Tab. 6.4, p. 6.4. The additional band in the Drebrin-lane represents laterally diffused Grb2 and is attributed to the high viscosity of whole cell lysates.

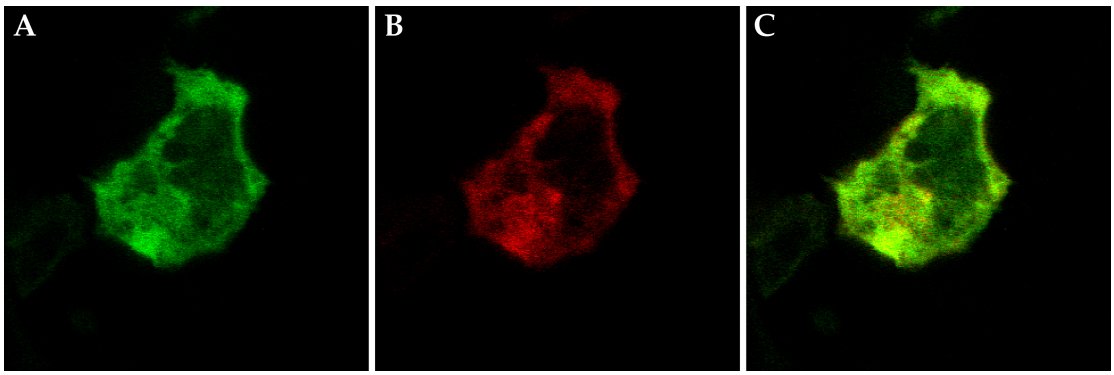

Figure 6.9.: Co-expression of eGFP-srGAP3 and mCherry-tagged candidates in HEK293T cells. Shown is a representative HEK293T cell expressing eGFP-srGAP3 (A) and mCherry-EB1 (B). C: Composite image of both channels. The image was aquired with a Zeiss LSM 510 Meta with a 63x oil objective and the images processed with Fiji [204].

6.3.2. Results of the Fluorescence-Based Co-IP Assay

In order to distinguish direct interaction partners of srGAP3 from those that were indirectly pulled-down in the GST pull-down experiment, I carried out the fluorescence-based Co-IP assay for the 19 candidate proteins and measured the relative amount of bound mCherry-tagged candidate of co-immunoprecipitations with eGFP-srGAP3 to co-immunoprecipitations with eGFP. MCherry-srGAP3, which was expected to form heterodimers with eGFP-srGAP3 [163] and for this reason included as a positive assay control, produced a strong binding signal (Fig. 6.10, p. 56). In contrast, the mCherry-fluorescence intensity of the negative assay control, GST, differed only insignificantly between Co-IPs with either eGFP-srGAP3 or eGFP (Fig. 6.10, p. 56). From these results, I concluded that the assay captures true binding events.

Within the final data set of the 19 candidates, a significant increase in the mCherry-fluorescence intensity compared to control precipitations was detected for α-Centractin, the 14-3-3 isoforms γ, ζ and θ/τ, and the SH3 domain-containing proteins Grb2, Endophilin-A1, Endophilin-A2, and Amphiphysin (Fig. 6.10, p. 56), indicating that these proteins can interact with full-length srGAP3 in HEK293T cells. Therefore, I was able to validate approximately 42 % of the total set of candidate proteins. Endophilin-A2 was the only candidate, for which mCherry-fluorescence intensities of the control experiments were not close to background levels (marked by grey line in Fig. 6.10, p. 56), which could have been caused by either unspecific binding of mCherry-Endophilin-A2 to eGFP or precipitation of this construct during the assay. The amount of mCherry-tagged protein bound by eGFP-srGAP3 varied between different constructs, but since the measured intensities represented relative values (compare Discussion, 7.1, p. 77), it is impossible to interpret them in terms of binding affinities. Nevertheless, candidate proteins exhibiting weak mCherry-fluorescence intensities in this assay (α-Centractin and 14-3-3ζ) were excluded from further analyses for two reasons: Firstly, they possessed a higher probability to originate from indirect binding events and secondly, low affinities, poor folding as well as low expression levels might have prevented binding of the respective protein and might similarly complicate their analysis *in vitro* (compare Discussion, 7.1, p. 76).

To show that complex formation with the remaining set of validated interaction partners (Grb2, Endophilin-A1, Endophilin-A2, Amphiphysin, as well as the 14-3-3 isoforms γ and θ/τ) was in fact mediated by the C-terminal region of srGAP3, I continued with the mapping of the binding sites *in vitro* and *in vivo*.

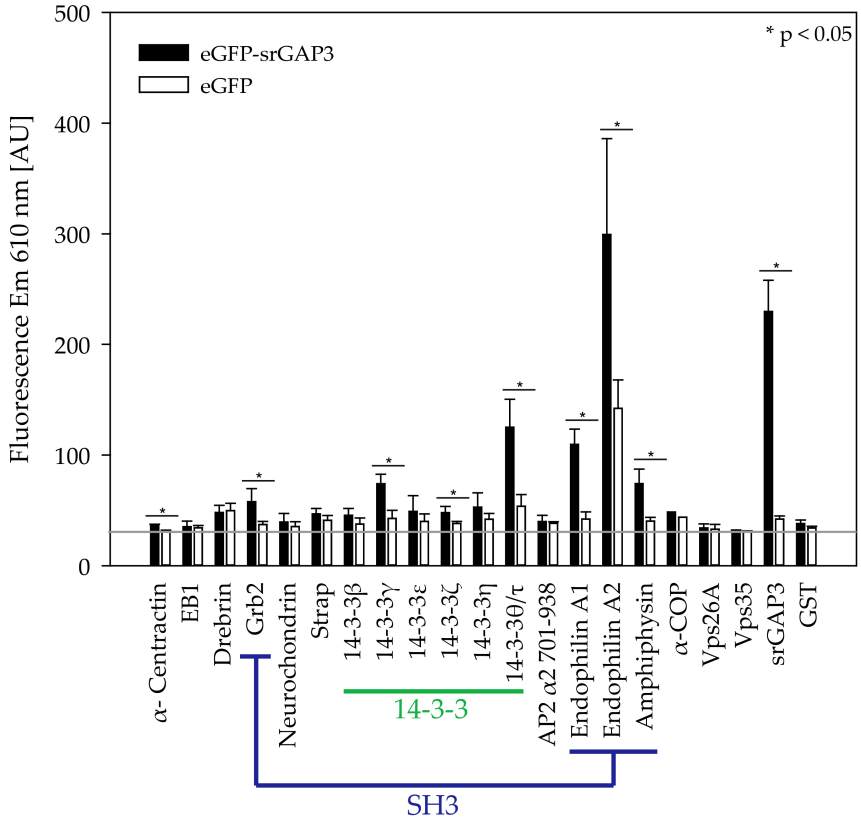

Figure 6.10.: SrGAP3 interacts with SH3 domain-containing and 14-3-3 proteins *in vivo*. MCherry-tagged candidate proteins and eGFP-tagged srGAP3 or eGFP were co-transfected into HEK293T cells and the complex formation measured with a fluorescence-based co-immunoprecipitation assay. The average mCherry-fluorescence intensity (emission, Em, at 610 nm, in arbitrary units, AU) from co-immunoprecipitations of each candidate with either eGFP-srGAP3 or eGFP is indicated. For each sample, two (α-COP) to four independent replicates were measured (standard deviation of samples is indicated, when three to four replicates were measured). Asterisks mark samples in which the difference between eGFP-srGAP3 and eGFP differs significantly ($p < 0.05$ in unpaired t-test). With the exception of α-Centractin, positive candidates could be grouped into SH3-domain-containing proteins (blue) and 14-3-3 (green). The grey line marks the average plate background before incubation (31 ± 5 AU). SrGAP3, which dimerises [163], served as positive control. GST was used as negative control. The statistical analysis was performed with SigmaPlot (version 12.3, Systat Software Inc.).

6.4. Confirmation of the Interaction of SrGAP3 with SH3 Domain-Containing Proteins *In Vitro*

The SH3 domain is the shared feature of Endophilin-A1, Endophilin-A2, Amphiphysin, and Grb2 (Fig. 6.11, p. 57) and potential SH3-binding motifs reside in the C-terminal region of srGAP3 (Fig. 6.2, p. 42). Therefore, we hypothesised that the SH3 domain constitutes the interaction surface for srGAP3-CTR. For this reason, I measured the association of the isolated SH3 domains with GST-srGAP3-CTR using ITC.

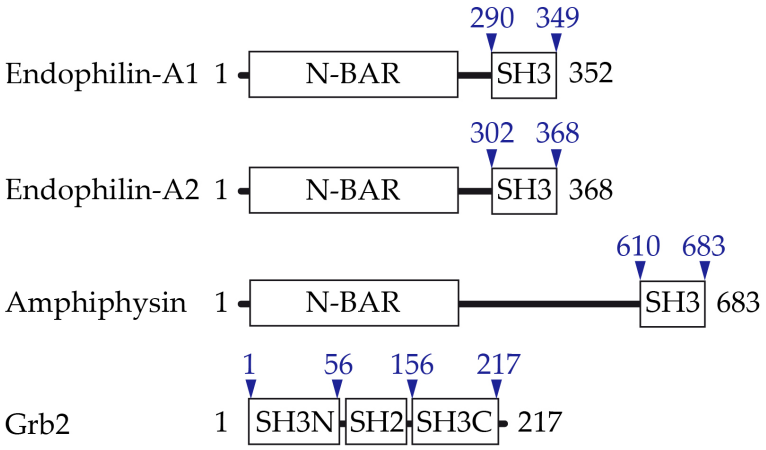

Figure 6.11.: Domain architecture of srGAP3 interaction partners containing SH3 domains. N-BAR, Bin-Amphiphysin-Rvs domain with additional N-terminal helix; SH3, Src-homology 3 domain; SH3N/SH3C, N-terminal and C-terminal SH3 domain, respectively; SH2, Src-homology 2 domain. The SH3 domain construct boundaries are indicated in blue. For sequence identifiers, see Tab. B.3, p. 167.

6.4.1. Production of SH3 Domains

Constructs of SH3 domains were expressed as GST-fusion proteins in *E. coli* and purified to homogeneity as assessed by SDS-PAGE (Fig. 6.12, p. 58). Amphiphysin was of rat origin, but its SH3 domain shares a high amino acid sequence identity of 97.3 % with the human protein: only two positions at the C-terminus differ (H681R, E683D), while the binding and specificity pocket are fully conserved (data not shown). Consequently, the genetic origin of the SH3 domain was expected to be irrelevant to the outcome of the *in vitro*-binding studies. In order to exclude that the absence of complex formation is related to improperly folded proteins, I analysed the folding status of the SH3 domains with CD spectroscopy. I found that all SH3 domains unfolded cooperatively

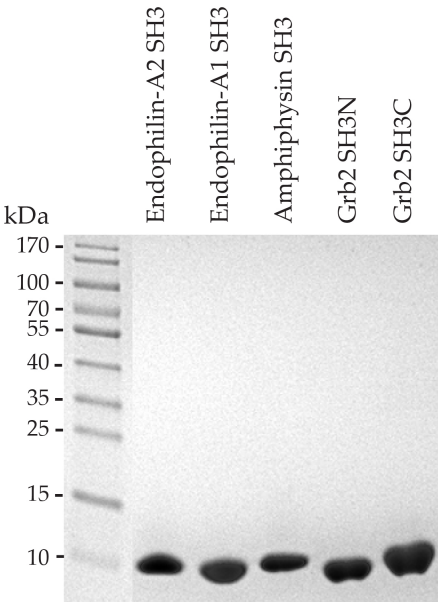

Figure 6.12.: Purity controls of SH3 domains. SDS-PAGE of the final protein pools from purifications of SH3 domains from Endophilin-A2 (residues 302-368, 8.3 kDa), Endophilin-A1 (residues 290-349, 7.7 kDa), Amphiphysin (residues 610-683, 9.2 kDa), and Grb2 (N-terminal SH3 domain, SH3N: residues 1-56, 7.3 kDa; C-terminal SH3 domain, SH3C: residues 156-217, 7.6 kDa).

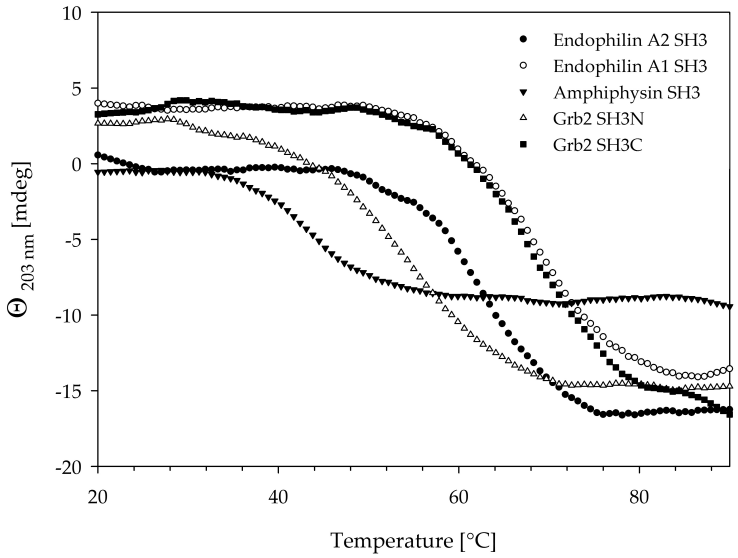

Figure 6.13.: Purified SH3 domains unfold cooperatively. Melting curves of SH3 domains (0.2 mg/ml) were obtained from measurements of circular dichroism at 203 nm (largest difference between native and unfolded state, compare [238]) from 20 °C to 90 °C. The average melting temperature of two independent measurements was calculated from the inflexion point of the curve with Spectra Manager II (Jasco): Endophilin-A2 SH3: T_M = 64.1 ± 0.6 °C; Endophilin-A1 SH3: T_M = 68.7 ± 0.5 °C; Amphiphysin SH3: T_M = 43.6 ± 0.5 °C; Grb2 SH3N: T_M = 55.1 ± 0.2 °C; Grb2 SH3C: T_M = 69.5 ± 1.1 °C.

with increasing temperature, which provided evidence for their folded nature (Fig. 6.13, p. 58). Nevertheless, the SH3 domains failed to produce very dis-

tinct CD spectra (data not shown). All SH3 domains were sufficiently stable at 20 °C, which was chosen as measurement temperature in subsequent experiments. Unfortunately, srGAP3-CTR degraded quickly after removal of the GST-tag and could therefore only be used as GST-fusion protein, which also precluded a structural analysis of this region.

6.4.2. The C-terminal Region of SrGAP3 Confers Binding to SH3 Domains *In Vitro*

To confirm that the newly identified complexes between srGAP3 and the SH3 domain-containing proteins Endophilin-A1, Endophilin-A2, Amphiphysin, and Grb2 were in fact mediated by the CTR of srGAP3, I conducted isothermal titrations with the individual SH3 domains of these proteins and GST-tagged srGAP3-CTR. These experiments revealed that the SH3 domains of the two Endophilins and the C-terminal SH3 domain of Grb2 (Grb2 SH3C) indeed directly bound to GST-srGAP3-CTR (Fig. 6.14, p. 61). The affinity of the complexes of Endophilin-A1 and -A2 (K_d = 17 μM and 24 μM, respectively, Tab. 6.5, p. 60) was in the expected range for SH3-mediated interactions (K_d = 1-100 μM, [51]). Grb2 SH3C produced ambiguous isotherms when used at the high concentrations that were required to observe the interaction. At lower concentrations the resulting binding isotherm could not be fitted reliably. For this reason, I omitted the quantification of this titration even though a binding isotherm was detected (Tab. 6.5, p. 60). GST-srGAP3-CTR also weakly interacted with the N-terminal SH3 domain of Grb2 (Grb2 SH3N), but the signal was too weak to be quantified reliably (Tab. 6.5, p. 60). On the contrary, binding to Amphiphysin SH3 was undetectable with the employed experimental settings (Fig. 6.14, Tab. 6.5), which were dictated by the limited solubility of GST-srGAP3-CTR. For this reason, I could not exclude that I failed to capture this interaction for technical reasons (compare 6.4.3, p. 61 for additional data). Taken together, these results confirm that the C-terminal region of srGAP3 mediates binding to SH3 domains, presumably via yet to be identified linear motifs. Therefore, I investigated these SH3-dependent interactions in the following set of experiments in greater detail.

Table 6.5.: Thermodynamic data from isothermal titrations of SH3 domains and various srGAP3 fragments.

Syringe Component	Conc. [μM]	Cell Component	Conc. [μM]	K_d[a] [μM]	N[a]	ΔH_{obs}[a] [kcal/mol]
Endophilin-A1 SH3						
Endophilin-A1 SH3	300	GST-srGAP3-CTR[b]	30	17 ± 1	1.1 ± 0.0	-9.8 ± 0.2
Endophilin-A1 SH3	1000	srGAP3 PxxP-fragment[b]	100	17 ± 1	1.0 ± 0.0	-9.3 ± 0.1
Endophilin-A1 SH3	1000	srGAP3 AxxA-fragment[b]	100	n. d.[b]	n. d.	n. d.
Endophilin-A2 SH3						
Endophilin-A2 SH3	300	GST-srGAP3-CTR	30	24 ± 3	0.7 ± 0.1	-12.0 ± 1.3
Endophilin-A2 SH3	1000	srGAP3 PxxP-fragment	100	20 ± 1	1.1 ± 0.3	-8.5 ± 0.3
srGAP3 PxxP-fragment	1000	Endophilin-A2 SH3	100	23 ± 0	1.3 ± 0.1	-6.3 ± 1.0
Endophilin-A2 SH3	1000	srGAP3 AxxA-fragment	100	n. d.	n. d.	n. d.
Amphiphysin SH3						
Amphiphysin SH3	300	GST-srGAP3-CTR	30	n. d.	n. d.	n. d.
Amphiphysin SH3	1000	srGAP3 PxxP-fragment	100	27 ± 6	1.2 ± 0.1	-1.4 ± 0.4
Amphiphysin SH3	1000	srGAP3 AxxA-fragment	100	n. d.	n. d.	n. d.
Grb2 SH3N[b]						
Grb2 SH3N	300	GST-srGAP3-CTR	30	NQ[b]	NQ	NQ
Grb2 SH3N	500	srGAP3 PxxP-fragment	50	NQ	NQ	NQ
Grb2 SH3N	500	srGAP3 AxxA-fragment	50	NQ	NQ	NQ
Grb2 SH3C[b]						
Grb2 SH3C	300	GST-srGAP3-CTR	30	NQ	NQ	NQ
srGAP3 PxxP-fragment	300	Grb2 SH3C	30	15 ± 5	1.2 ± 0.1	-4.7 ± 1.8
srGAP3 AxxA-fragment	300	Grb2 SH3C	30	n. d.	n. d.	n. d.

[a] Analysis performed with single-site binding model; K_d = dissociation constant; N = stoichiometry (syringe component to cell component); $\Delta H_{(obs)}$ = observed binding enthalpy. Indicated is the standard deviation between 2 to 3 independent experiments. Grb2 SH3N and Grb2 SH3C were measured only once due to limited availability of GST-srGAP3-CTR.

[b] GST-srGAP3-CTR: srGAP3 (residues 810-1099) N-terminally tagged with GST; n. d., not detected; srGAP3 PxxP-fragment: residues 1047-1079; srGAP3 AxxA-fragment: residues 1047-1079 with mutation of P1056 and P1059 to alanine. NQ, non-quanitfiable; SH3N: N-terminal SH3 domain; SH3C: C-terminal SH3 domain.

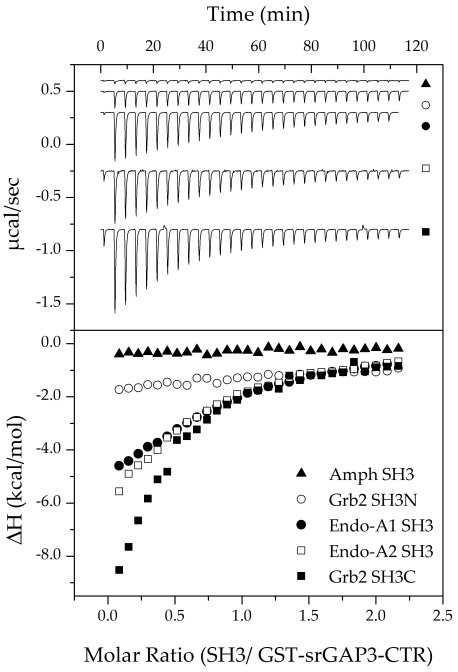

Figure 6.14.: GST-srGAP3-CTR directly interacts with SH3 domains. Isothermal titrations of 300 µM SH3 domain into 30 µM GST-srGAP3-CTR (C-terminal region, residues 810-1099 of srGAP3) at 20 °C. The upper panel shows the raw heat signals (separated by shifting of the baselines), whereas the lower panel contains the integrated heat signal per injection corrected for the heat of dilution.

6.4.3. Characterisation of a Multi-Class SH3-Binding Motif in SrGAP3

Linear motifs usually consist of stretches of 3 to 11 amino acids [45] and are inherently more difficult to predict than globular domains due to their shortness as well as the resulting high number of false-positive results [45]. For this reason, I used high stringency settings and the consensus prediction of the ELM resource [188, 189] and Scansite [190, 191] as a basis to narrow down the list of potential interacting motifs (compare alignment, Fig. 6.2, p. 42). Since SLiMPred was reported to perform especially well in the prediction of polyproline type II motifs compared to other *de novo* predictors [194], its results were included in this analysis in order to prioritise potential binding regions. Interestingly, only a single SH3-binding motif (residues 1053-1062) was predicted with high confidence by all algorithms (compare Fig. 6.15A, p. 62): RPPPMRPVRP. This motif is present in srGAP3 sequences with only three exceptions (*Melea-*

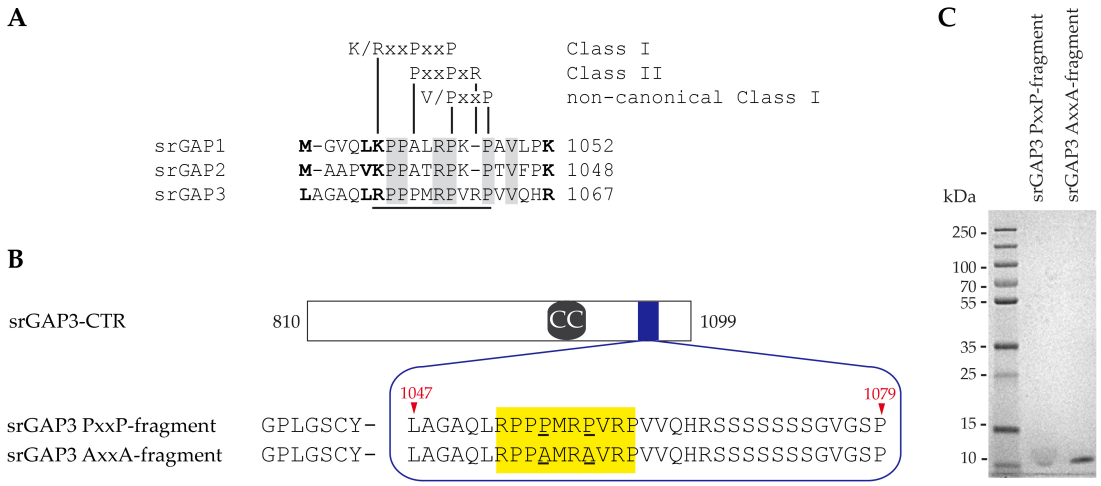

Figure 6.15.: A multi-class SH3-binding motif is present in srGAP3. A: MUSCLE alignment [179, 180] of srGAP1, 2, and 3 from *H. sapiens* of the SH3-binding motif region. Conserved (light grey) and similar (bold) positions are highlighted. The motif classes are indicated above (ELM resource classification, http://elm.eu.org/). **B:** Amino acid sequence (+GPLGSCY from vector) of the purified srGAP3 fragment and the mutant thereof (P1056A/ P1059A) as well as their location within the CTR. CTR, C-terminal region; CC, predicted coiled-coil segment. The SH3-binding motif is highlighted in yellow and the mutated proline residues are underlined. **C:** SDS-PAGE purity control of the srGAP3 PxxP-fragment (4.1 kDa) and AxxA-fragment (4.0 kDa).

gris gallopavo, *Camelus ferus*, and *Poecilia formosa*). These sequences originated from predicted and unverified sequence annotations and, thus, it remains unclear whether they also harbour the motif. Nevertheless, this sequence analysis implies that I have identified a potential SH3-binding motif that is universally conserved among srGAP3 proteins.

A unique feature of this motif is its multi-class nature (Fig. 6.15A), which could equip srGAP3 with a flexible interaction surface for recognition of different SH3 domains and hence depicted an ideal candidate to mediate binding to Endophilin-A1, Endophilin-A2, and Grb2. Moreover, the SH3 domain of Amphiphysin was shown to specifically bind to a short linear motif in the proline-rich region of Dynamin with the sequence PSRPNR [239]. As this motif resembles the predicted SH3-binding motif in class II orientation (Fig. 6.15A), whereby both conform to the consensus PxRPxR, Amphiphysin might likewise engage this region in srGAP3 for complex formation. SrGAP1 and srGAP2, on the contrary, lack a classical type I or type II polyproline consensus motif at this position (Fig. 6.15A),which potentially renders it a characteristic that

distinguishes srGAP3 from srGAP1 and srGAP2 (compare Discussion 7.2.1, p. 80).

Based on these bioinformatic predictions, I designed a shorter srGAP3 construct comprising this linear motif (aa 1047-1079, "PxxP-fragment", Fig. 6.15B) and tested, whether it exhibited binding to the SH3 domains in isothermal titrations. In order to delineate interacting residues, I also prepared a mutated fragment, in which the core proline residues P1056 and P1059 were replaced by alanines ("AxxA-fragment", Fig. 6.15B). The two protein constructs were expressed in *E. coli* and purified to homogeneity (Fig. 6.15C).

Analysis of the Interaction Between the SrGAP3 PxxP-Fragment and the SH3 Domains of Endophilins

The ITC experiments revealed that this smaller srGAP3 PxxP-fragment containing the predicted linear motif indeed interacted with the SH3 domains of Endophilins in a 1:1 stoichiometry (Fig. 6.16A and B, p. 66). The affinities of the complexes (K_d = 17 and 20 μM, Tab. 6.5, p. 60) were similar to the complexes involving the full C-terminal region. Reverse titrations yielded similar thermodynamic parameters, which corroborated a single-site interaction model. In order to demonstrate that binding to both Endophilins in fact depended on the presence of the predicted SH3-binding motif, I conducted titrations with the mutated srGAP3 fragment (AxxA-fragment, Fig. 6.15B, p. 62). This mutant failed to bind either Endophilin-A1 SH3 or Endophilin-A2 SH3 (Fig. 6.16A and B, p. 66) and these results, thus, indicated that the predicted multi-class SH3-binding motif between residues 1053 and 1062 of srGAP3 mediated the interaction.

Analysis of the Interaction Between the SrGAP3 PxxP-Fragment and the SH3 Domains of Grb2

In the previous set of ITC experiments, I demonstrated that Grb2 assembled with srGAP3-CTR *in vitro* and complex formation was governed by the C-terminal SH3 domain of Grb2, while the N-terminal SH3 domain depicted a potential low-affinity interaction site (see 6.4.2, p. 59). McDonald *et al.* [240] reported that the two SH3 domains of Grb2 can recognise the same linear motif in Sos1, yet bind it with different affinities. As the linear motif in the srGAP3 PxxP-fragment might behave similarly, I determined the binding characteristics of both SH3 domains to this protein construct using ITC: The measured affinities (Tab. 6.5, p. 60) suggested that binding sites for both domains might be located within the PxxP-fragment, but that the affinity for Grb2 SH3C (K_d = 14 μM) is at least an order of magnitude higher than for Grb2 SH3N (affinity

too low to be quantified reliably). Furthermore, the complex with Grb2 SH3C exhibited a 1:1 stoichiometry and an affinity in the same range as complexes between srGAP3 and the Endophilins (Tab. 6.5, p. 60). Reverse titrations yielded non-reproducible binding isotherms for unknown reasons and were therefore omitted in this analysis.

In order to test whether the predicted SH3-binding motif was likewise responsible for complex formation with Grb2, I carried out isothermal titrations with the srGAP3 AxxA-fragment. Indeed, titrations of Grb2 SH3C with this mutated srGAP3 fragment revealed that this interaction also depended on this linear motif (Fig. 6.16C, p. 66). In contrast, the two proline residues were not required for the interaction with Grb2 SH3N: Although the measured signal of titrations with the srGAP3 AxxA-fragment was too weak to be reliably quantified (Tab. 6.5, p. 60), it displayed a similar shape as the isotherms from titrations with the wild-type fragment (data not shown). Therefore, it can be concluded that the C-terminal SH3 domain of Grb2 directly bound to the proline-rich motif within the srGAP3 PxxP-fragment, while the N-terminal SH3 domain either recognised a different motif or non-specifically interacted with the srGAP3 PxxP-fragment (compare Discussion 7.2.1, p. 80).

Analysis of the Interaction Between the SrGAP3 PxxP-Fragment and Amphiphysin SH3

As outlined above, the predicted SH3-binding site contained a consensus sequence recognised by the Amphiphysin SH3 domain. Therefore, I explored the binding behaviour of Amphiphysin SH3 to this smaller srGAP3 fragment, although I failed to detect a direct interaction between Amphiphysin SH3 and the full C-terminal region of srGAP3 in earlier experiments (see Tab. 6.5, p. 60 and Fig. 6.14, p. 61). Indeed, the srGAP3 PxxP-fragment bound the SH3 domain of Amphiphysin in a 1:1 stoichiometry (Fig. 6.16D, p. 66) and affinities that were comparable to the data obtained from titrations with Endophilin-A1 and -A2 SH3 as well as Grb2 SH3C (K_d = 27 μM, Tab. 6.5, p. 60). The enthalpic contribution of these interactions was generally smaller (Tab. 6.5, p. 60), which explains, why binding was undetectable in titrations with the full C-terminal region: Only at these higher protein concentrations the generated heat of binding was large enough to surpass the detection limit at the employed experimental settings. Reverse titrations of the SH3 domain with the srGAP3 fragment were accompanied by a large heat of dilution from titrating a highly concentrated unfolded peptide into buffer, which masked the binding isotherm (data not shown). For this reason, the data set lacks additional support for a single-site binding mode from the reverse experiment.

Following up on these results, I analysed whether the binding event likewise required the presence of the SH3-binding motif. I found that, similar to ex-

periments with Endophilin-A2, Endophilin-A1, and Grb2, mutations in core interacting residues within the motif abrogated binding (Fig. 6.16C). Taken together, these results demonstrated an unexpected flexibility of a single SH3-binding motif in srGAP3 in engaging in different SH3-dependent interactions.

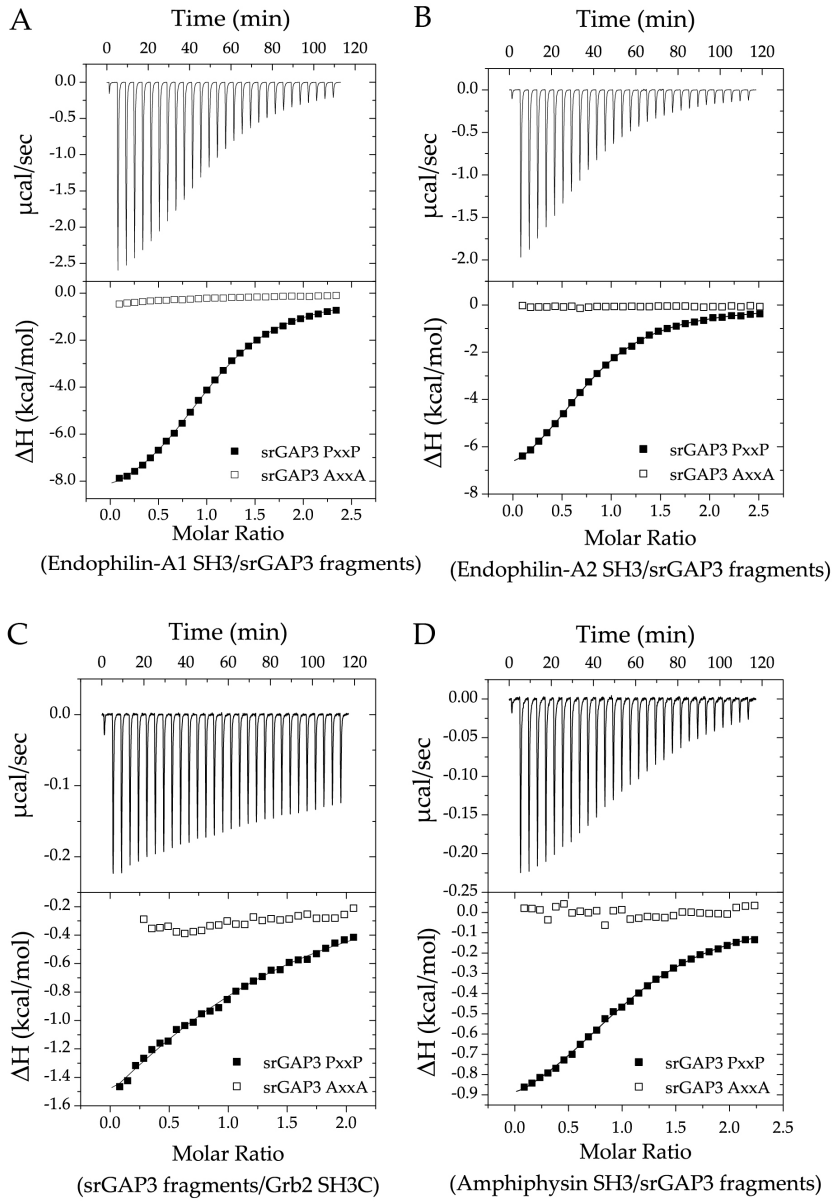

Figure 6.16.: A single SH3-binding motif in srGAP3 mediates binding to Endophilin-A1 SH3, Endophilin-A2 SH3, Grb2 SH3C, and Amphiphysin SH3. Interactions were measured with isothermal titration calorimetry at 20 °C. The upper panel shows the raw heat signal of titrations with the srGAP3 PxxP-fragment (residues 1047-1079) only. The lower panel shows the integrated heat signal per injection corrected for the heat of dilution for the srGAP3 PxxP-fragment and the mutated AxxA-fragment (P1056A/ P1059A). Binding isotherms were analysed assuming a single-site binding model. **A:** 1000 µM Endophilin-A1 SH3 were titrated into 100 µM srGAP3 PxxP-fragment or 100 µM srGAP3 AxxA-fragment. **B:** 1000 µM Endophilin-A2 SH3 were titrated into 100 µM srGAP3 PxxP-fragment or 100 µM srGAP3 AxxA-fragment. **C:** 300 µM srGAP3 PxxP-fragment or srGAP3 AxxA-fragment were titrated into 30 µM C-terminal SH3 domain of Grb2 (Grb2 SH3C) and **D:** 1000 µM Amphiphysin SH3 into 100 µM srGAP3 PxxP-fragment or 100 µM srGAP3 AxxA-fragment. In titrations with Grb2 SH3C syringe and cell component were switched due to technical reasons.

6.5. Characterisation of the 14-3-3/srGAP3-Complex *In Vivo*

The second group of srGAP3-interaction partners validated in the *in vivo*-binding assay comprised the 14-3-3 proteins (see results of Co-IP assay, p. 55, 14-3-3γ and 14-3-3θ/τ). As mentioned earlier, the association between srGAP3 and this protein family has already been described by others [207, 241], but these data sets lacked information on specific interaction motifs or the corresponding 14-3-3 isoforms.

6.5.1. Phosphorylation Analysis of SrGAP3

14-3-3 proteins typically bind to linear motifs, which incorporate a phosphorylated serine or threonine [84], although non-phosphorylated motifs have also been reported [213–216] (compare Bioinformatic Analysis for motif descriptions 6.1.2, p. 38). Database searches revealed that proteomic studies had identified numerous phosphorylation sites within the C-terminal region of srGAP3 and some of these phosphorylation sites even colocalised with predicted 14-3-3-binding motifs (Fig. 6.17, p. 69). But since phosphorylation depends on many different factors such as tissue type or developmental stage [242, 243], we decided to analyse the phosphorylation state of srGAP3 used in my experiments.

We determined the phosphorylation states of endogenous srGAP3 from rat brain (stage P14) and of overexpressed human srGAP3 from HEK293T cells with mass spectrometry. SrGAP3 was almost exclusively phosphorylated in the C-terminal region (Fig. 6.17) with S759 being the only exception. The phosphorylation sites S837, S858, S874, S895, and S919 were conserved between rat and human as well as different cell types and the residues S858 and S919 additionally colocalised with or lay adjacent to predicted 14-3-3-binding sites. As phosphorylation is often tissue-specific [242], we were not surprised to find several cell type-specific phosphorylation sites and two of those were, at the same time, positioned within or close to 14-3-3-binding motifs: S932 and S1070. Moreover, we not only confirmed several phosphorylation sites identified in other studies, but also found additional phosphorylated residues: T885, S894/S895, S932, S1011, and T1082 (Fig. 6.17, p. 69).

On the one hand, the goal of this project consisted of the characterisation of brain-specific srGAP3-complexes, while the methodology was, on the other hand, restricted to the usage of HEK293T cells. For this reason, I solely considered those phosphorylation sites within or close to predicted 14-3-3-binding sites in the following experiments that were present in both samples: S858 and S919. As revealed by my sequence analysis, both motifs are not only present in

human srGAP3, but invariably conserved within vertebrate srGAP3 proteins (data not shown) suggesting that their function might even be conserved in non-mammalian species and therefore over larger evolutionary distances.

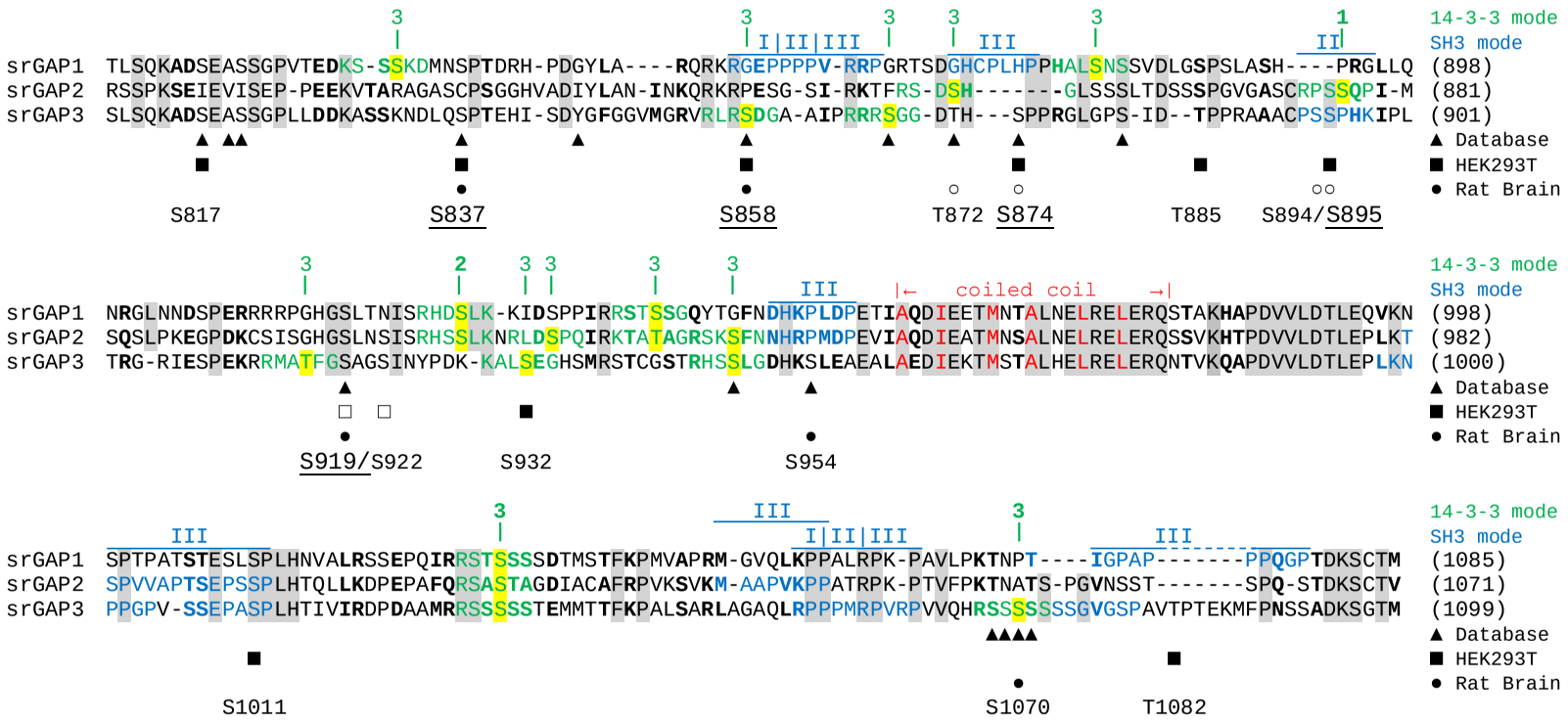

Figure 6.17.: Several phosphorylation sites of srGAP3-CTR colocalised with predicted 14-3-3-binding motifs. MSAProbs [178] alignment of the C-terminal regions (CTR) of srGAP1, 2, and 3 from *H. sapiens*. Conserved positions are highlighted in grey and similar residues are printed in bold. Predicted 14-3-3-binding sites (green) and the corresponding motif class of the ELM classification scheme (see http://elm.eu.org/) are indicated. Predicted phosphorylated residues within these motifs are highlighted in yellow. Predicted SH3-binding sites (blue) with the corresponding motif class from the ELM resource and the predicted coiled-coil region (red) are also marked. Phosphorylation sites of srGAP3 enlisted in the PhosphoSite database (http://www.phosphosite.org/) are marked with ▲. Phosphorylation sites of srGAP3 transiently expressed in HEK293T (▪) and endogenous srGAP3 in rat brain lysate (•) were identified by mass spectrometry. If the position could not be determined unambiguously (position score = 0.5), both possible amino acids are marked with the respective empty symbols (e. g. T872/S874). Phosphorylation sites, which are shared between the two samples, are underlined. Linear motifs were obtained from Scansite (http://scansite3.mit.edu/) and the ELM resource.

6.5.2. Do the Mutations S858A and S919A Affect Complex Formation with the 14-3-3 Isoforms γ and θ/τ?

To test, whether phosphorylation of S858 and S919 affected binding to 14-3-3 proteins, I constructed phosphorylation-incompetent srGAP3 mutants by replacing S858 and S919 with alanines (see Fig. 6.17, Tab. 6.6) and determined whether these mutations impaired binding of srGAP3 to the 14-3-3 isoforms γ and θ/τ. The mutant S895A depicted a negative control, since this phosphorylation site was positioned outside of predicted 14-3-3-binding sites, but at the same time conserved between different cell types (Fig. 6.17).

Table 6.6.: Constructs for 14-3-3 motif characterisation. 14-3-3 isoforms are were tagged with mCherry and srGAP3 full-length and point mutants thereof with eGFP.

Protein Name	Species[a]	MW[a] [kDa]	mCherry/eGFP-Fusion MW [kDa]
14-3-3γ	Rn	28.3	57.2
14-3-3θ/τ	Hs	27.8	56.0
srGAP3	Hs	124.5	154.1
srGAP3 S858A	Hs	124.5	154.1
srGAP3 S919A	Hs	124.5	154.1
srGAP3 S858A S919A	Hs	124.5	154.1
srGAP3 S895A	Hs	124.5	154.1
eGFP	from pEGFPC23C[a]	30.3	–

[a] Rn, *Rattus norvegicus*; Hs, *Homo sapiens*; pEGFPC23C, vector; MW, molecular weight.

I measured complex formation with the fluorescence-based Co-IP assay (compare 6.3, p. 48) and could show that the mutations S858A and S919A affected the interaction with either isoform (Fig. 6.18). In case of 14-3-3θ/τ, the mutation of either S858 or S919 to alanine reduced binding to 58 % and 62 % compared to srGAP3 wild-type. The simultaneous presence of both mutations compromised complex formation even further (bound fraction reduced to 41 %, Fig. 6.18B). Interestingly, S919 lay adjacent to and not within the respective linear motif, but still affected its binding capabilities (compare Fig. 6.17, p. 69), which demonstrates the complexity of phosphorylation-dependent 14-3-3-interactions (compare Discussion 7.2.2, p. 83).

In case of 14-3-3γ, on the other hand, I only observed significantly less binding in Co-IPs with the srGAP3 double mutant (reduced to 68 % of wild-type, Fig. 6.18A). Nevertheless, the two point mutations failed to fully abrogate binding

to 14-3-3s with the employed experimental settings,which points towards the presence of additional binding sites.

In summary, multiple sites within the C-terminal region of srGAP3 seemed to be involved in binding of 14-3-3s suggesting a complex mode of interaction. Two of these sites, S858 and S919, could be validated in this project and were involved in binding to the 14-3-3 isoforms γ and θ/τ in HEK293T cells. Since their phosphorylation pattern was tissue-invariant, they are expected to hold the same function in brain-specific srGAP3/14-3-3-complexes.

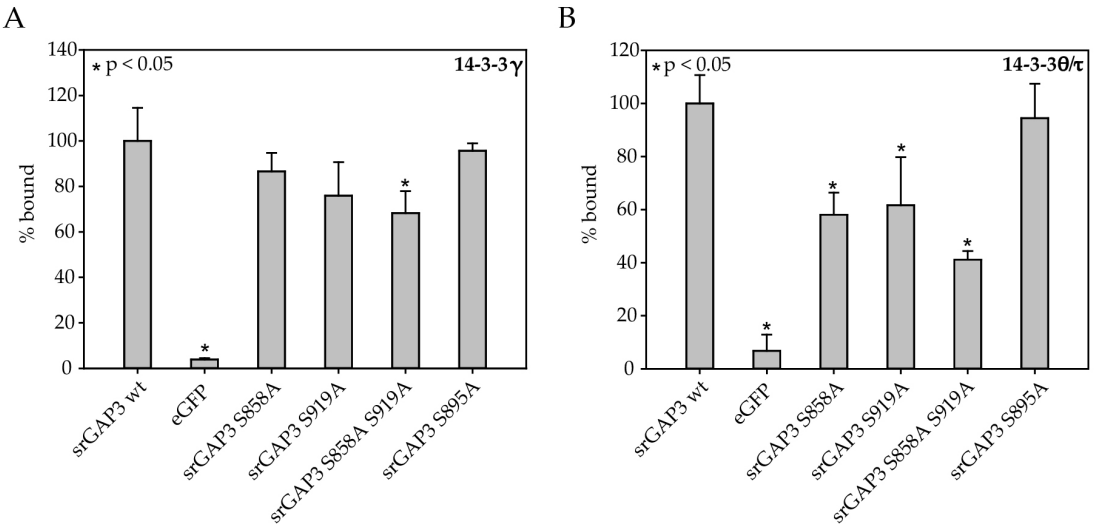

Figure 6.18.: Binding of 14-3-3γ and θ/τ to srGAP3 involves phosphorylation of S858 and S919. MCherry-tagged 14-3-3γ and θ/τ and eGFP-tagged srGAP3 were co-expressed in HEK293T cells and the interaction analysed in a fluorescence-based co-immunoprecipitation assay. The fraction of bound 14-3-3γ and 14-3-3θ/τ in percent of co-immunoprecipitations with srGAP3, mutants thereof, or eGFP are indicated. The average mCherry fluorescence intensity of three independent experiments was corrected for the instrument background and normalised to the wild-type sample (srGAP3 wt). Error bars correspond to the standard deviation between replicates and asterisks mark samples that are significantly different from co-immunoprecipitations with srGAP3 wild-type ($p < 0.05$ in unpaired t-test). EGFP and srGAP3 S895A served as assay and negative control, respectively. The statistical analysis was performed with SigmaPlot (version 12.3, Systat Software Inc.).

7. DISCUSSION

The srGAP family of proteins has been implicated in various aspects of neuronal development [151, 152, 155–158, 244] and these findings were, on a molecular level, mainly substantiated through functional characterisations of the N-terminal domains [127, 151, 154, 156, 163, 165], whereas less attention has been given to the C-terminal region [207, 245]. The C-terminal region exhibits the highest divergence between paralogous srGAP proteins [151] and my bioinformatic analysis predicted it to be natively disordered (Fig. 6.2, p. 42). Since database searches revealed the presence of potential short linear motifs for protein-protein interactions, I attempted to characterise protein complexes formed by the C-terminal region of srGAP3. With a combination of different biochemical and biophysical methods, I was able to show that srGAP3 uses such linear motifs for binding of 14-3-3 proteins as well as the SH3 domain-containing proteins Endophilin-A1, Endophilin-A2, Amphiphysin, and Grb2 (Fig. 7.1). In the following sections, I will discuss my methodology (7.1), specific characteristics of the identified interactions (7.2, 7.3), hypothetical functions of the formed complexes (7.4), and I will finally try to answer the question, whether the C-terminal region is natively unstructured (7.5).

7.1. Top-Down Approach for the Identification of Direct Interaction Partners of SrGAP3-CTR

The identification of direct interaction partners for a specific protein or protein domain is not a trivial task. About 300 SH3 domains are, for example, encoded in the human genome [50] and isolating the subset of SH3 domains that directly binds to a protein of interest confronts the researcher with a difficult combinatorial problem that has to be solved in a reasonable amount of time. In principle, two different starting points exist to dissect the cellular machinery associated with a specific protein without prior knowledge: The first comprises multiplexed screening of binary interactions ("bottom-up"), which is realised in library-based methods and is generally performed outside the native environment of the protein [246, 247]. The second constitutes the isolation of multi-protein complexes from the native tissue containing the target protein ("top-down"), which is the focus of pull-down or co-immunoprecipitation experiments that are usually combined with mass spectrometry methods [233].

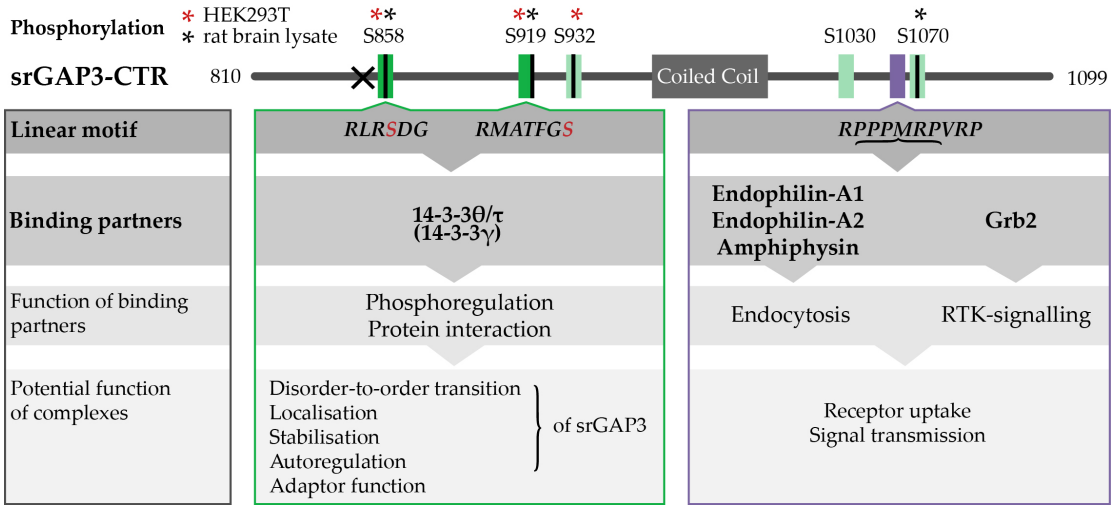

Figure 7.1.: Protein interactions of the C-terminal region of srGAP3 and functional implications. An interaction model of srGAP3-CTR with the relative positions of the identified linear motifs and the respective binding partners is displayed. Shown in blue is the multi-class SH3 domain-interaction motif and marked with a cross is the approximate position of a predicted multi-class SH3-binding motif in srGAP1 (see 7.2.1 for further discussion). The analysed 14-3-3-binding motifs with the corresponding phosphorylation sites are marked in dark green, whereas potential additional motifs are depicted in light green (see 7.2.2 for discussion). Asterisks mark identified phosphorylation sites located within 14-3-3 motifs. The amino acid sequences of the motifs, as well as functional associations derived from Gene Ontology terms and literature data, and potential functional implications of the identified complexes are displayed below. 14-3-3 functions were subsumed under the category phosphoregulation/protein interaction, whereas Endophilins and Amphiphysin belong to the endocytic machinery, and Grb2 is associated with receptor tyrosine kinase (RTK) signalling (see 7.4 for further discussion).

In vivo-crosslinking (e.g. [248]) represents an intermediate approach, but is irrelevant to the following discussion paragraphs and therefore not explained in greater detail.

In this project, I pursued a top-down strategy for the identification of binding partners for srGAP3-CTR, in which the initial GST pull-down from rat brain lysate was followed by a validation experiment relying on co-immunoprecipitations from HEK293T cells and a subsequent analysis of interacting domains and motifs. Ultimately, this led to the identification of six previously unknown protein complexes (Fig. 7.1, p. 74). Why did this methodology yielded results in contrast to the library-based approach from Haussmann [220] employing a yeast-two-hybrid screen?

GST Pull-Down from Rat Brain Lysate

The main difference lies in the isolation of multi-protein complexes from native tissue in the initial pull-down experiment, in which several linear motifs in srGAP3-CTR could, for example, have acted in parallel to bind different members of larger protein assemblies (compare 7.3, p. 89). Furthermore, the bait protein GST-srGAP3-CTR was presented as an immobilised dimer through the N-terminal GST-tag and within the framework of the resulting multiple attachment sites, low affinity complexes - like the identified SH3 domain-interactions - were potentially stabilised through cooperative effects [48, 233]. In contrast, the detection limit of yeast-two-hybrid experiments, which only detects binary interactions [246], is a K_d of approximately 1 μM [246]. This cut-off is smaller than the measured affinities and might explain, why Haussmann [220] was unable to detect these complexes.

Another advantage of GST pull-down experiments is their ability to detect phosphorylation-dependent interactions, which cannot be captured by yeast-two-hybrid screens due to a different phosphorylation pattern in yeast [249]. This aspect might be especially important in the light of the identified 14-3-3 interactions, which usually, but not always involve phosphorylation of the binding motif in the ligand (Fig. 7.1, p. 74) [79, 84]. If phoshorylation of GST-srGAP3-CTR had, however, been absolutely required for complex formation between srGAP3 and 14-3-3s, the bait protein would have had to be phosphorylated by kinases present in the lysate. And although we treated the lysate with phosphatase inhibitors, which stabilise the phosphorylated states of proteins, we omitted the parallel application of kinase activators or ATP, which might be required for a quantitative phosphorylation of the bait protein *in vitro* (compare [250]). It is therefore likely that phosphorylation of GST-srGAP3-CTR was dispensable for complex formation with 14-3-3s in this experimental setup, although we did not analyse its phosphorylation state after incubation with

the rat brain lysate. On the other hand, even if complex formation was independent of phosphorylation of a bait protein, phosphorylation of binding partners might have been necessary for the interaction and a comparative analysis of GST pull-down experiments in presence and absence of phosphatase inhibitors should help to clarify this issue. Despite these caveats of our own results, GST pull-down experiments should perform superior to yeast-two-hybrid screens in the analysis of 14-3-3-dependent interactions.

It is clear that the outcome of a pull-down experiment will directly depend on the type and origin of the tested tissue. This becomes especially important, if the bait protein - as in this case - is developmentally regulated [159, 160, 221], which might similarly apply to expression patterns of binding partners making them potentially exclusively detectable at certain developmental stages. After postnatal day 14, srGAP3 mainly relocates from the cytosol to the nucleus [159], which means that repeating the experiment with earlier developmental stages might help to identify different or additional cytosolic binding partners for srGAP3-CTR, whereas later stages would aim at the isolation of nuclear srGAP3-containing complexes.

An obvious drawback of the pull-down approach is its high amount of false-positive results originating from indirect interactions [251]. In order to improve the signal-to-noise ratio, we utilised srGAP1-CTR in parallel to dissect binding partners, that are potentially specific for either srGAP-family member. On the other hand, we had expected that the CTRs bind their ligands mainly through linear motifs, which typically engage in low-affinity interactions [45] and for this reason we omitted extensive washing procedures to increase the detection probability. The mass spectrometry results thus likely contained a considerable amount of background signal, which rendered the validation of the pull-down results through an alternative method especially important. Therefore, we selected a subset of 19 proteins, which was mainly specific for srGAP3-CTR, and I subsequently analysed the interactions with srGAP3 in an orthogonal approach, which permitted the detection of direct protein-protein interactions.

Fluorescence-Based Co-IP Assay

The established Co-IP assay was based on an immobilised nanobody directed against GFP [196] and nanobodies feature special characteristics that might have been advantageous in this particular experimental set-up: Due to their small size, nanobodies achieve higher probe densities on solid supports compared to conventional antibodies [252, 253]. In my assay, relatively high protein concentrations (upper limit of the plate supplier's recommendations) were necessary to saturate the plate surface with the GFP-nanobody, which maybe

indicates such higher probe densities. Increased amounts of immobilised nanobody were reported to positively affect the sensitivity of surface plasmon resonance experiments [252, 253] and might have likewise improved the sensitivity of my assay.

I utilised the GFP-nanobody to co-precipitate mCherry-tagged candidate proteins through eGFP-tagged srGAP3 full-length and was able to confirm the interaction of srGAP3 with eight of the 19 candidate proteins *in vivo*: α-Centractin, Grb2, Endophilin-A1, Endophilin-A2, Amphiphysin, as well as the 14-3-3 isoforms γ, θ/τ, and ζ (Fig. 6.10, p. 56). These interactions were likely to be direct, since overexpression and the resulting high protein concentrations of both interaction partners in HEK293T cells rendered indirect binding events improbable (compare Fig. 6.5, p. 48 for set-up). Of course, indirect interactions cannot be formally excluded, which especially applies to cases, where the binding signal was weak (such as α-Centractin and 14-3-3ζ).

These eight binding partners (Fig. 7.2, p. 78, displayed in green) have been implicated in a subset of cellular networks, which also involved several candidates, which I was unable to validate in the Co-IP assay (Fig. 7.2, p. 78). Indirect interactions in larger protein assemblies presumably caused the occurrence of these and other proteins in the initial pull-down experiment. However, it is likewise conceivable that non-validated candidates either represented unspecific background due to insufficient washing (see above, 76) or were unable to bind srGAP3 in this specific experimental set-up, for example due to masking of binding sites through phosphorylation (e.g. [254]).

The amount of bound mCherry-tagged binding partners varied considerably between different srGAP3/candidate pairs in the fluorescence-based Co-IP assay (Fig. 6.10, p. 56), which might imply that they interacted with different strength with srGAP3. Nevertheless, it is impossible to draw conclusions about the affinity of the interactions for several reasons: Firstly, the nature of the interaction (transient or stable) or the concentration of active protein inside the cell might affect the amount of bound protein in a similar fashion. Secondly, transient transfections for each srGAP3/candidate pair were optimised to maximise the expression of both constructs and the fluorescence levels solely normalised to its own eGFP control, but not to other srGAP3/candidate combinations. Therefore, the obtained mCherry-fluorescence intensities represent relative values to the respective eGFP control and the overall amount of bound protein in individual samples might have been influenced by the respective expression levels. However, I decided to exclude candidates that weakly co-precipitated with eGFP-srGAP3 (α-Centractin, 14-3-3ζ) from further analyses due to the higher probability that they represented indirect binding events (see above) or that specific protein features - such as low affinity-binding or poor folding - could complicate a characterisation *in vitro*. The remaining set of val-

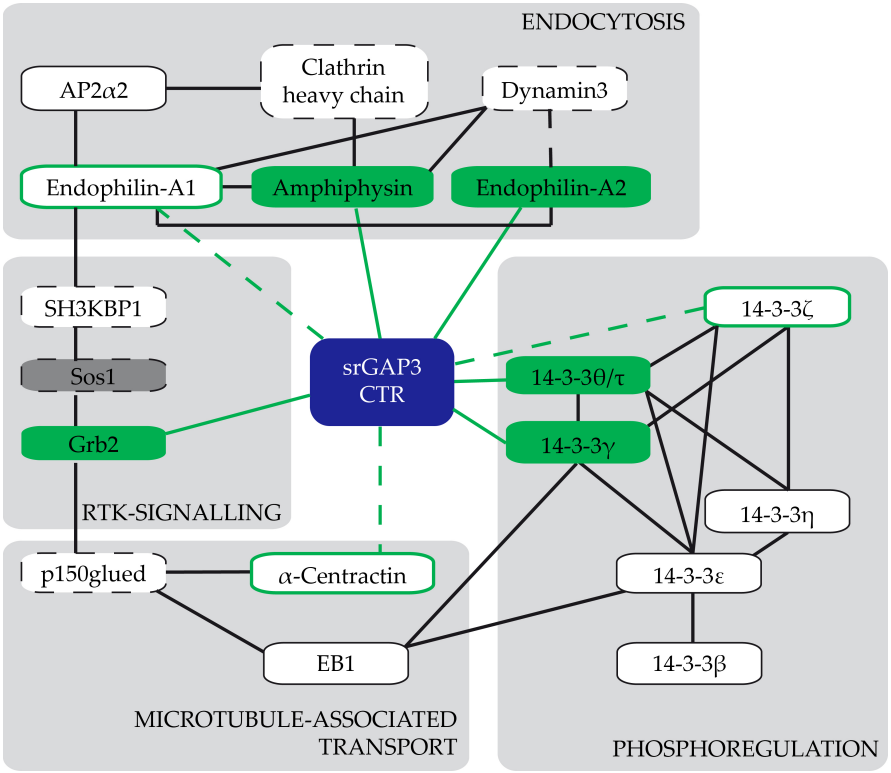

Figure 7.2.: Functional networks involving srGAP3. Interaction data with experimental support was retrieved from the STRING database (http://string-db.org/ [255]), from the literature, or identified in this project. Solid lines depict connections with high confidence, whereas dashed lines illustrate weak experimental support. Binding partners of srGAP3-CTR that were identified in this study are shown in green (filled green box: interaction with CTR validated; encircled in green: interaction with full-length srGAP3). Encircled in solid black are non-validated candidates from the co-immunoprecipitation assay. Proteins that were identified in the mass spectrometric analysis of the GST pull-down experiment, but not investigated further, are marked with a dashed black line. Son of sevenless 1 (Sos1) was identified in co-immunoprecipritations of endogenous srGAP3 from rat brain lysate (data not shown). RTK: receptor tyrosine kinase. Functional associations were retrieved from either the Gene Ontology database (http://geneontology.org/) or the literature.

idated interaction partners belonged to the SH3 domain-containing proteins (Endophilin-A1, Endophilin-A2, Amphiphysin, Grb2) and 14-3-3s (isoform γ and θ/τ).

Characterisation of SH3 Domain-Complexes with ITC

Utilising ITC, I confirmed the direct interaction of the SH3 domains of Endophilin-A1, Endophilin-A2, Amphiphysin, and Grb2 with the full C-terminal region as well as a shorter PxxP-fragment of srGAP3. The affinities were low with K_d values in the micromolar range and specific characteristics of the formed complexes are discussed in section 7.2.1. Through a mutational analysis, I was able to delineate a single proline-rich motif in srGAP3-CTR that conferred binding to at least three of these proteins (data for Endophilin-A1 only preliminary, Fig. 7.1, p. 74).

An obvious advantage of isothermal titration calorimetry is the potential to determine all biophysical parameters (enthalpy, affinity, stoichiometry, and - derived from that - the entropy) in a single experiment without the need to label the components [256]. A drawback of this method is clearly the requirement for large amounts of soluble protein to obtain meaningful data in the investigation of such low affinity interactions [141]. In case of the SH3 domain of Amphiphysin, I was for this reason unable to detect the direct interaction with the full C-terminal region of srGAP3: At the employed protein concentration and measurement temperature, the enthalpic change - which depends on these settings [256] - was below the detection limit. In contrast, the interaction of this SH3 domain with a smaller srGAP3 fragment, which was soluble at higher protein concentrations, was successfully detected.

Mutational Analysis of 14-3-3-Dependent Interactions

In most cases, binding to 14-3-3 proteins requires phosphorylation of a serine or threonine residue in the target motif [84, 85] and, for this reason, I focused on the analysis of predicted 14-3-3-binding motifs in srGAP3-CTR that were phosphorylated in our samples. I employed HEK293T cells to validate the interaction of 14-3-3 proteins with srGAP3, but the phosphorylation pattern of srGAP3 transiently expressed in this cell type only partially matched its phosphorylation pattern in rat brain (Fig. 6.17, p. 69). As the goal of this project was the identification of brain-specific srGAP3-complexes, which is the tissue srGAP3 is mainly expressed in [161], I took only those phosphorylation sites into account that were shared between both cell types (S858 and S919). Consequently, the identified residues within srGAP3 that are involved in complex formation with 14-3-3s in HEK293T cells should carry out the same function in the rat brain.

To investigate the binding behaviour of these predicted motifs, I initially attempted to analyse their interaction with the 14-3-3 proteins *in vitro* using fragments of srGAP3-CTR, which carried phosphomimetic mutations (phosphorylated positions mutated to aspartate). This approach was unsuccessful and,

therefore, I performed a mutational analysis of full-length srGAP3, in which I screened for loss of interactions with 14-3-3 proteins in the fluorescence-based Co-IP assay. With this methodology, I was able to identify two of several positions within the C-terminal region of srGAP3 that are involved in the complex formation with 14-3-3s (Fig. 7.1, p. 74), which will be discussed in detail in section 7.2.2.

In summary, a top-down approach employing a panel of different *in vivo* and *in vitro* methods uncovered six previously unknown direct interaction partners of srGAP3, which bind to its C-terminal region: Amphiphysin, Endophilin-A2, Endophilin-A1, Grb2, 14-3-3γ, 14-3-3θ/τ.

7.2. Protein-Peptide Interactions Mediated by SrGAP3-CTR

Bioinformatical structure predictions revealed that the C-terminal region of srGAP proteins likely lacks secondary structure elements that can be combined to produce a classically folded tertiary structure and, therefore, this region is possibly intrinsically disordered (see section 7.5 for further discussion). The functions attributed to unstructured segments are diverse and can range from chaperone activity or flexible connections of folded domains to assembly of protein complexes or scavenging of small molecules [37]. Protein-protein interactions of disordered regions are often mediated by linear motifs [37], which usually bind to globular domains [46] and represent versatile interaction modules that can be combined in numerous ways in a single polypeptide chain [45]. Employing database searches, I detected such linear motifs in the C-terminal region of srGAP3 for binding to 14-3-3 proteins and SH3 domains, which I was able to validate experimentally. In the following subsections, I will discuss specific features of the identified motifs and how they might have contributed to the selective binding of the respective proteins.

7.2.1. SH3 Domain-Dependent Interactions

In the canonical binding mode, SH3 domains recognise proline-rich sequences, which form a type II polyproline helix and contain a PxxP core motif [55, 212]. Positively charged amino acid preceding (class I: *[RK]xxPxxP*) or following (class II: *PxxPx[KR]*) the PxxP core are accommodated by an acidic specificity pocket, which determines the binding orientation of the ligand peptide [57–59, 257]. Additional residues within or close to the motif as well as variable loop regions in the SH3 domain that contribute to the specificity pocket not only affect the affinity of the interaction, but are also instrumental to the

diverse specificity landscape of SH3-mediated interactions, which can range from exclusive to promiscuous [257, 258].

Using the outlined experimental set-up (compare section 7.1, p. 73), I was able to show that the SH3 domains of the Endophilins, Amphiphysin, and the C-terminal SH3 domain of Grb2 share the ability to bind to a single proline-rich motif in the C-terminal region of srGAP3 with a K_d of 14 - 27 μM. Weak interactions like these are typical for SH3-mediated complexes (K_d = 1-100 μM [51]) and can partially be attributed to the relatively small buried surface area in domain-peptide interactions (200-500 *Å* [259]) compared to complexes involving two structured domains (2000 *Å* [260]). The linear motif in srGAP3 with the sequence RPPPMRPVRP is positioned at the end of the C-terminal region (residues 1053-1062, Fig. 7.1, p. 74) and carries properties of class I and class II peptides, which we assumed to be important in binding of SH3 domains with differing class preferences. Nevertheless, the motif must contain additional sequence features that allowed it to selectively bind the above-mentioned SH3 domains, but not all SH3 domains tested, such as the SH3 domain of the Abelson interactor 1 (data not shown) or the N-terminal SH3 domain of Grb2 (see results on Grb2 SH3N, 6.4.3, p. 63).

The SH3 domain of Amphiphysin was, for example, reported to specifically recognise class II motifs containing two arginines [239] that are accommodated by a negatively charged patch covering its binding surface [261]. Dynamin1 and Synaptojanin associate with the SH3 domain of Amphiphysin through such motifs (PSRPNR and PIRPSR, respectively [262]) and the resulting consensus sequence PxRPxR is also incorporated in the srGAP3 sequence (RPPPMRPVRP). Therefore, it is not surprising that Amphiphysin SH3 interacted with this multi-class SH3-binding motif in srGAP3. The affinity of this interaction is three times higher than the previously reported affinity of the Amphiphysin-Dynamin complex [263], rendering it to my knowledge the strongest interaction for this SH3 domain described so far.

The binding specificity of the SH3 domains of Endophilins was reported to be more complex [54, 262], with certain preference for class I motifs with an additional arginine in position +2 relative to the first proline in the PxxP core [54, 264]. This consensus is likewise present in the identified motif in srGAP3 (RPPPMRPVRP). The more extensively studied Endophilin-A1 can also recognise the Amphiphysin-binding class II motif in Dynamin1 (PSRPNR [262]) and, thus, might either recognise the same class II consensus sequence in srGAP3 as Amphiphysin or select the class I orientation. Interactions of Endophilin-A1 and Endophilin-A2 thermodynamically resembled each other (Tab. 6.5, p. 60), which might reflect similar complex interfaces. This might even be expected, as the two domains share a high degree of sequence identity (80 %) and the residues lining the canonical SH3 domain binding pocket are almost fully con-

served [265]. However, NMR-based binding studies would be required to fully understand the complex formation with the SH3 domains of Endophilins.

The interaction of Grb2 was mediated by its C-terminal SH3 domain, while the N-terminal SH3 domain might constitute a secondary interaction site that is able to recognise the same region, yet interacts with a different motif. Although I detected a weak binding signal in titrations of Grb2 SH3N and the PxxP-fragment, I obtained a similar signal with the mutated AxxA-fragment (compare Tab. 6.5, p. 60). These findings indicate either that the interaction was independent of the two mutated prolines or that the observed enthalpic change in titrations with Grb2 SH3N represented an unspecific signal. In the following paragraph, I will therefore discuss both possibilities, but mainly focus on the interactions mediated by Grb2 SH3C.

SrGAP3 has the ability to dimerise [163] and simultaneous binding of SH3N and SH3C to one srGAP3 dimer would somewhat be reminiscent of the Grb2/Sos1 complex, which is conversely governed by the N-terminal SH3 domain of Grb2 [266]. In this complex, Grb2 SH3N can bind to each of four motifs in Sos1 with high affinity, whereas SH3C only engages with the first motif in a low-affinity interaction [240]. Although one might expect that SH3N out-competes SH3C, simultaneous binding of both SH3 domains of Grb2 to Sos1 was found to be crucial for efficient activation of Ras signalling [240, 267–269]. Consequently, this model illustrates, how the secondary interaction site Grb2 SH3N in the Grb2-srGAP3 complex could become important in a specific functional context.

Similar to srGAP3, Grb2 possesses the ability to form dimers [163, 270, 271] and, thus, two Grb2 SH3C domains could bind to one srGAP3 dimer, which would resemble the Grb2/Gab1 complex [60, 272]. In this complex, Grb2 SH3C was shown to interact with two RxxKP motifs in Gab1 [60, 272], in which the RxxK core is crucial for binding [273]. This consensus is similar to the RxxRP motif contained in the srGAP3 sequence RPPPMRPVRP, in which the lysine is substituted by arginine. This amino acid exchange and the preference of Grb2 SH3C against prolines in position +1 relative to the first arginine [273] might explain, why this SH3 domain interacted with srGAP3 with a fivefold lower affinity than with Gab1, which contains the RxxK consensus (compare [273]). On the other hand, mutation of two proline residues (RPPPMRPVRP) instead of the two arginines abrogated binding in my experimental set-up, which suggests an entirely different interaction mechanism that is independent of the RxxR core. Again, additional experiments, such as mutational analyses or a structure determination of the complex, would be required to reveal the underlying mode of interaction.

The identified motif was - with only three exceptions - conserved among srGAP3 sequences, which suggests a general importance for the function of srGAP3 and might support the idea that the identified complexes universally occur in vertebrates (compare Results 6.4.3, p. 61). Noteworthy, srGAP1 also

contains a predicted multi-class SH3-binding motif at a different position within the CTR (relative position indicated in Fig. 7.1, p. 74). The motif with the sequence RGEPPPPVRRP is likewise conserved with only a few exceptions, but whether it indeed confers binding to SH3 domains remains to be demonstrated. Interestingly, two of the six srGAP1 sequences that lacked the motif at the conserved position (*Poecilia formosa* and *Danio rerio*), shared a multi-class motif with srGAP3 proteins at the end of the C-terminal region (compare Fig. 7.1, p. 74). Therefore, the precise location of SH3-binding motifs within the C-termini of srGAP1 and srGAP3 might, in addition to their amino acid sequence, be important for effective complex formation with SH3 domain-containing proteins. Apart from these two exceptions, srGAP1 and srGAP2 sequences are at this position devoid of typical class I and class II SH3-binding motifs or specific consensus sequences for Endophilins, Amphiphysin, or Grb2, which renders the interactions potentially specific for srGAP3. As linear motifs are often lost in paralogous sequences [45, 274], this finding might even be expected, but it is, of course, possible that srGAP1 and srGAP2 likewise employ this region for SH3 domain-dependent interactions via non-canonical proline-rich motifs.

Additional predicted proline-rich motifs with similar consensus sequences are absent from srGAP3, but whether the identified motif constitutes the only binding site within srGAP3 for these interaction partners awaits experimental demonstration. The associated question, whether the motif is also essential for the interaction in the context of full-length proteins, could be answered with the fluorescence-based Co-IP assay employing a mutated version of full-length srGAP3, in which the core proline residues of the motif are replaced by alanine.

In summary, I found a single SH3 domain-binding motif in the C-terminal region of srGAP3 that displayed a surprising flexibility in engaging in different SH3 domain-dependent interactions. The versatile, yet specific recognition of this motif by the SH3 domains of Endophilin-A1, Endophilin-A2, Amphiphysin, Grb2, and was potentially attributed to its multi-class nature as well as the presence of an additional arginine residue in the +2 position relative to the first proline in the PxxP core. Therefore, these results may provide an example how additional amino acids in conjunction with the canonical PxxP motif can contribute to the specificity in SH3 domain-mediated interactions.

7.2.2. 14-3-3-Dependent Interactions

The family of 14-3-3 proteins comprises seven isoforms in mammals (β, γ, ϵ, η, σ, θ/τ, and ζ), which share high sequence similarities [79] and bind to their targets as rigid, saddle-shaped dimers (reviewed in [81]). The C-terminal regions of srGAP1, srGAP2, and srGAP3 contain multiple linear motifs that are

predicted to confer binding to 14-3-3s and the association between these protein families in HEK293T cells has already been noticed by others [86, 207]. In contrast, ARHGAP4 proteins seem to have lost the ability to bind 14-3-3 proteins [207] and are devoid of predicted 14-3-3-binding motifs. In this project, I was able to show that srGAP3 also forms complexes with this protein family in the developing rat brain and could confirm the interaction in HEK293T cells. Moreover, I demonstrated that srGAP3 selectively bound the 14-3-3 isoforms γ and θ/τ in the latter cell type. In murine embryonic brain, srGAP3 was reported to represent a substrate for 14-3-3 ϵ [241], whereas it was unable to associate with this isoform in HEK293T cells. Therefore, 14-3-3-binding seems to be a general function of srGAP proteins and is conserved in different organisms and cell types, yet might depend on distinct 14-3-3 isoforms in different tissues, which is potentially related to tissue-specific phosphorylation patterns and binding sites (Fig. 7.1, p. 74) [242, 243].

Another level of complexity is added through the ability of 14-3-3 proteins to form homo- or heterodimers (Fig. 7.2, p. 78, reviewed in [79]). 14-3-3 γ, for example, prefers to bind targets in a homodimeric fashion, whereas 14-3-3 ϵ usually heterodimerises [275]. The formation of unfavourable and less stable homodimers of 14-3-3 ϵ [79] could thus also have prevented complex formation with srGAP3 in my assay.

From the work of Ivan Blasutig [207], it was known that the C-terminal region of srGAP3 is necessary for the interaction with 14-3-3s, but specific linear motifs remained undefined. In the majority of complexes, 14-3-3s bind to linear motifs featuring a phosphorylated serine or threonine residue [84, 85]; although all 14-3-3 isoforms were reported to recognise the canonical sequences *RSx[pS]xP* (mode I) and *Rx[F/Y]x[pS]xP* (mode II) [80], identified motifs of *in vivo*-ligands, like srGAP3, often diverge from this consensus (reviewed in [79]). In fact, numerous 14-3-3-binding motifs were predicted in the C-terminal region of srGAP3, but all belonged to the motif class with the divergent consensus *[RHK][STALV]x([ST])x[PESRDFTQ]* (class 3, Fig. 6.17, p. 69), which underlines the difficulty in predicting true 14-3-3-binding sites. Because of the high complexity of this interaction system with numerous predicted motifs, multiple 14-3-3 isoforms, and tissue-specific phosphorylation sites (see Discussion, 7.1), I restricted the analysis to predicted 14-3-3-interaction motifs that were phosphorylated in HEK293T cells as well as in the rat brain (compare Fig. 7.1, p. 74).

Employing the Co-IP assay in HEK293T cells, I found that phosphorylation of S858 and S919 in the C-terminal region of srGAP3 promoted complex formation with 14-3-3 γ and θ/τ (Fig. 7.1, p. 74). These residues are embedded in or lie adjacent to predicted 14-3-3-binding motifs and the respective motifs might therefore directly participate in the interaction. My bioinformatical analysis

further revealed that these motifs are universally conserved in srGAP3 sequences, which clearly argues for their importance. Nevertheless, mutation of these serine residues to alanine only reduced, but failed to fully abrogate binding, which points towards the presence of additional 14-3-3-binding sites and suggests a complex mode of interaction between srGAP3 and 14-3-3s. This would be in accordance with the findings of Blasutig [207], who noticed a gradual loss of 14-3-3-binding in co-immunoprecipitations with srGAP3 constructs that were stepwise truncated from the C-terminus.

Nevertheless, the two mutations S858A and S919A might physiologically affect the srGAP3/14-3-3 complex *in vivo*, since simultaneous binding of two motifs of one ligand molecule to a 14-3-3 dimer can be instrumental to the function of the respective protein complex (reviewed in [87]). The Bcl2-associated agonist of cell death (BAD) protein, for example, stably interacts through either of two motifs with 14-3-3s, but only if both motifs engage in the interaction at the same time, binding of BAD to BCL-X_L and therefore apoptosis is efficiently prevented [276]. This means that, although the two point mutations in srGAP3 were insufficient to abolish the interaction with 14-3-3 proteins due to the presence of additional motifs, either one of them could - in analogy to the BAD/14-3-3 complex - be important in a specific functional context (see 7.4.2 for further discussion of functional implications).

With truncated srGAP3 constructs, Blasutig [207] further mapped the binding region of 14-3-3 proteins to the residues 883 to 954 and the potential binding motif surrounding S858, which I identified in this project, lies N-terminal to that region. This finding demonstrates either the requirement of multiple attachment sites for stable complex formation [80] or a dependence of phosphorylation at S858 on sites located further downstream (see below, [85]). Mutation of S919 to alanine also resulted in impaired binding of 14-3-3 proteins to srGAP3, although this residue is positioned adjacent to, but not within a predicted 14-3-3-interaction site. These findings illustrate the difficulty of identifying true 14-3-3-binding sites *in vivo* through mutation of phosphorylation sites or truncated constructs (compare [85]). Although it is, of course, possible that the neighbouring motif of S919 forms direct contacts with 14-3-3s and is affected by this phosphorylation event, it is likewise conceivable that phosphorylation of S919 is part of a hierarchical phosphorylation system, in which phosphorylation of this primary site triggers phosphorylation of the actual 14-3-3-binding motif and therefore complex formation [85]. The forkhead in rhabdomyosarcoma (FKHR) protein, for example, is phosphorylated by protein kinase B (PKB) at S256, which in turn leads to phosphorylation at Thr24 and binding of 14-3-3 at this secondary site [277]. In order to unambiguously show that the motifs surrounding S858 and S919 represent bona fide 14-3-3-interaction sites, the complex formation with 14-3-3 proteins would have to be analysed *in vitro* employing phospho-peptides or *in vitro*-phosphorylated srGAP3-CTR.

This obviously poses the question which kinase(s) phosphorylate these sites *in vivo*. Usually, the amino acid sequence of the target motif determines the kinase specificity [278, 279] and 14-3-3 proteins typically recognise linear motifs that are phosphorylated on serine and threonine residues by basophilic kinases, for example PKA or PKB [78, 86]. Indeed, NetPhosK (http://www.cbs.dtu.dk/services/NetPhosK/) [280] predicts a preference for PKB and PKA at S858, but no phosphorylation at S919. Blasutig [207], on the other hand, reported that the complex formation between srGAP proteins and 14-3-3s depends on phosphorylation by protein kinase C, which is likewise known to phosphorylate 14-3-3 motifs [281]. As outlined above, it is again possible that hierarchical phosphorylation events come into play and, thus, it might be difficult to find the respective kinase, which directly phosphorylated the 14-3-3-binding motifs. How could this question be tackled experimentally? First of all, neuron-derived cell lines (e.g. Neuro2A) might depict model systems that are better suited to study brain-specific 14-3-3-interactions. If the phosphorylation pattern of srGAP3 in these cells matches its pattern in the rat brain, specific kinase inhibitors could be applied in the fluorescence-based Co-IP assay to obtain a set of relevant kinases, which could subsequently be tested in *in vitro* phosphorylation assays.

From the presented experimental results, it is clear that the C-terminal region of srGAP3 must contain additional 14-3-3-binding motifs, which might, for example, involve tissue-specific phosphorylation and binding sites, such as the predicted motif surrounding the HEK293T-specific phosphorylation site S932 or the brain-specific S1070 (Fig. 7.1, p. 74). This latter motif is especially interesting, since it is positioned close to the identified SH3 domain-binding motif and 14-3-3-binding at this site could either positively or negatively regulate SH3-dependent interactions through masking of the proline-rich motif or allosteric effects (compare [81] and section 7.4.2).

Alternatively, srGAP3 could engage unconventional binding motifs for the interaction with 14-3-3 proteins. Although phosphorylation of the ligand peptide is required in most 14-3-3-dependent interactions [85], exceptions to that rule have been reported [213–215]. The respective motifs either follow the canonical consensus sequence, but remain unphosphorylated [214, 282], or are entirely different and enriched in hydrophobic residues (e.g. GLLDALDLAS [215]). With respect to non-phosphorylated canonical consensus sequences, one motif in the C-terminal regions of srGAP proteins stands out: Only at a single site, srGAP1, srGAP2 as well as srGAP3 share the prediction for a 14-3-3-binding motif (S1030, Fig. 6.17, p. 69). The respective motif in srGAP3 follows the sequence RSSSSS (residues 1027-1032, Fig. 7.1, p. 74) and lacked any detectable phosphorylation in either HEK293T cells or rat brain. Since mass spectrometry can only provide a snapshot of the native phoshorylation state and the obtained sequence coverage will depend on a variety of factors, such as sample processing and the specific spectrometry method [283] or the origin, quality, or

type of protein to be analysed [242, 283], we might have simply failed to capture its phosphorylation. But even if this motif was unphosphorylated under native conditions, it would still depict a prime candidate for complex formation with 14-3-3s: Given the low sequence and positional conservation on the level of predicted binding motifs between the different srGAP paralogs, it would be truly surprising if this motif would have been kept intact without experiencing any evolutionary constraints related to its assumed function in 14-3-3-binding or would have been acquired by chance at exactly this position in all three paralogs. Whether the motif depicts a true 14-3-3-binding site, is certainly controversial and its location outside the predicted 14-3-3-binding region (see above, compare Blasutig [207]) argues against it. Other 14-3-3-binding motifs that are present upstream of this motif could, however, have acted as alternative binding sites in the absence of this motif in C-terminally truncated srGAP3, which might explain why it remained undetected in the experimental set-up of Ivan Blasutig [207] (Fig. 7.1, p. 74).

In summary, multiple motifs present in the C-terminal region of srGAP3 confer binding to 14-3-3 proteins, which might not only ensure a robust interaction even in the absence of single binding sites, but could also open up the possibility to dynamically modulate the interaction surface of srGAP3 through phospho-regulation of individual motifs through different kinases [284].

7.2.3. The Specificity Issue

Low affinities measured *in vitro* are always associated with the question, how the respective complexes can be specific or occur at all given the lower protein concentrations inside the cell and the high probability that a short motif will appear by chance in unrelated proteins [285]. The answer is that the cell can make use of a number of different mechanisms to facilitate their formation in the native context. First of all, through multimerisation, which is the shared feature of all interaction partners described in this work [95, 163, 270, 286, 287], initially weak monomeric interactions can be stabilised and therefore become relevant in the cell. In the same line of reasoning, the presence of several 14-3-3-binding sites in srGAP3-CTR might likewise positively affect the affinity of 14-3-3-involving complexes either through cooperative effects, when two motifs simultaneously bind to a 14-3-3 dimer [80], or local increase in binding site concentration in an avidity-guided fashion [288, 289].

Secondly, the proteins srGAP3, Endophilin-A1, Endophilin-A2, and Amphiphysin contain BAR domains, which represent membrane-interaction modules (see introduction on BAR domains, 1.1.3, p. 6) [95, 163], and membrane confinement is believed to facilitate the recognition of binding partners

through reduction of dimensions in a "matricity-driven" process [289]. Another important contribution to specificity comes from flanking regions of the motif, which not only help to improve the affinity through additional contacts, but can also prevent non-native interactions through steric hindrance [65]. This intimate connection between linear motifs and their flanking regions is additionally underlined by the finding that they evolve in a concerted fashion [290].

Although these mechanisms might guide the selective association of srGAP3 with the identified binding partners, it is still unclear, how srGAP3 could discriminate between three different SH3 domain-containing proteins, which bind to a single motif with similar affinities. It is, of course, possible that simultaneous binding of at least two interaction partners could be realised through multimerisation of srGAP3 [163]. Furthermore, the regulated and directional assembly of multi-protein complexes, in which the identified SH3-mediated interactions are expected to occur (see section 7.3, p. 89 for further discussion), might either promote or prevent individual interactions in the context of cooperative binding and ordered complex assembly [48].

Another important factor might be differences in local protein concentration [48], which can be regulated through a variety of mechanisms: Firstly, the localisation of signalling proteins rather seems to depend on active processes than mere diffusion [48]. Through active transport [291], restricted localisation via interaction partners (as for example through binding of srGAP3 to 14-3-3s, see 7.4.2, p. 93 for further discussion), or localised translation, which is especially important in neurons [292], the cell might impose a spatio-temporal regulation pattern onto individual srGAP3-containing complexes. Secondly, multivalent protein-peptide interactions have been reported to promote phase separation inside the cell [293], which has also been suggested for Grb2-involving protein complexes [294, 295]. Such phase separations via multivalent binding events have recently been shown to cluster surface receptors into microdomains thereby creating locally organised signalling zones [296]. These transitions will generate sharp and dynamic concentration gradients in a local environment and will probably affect binding affinities as well as binding kinetics of associated protein complexes [293].

Where and when the identified srGAP3-containing complexes occur inside the cell and whether they are mutually exclusive, remains to be elucidated, but they will likely depend on a complex panel of different regulatory mechanisms.

7.3. Transient Protein-Protein Interactions in Signal Transduction

Transient protein-protein interactions play crucial roles in cellular signalling pathways [36, 297] and are often mediated by adaptor modules, such as SH3 domains or 14-3-3s, which recognise short linear motifs with moderate affinity and variable specificity [32, 45, 285]. SrGAP3 was implicated in Slit-Robo signalling [151] through binding of its SH3 domain to a proline-rich region in the intracellular domain of Robo receptors [151] and its affinity for a Robo1-derived peptide was determined at a K_d of 5.6 μM [166]. In this project, I furthermore found that srGAP3 engages its C-terminal region and the linear motifs therein for interactions with SH3 domains that are characterised by similar weak affinities. Are there possibly reasons, why low affinities could be beneficial for signalling processes in general?

Protein-peptide interactions are entropically disfavoured due to the ordering of unstructured residues in an unfolded peptide [34, 50], which often results in low affinities and fast association/dissociation rates [34, 298–300]. This is a prerequisite for the formation of reversible and highly dynamic signalling complexes [34]. Additionally, such transient complexes mediated by linear motifs usually do not occur in isolation, but are part of large protein assemblies (compare 7.2.3, p. 87 and Fig. 7.2, p. 78), in which several low affinity interactions become stabilised through cooperative effects [45, 48] and thereby allow signal integration from different pathways for highly combinatorial and discrete decision making [45, 48, 49]. Cooperativity will also provide the basis for robust signalling systems [48] and robustness might also have been the underlying driving force for the stable association between 14-3-3s and srGAP3 even in the absence of individual binding motifs.

The question whether initially weak and promiscuous protein-peptide interactions could in principle be evolved into high affinity-complexes has been exemplarily answered with SH2 domains [301], which bind phosphorylated motifs with mediocre affinities [302]: Three mutations in the Fyn SH2 domain were sufficient to create a superbinder SH2 domain, which bound its ligands with about 340x higher affinity than its wild-type version [301]. This combination of mutations also efficiently turned other SH2 domains into superbinders, but, however, never occurs in this subcluss of SH2 domains in nature [301]. Could evolution have even selected against strong motif-mediated interactions [303]? As linear motifs can be acquired by chance in unrelated proteins [285] or be easily hijacked by pathogens [304], they might generally represent untrustworthy binding surfaces [303, 304]. Consequently, the low affinity could serve to protect the cell from deleterious off-target binding [303]. Therefore, it is possible that srGAP3 preferentially associates with several, but not all of the newly identified binding partners under native conditions. First evidence that some

of these complexes indeed occur *in vivo*, stemmed from the isolation of native srGAP3-containing complexes from rat brain lysate, in which we were able to identify Grb2 as well as 14-3-3 proteins (data not shown).

On the other hand, the described evolutionary flexibility of linear motifs, which is also reflected by the apparent lack in conservation between different srGAP paralogs, imparts evolutionary plasticity onto networks [303, 305] and leads to rewiring and tuning of the respective pathways [306]. Therefore, the potential ability of the C-terminal regions of paralogous srGAPs in binding different proteins might account - in addition to temporal and spatial regulation patterns [159] - for the functional diversity observed within this protein family [151–153, 155–157, 218].

Although direct evidence is still missing, we have good reasons to believe that the identified complexes also exist *in vivo*, since the identified transient protein-protein interactions mediated by linear motifs in the C-terminal region or by the SH3 domain of srGAP3 are in good agreement with the established principles of signal transduction in eukaryotes.

7.4. Functional Implications of the Identified Complexes

Correct neural development is required for normal brain function and regulated, among other signalling networks (reviewed in [307]), by the Slit-Robo pathway [148, 150, 307]. SrGAP proteins act downstream of Robo receptors [151] and a more general role at the intersection of signal transmission, actin cytoskeleton regulation, and membrane deformation during different steps of vertebrate neural development has been established (compare introduction on the function of srGAP3, p. 25) [127, 153–157, 161, 163–165, 308].

Using sensitive homology detection methods, I identified a remote srGAP ortholog in the genomes of the choanoflagellate *Salpingoeca rosetta* and the filasterean *Capsaspora owczarzaki*. These phyla of unicellular organisms represent the closest relatives to metazoans and possess the ability to form colonies as well as different cell types [206, 309]. They are, thus, at the boundary of multicellularity [310] and evidence is increasing that the processes driving cellular differentiation in these organisms are governed by homologous proteins participating in vertebrate signalling pathways and establishing the tissue architecture [310–315]. This finding would put srGAPs already at the onset of metazoan evolution, in which they might have been part of a set of proteins that was essential to establish and subfunctionalise inter-cellular networks, and further suggests a general importance of srGAPs in cellular differentiation.

Finally, my bioinformatic analysis furthermore revealed that paralogous srGAP sequences (srGAP1, 2, and 3, ARHGAP4) emerged in vertebrates. Although the paralogs share a role in neural development [151, 155, 161, 163, 316], they were found to be important for different steps of these processes [155, 157, 158, 163, 218]. This functional divergence partially arises from differential spatio-temporal regulation patterns [159, 160, 219], but might likewise depend on structural differences in protein domains that can, for example, result in unequal ligand-recognition specificities [127, 151, 308]. The presented results provide first examples on how srGAP3 could employ its C-terminal region in protein-protein interactions that are potentially specific for this paralogous subgroup. As a functional characterisation of these complexes was beyond the scope of this project, I will, in the following sections, develop working hypotheses for future projects that are mainly guided by known functions of the identified interaction partners.

7.4.1. Potential Functions of SH3 Domain-Mediated Complexes

As outlined above, srGAP3 associated in HEK293T cells and *in vitro* with the SH3 domain-containing proteins Endophilin-A1, Endophilin-A2, Amphiphysin, and Grb2 (compare Fig. 7.1, p. 74).

With respect to cellular functions, Endophilins and Amphiphysin belong to the clathrin-dependent endocytic machinery (compare introduction, Fig. 1.4, p. 12): Amphiphysin is the major binding partner of Dynamin in nerve terminals [317] and engages its SH3 domain for this interaction [239, 261, 262]. Overexpression of its SH3 domain was furthermore found to block receptor-mediated endocytosis by interfering with Dynamin recruitment [318]. Endophilins are likewise enriched in nerve terminals [264], where they bind Dynamin [264] and also Synaptojanin [262]. All of these srGAP3-binding partners have been implicated in synaptic vesicle endocytosis [317, 319, 320], whereas only Endophilin-A2 and Amphiphysin were additionally reported to regulate AMPA receptor trafficking at postsynaptic sites [321, 322].

Grb2 is implicated in growth factor receptor signalling, where it binds activated receptor tyrosine kinases and links them to Ras signalling through simultaneous binding of the Ras guanine-nucleotide exchange factor Sos1 [268, 269, 323–327]. Grb2 was also found to be involved in associated receptor-uptake mechanisms [328–330] and its general importance in developmental processes is underlined by its constant expression levels throughout neural development [331] and the severe phenotype of Grb2 knockout mice, which die after embryonic day 7.5 [332].

The common theme present in the functional repertoire of these binding partners thus seems to be their involvment in endocytic processes. Endocytosis is not only important at presynaptic sites to balance synaptic vesicle release [333], but also affects the position and the amount of neuronal receptors at the entire cell surface [3]. Receptor-uptake can serve to adjust the responsiveness of a neuron to guidance cues [13, 16, 17] and has been found to be essential for signal transduction itself in certain cases (e.g. TGFβ [18, 334] or G-protein-coupled receptors [335]). Therefore, I would speculate that srGAP3 recruits the endocytic machinery through its association with Endophilins, Amphiphysin, or Grb2 to activated receptors to trigger their uptake and downstream signalling, for example via Ras. Another possibility is the recruitment of Endophilins and Amphiphysin at presynaptic sites for the regulation of synaptic vesicle endocytosis. In fact, recruitment of endocytic factors by GAP proteins has already been described: Oligophrenin-1, which is a BAR domain-containing RhoGAP protein of the GRAF family [336], was reported to recruit Endophilins at pre- and postsynaptic sites, thereby controlling synaptic vesicle endocytosis and AMPA receptor uptake [337, 338]. Similar to srGAP3, Oligophrenin-1 employs a single proline-rich motif, which contains internal and flanking positively charged amino acids (aa 739 - 750, RPPVRPPDPPCR) and is located at the end of a putatively disordered C-terminal region, for binding the SH3 domains of these proteins [337, 338]. Therefore, these findings not only support the relevance of my identified srGAP3 complexes *in vivo*, but also suggest a more general mechanism, by which certain GAP proteins can recruit endocytic factors through C-terminal SH3 domain-binding motifs.

It will, undoubtedly, be difficult to identify the respective receptors, but the Robo family surely constitute prime candidates, as srGAP3 was reported to bind via its SH3 domain to the intracellular domains of Robo1 and Robo2 [152]. The Slit/Robo pathway regulates midline crossing of axons [148, 149, 339, 340] and srGAP3 has been implicated in the positioning of post crossing axons in the ventrolateral funiculus through a functional interplay with Robo receptors, although the precise mode of action remained unclear [152]. Robo receptors are also endocytosed [341], but so far nothing is known about the uptake mechanism and its impact on Robo signalling.

Another potential target for srGAP3-mediated receptor uptake could be the gamma-amminobutyric acid A ($GABA_A$-)receptor, since srGAP3 was found to be important for its clustering at inhibitory synapses in the CA1 region of the Hippocampus (specifically in the stratum radiatum) through an interaction of srGAP3's SH3 domain with Gephyrin [248]. The regulation of surface levels of the $GABA_A$-receptor through endocytosis and recycling is required for its function [342], but the uptake mechanism and involved downstream factors are unknown. Importantly, Endophilin-A2 is also expressed in this brain region [264] and it could be possible that srGAP3 might not only regulate clus-

tering, but also endocytosis of the $GABA_A$-receptor through the recruitment of Endophilin-A2.

How could a general hypothesis of uptake be tested? It would be possible to compare surface receptor levels of neuronal cells (e.g. Neuro2A, [153]) that overexpress srGAP3 wild-type to those carrying a mutated srGAP3-construct, in which the two core proline residues are exchanged to alanines (see Fig. 6.15B, p. 62). Since probably all neuronal cells will contain endogenous srGAP3 (compare [145, 153, 160]), a parallel knockdown of the endogenous srGAP3 wild-type might be required. Moreover, endocytosis and subsequent recycling might be restricted to activated receptors and, thus, it could be necessary to treat the cells with activating factors, such as the Slit protein (compare introduction on the Slit-Robo pathway, p. 25) [151, 343]. Evidence for complex formation between srGAP3 and the identified endocytic proteins could furthermore stem from co-localisation experiments before and after treatment with activating factors or in presence or absence of the interfering srGAP3 PxxP-fragment. As the expression level and pattern of srGAP3 is developmentally regulated [157, 159, 160, 344], a comprehensive co-localisation study from different neuronal stages and regions would additionally be required to track these complexes *in vivo*.

On the basis of the presented results, it is therefore possible to deduce clear working hypotheses regarding functional implications of the identified complexes, which might argue for their existence *in vivo*. In summary, my results not only revealed a link between srGAP3 and the endocytic machinery as well as the Ras signalling pathway, but also provided evidence that the C-terminal region carries an adaptor function to connect srGAP3 with different cellular networks.

7.4.2. Potential Functions of 14-3-3-Mediated Complexes

14-3-3 proteins are expressed in all eukaryotic cells and involved in numerous cellular pathways, such as apoptosis, metabolism, cell cycle progression, or transcription, in which they regulate the activity of their binding partners through various mechanisms (reviewed in [78]). How could they specifically affect the function of srGAP3?

Firstly, the relatively rigid 14-3-3 dimer (compare introduction, Fig. 1.2, p. 7) [84] is believed to impose its structure onto ligands upon binding [81] and could thereby lock the flexible C-terminal region of srGAP3 in a specific conformation [345]. The resulting disorder-to-order transition [87, 345–347] could either affect srGAP's affinity for other binding partners via allosteric effects [345] or increase its half-life through shielding of disordered residues [348], which might otherwise accelerate its degradation [349].

Secondly, 14-3-3s could orchestrate the interactions of srGAP3 with other proteins through exposing or masking of binding sites in response to different incoming signals [276, 350, 351]. As outlined above (see 7.2.2, p. 83), this aspect might be especially relevant to the predicted binding site S1070 (see Fig. 7.1, p. 74), which is located adjacent to the identified SH3-binding motif. Moreover, the subcellular localisation of srGAP3 changes from cytoplasmic to nuclear in older cell stages [159, 221] and 14-3-3 proteins could assist in establishing this distribution pattern, for example through masking of nuclear localisation signals [352], which were proposed to reside in the C-terminal region [221].

Thirdly, dimeric 14-3-3 proteins might act as bridging adaptors [79, 81] by tethering otherwise non-interacting proteins to srGAP3. Although this function of 14-3-3s is only weakly supported by experimental data compared to other assigned functions [80, 81, 353–355], it potentially explains the occurrence of certain false-positive candidates in the initial pull-down experiment that might have been pulled down indirectly through a 14-3-3 dimer (e.g. EB1, see Fig. 7.2, p. 78).

How could these hypotheses be analysed experimentally? A relatively simple approach would involve the overexpression of the inhibiting R18 peptide that was found to interfere with all 14-3-3 interactions inside the cell [86, 356, 357]. Although the system would be completely dysregulated and validation experiments would be required to demonstrate direct effects on the interaction between 14-3-3s and srGAP3, this approach might nonetheless provide first inside into the functional repertoire of these protein complexes. It would, for example, be possible to analyse changes in the subcellular localisation of srGAP3 or to measure its stability over time in different cell types. Whether 14-3-3s also affect the ability of srGAP3-CTR to bind SH3 domains, could be tested with co-immunoprecipitation or co-localisation experiments in presence or absence of the R18 peptide.

In any case, a functional analysis of srGAP3/14-3-3 complexes will either support a role of the C-terminal region in establishing the spatio-temporal regulation pattern of srGAP3 [221] or provide a solution to the question how the availability of linear motifs and therefore complex formation through the C-terminal region could be finely tuned for specific cellular functions.

7.5. Is the C-Terminal Region of SrGAP3 Natively Unstructured?

Intrinsic disorder describes a set of very different conformational states of polypeptide chains, which can range from the absence of any recognisable structure

over partially folded elements to molten or collapsed globules, which are reasonably stable [37]. Despite of this diversity, they all share the lack of a classically folded tertiary structure with a hydrophobic core [37].

My bioinformatic analysis demonstrated that none of the investigated C-terminal sequences of srGAP proteins contain - apart from short helical or coiled-coil segments - predicted secondary structure elements that are likely to be combined in a fixed 3D-structure. Conversely, disorder was reliably predicted over the full CTR with exception of regions that might harbour secondary structure elements. Furthermore, sequences of C-terminal regions clustered according to the phylogenetic relationship, which would be expected from sequences experiencing few evolutionary constraints in sequence space. This characteristic is often, but not necessarily a trait of disordered regions [358] and might be restricted to exposed residues that are located outside of interfaces [359–361] or "functional hot spots" [362]. Linear motifs represent such "functional hot spots", are enriched in disordered segments [217], and database searches revealed that they are likewise enriched in the C-terminal region of human srGAP3. Moreover, I was able to validate at least two of the predicted motifs experimentally. Taken together, the bioinformatical analysis strongly supports the hypothesis that the C-terminal region of srGAP3 and srGAP proteins in general is intrinsically disordered.

Nevertheless, it was impossible to prove this hypothesis experimentally, since the instability of srGAP3-CTR precluded a structural analysis (compare Results 6.4.1, p. 57). At the same time, this finding also argues for its disordered state, whereby its high flexibility might have made it amenable to protease cleavage [363–365]. Such faster degradation kinetics of unstructured regions [349] are used inside the cell as a means to regulate the abundance of intrinsically disordered proteins [366]. The analysis of intrinsic disorder is experimentally challenging, but accessible through NMR or CD spectroscopy in conjunction with functional studies [40]. In more recent examples, single-molecule Förster resonance energy transfer (smFRET) has been applied to specifically investigate conformational ensembles of intrinsically disordered regions [367] or folding upon binding [368]. Due to the instability of the full CTR, I mainly employed smaller fragments for *in vitro*-experiments that covered the full length of the CTR with the exception of the predicted coiled-coil segment. All of these fragments were highly soluble and exhibited considerable heat stability (data for residues 904-954, 810-910, 995-1079 not shown), which is a general characteristic of natively disordered regions due to the lack of extensive secondary and tertiary contacts [37].

Furthermore, disordered segments have been reported to be enriched in phosphorylation sites (reviewed in [37]). As part of our interaction studies with 14-3-3 proteins, we analysed the phosphorylation pattern of endogenous srGAP3 from rat brain and found that it was almost exclusively phosphorylated

in the C-terminal region. Although conclusive experimental evidence is still missing, it can be concluded from all of this evidence that the C-terminal region of srGAP3 likely depicts a natively unstructured region.

Part II.

Regulation of Syndapin1 by EHD1

8. INTRODUCTION

Vesicle trafficking relies on a complex machinery of membrane-interacting and -bending proteins as well as factors involved in actin cytoskeletal dynamics and microtubular transport [23, 27]. F-BAR proteins, such as Syndapins (for synaptic Dynamin-associated protein [369]), have been suggested to interconnect these processes *in vivo* [370, 371]. The proteins of the Syndapin family, which are also termed PACSINs (for Protein Kinase C and Casein Kinase 2 substrate in neurons [372]), are conserved in metazoa [373] and comprise the paralogs Syndapin1, Syndapin2, and Syndapin3 in mammals [369, 372–376], which have differential expression patterns: Syndapin1 constitutes the brain-specific isoform, whereas Syndapin2 is ubiquitously expressed and Syndapin3 is found in heart, lung, and muscle [376]. They share a conserved domain architecture with an N-terminal F-BAR domain followed by a variable linker region and a C-terminal SH3 domain (Fig. 8.1E, p. 101) [369, 372].

Via the SH3 domain, all Syndapin isoforms were found to bind the endocytic proteins Dynamin and Synaptojanin as well as the Arp2/3-complex activator N-WASP (neuronal Wiskott-Aldrich syndrome protein), which promotes actin polymerisation [369, 375, 376] (compare introduction on endocytosis 1.2.1, p. 10, and actin polymerisation, section 1.2.2, p. 11). For this reason, Syndapins were suggested to function at the intersection of endocytic processes and actin dynamics [371, 375, 377]. Although Syndapins share a role in membrane trafficking, individual isoforms have been implicated in different endocytic pathways (reviewed in [378]). Syndapin1, in particular, participates in activity-dependent bulk endocytosis, which is launched upon repetitive neuronal stimulation (compare general introduction, p. 1) [379].

Targeting of Syndapin1 to membranes depends on its F-BAR domain (see introduction on lipid binding domains, section 1.1.3, p. 6) [99–101, 130]. Like conventional F-BAR domains, the F-BAR domain of Syndapin1 forms an elongated dimer (compare Fig. 1.3, p. 9), but due to strongly kinked tips it possesses a unique tilde shape (Fig. 8.1A, p. 101) [92, 99]. In contrast to conventional F-BAR architectures, this results in a doubly bent membrane binding surface (Fig. 8.1D, p. 101), which enables stabilisation of various curvature types [99, 130, 131]. A hydrophobic wedge loop (Fig. 8.1A, p. 101), which is believed to insert into one leaflet of the bilayer, acts in concert with the curved surface to drive Syndapin1-dependent membrane deformations (see introduction on deformation mechanisms, p. 8) [99].

Artificial liposomes often serve as a model system to study BAR domain-mediated membrane-bending *in vitro*. The F-BAR domain of Syndapin1 has been shown to deform such liposomes into tubules (Fig. 8.1F, p. 101) [99, 100, 130], but this activity is downregulated in the full-length protein through an autoinhibitory clamp between the SH3 and F-BAR domain (Fig. 8.1A-E, p. 101) [130]. The autoinhibition can be released through binding of ligands to the SH3 domain, which leads to prominent tubulation of liposomes [130]. Since the binding surface for the F-BAR domain overlaps with the canonical SH3-binding pocket, SH3 domain ligands probably activate Syndapin1 through a displacement mechanism (Fig. 8.1C, p. 101) [130].

A flexible linker connects the F-BAR domain with the SH3 domain and this region is, compared to the globular domains, most divergent between different Syndapin isoforms [129]: The linker does not only vary in length and amino acid sequence, but also in the number of contained Asn-Pro-Phe (NPF) motifs, which can range from zero in Syndapin3 to three in Syndapin2 (Fig. 8.2, p. 102). NPF motifs mediate binding to EH domains [72] and - in case of Syndapins - to the EH domains of the EHD (for EH domain-containing [380]) family of proteins [129, 381] (compare introduction on EH domains, subsection 1.1.2, p. 5). Moreover, both NPF motifs of Syndapin1 were found to be required for a stable association with EHD1 [129].

In mammals, the EHD family of proteins consists of four paralogs (EHD1-4) [380, 382–384], which have been implicated in various types of membrane trafficking at the plasma membrane and endosomal compartments (compare introduction, Fig. 1.1, p. 3 for description of the endosomal system) [22, 384]. EHD1, in particular, was found to be important for recycling of cargo from the endocytic recycling compartment (ERC) back to the plasma membrane [385–388]. However, it might possess a divergent function in neurons, as it mainly labelled early endosomes in this cell type and was required for cargo-specific endocytosis [18, 388, 389]. EHD proteins are composed of a G-domain, which structurally resembles the GTPase-domain of Dynamins, yet is specific for ATP, followed by a helical domain, and a C-terminal EH domain (Fig. 8.3A, p. 103) [390]. Furthermore, EHD proteins can form homo- and heterodimers [384, 390–392] via their G-domain and the EH domain-binding pocket is occupied by an internal Gly-Pro-Phe (GPF) motif located in a linker connecting the helical domain with the EH domain (Fig. 8.3B, p. 103) [390]. The structural and biophysical characterisation of the isoform EHD2 suggests that EHD proteins assemble in ring-like fashion around membrane tubes and promote curvature generation by inserting the tips of their helical domain in a wedging mechanism into the lipid bilayer (Fig. 8.3B-D, p. 103) [390, 393]. Moreover, membrane-binding released the ATPase-activity of EHD2, but the hydrolysis rate was 600x slower than the GTP-hydrolysis rate of Dynamin [386, 390]. Despite this low activity, EHD proteins have been suggested to act as “pinchases” at endosomal compartments in analogy to Dynamins in endocytic processes (see introduction on

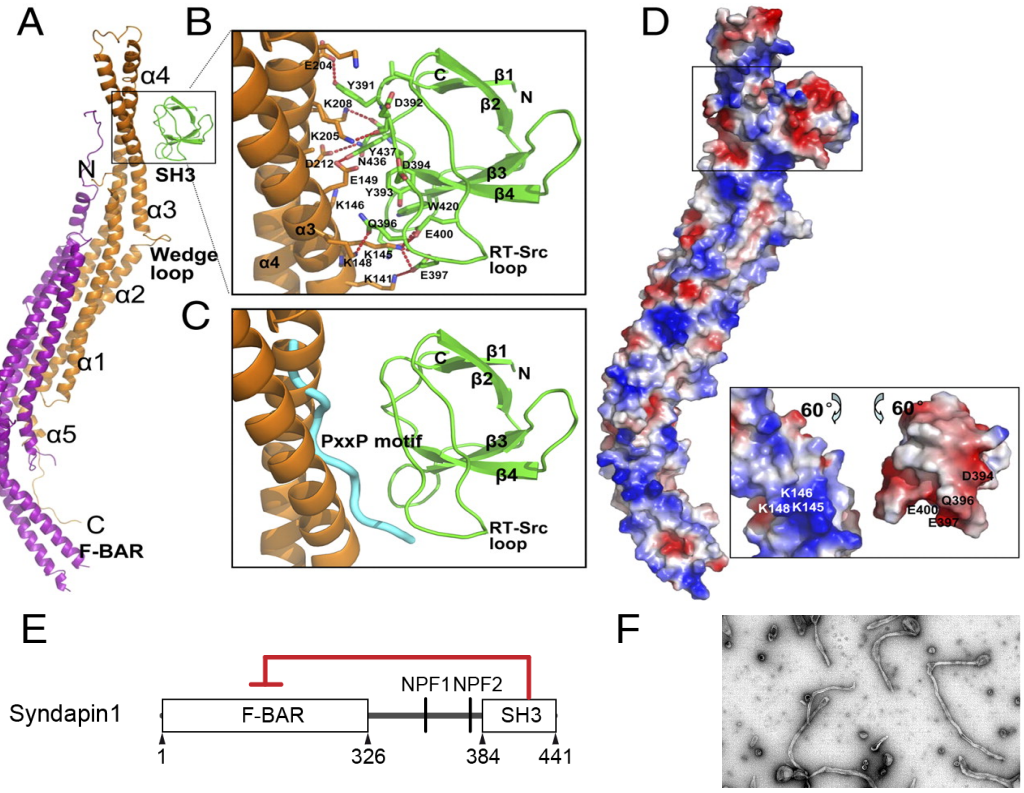

Figure 8.1.: The F-BAR domain of Syndapin1 is autoinhibited by an interaction with the SH3 domain. The structure of full-length Syndapin1 is shown (PDB ID 2X3W and 2X3X). **A:** Syndapin1 in secondary-structure representation. The F-BAR domain monomers are depicted in gold and purple, respectively, whereas the SH3 domain is shown in green. The N and C termini as well as the secondary-structure assignment, and the wedge loop are only marked on one chain. **B:** Close-up of the interface between the F-BAR domain and the SH3 domain. The β-strands of the SH3 domain are labelled according to the conventional nomenclature (see introduction on SH3 domains, 1.1.2, p. 5). Residues involved in binding are represented as sticks and polar contacts as red dashed lines. **C:** The peptide (blue) derived from the proline-rich region of Dynamin1 is modelled into the expected PxxP-binding groove of the SH3 domain. **D:** Coloring of the protein surface according to the electrostatic potential: red (negative) through white (neutral) to blue (positive). The lower panel depicts an open-up view of the interface. Important residues that were mutated in functional assays are labelled. Note, that the interface is mainly composed of positively charged residues in the F-BAR and negatively charged residues in the SH3 domain. **E:** Domain architecture of mouse Syndapin1 (GI: 557948024). **F:** Electron micrograph of phosphatidylserine-liposomes incubated with Syndapin1 F-BAR. F-BAR, Fes-Cip4-homology-BAR (Bin-Amphiphysin-Rvs) domain; SH3, Src-homology 3 domain; NPF, peptide motif composed of Asn-Pro-Phe. The domain boundaries are indicated. Panel A-D and F as well as the figure legend were adopted from Rao *et al.* [130].

```
Syndapin1  NATGAVEST--SQAGD---------------------------------      (337)
Syndapin2  GINQTGDQSGQNKPGSNLSVPSNPAQSTQLQSSYNPFEDEDDTGSSISEKE    (378)
Syndapin3  SIVPTRDGT--APPPQ---------------------------------      (337)

Syndapin1  ---RGSVSSYDRGQTYATEWSDDESGNPFGGNEANGGANPFEDD---AKG     (384)
Syndapin2  DIKAKNVSSYEKTQTYPTDWSDDESNNPFSSTDANGDSNPFDEDTTSGTE    (428)
Syndapin3  -----SPSSPGSGQ--DEDWSDEESPRK--------------V---ATG     (365)
```

Figure 8.2.: The linker region of mouse Syndapin1 and Syndapin2, but not Syndapin3 contain NPF motifs. MSAProbs [178] alignment of mouse Syndapin sequences (Syndapin1, GI: 557948024; Syndapin2, GI: 226958422; Syndapin3, GI: 576067844). Conserved positions are highlighted in grey and similar residues are printed in bold. NPF motifs are displayed in red. The full variable region of mouse Syndapins is shown.

endocytosis, p. 10) [390, 394] and ATP hydrolysis was indeed found to be necessary for EHD-mediated vesiculation of membranes *in vivo* [390] and *in vitro* [394, 395], although direct experimental evidence is still missing.

Complex formation of EHD1 with either Syndapin1 or Syndapin2 is necessary for membrane trafficking and receptor recycling, as overexpression of either Syndapin's variable linker region or the EH domain, which both interfere with the interaction, impaired transferrin receptor uptake [129]. The complex labels tubular and vesicular structures in HeLa cells and co-distributes at postsynaptic sites in primary hippocampal neurons [129]. Further evidence for a function in recycling stems from studies in *Caenorhabditis elegans*, in which Syndapin1 and EHD1 colocalise on recycling endosomes [396]. However, the specific role of the Syndapin1-EHD1 complex in neurons as well as molecular mechanisms associated with its function remain to be elucidated.

In order to gain further insight into membrane rearrangements of Syndapin1 in presence of its binding partner EHD1, we reconstituted this complex on artificial membranes *in vitro*.

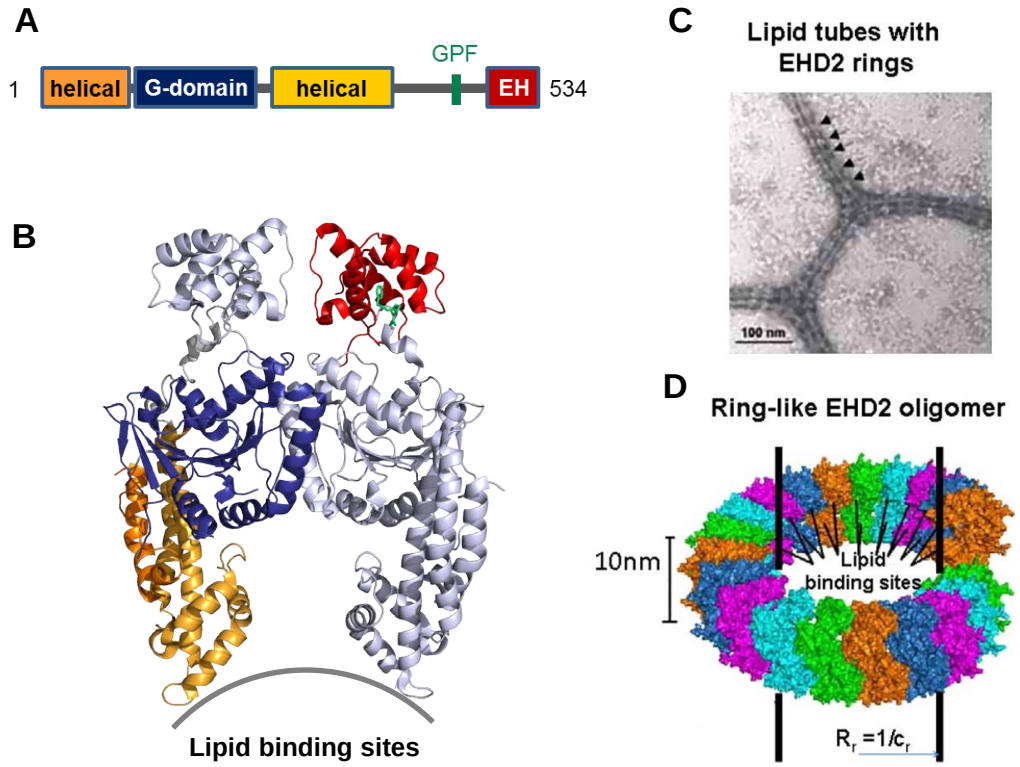

Figure 8.3.: Structural model of EHD2. **A:** Domain architecture of EHD proteins. G domain, GTPase domain (ATP-specific in EHD proteins [390]); Helical, helical domain; EH, Eps15-homology domain. The location of the Gly-Pro-Phe (GPF) motif, which occupies the EH domain-binding pocket, is marked. **B:** Structure of the EHD2 dimer in the presence of the nonhydrolyzable ATP analog AMPPNP (PDB ID: 2QPT) **C:** Electron micrograph of phosphatidylserine-liposomes incubated with EHD2. **D:** Structural model of an oligomeric ring of EHD2 on lipid tubes derived from the crystal structure. Panel C and D were adopted from Daumke *et al.* [390].

9. MATERIALS AND METHODS

9.1. Cloning Strategies and DNA Constructs

The Syndapin1 clone was obtained from BioCat Gmbh (Heidelberg). For expression in *E. coli*, mouse Syndapin1 (residues 1-441) was cloned into pGEX6P1 and pGEX4T1 (GE Healthcare). The construct for the Syndapin1 F-BAR domain was obtained by introduction of a stop codon after aa 326 of Syndapin1 by site-directed mutagenesis of pGEX4T1-Syndapin1. Syndapin1 ΔSH3 (aa 1-384) and the linker region between the F-BAR domain and the SH3 domain (aa 327-384) were cloned into pGEX4T1. The NPF motifs in Syndapin1 were mutated to AAA by two consecutive rounds of site-directed mutagenesis. The clone for human EHD1 was obtained from BioCat Gmbh (Heidelberg). Full-length EHD1 (residues 1-534) was cloned into the pET_Trx_1b vector (provided by Gunter Stier, Heidelberg), which contained a N-terminal thioredoxin-tag followed by a His_6-tag. The mutant EHD1 W485A, in which the conserved tryptophan in the EH domain-binding pocket was replaced by alanine, was obtained by site-directed mutagenesis. The EH domain of mouse EHD1 (residues 438-534) was cloned into pGEX6P1. An overview of all constructs and primers can be found in the appendix (Tab. C.1, p. 170).

9.2. Protein Expression and Purification

Syndapin1 full-length, **Syndapin1** ***mNPF*** and **EHD1 EH** were expressed as GST-fusion proteins in *E. coli* BL21 Gold (DE3) cells. Protein expression was induced with 0.5 mM IPTG and the cells were harvested after 5 h at 28 °C. The cells were lysed in 50 mM Tris/HCl (pH 8.0), 300 mM NaCl, 4 mM DTE, 4 mM Benzamidine, 2 mM EDTA, as well as cOmplete Protease Inhibitor Cocktail (Roche) and the cleared lysate was applied to a Glutathione Sepharose 4B column (GE Healthcare). After washing with a high salt buffer (1 M NaCl), bound protein was eluted in a linear GSH gradient and the free protein produced by incubation with PreScission protease (GE Healthcare). GST was removed with a second affinity column and the flow-through, which contained the target protein, subjected to size exclusion chromatography (Superdex 200 for Syndapin1 full-length, Superdex 75 for EHD1 EH) in 50 mM Tris/HCl (pH 8.0), 150 mM NaCl, 2 mM DTE, and - in case of EHD1 EH - 2 mM $CaCl_2$.

Syndapin1 full-length, Syndapin1 *mNPF* and EHD1 EH were concentrated to 24 mg/ml, 9 mg/ml, and 32 mg/ml, respectively.

The **Syndapin1 Linker**, **Syndapin1 F-BAR**, and **Syndapin1 ΔSH3** constructs were also expressed as GST-fusion proteins in *E. coli* BL21 Gold (DE3) cells with the same protocol as employed for full-length Syndapin1. The crude extracts were applied to a Glutathione Sepharose 4B column in 50 mM Tris/HCl (pH 8.0), 300 mM NaCl, 4 mM DTE, 4 mM Benzamidine, 2 mM EDTA, and cOmplete Protease Inhibitor Cocktail, washed with a high salt buffer (1 M NaCl), and eluted in a linear GSH gradient. DnaK, which often co-purifies with unfolded peptides, was removed from Syndapin1 Linker protein pools according to Thain *et al.* [199]. The GST-tag was cleaved off with Thrombin (Sigma) during dialysis in 50 mM Tris/HCl (pH 8.0), 50 mM NaCl, 2 mM DTT, and 2 mM $CaCl_2$ and removed with a second affinity column. Subsequently, the protein was bound to an anion exchange column (Source Q, GE Healthcare) and eluted in a linear salt gradient. The eluates were subjected to size exclusion chromatography (Superdex 75 for Syndapin1 Linker, Superdex 200 for Syndapin1 F-BAR and ΔSH3) in 50 mM Tris/HCl (pH 8.0), 300 mM NaCl, and 2 mM DTT. The final protein pools of Syndapin1 Linker, Syndapin1 F-BAR, and Syndapin1 ΔSH3 were concentrated to 29 mg/ml, 23 mg/ml, and 11 mg/ml, respectively.

EHD1 and **EHD1** ***W485A*** were expressed in *E. coli* Rosetta 2 (DE3) cells. Protein expression was induced with 0.5 mM IPTG and the cells harvested after 16 h at 22 °C. The bacteria were lysed in 20 mM Hepes (pH 8.0), 400 mM NaCl, 1 mM $MgCl_2$, 2.5 mM β-Mercaptoethanol, 1 % NP-40, as well as cOmplete Protease Inhibitor Cocktail and the cleared lysate applied to a Ni Sepharose (GE Healthcare) column. After washing with high salt buffer (1 M NaCl), the fusion protein was eluted in a linear imidazole gradient. The thioredoxin- and His_6-tags were removed by incubation with Tobacco Etch Virus protease during dialysis against 50 mM Tris/HCl (pH 8.0), 50 mM NaCl, and 2 mM DTE. Since the protein precipitated at 4 °C, the dialysis as well as all subsequent steps were carried out at 23 °C. The free protein was further purified with anion exchange chromatography and eluted in a linear salt gradient. The fractions containing the target protein were applied to a Superdex 200 column in 50 mM Tris/HCl (pH 8.0), 300 mM NaCl, and 2.5 mM β-Mercaptoethanol and EHD1 and EHD1 *W485A* concentrated to 35 mg/ml and 11 mg/ml, respectively.

9.3. Lipid Biochemistry Methods

9.3.1. Liposome Preparation

Total lipid extract from bovine brain (Folch I fraction) from Avanti (131101) and Sigma (B1502) were mixed 1:1 in chloroform and supplemented with 1 % (w/w) PtdIns(4,5)P_2 (Sigma, P9763) as well as 1 % (w/w) Rhodamine-labelled phosphatidylethanolamine (PE, Avanti, 810150) (modified lipid mix from [397]). The Endomix (protocol provided by Felix Wieland, Universität Heidelberg) was prepared with 35 mol% Cholesterol (Avanti, 700000), 10 mol% sphingomyelin (Avanti, 860062), 10 mol% PE (Avanti, 840026), 10 mol% phosphatidylserine (PS, from Avanti, 840032), 5 mol% phosphatidylinositol (Avanti, 840042), 25 mol% phosphatidylcholine (PC, from Avanti, 840055), and 5 mol% PtdIns(4,5)P_2 (Sigma, P9763). Lipids were dried at 37 °C under a N_2-stream and residual solvent removed in a vacuum manifold for 16 h. The dried lipid film was hydrated for 3 h at 37 °C in 20 mM Hepes (pH 7.5), 140 mM KCl, 10 mM NaCl, 1 mM $MgCl_2$ to yield a final lipid concentration of 5 mg/ml for Folch I liposomes and 4 mM for Endomix liposomes. Multi-lamellar liposomes were produced by nine freeze-thaw cycles with liquid nitrogen and a water bath at 37 °C [398, 399] and the liposome solution was stored at -80 °C until further usage. For co-pelleting and tubulation assays, small unilamellar vesicles were produced by sonication for 3 min [97, 131], which yielded a clear solution.

9.3.2. Liposome Co-Pelleting Assay

The liposome co-pelleting assay was performed as described by Goh *et al.* [131]. In particular, 0.5 mg/ml sonicated Folch I liposomes were mixed with 5 to 100 µM of protein in 20 mM Hepes (pH 7.5), 140 mM KCl, 10 mM NaCl, 1 mM $MgCl_2$ and incubated for 15 min at 25 °C. Liposomes were pelleted by centrifugation at 87000 rpm for 15 min at 20 °C and the supernatant and pellet fractions analysed by SDS-PAGE. Quantification of protein bands was performed with the FusionCapt Advance software (Vilber Lourmat). For this purpose, the amount of protein in supernatant or pellet was calculated as percentile of the summed intensities of both fractions (100 %).

9.3.3. Liposome Tubulation Assay

For investigation of the tubule formation potential of individual proteins and protein complexes, 0.25 mg/ml sonicated Folch I liposomes or 200 µM sonicated Endomix liposomes were incubated with 10 to 1000 µM protein in 20 mM Hepes (pH 7.5), 140 mM KCl, 10 mM NaCl, 1 mM $MgCl_2$ for 20 min

at 25 °C, spotted onto glow-discharged carbon-coated copper grids with picoloform film, and incubated for additional 10 min. The solution was removed by blotting, the grid washed once with buffer, and the specimen was stained by incubation with 1 % filtered uranyl acetate solution for 45 sec. Excessive liquid was removed by blotting and the samples were imaged with a TECNAI Spirit transmission electron microscope (FEI). Tubule diameters were quantified with Fiji [204] and statistically analysed with SigmaPlot (version 12.3, Systat Software Inc.).

9.4. Isothermal Titration Calorimetry

All measurements were carried out at 20 °C and the ligand was titrated under constant stirring at 300 rpm into the cell (cell volume 1.4295 ml) in 28 steps of 10 µl, and a spacing between titration steps of 240 sec. 180 to 300 µM ligand were titrated into 18 to 30 µM protein solution. Prior to measurements, all proteins were extensively dialysed against 50 mM Tris/HCl (pH 8.0), 150 mM NaCl, and 0.5 mM tris(2-carboxyethyl)phosphine.

10. RESULTS

Syndapin1 is an accessory protein in dynamin-dependent endocytosis [371, 375, 400] and has - via its association with EHD1 - also been implicated in endocytic receptor recycling [129]. How the latter protein complex carries out its function on a molecular level is not understood and, therefore, we specifically wanted to investigate how binding of EHD1 affects the membrane sculpting potential of Syndapin1 by reconstituting this protein complex on artificial liposomes.

10.1. Production of Proteins

We purified mouse Syndapin1, human EHD1, as well as different fragments thereof (Fig. 10.1) from bacteria expressing these proteins. Since mouse and human EHD1 have an amino acid sequence identity of over 99 % and, we expected that the results of our experiments would not be influenced by the hu-

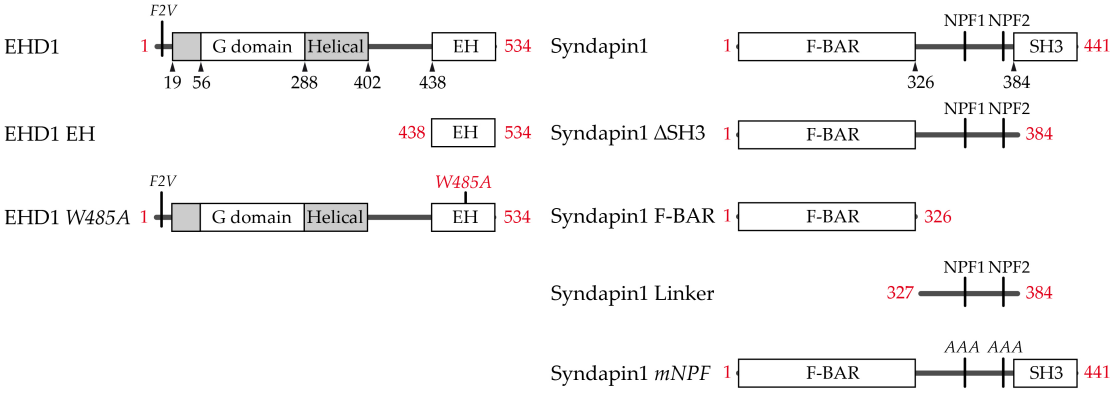

Figure 10.1.: Domain architecture of EHD1 and Syndapin1. Protein constructs of EHD1 and Syndapin1 used in this study. Mutations are indicated in italics. G domain, GTPase domain (ATP-specific in EHD1 proteins [390]); Helical, helical domain that composes the membrane interaction surface [390]; EH, Eps15-homology domain; F-BAR, Fes-Cip4-homology-BAR (Bin-Amphiphysin-Rvs) domain; SH3, Src-homology 3 domain; NPF, peptide motif composed of Asn-Pro-Phe. The domain boundaries of human EHD1 and mouse Syndapin1 are shown in black and the construct boundaries in red.

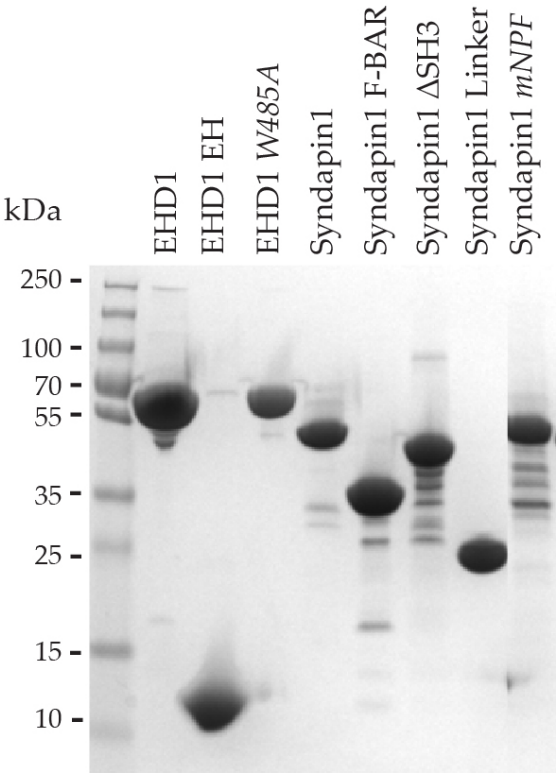

Figure 10.2.: Purification controls EHD1 and Syndapin1. SDS-PAGE of final protein pools from purifications of EHD1 (residues 1-534, 60.7 kDa), EHD1 EH (residues 438-534, 11.3 kDa), EHD1 *W485A* (residues 1-534, 60.6 kDa), Syndapin1 (residues 1-441, 50.0 kDa), Syndapin1 F-BAR (residues 1-326, 38.4 kDa), Syndapin1 ΔSH3 (residues 1-384, 44.3 kDa), Syndapin1 Linker (residues 327-384, 6.0 kDa), Syndapin1 *mNPF* (residues 1-441, 50.7 kDa). Syndapin1 Linker appears at higher molecular weigths, which is probably related to reduced SDS-binding of an unfolded peptide in conventional Tris-glycine SDS-PAGE [401].

man origin of the EHD1 constructs. Our EHD1 full-length construct contained, however, the mutation F2V (Fig. 10.1), which resides in a conserved region that was recently found to be functionally important in the related isoform EHD2 [393] (see 11.2.2, p. 125 for further discussion). The final protein pools were mainly homogeneous as assessed by SDS-PAGE (Fig. 10.2).

10.2. Syndapin1 and EHD1 Affect Membrane Shape *In Vitro*

EGFP-tagged Syndapin1 overexpressed in COS7 cells was reported to be mainly distributed in the cytoplasm, while the isolated F-BAR domain was located at the membrane [130]. In a less complex *in vitro*-environment, Syndapin1 full-length and the F-BAR domain can, however, both interact with liposomes [99–101, 130]. It was hypothesised that this labile interaction of Syndapin1 full-length with membranes is caused by its inability to form stabilising higher-order oligomers in the closed conformation [130]. Nevertheless, it is also possible that phosphorylation of Syndapin1 is involved in its membrane targeting *in vivo* [397, 402] and its assembly in specific oligomers [243] (see 11.1, p. 121 for discussion). The binding partner EHD1 was likewise reported to bind membranes *in vivo* and *in vitro* [387, 391, 395].

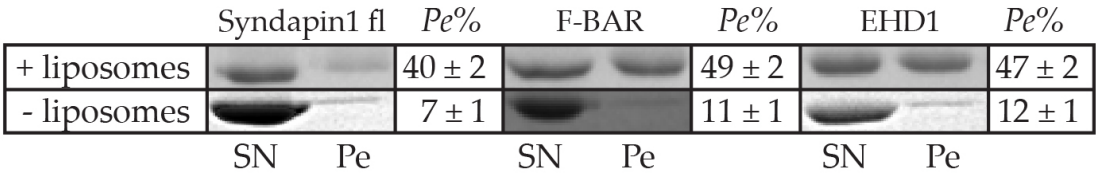

Figure 10.3.: Syndapin1 and EHD1 bind Folch I vesicles. SDS-PAGE of fractions from liposome co-pelleting assay. 0.5 mg/ml sonicated Folch I liposomes (see Materials and Methods 9.3.1, p. 107 for composition) were incubated with either 5 µM Syndapin1 full-length (left), Syndapin1 F-BAR (middle), or EHD1 (right) and pelleted by centrifugation. SN: supernatant, Pe: pellet. The fraction in percent of protein in the pellet is indicated (100 % = SN% + Pe%), which was calculated from duplicates.

As we intended to study the effect of the complex formation between these proteins on artificial membranes, we carried out a control experiment in which we tested binding of the individual proteins to our Folch I liposomes using a liposome co-pelleting assay. We incorporated 1 % PtdIns(4,5)P_2 in the Folch I lipid mix, as this component was reported to be part of EHD1-containing tubules in the endocytic recycling compartment [19, 403, 404]. Furthermore, PtdIns(4,5)P_2 has been shown to increase Syndapin1-binding to PS in PC- and PE-containing liposomes [101], which are all contained in the Folch I mix according to the supplier's analysis. As expected, the results demonstrated that Syndapin1 as well as EHD1 were enriched in liposome-containing fractions (Fig. 10.3), indicating that they also interacted with Folch I liposomes in our experimental set-up. Additional experiments with the isolated F-BAR domain furthermore revealed that the amount of membrane-associated Syndapin1 full-length and the F-BAR domain differ by only 9 % (40 % compared to 49 %, Fig. 10.3), which corroborated the results from Wang *et al.* [99] and Rao *et al.* [130].

The F-BAR domain of Syndapin1 can deform native and artificial membranes into tubules [99, 100], but this activity is inhibited in the full-length protein [99, 130]. EHD proteins are ATPases [390, 405] and the isoform EHD2 was also found to tubulate vesicles *in vitro* with increased efficiency in the presence of ATP or ADP [390]. Whether EHD1 shares the ability to deform membranes *in vitro* has not been studied in detail (see [395] for primary experiments), but from cell-based experiments EHD1 is known to be important for the generation of tubular recycling endosomes [387, 406] and their vesiculation [394, 395] in an ATP-dependent manner [395]. To analyse the effect of Syndapin1 in conjunction with EHD1 on the shape of artificial membranes, we imaged Folch I liposomes incubated with these proteins with transmission electron microscopy.

The microscopic analysis of the Folch I liposomes revealed that sonication produced liposomes with a broad range of sizes and therefore curvatures (Fig. 10.4A), which is consistent with data from Goh *et al.* [131]. To test our assay,

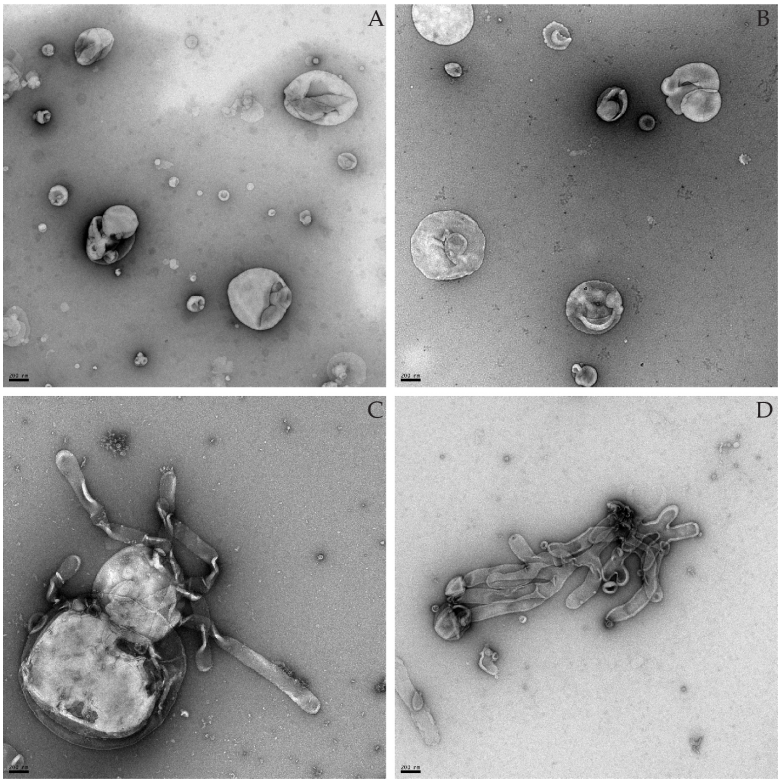

Figure 10.4.: Syndapin1 is autoinhibited and tubule formation depends on release of the F-BAR domain. Syndapin1 was reported to be autoinhibited [99, 130] through binding of its SH3 domain to the F-BAR domain [130]. Deletion of the SH3 domain and the linker promotes tubule formation. Representative transmission electron micrographs of **A:** sonicated Folch I liposomes incubated with **B:** 10 µM Syndapin1, **C:** 10 µM Syndapin1 ΔSH3, and **D:** Syndapin1 F-BAR. Scale bar corresponds to 200 nm. Samples were negatively stained with uranyl acetate.

we incubated the Folch I liposomes with full-length Syndapin1, which should be autoinhibited [99], as well as truncated constructs thereof, which had been reported to deform membranes *in vitro* [99, 130]. As expected, tubules were absent from samples that contained full-length Syndapin1 (Fig 10.4B), whereas we observed tubule formation in samples with either Syndapin1 ΔSH3 (Fig. 10.4C) or the isolated F-BAR domain (Fig. 10.4D). These findings are in line with the autoinhibition model of Wang *et al.* [99] and Rao *et al.* [130] and demonstrated that we successfully established the tubulation assay.

We next tested EHD1 in our assays and found that, similar to Syndapin1, EHD1 was unable to deform Folch I liposomes on its own (Fig. 10.5A and B, p. 113). EHD1, however, strongly aggregated vesicles for unknown reasons. When we incubated Folch I liposomes with both proteins at the same time, we observed - in contrast to samples with the individual proteins - numerous tubules (Fig.

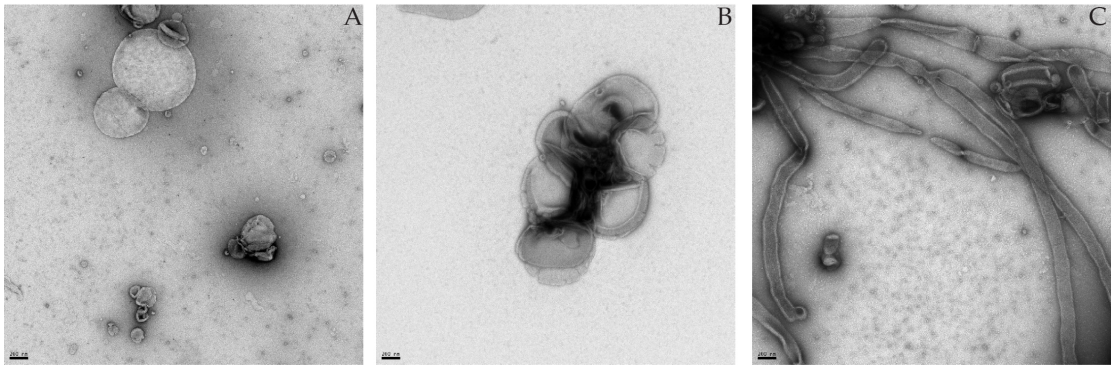

Figure 10.5.: The Syndapin1-EHD1 complex tubulates liposomes *in vitro*. Representative transmission electron micrographs of sonicated Folch I liposomes incubated with **A:** 10 μM Syndapin1, **B:** 10 μM EHD1 or **C:** both proteins. Scale bar corresponds to 200 nm. Samples were negatively stained with uranyl acetate.

10.5C). Since this effect could also have been caused by the membrane interaction of the individual proteins independent of complex formation, we then determined, whether the generation of tubules required binding of Syndapin1 to EHD1.

10.3. Influence of the Interaction Between Syndapin1 and EHD1 on Tubule Formation

Using co-immunoprecipitation and pull-down experiments, Braun *et al.* [129] had shown that the EH domain of EHD1 and the linker region of Syndapin1 containing the NPF motifs are necessary and sufficient for complex formation between these proteins. Furthermore, mutation of either or both NPF motifs to NPV abrogated binding to EHD1 in GST pull-downs [129].

In order to confirm that Syndapin1 and EHD1 used in our experiments indeed form a direct complex, we carried out isothermal titrations with the purified proteins. Our results demonstrated that Syndapin1 bound EHD1 with a K_d of 18 μM (Tab. 10.1), which is in the same range as the published affinity of the cognate Syndapin2-EHD2 complex (K_d = 37 μM [407]). A precise determination of the affinity and the stoichiometry of the Syndapin1-EHD1 complex was, however, hampered by the fact that both proteins precipitated in each other's presence at the required high concentrations. With additional titrations employing either a single EH domain of EHD1 or the NPF-containing linker region of Syndapin1 (EHD1 EH and Syndapin1 Linker, Fig. 10.1, p. 109), we could confirm that these regions are sufficient for complex formation (Tab. 10.1, compare [129]). The determination of the stoichiometry of these complexes yielded inconsistent results and ranged between 1:2 (one Syndapin1 molecule

Table 10.1.: Thermodynamic data from isothermal titrations of Syndapin1 and EHD1.

Syringe Component	Conc. [μM]	Cell Component	Conc. [μM]	K_d[a] [μM]	N[a]	ΔH_{obs}[a] [kcal/mol]
Syndapin1	180	EHD1	18	21[c]	0.23[c]	-22
Syndapin1 Linker[b]	300	EHD1	30	15 ± 4	0.6 ± 0.0	-4.5 ± 1.5
EHD1 EH[b]	300	Syndapin1	30	35	1.1	-7.7
EHD1 EH		Syndapin1 *mNPF*[b]	n. d.[b]	n. d.	n. d.	n. d.
Syndapin1 Linker		EHD1 *W485A*	n. d.	n. d.	n. d.	n. d.

[a] Analysis performed with single-site binding model; K_d = dissociation constant; N = stoichiometry (syringe component to cell component); $\Delta H_{(obs)}$ = observed binding enthalpy. Indicated is the standard deviation between two independent experiments. This data set is preliminary and at the time of writing several complexes had only been measured once.

[b] Syndapin1 Linker, residues 327-384, which contain NPF motifs; EH, Eps15-homology domain (residues 438-534 of EHD1); Syndapin1 *mNPF*, full-length Syndapin1 with both NPF motifs mutated to AAA; n. d., non detectable.

[c] Complex of full-length proteins precipitates and, for this reason, the parameters probably contain considerable errors.

with two NPF motifs per EHD1 dimer) to 1:1 (one Syndapin1 per single EH domain, Tab. 10.1). Titrations with mutated constructs, in which we either replaced the NPF motifs by alanines (Syndapin1 *mNPF*, Fig. 10.1, p. 109) or exchanged the conserved tryptophan in the EH domain-binding pocket with alanine (EHD1 *W485A*, Fig. 10.1, p. 109, compare [72, 76]), revealed that the interaction depended on a functional EH domain and the NPF motifs (Tab. 10.1).

We then asked whether tubule formation depended on the interaction between EHD1 and Syndapin1 and, therefore, we repeated the electron microscopy assay with different binding-deficient mutants: First, we tested Syndapin1 *mNPF* and found that, in contrast to wild-type Syndapin1, it occasionally deformed Folch I liposomes into tubules (Fig. 10.6B, p. 116). This finding was probably related to partial degradation of the construct (compare purification controls in Fig. 10.2, p. 110), which partially released the autoinhibition of the F-BAR domain. Folch I liposomes incubated with Syndapin1 *mNPF* and wild-type EHD1 were significantly less tubulated (Fig. 10.6C, p. 116) compared to samples containing both wild-type proteins (Fig. 10.6A, p. 116), and occasional tubules likely originated from the activity of Syndapin1 *mNPF* alone. Therefore, tubule formation by Syndapin1 in conjunction with EHD1 depended on the presence of the NPF motifs.

In a second experiment, we tested the mutant EHD1 *W485A* and found that, like wild-type EHD1, it was unable to form tubules (Fig. 10.6D, p. 116). Moreover, tubulation was significantly impaired, when EHD1 *W485A* was applied together with wild-type Syndapin1 to liposomes (Fig. 10.6E, p. 116). From

these experiments we concluded that a functional EH domain was required for reshaping of the liposomes.

To confirm that the inability to generate tubules was indeed caused by the absence of the protein-protein interaction and not simply by improperly folded mutant proteins, we carried out competition experiments employing the Syndapin1 Linker, which was reported to interfere with the interaction of Syndapin1 and EHD1 [129]. The Syndapin1 Linker itself was unable to induce tubules in the electron microscopic assay (Fig. 10.6F, p. 116) and considerably decreased the tubulating potential of the Syndapin1-EHD1 complex (Fig. 10.6A and G, p. 116). Moreover, this linker region had to be applied in excess in order to outcompete full-length Syndapin1, which suggested that Syndapin1 and EHD1 stably interact with each other.

In summary, complex formation via the EH domain of EHD1 and the NPF motifs of Syndapin1 was required for the formation of tubules in our assays. Interfering with this interaction by either mutating both NPF motifs to AAA or by mutating the EH domain binding pocket efficiently blocked reshaping of the vesicles.

10.4. Effect of a Single EH Domain of EHD1 on Tubule Formation

In the previous experiments, we had employed full-length constructs of Syndapin1 as well as EHD1 and both proteins interacted with our vesicles (see above). Since we wanted to focus on the investigation of the morphogenic potential of Syndapin1, but not EHD1, on artificial membranes, we needed to rule out an influence of membrane-tethering through EHD1 on tubule formation. Therefore, we restricted subsequent assays to the single EH domain and asked, whether it was sufficient to drive the observed membrane rearrangements together with Syndapin1.

However, the EH domain of EHD1 has been reported to interact with phosphorylated phosphatidylinositols and phosphatidic acid [403, 408]. Folch I extracts indeed contain phosphatidylinositol phosphates [409], mainly PtdIns(4,5)P_2 [410], and also phosphatidic acid (according to supplier's analysis). Therefore, we tested whether the EH domain of EHD1 also binds to our Folch I vesicles. Employing the liposome co-pelleting assay, we could demonstrate that the isolated EHD1 EH domain was not enriched in liposome-containing fractions (Fig. 10.7, p. 117) and, thus, unable to bind to Folch I vesicles in the employed concentration range. For this reason, membrane reshaping in subsequent assays should presumably have originated from the interaction of Syndapin1 with the liposomes.

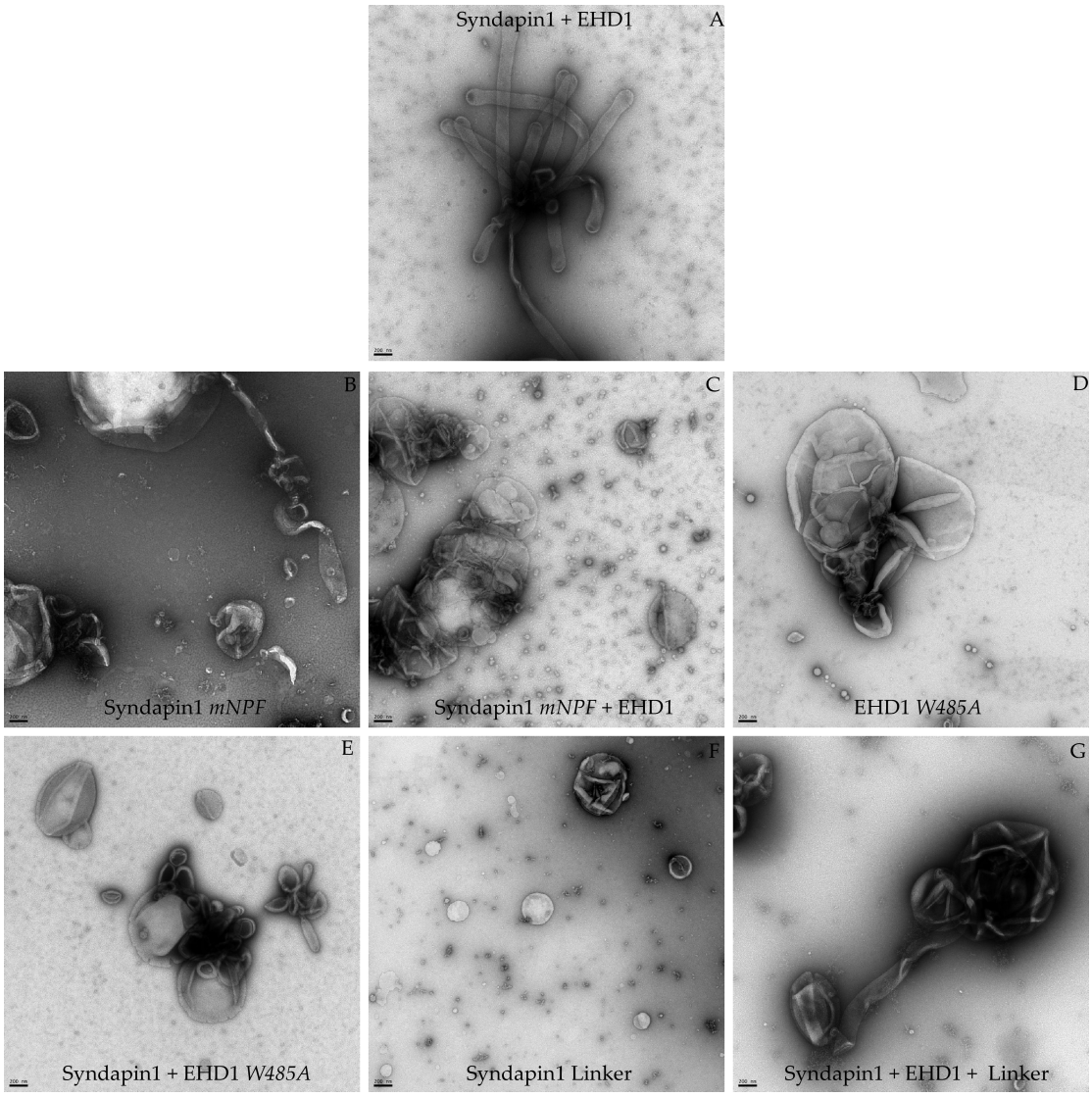

Figure 10.6.: The interaction between Syndapin1 and EHD1 is required for tubule formation *in vitro*. Representative transmission electron micrographs of Folch liposomes incubated with **A:** 10 µM Syndapin1 and 10 µM EHD1, **B:** 10 µM Syndapin1 *mNPF* (NPF motifs mutated to AAA), **C:** 10 µM Syndapin1 *mNPF* and 10 µM EHD1, **D:** 10 µM EHD1 *W485A* (inactivated EH domain), **E:** 10 µM Syndapin1 and 10 µM EHD1 *W485A*, **F:** 1000 µM Syndapin1 Linker (region containing NPF motifs), **G:** 10 µM Syndapin1, 10 µM EHD1, and 1000 µM Syndapin1 Linker. Scale bar corresponds to 200 nm. Samples were negatively stained with uranyl acetate.

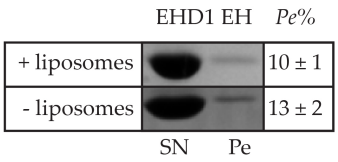

Figure 10.7.: The EH domain of EHD1 is unable to bind Folch I vesicles. SDS-PAGE of fractions from liposome co-pelleting assay. 0.5 mg/ml sonicated Folch I liposomes were incubated with 100 µM EHD1 EH domain and pelleted by centrifugation. SN: supernatant, Pe: pellet. The fraction in percent of protein in the pellet is indicated (100 % = SN% + Pe%), which was calculated from duplicates.

We then incubated Folch I liposomes with Syndapin1 and the EH domain of EHD1 and found that tubules were present, similar to samples with the full-length proteins (Fig. 10.8B, p. 118). On the contrary, the EH domain alone was unable to deform the vesicles (Fig. 10.8A, p. 118). Therefore, it can be concluded that a single EH domain of EHD1 in complex with Syndapin1 is sufficient for tubulation. The EH domain was, however, less effective than full-length EHD1 (see 11.2.2, p. 125 for discussion). Employing the liposome co-pelleting assay, we could show that the amount of Syndapin1 in the liposome-containing fraction increased only by 3 % in presence of the EH domain (data not shown), indicating that tubule formation was not caused by increased membrane-targeting of Syndapin1.

Since Folch I lipids are natural extracts with a large batch-to-batch variability, we wanted to confirm our results with a synthetic lipid mixture of known composition resembling internal membranes (Endomix, compare methods section 9.3.1, p. 107, composition determined by the lab of Felix Wieland, Heidelberg). Syndapin1 and EHD1 similarly interacted with the Endomix liposomes (data not shown) and we then carried out the tubulation assay with these vesicles. We found that, similar to our results with Folch I liposomes, tubules were absent from incubations with Syndapin1 full-length (Fig. 10.9B, p. 119), while the F-BAR domain produced numerous tubules (Fig. 10.9C, p. 119). In contrast to our results with Folch I vesicles, we observed additional membrane topologies in samples with Endomix liposomes and the isolated F-BAR domain: striated tubules (Fig. 10.9C, p. 119, inset) and small vesicles with a diameter of 36 nm (quantification not shown).

We next tested, whether the EH domain of EHD1 was also able to induce tubule formation by Syndapin1 full-length with Endomix liposomes. The EH domain of EHD1 alone had no effect on the shape of Endomix vesicles at these higher concentrations (data not shown). Employing a series of EH domain concentrations, we showed that the Syndapin1-EHD1 EH complex likewise tubulated our synthetic liposomes and that tubule abundance was positively correlated with the concentration of the EH domain (Fig. 10.9D-E, p. 119). A reasonable explanation for this finding is that increasing amounts of Syndapin1 are found in complex with the EH domain. Due to the low affinity of the interaction, the EH domain had to be applied in excess (compare ITC data, Tab. 10.1, p. 114).

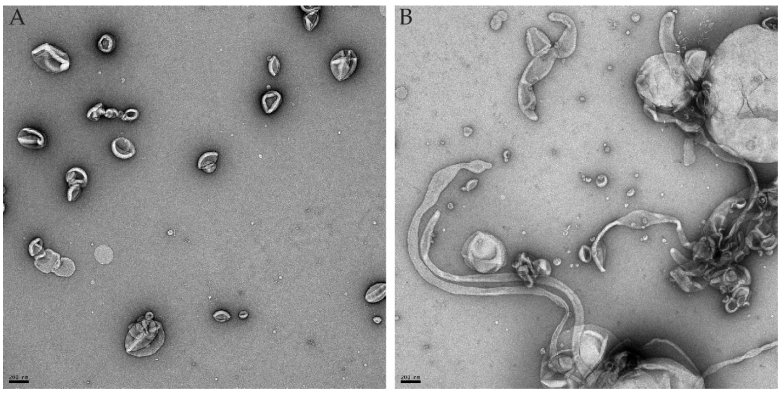

Figure 10.8.: A single EH domain of EHD1 in complex with Syndapin1 is sufficient for tubule formation *in vitro*. Representative transmission electron micrographs of sonicated Folch I liposomes incubated with **A:** 300 μM EHD1 EH domain and **B:** 10 μM Syndapin1 and 300 μM EHD1 EH domain. Scale bar corresponds to 200 nm. Samples were negatively stained with uranyl acetate.

Furthermore, a quantification of Endomix tubule diameters revealed that the tubules formed by the complex of Syndapin1 and EHD1 EH were wider than the tubules formed by the F-BAR domain alone (130 nm compared to 112 nm, respectively, $p < 0.001$ in Mann-Whitney Rank Sum Test, Fig. 10.10, p. 119). On Folch I liposomes, the F-BAR domain generated tubules with a similar diameter (99 nm, data not shown).

From these results, we concluded that binding of the EH domain of EHD1 to the NPF motifs of Syndapin1 likely opens up the autoinhibitory conformation and that this alternative route for the activation of Syndapin1 is independent of ligand-binding to the SH3 domain (compare [130]).

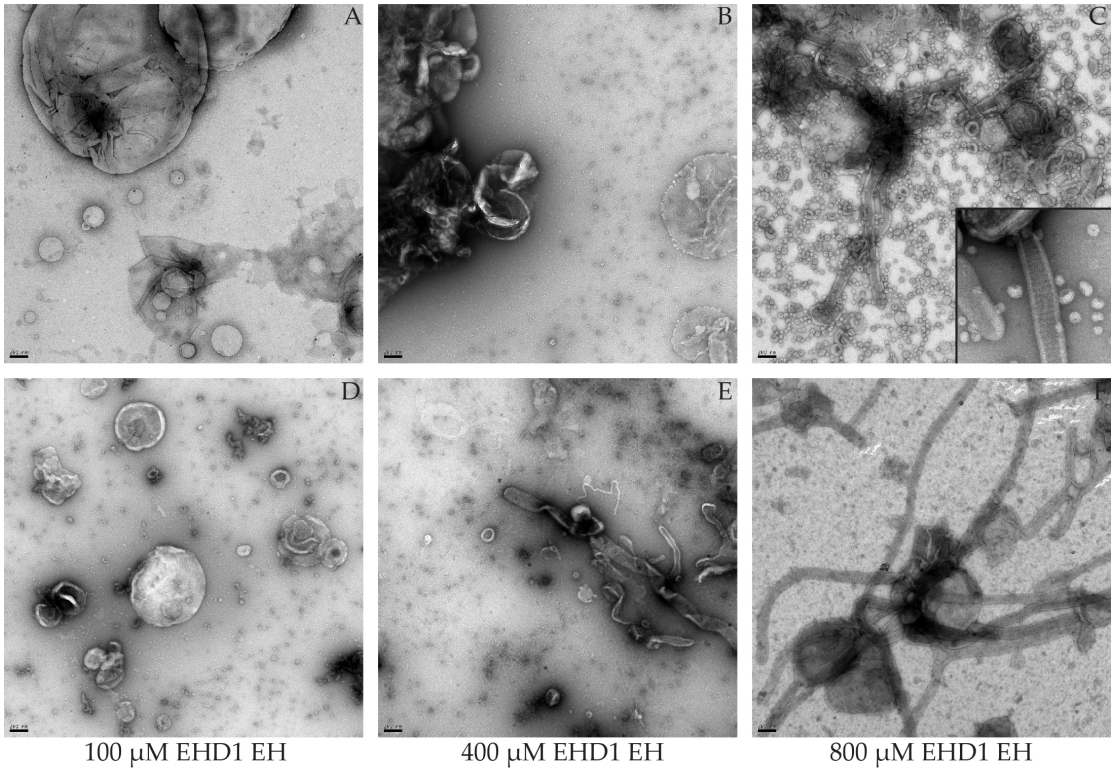

Figure 10.9.: Tubule abundance is positively correlated with the concentration of EHD1 EH. Representative transmission electron micrographs of **A:** sonicated Endomix liposomes, incubated with **B:** 10 µM Syndapin1, **C:** 10 µM Syndapin1 F-BAR (the inset shows a close-up of a striated tubule), **D-E:** 10 µM Syndapin1 and 100/400/800 µM EHD1 EH domain. Scale bar corresponds to 200 nm. Samples were negatively stained with uranyl acetate.

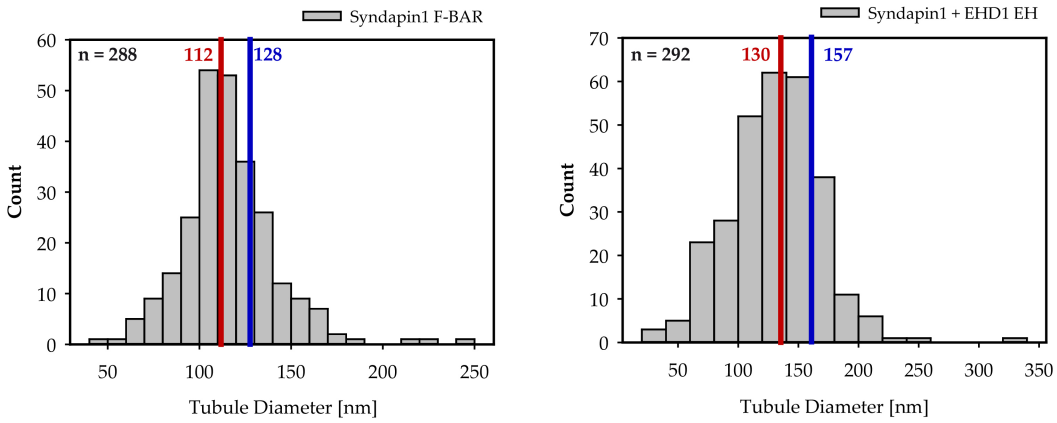

Figure 10.10.: Quantification of tubule diameters generated by different Syndapin1 constructs. Diameters of tubules formed by Syndapin1 F-BAR (left) as well as Syndapin1 full-length in complex with EHD1 EH (right) on Endomix liposomes and imaged with transmission electron microscopy were measured with Fiji [204] and statistically analysed with SigmaPlot (version 12.3, Systat Software Inc.). The red line denotes the median and the blue line the 75%ile.

11. DISCUSSION

The membrane system of eukaryotic cells undergoes constant remodelling to realise a certain cellular morphology, to exchange material with the environment and between different cellular compartments, or to transmit signals between or within cells [27]. For these purposes, membranes need to be bent, for example, into tubular structures, separated by vesiculation, or interconnected through fusion events [27]. Membrane reshaping is considered to be an active process driven by a finely tuned interplay between membrane-interacting proteins, the lipid composition, and the actin cytoskeleton [29, 30]. The BAR domain superfamily of proteins depict such membrane-interacting scaffolds that can stabilise and/or induce curvature [92] and that have been implicated in various aspects of membrane rearrangements [30].

All BAR domains share the ability to form rigid dimers with an intrinsically curved membrane-interaction surface that is positively charged and enables binding to negatively charged phospholipid-headgroups via electrostatic interactions [30, 95, 98, 99, 103]. It is generally believed that they induce or stabilise different membrane shapes by a scaffolding mechanism, in which the degree of membrane bending corresponds to the overall topology of their intrinsic curvature (compare introduction on BAR domains, 1.1.3, p. 6) [27, 95].

11.1. Tubule Formation by the F-BAR Domain of Syndapin1

From a structural perspective, the F-BAR domains of Syndapins represent a unique subgroup within the BAR domain superfamily, since the tips are strongly bent away from the central helical bundle, thereby realising an S-shape (Fig. 8.1, p. 101), which is in principle able to support two types of curvatures [92, 99]. The wedge loop, which is an additional membrane-interacting feature and believed to insert into one leaflet of the bilayer, acts in concert with the concave surface to drive membrane rearrangements (see introduction, Fig. 8.1, p. 101) [99]. This structural model was substantiated by the versatile deformation potential that the F-BAR domain of Syndapin1 displays on artificial liposomes: It was found to form tubules with different diameters (98 nm and 17 nm), as well as small vesicles with a diameter of 31 nm [99, 131]. Disrupting the membrane association by introducing mutations into either the curved interaction surface

or the wedge loop abrogated tubulation as well as vesiculation [99]. In our experiments, the isolated F-BAR domain of Syndapin1 produced only wide tubules on Folch I liposomes (99 nm) and wide tubules (112 nm) as well as small vesicles (36 nm) with our synthetic lipid mix (Fig. 10.4, p. 112 and Fig. 10.9, p. 119).

Why did we observe different membrane morphologies dependend on the employed lipid mix and compared to published results? It was reported that the composition and curvature of the liposomes as well as the precise experimental conditions can influence the ability of the F-BAR domain to support different membrane shapes [99, 131], which likely explains these heterogeneous results. Folch lipids are, for example, natural extracts with a large batch-to-batch variability and differences in lipid compositions will alter the mechanical properties of the artificial membrane [30, 131]. This, in turn, will influence Syndapin1's membrane-bending ability [30, 131] and might explain why Wang *et al.* [99] observed different morphologies with Folch I liposomes. Furthermore, it is known that the initial size and lamellarity and, thus, the elasticity of the liposomal membrane can affect the outcome of tubulation assays with Syndapin1 [131]: Usage of smaller vesicles (50 to 200 nm) as starting material was, for example, found to support vesiculation through the F-BAR domain, whereas larger vesicles promoted the formation of wide tubules [99]. Therefore, differences in the size distribution and lamellarity of the vesicles between our and published assays [99], which are difficult to control in different sonication set-ups, could also have contributed to the variability in produced curvatures.

Furthermore, F-BAR domains bind to the membrane mainly through electrostatic contacts, which renders their deformation activity highly salt dependent [130, 131]. The higher ionic strength of our assay buffer compared to Wang *et al.* [99] and Goh *et al.* [131] (150 mM NaCl and 50 mM NaCl, respectively) could likewise account for the observed differences. Therefore, *in vitro* tubulation should be tested under several conditions in order to be able to eliminate effects originating from a specific experimental set-up. However, despite these shortcomings, *in vitro* assays employing artificial membranes together with structural analyses have proven to be valuable tools in the investigation of BAR domain-mediated membrane sculpting.

In addition to the unique geometry of Syndapin1's F-BAR domain with its two inherent curvatures, the bending angle of the F-BAR homodimer can be modulated by phosphorylation [243], which brings another level of complexity to Syndapin's ability to support different membrane shapes *in vivo*. Although our construct expressed in *E. coli* was not phosphorylated (assessed by mass spectrometry, data not shown), we cannot exclude the possibility that phosphorylation of the F-BAR domain in published assays [99, 131] caused the observed differences. Moreover, phosphorylation of the F-BAR domain was suggested to regulate lateral inter-dimer contacts [243], and arrangement into specific higher

order oligomers, such as spirals, sheets, or chains, on the membrane is generally believed to drive BAR domain-mediated membrane deformation [30, 97, 130, 131]. Indeed, in cryo-electron microscopy-based reconstructions the F-BAR domains of Cip4 and FBP17 [97, 109], as well as the N-BAR domain of Endophilin-A1 [110], were arranged in spiral-like lattices on tubules [30]. Importantly, under certain experimental conditions we and others have observed striated tubules with the F-BAR domain of Syndapin1 (Fig. 10.9C, inset, p. 119) [99], which indicate such ordered arrangements [97, 109, 110].

Finally, such higher order structures can be stabilised by lateral and tip-to-tip contacts between adjacent dimers, as demonstrated for the F-BAR domain of Cip4 [97]. Tip-to-tip interactions have also been suggested to be important for the oligomerisation of the Syndapin2 F-BAR domain [411] and its tubulation activity [412]. Although direct evidence for similar inter-dimer contacts in Syndapin1 is still missing, it is clear that many Syndapin1 dimers need to act in concert to induce or stabilise a certain membrane curvature [92]. Whether the F-BAR domain of Syndapin1 actively generates curvature *in vivo* or is simply required to stabilise curved membrane topologies formed by other proteins, is still an open question, but its tight regulation through the SH3 domain (see subsequent section) and phosphorylation might argue for an active contribution [30].

11.2. The Extended Autoinhibition Model of Syndapin1

11.2.1. Binding to the SH3 Domain

Many BAR domain proteins involved in endocytic processes harbour an SH3 domain for the interaction with or the recruitment of other endocytic coat components [27], but so far only the SH3 domain of Syndapin1 has been shown to serve additional autoregulatory purposes [30, 99, 130]. In the closed state, the SH3 domain folds back onto the F-BAR domain, thereby inhibiting its membrane sculpting activity [130] (Fig. 11.1, p. 124). This model is consistent with our finding that Syndapin1 full-length is unable to deform vesicles, whereas the isolated F-BAR domain and a truncated construct lacking the SH3 domain potently induce tubulation (Fig. 10.4, p. 112). This autoinhibitory clamp was shown to be released by binding of the proline-rich region of Dynamin1 to the SH3 domain, thereby probably displacing it from the F-BAR domain (Fig. 11.1, p. 124) [130, 131].

How the activity is released upon displacement of the SH3 domain is not immediately clear from the available data [131]. In the closed conformation,

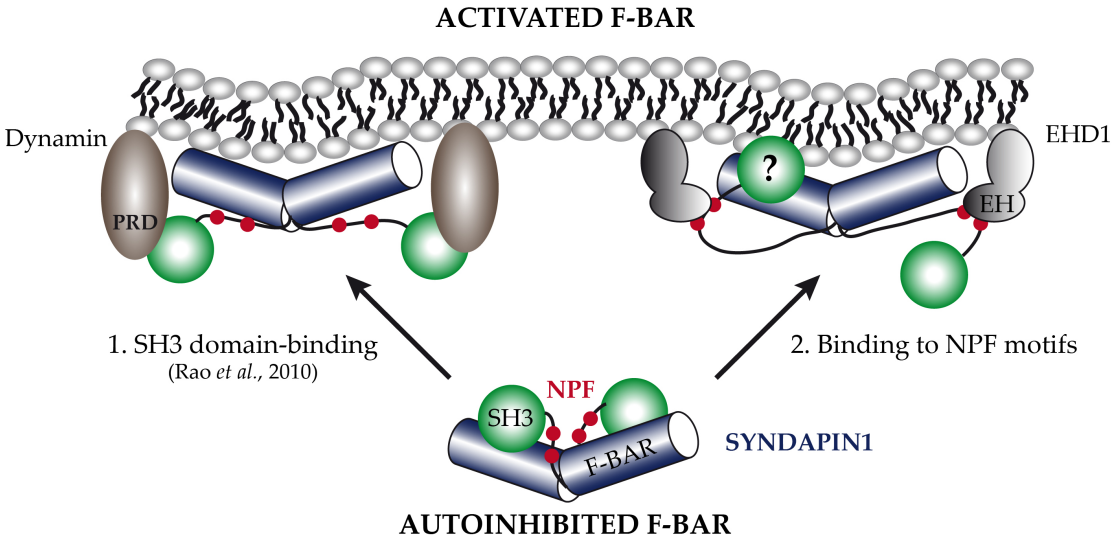

Figure 11.1.: Extended model for the release of the autoinhibition of Syndapin1. The membrane deforming potential of the F-BAR domain of Syndapin1 is released either upon binding of ligands to the SH3 domain, e. g. Dynamin1 (via its PRD, proline-rich domain) [130] or binding of EHD1 (via its EH domain) to the NPF motifs. Whether the SH3 domain is displaced in the Syndapin1-EHD1 complex is unclear and therefore two possible positions are indicated. Figure adapted from Rao *et al.* [130].

Syndapin1 is likewise able to associate with artificial membranes, as demonstrated by our and published liposome binding assays [99, 101, 130, 131]. Instead, it was hypothesised that displacing the SH3 domain releases conformational restraints [130] and triggers the formation of the aforementioned functional higher order assemblies [30, 130, 131]. In fact, SH3 domain-mediated regulation of BAR modules might be more widespread than initially anticipated: Recent data on the N-BAR proteins Endophilin and Amphiphysin suggest that their ability to associate with membranes is inhibited in the full-length context, but released upon binding of Dynamin's proline-rich region to the SH3 domain (compare introduction on endocytosis, Fig. 1.4, p. 12) [119]. Moreover, binding of N-WASP to the SH3 domain of SNX9 was also proposed to open an autoinhibtory clamp [27, 413].

11.2.2. Binding to the NPF Motifs

In this project, we investigated the effect of complex formation between Syndapin1 and EHD1 on the membrane-deforming activity of Syndapin1. EHD1 possesses an EH domain, which was reported to interact with both NPF motifs of Syndapin1 in pull-down experiments [129] and these motifs are located in the flexible linker connecting the F-BAR domain and the SH3 domain

(Fig. 11.1). Through isothermal titrations, we were able to show that this interaction is indeed direct and dependent on the EH/NPF modules. The affinity of the interaction between Syndapin1 and EHD1 (K_d = 15-35 μM) was similar to the published affinity of a related complex between Syndapin2 and EHD2 (K_d = 37 μM, [407]). Although the interaction is in the expected low affinity range of EH domain-mediated complexes (our unpublished data and reviewed in [69]), the complex might become stabilised under native conditions through membrane tethering of both proteins [131, 289], which could in turn also lead to mutual enhanced membrane binding. However, whether the two proteins reciprocally recruit each other could not be tested with our co-pelleting assay, since the complex precipitated in the absence of membranes. Floatation of liposomes in sucrose gradients [101] constitutes an alternative approach to measure enhancement, but giant unilamellar vesicles, which can be observed with conventional fluorescence microscopy, should provide the optimal platform to analyse the time-dependent recruitment of the two proteins to membranes [119].

With our electron microscopic assay, we showed that binding of the EH domain of EHD1 to the NPF motifs is sufficient and required to unlock Syndapin1's tubulation activity on Folch I as well as Endomix vesicles (Fig. 11.1, p. 124). The generated curvatures likely originated from an interaction of Syndapin1 with the vesicles, since the EH domain failed to associate with the Folch I or Endomix liposomes on its own. However, the EH domain of EHD1 was reported to bind membranes [403, 408] and the Folch I extract should (according to the supplier's analysis) contain lipids recognised by this domain, specifically phosphatidic acid [408]. The concentration of these lipids might have been insufficient to allow recruitment of the EH domain. Since the presence of the EH domain did not increase membrane recruitment of Syndapin1 (compare results, p. 117), we can furthermore exclude that tubule formation resulted from protein crowding on our vesicles, which has been shown to cause tubulation *in vitro* (compare [414]).

Although the EH domain was sufficient for tubulation, a complex between the two full-length proteins was much more potent in generating tubules compared to the Syndapin1-EH complex. This might have been related to more efficient membrane-targeting of Syndapin1 through the interaction of EHD1 with the vesicles (Fig. 10.3, p. 111). The isoform EHD2 was proposed to assemble in ring-like fashion around membrane tubes, thereby promoting tubule formation (compare introduction, Fig. 8.3, p. 103) [390, 393], but whether EHD1 shares this ability is unclear. However, although EHD1 failed to produce tubules on its own, it is possible that - through a structured assembly guided by Syndapin1 - the two proteins acted in concert to drive membrane deformation. Furthermore, EHD proteins are ATPases and were suggested to promote vesicle scission similar to Dynamins (compare introduction on endocytosis, Fig. 1.4, p. 12) [390]. In particular, EHD1 has been implicated in the exit of recycling vesicles from endosomal compartments (compare introduction on endosomal

recycling, Fig. 1.1, p. 3) [394, 395] and this function might depend on its ATPase activity [395]. Therefore, nucleotide addition in our assays might not only alter the morphogenic potential of EHD1 itself, but also that of the Syndapin1-EHD1 complex.

Unfortunately, we could not exclude the possibility that our results were influenced by the mutation F2V at the N-terminus of our EHD1 construct, which might be of functional importance: In EHD2, this residue is part of a conserved stretch of amino acids, which constitutes a secondary membrane interaction site and promotes a highly ordered arrangement of the EHD2 coat on membranes, yet is not required for EHD2-mediated tubulation in general [393]. However, whether this region also regulates the oligomeric assembly of EHD1 remains to be shown.

How could binding of the EH domain to the linker activate the tubulation activity of the Syndapin1 F-BAR domain? Our results of the isothermal titrations suggested that the NPF motifs were accessible in the full-length context, since the affinities of Syndapin1 full-length and Syndapin1 Linker for EHD1 were comparable (Tab. 10.1, p. 114). Furthermore, the linker was invisible in the crystal structure also implying that it is rather flexible [130]. Therefore, it is not obvious why ligand binding to the NPF motifs would release the autoinhibitory clamp. As the second NPF motif is positioned close to the SH3 domain boundary, one possibility would be a displacement mechanism via steric hindrance. Since the buried surface area between the F-BAR domain and the SH3 domain is small (460 $\AA$, [130]) and, thus, the interaction expected to be weak [130, 131], binding to the NPF motifs - especially in the context of a stabilised protein complex on the membrane - might be sufficient to displace the SH3 domain. Another possibility is that the linker becomes structured upon EH-domain binding, thereby adopting a conformation that is incompatible with autoinhibition [415].

Another open question is the precise function of the NPF-containing linker region in the autoinhibition. It has been reported that Syndapin1 ΔSH3 is not as potent in deforming vesicles as the isolated F-BAR domain [130, 131]. Moreover, the different human Syndapin isoforms exhibit varying degrees of autoinhibition in the full-length context [131]: Whereas Syndapin1 is inhibited and Syndapin2 shows impaired activity compared to its isolated F-BAR domain, Syndapin3 is fully active. It was hypothesised that not only structural differences between the F-BAR domains, but also the variability in the amino acid sequence and length of the linker regions could contribute to the observed differences between Syndapin isoforms [131]. Hence, the variable region might be required to establish the full autoregulatory conformation of Syndapin1, possibly binding to the F-BAR domain itself. Binding of the EH domain could then trigger a conformational change in the linker, thereby allowing

Syndapin1 to form functional assemblies. Indeed, our initial experiments support this hypothesis, as Syndapin1 ΔSH3 was less potent in deforming vesicles, which is consistent with reported data [99, 131], but exhibited increasing activity when incubated with increasing concentrations of the EH domain (data not shown). Moreover, initial NMR-based studies also revealed a potential direct interaction between the linker region and the F-BAR domain, which could be outcompeted by the addition of the EH domain (data not shown). Additional experiments are required to confirm these results.

In summary, we have identified an alternative path to release the autoinhibitory conformation of Syndapin1 by binding of EHD1 to the NPF motifs in the variable linker region. This route of Syndapin1 activation is independent of ligand-binding to the SH3 domain and, although the underlying mechanisms remains unclear, we have uncovered an unexpected function of the NPF motifs in regulating membrane scaffolding by the F-BAR domain.

11.2.3. Membrane Deformation by Activated Syndapin1

The membrane sculpting potential of activated Syndapin1 was reported to be as diverse as that of the isolated F-BAR domain [131]: Binding of a small peptide derived from the proline-rich region of Dynamin1 to the SH3 domain promoted the formation of tubules [130], whereas binding of its full proline-rich region led to prominent vesiculation [131]. It was suggested that these disparate results originated from an additional membrane contact provided by the full proline-rich region of Dynamin1 itself, which interacted with liposomes through a polybasic stretch [131]. On the other hand, we found that binding of the EHD1 EH domain to the NPF motifs leads to the formation of tubules with a wider diameter than those formed by the F-BAR domain alone (130 nm compared to 112 nm, respectively; Fig. 10.10, p. 119). Therefore, it is likely that opening of the autoinhibitory clamp of Syndapin1 results in the formation of a number of different lattices and their architecture might depend on inherent features of the F-BAR domain as well as modulation through binding partners, the lipid composition of the membrane, or phosphorylation [30, 131, 243]. Regulation of the F-BAR coat geometry through binding partners would also ensure the formation of context-specific lattices and, hence, membrane topologies that are tailored to specific steps in the respective cellular process.

Under *in vitro* conditions, activated Syndapin1 seems to support tubules with wide, as well as narrow diameters down to the point where spontaneous vesiculation occurs, which is indicated by the formation of small vesicles [131]. This is in line with the current model of membrane invagination, neck constriction and subsequent vesicle fission in endocytic processes (compare introduction on endocytosis, 1.2.1, p. 10) [27, 92]. Although we only observed wide

tubules in our assays, nucleotide addition and a concerted action of EHD1 might allow the assembly of different lattices and thereby promote constriction. However, it is questionable whether under more physiological conditions a complex between Syndapin1 and EHD1 is sufficient to drive membrane deformation or even vesiculation of endosomal membranes. This energetically expensive process might instead require the recruitment of additional factors, such as N-WASP, which triggers actin polymerisation [124, 416] and interacts with Syndapin1 (see introductory section 8 on functions of Syndapin1, p. 99) [369, 375]. In fact, Syndapin1 is known to interconnect the endocytic machinery with the actin cytoskeleton [371, 400] and, although the precise function of the Syndapin1-EHD1 complex in neurons remains unclear, Syndapin1 might serve similar functions in EHD1-mediated membrane rearrangements.

12. CONCLUSIONS AND OUTLOOK

In this thesis, I have presented two projects on F-BAR domain-containing proteins, of which the starting points were, admittedly, rather different: The first project aimed at the identification of binding partners for a previously uncharacterised variable region, while the second project aimed at elucidating the functional implication of a known complex mediated by linear motifs in a flexible linker:

In the first part, I have provided evidence that the C-terminal region of srGAP proteins is likely to be intrinsically disordered and acts as a versatile binding platform through contained linear motifs. Via the identified interactions, srGAP3 is not only linked to the endocytic machinery as well as the Ras signalling cascade, but might also connect with yet to be identified pathways via 14-3-3 proteins. Furthermore, I have shown that this region is highly phosphorylated and that phosphorylation modulates the association with 14-3-3 proteins. In this sense, the C-terminal region of srGAP3 exhibits a broader binding spectrum than classical adaptor domains and presents typical features of intrinsically disordered segments of signalling proteins: the potential for signal integration and cross-talk between different pathways as well as mutability through phosphoregulation [36, 37].

In the second part, I have shown that the autoinhibition of the F-BAR domain of Syndapin1 can not only be released through binding of ligands to the SH3 domain, but also via binding of the EH domain of EHD1 to the NPF motifs. Furthermore, I have found an additional type of curvature supported by activated Syndapin1, which provides yet another example of its versatile membrane deforming ability. From these results, we can draw the conclusion that, although the underlying mechanism of membrane rearrangements driven by the Syndapin1-EHD1 complex are still unclear, the activation of Syndapin1's membrane sculpting activity upon binding of EHD1 likely constitutes an important step.

At first sight, the presented results seem unrelated to each other, but we might reduce them to the following common denominators: In both projects, the identified linear motifs seem to hold functions in the recruitment and/or scaffolding of other proteins. SrGAP3 could recruit endocytic factors or the Ras signalling proteins, but might also be required for interconnecting upstream receptors with these machineries. The same applies to Syndapin1, which might

not only arrange EHD1 in specific oligomers, but could also recruit this protein to specific membranes similar to the function of Syndapin2 in recruiting EHD1 to the tubular recycling endosome [406]. Moreover, the NPF motifs of Syndapin1 carry an implicit role in regulating the activity of the N-terminal F-BAR domain through binding to EHD1. Similarly, the 14-3-3-binding sites in the C-terminal region of srGAP3 could serve indirect regulatory purposes regarding the availability of binding sites, the stability, or the localisation of the protein, which are typical functional outputs of 14-3-3 interactions [81]. All of these linear motifs are located in intrinsically disordered regions and this aspect might be important for their ability to establish certain regulatory states, as unstructured segments are especially tailored to enable switch-like behaviour [49, 415].

Finally, I have provided the first example for an association between N-BAR domain proteins (Endophilins and Amphiphysin), which promote membrane invaginations [95, 96], with a specific subgroup of F-BAR proteins, which are implicated in the formation of protrusions [154, 156]. If srGAP3 indeed recruits the endocytic machinery for receptor internalisation, how could we envision the formation of the endocytic pit mechanistically? On the one hand, this process might require a temporary inhibition of the F-BAR's counteracting activity. On the other hand, it could be possible that the F-BAR domain of srGAP3 carries an unexpected flexibility in stabilising different membrane shapes similar to the diverse effects of Syndapins. In fact, the F-BAR domain of srGAP proteins has been suggested to be autoregulated through regions located downstream [156, 417] and regulation of F-BAR domains through interdomain-contacts could be another unifying principle underlying the functions of Syndapin1 and srGAP3.

Bibliography

[1] T. Jessell and E. R. Kandel. "Synaptic transmission: a bidirectional and self-modifiable form of cell-cell communication". In: *Cell* (1993), pp. 1–30.

[2] Y.-N. Jan and L. Y. Jan. "Branching out: mechanisms of dendritic arborization". In: *Nat. Rev. Neurosci.* (2010), pp. 316–328.

[3] B. Winckler and I. Mellman. "Trafficking guidance receptors." In: *Cold Spring Harbor Perspec. Biol.* (2010), a001826.

[4] J. Del Castillo and B. Katz. "Quantal components of the end-plate potential". In: *J. Physiol.* (1954), pp. 560–573.

[5] J. Del Castillo and B. Katz. "Biophysical aspects of neuro-muscular transmission." In: *Prog. Biophys. Biop. Ch.* (1955), pp. 121–170.

[6] V. Whittaker and M. Sheridan. "The morphology and acetylcholine content of isolated cerebral cortical synaptic vesicles". In: *J. Neurochem.* (1965), pp. 363–372.

[7] V. Whittaker, I. Michaelson and R. J. A. Kirkland. "The separation of synaptic vesicles from nerve-ending particles (synaptosomes')". In: *Biochem. J.* (1964), p. 293.

[8] K. Takei *et al.* "The synaptic vesicle cycle: a single vesicle budding step involving clathrin and dynamin." In: *J. Cell Biol.* (1996), pp. 1237–1250.

[9] Q. Zhang, Y. Li and R. W. Tsien. "The dynamic control of kiss-and-run and vesicular reuse probed with single nanoparticles". In: *Science* (2009), pp. 1448–1453.

[10] E. L. Clayton, G. J. Evans and M. A. Cousin. "Bulk synaptic vesicle endocytosis is rapidly triggered during strong stimulation". In: *J. Neurosci.* (2008), pp. 6627–6632.

[11] P. Hoopmann *et al.* "Endosomal sorting of readily releasable synaptic vesicles". In: *Proc. Natl. Acad. Sci. U. S. A.* (2010), pp. 19055–19060.

[12] S. Watanabe *et al.* "Ultrafast endocytosis at mouse hippocampal synapses." In: *Nature* (2013), pp. 242–7.

[13] J. Allen and J. K. Chilton. "The specific targeting of guidance receptors within neurons: who directs the directors?" In: *Dev. Biol.* (2009), pp. 4–11.

[14] M.-P. Fache *et al.* "Endocytotic elimination and domain-selective tethering constitute a potential mechanism of protein segregation at the axonal initial segment". In: *J. Cell Biol.* (2004), pp. 571–578.

[15] J. J. Garrido *et al.* "Dynamic compartmentalization of the voltage-gated sodium channels in axons". In: *Biol. Cell* (2003), pp. 437–445.

[16] M. Piper *et al.* "Endocytosis-dependent desensitization and protein synthesis–dependent resensitization in retinal growth cone adaptation". In: *Nat. Neurosci.* (2005), pp. 179–186.

[17] G. J. Bashaw and R. Klein. "Signaling from axon guidance receptors." In: *Cold Spring Harbor Perspec. Biol.* (2010), a001941.

[18] C. C. Yap and B. Winckler. "Harnessing the power of the endosome to regulate neural development." In: *Neuron* (2012), pp. 1–12.

[19] B. D. Grant and J. G. Donaldson. "Pathways and mechanisms of endocytic recycling". In: *Nat. Rev. Mol. Cell Biol.* (2009), pp. 597–608.

[20] C. D'Souza-Schorey and P. Chavrier. "ARF proteins: roles in membrane traffic and beyond". In: *Nat. Rev. Mol. Cell Biol.* (2006), pp. 347–358.

[21] I. Jordens *et al.* "Rab proteins, connecting transport and vesicle fusion". In: *Traffic* (2005), pp. 1070–1077.

[22] J. Zhang, N. Naslavsky and S. Caplan. "Rabs and EHDs: alternate modes for traffic control". In: *Bioscience reports* (2012), pp. 17–23.

[23] F. R. Maxfield and T. E. McGraw. "Endocytic recycling". In: *Nat. Rev. Mol. Cell Biol.* (2004), pp. 121–132.

[24] J. Gruenberg and H. Stenmark. "The biogenesis of multivesicular endosomes". In: *Nat. Rev. Mol. Cell Biol.* (2004), pp. 317–323.

[25] M. J. Kennedy and M. D. Ehlers. "Organelles and trafficking machinery for postsynaptic plasticity". In: *Annu. Rev. Neurosci.* (2006), p. 325.

[26] V. W. Hsu, M. Bai and J. Li. "Getting active: protein sorting in endocytic recycling". In: *Nat. Rev. Mol. Cell Biol.* (2012), pp. 323–328.

[27] O. Daumke, A. Roux and V. Haucke. "BAR Domain Scaffolds in Dynamin-Mediated Membrane Fission." In: *Cell* (2014), pp. 882–892.

[28] M. M. Kozlov, H. T. McMahon and L. V. Chernomordik. "Protein-driven membrane stresses in fusion and fission." In: *Trends Biochem. Sci.* (2010), pp. 1–8.

[29] H. T. McMahon and J. L. Gallop. "Membrane curvature and mechanisms of dynamic cell membrane remodelling." In: *Nature* (2005), pp. 590–6.

[30] S. Suetsugu, S. Kurisu and T. Takenawa. "Dynamic Shaping of Cellular Membranes by Phospholipids and Membrane-Deforming Proteins". In: *Physiol. Rev.* (2014), pp. 1219–1248.

[31] H. Wu. "Higher-order assemblies in a new paradigm of signal transduction." In: *Cell* (2013), pp. 287–92.

[32] T. Pawson and P. Nash. "Assembly of cell regulatory systems through protein interaction domains." In: *Science* (2003), pp. 445–52.

[33] T. Pawson and P. Nash. "Protein-protein interactions define specificity in signal transduction." In: *Genes Dev.* (2000), pp. 1027–47.

[34] H. J. Dyson and P. E. Wright. "Intrinsically unstructured proteins and their functions". In: *Nat. Rev. Mol. Cell Biol.* (2005), pp. 197–208.

[35] L. M. Iakoucheva *et al.* "Intrinsic disorder in cell-signaling and cancer-associated proteins." In: *J. Mol. Biol.* (2002), pp. 573–84.

[36] J. R. Perkins *et al.* "Transient protein-protein interactions: structural, functional, and network properties." In: *Structure* (2010), pp. 1–11.

[37] R. van der Lee *et al.* "Classification of Intrinsically Disordered Regions and Proteins." In: *Chem. Rev.* (2014), pp. 6589–6631.

[38] W. Bode, P. Schwager and R. Huber. "The transition of bovine trypsinogen to a trypsin-like state upon strong ligand binding: The refined crystal structures of the bovine trypsinogen-pancreatic trypsin inhibitor complex and of its ternary complex with Ile-Val at 1.9 Å resolution". In: *J. Mol. Biol.* (1978), pp. 99–112.

[39] A. Bloomer *et al.* "Protein disk of tobacco mosaic virus at 2.8 Å resolution showing the interactions within and between subunits". In: *Nature* (1978), pp. 362–368.

[40] A. K. Dunker *et al.* "Intrinsically disordered protein". In: *J. Mol. Graph. Model.* (2001), pp. 26–59.

[41] P. Romero *et al.* "Identifying disordered regions in proteins from amino acid sequence". In: *Int. Conference Neural Networks, 1997.* IEEE. 1997, pp. 90–95.

[42] V. N. Uversky, J. R. Gillespie and A. L. Fink. "Why are "natively unfolded" proteins unstructured under physiologic conditions?" In: *Proteins: Struct., Funct., Bioinf.* (2000), pp. 415–427.

[43] V. N. Uversky and A. K. Dunker. "The case for intrinsically disordered proteins playing contributory roles in molecular recognition without a stable 3D structure". In: *F1000 Biol. Rep.* (2013).

[44] V. N. Uversky and A. K. Dunker. "Understanding protein non-folding". In: *Biochim. Biophys. Acta, Proteins Proteomics* (2010), pp. 1231–1264.

[45] F. Diella *et al.* "Understanding eukaryotic linear motifs and their role in cell signaling and regulation." In: *Front. Biosci.* (2008), pp. 6580–603.

[46] R. J. Weatheritt and T. J. Gibson. "Linear motifs: lost in (pre)translation." In: *Trends Biochem. Sci.* (2012), pp. 333–41.

[47] N. E. Davey *et al.* "Attributes of short linear motifs." In: *Mol. Biosyst.* (2012), pp. 268–81.

[48] T. J. Gibson. "Cell regulation: determined to signal discrete cooperation." In: *Trends Biochem. Sci.* (2009), pp. 471–82.

[49] K. Van Roey, T. J. Gibson and N. E. Davey. "Motif switches: decision-making in cell regulation". In: *Curr. Opin. Struct. Biol.* (2012), pp. 378–385.

[50] A. Stein *et al.* "Dynamic interactions of proteins in complex networks: a more structured view". In: *FEBS J.* (2009), pp. 5390–5405.

[51] S. Li. "Specificity and versatility of SH3 and other proline-recognition domains: structural basis and implications for cellular signal transduction". In: *Biochem. J.* (2005), pp. 641–653.

[52] H. Yu *et al.* "Solution structure of the SH3 domain of Src and identification of its ligand-binding site". In: *Science* (1992), pp. 1665–1668.

[53] M. Noble *et al.* "Crystal structure of the SH3 domain in human Fyn; comparison of the three-dimensional structures of SH3 domains in tyrosine kinases and spectrin." In: *EMBO J.* (1993), p. 2617.

[54] M. Carducci *et al.* "The protein interaction network mediated by human SH3 domains". In: *Biotechnol. Adv.* (2012), pp. 4–15.

[55] W. A. Lim, F. M. Richards and R. O. Fox. "Structural determinants of peptide-binding orientation and of sequence specificity in SH3 domains." In: *Nature* (1994), pp. 375–9.

[56] A. Musacchio *et al.* "Crystal structure of a Src-homology 3 (SH3) domain". In: *Nature* (1992).

[57] J. K. Chen *et al.* "Biased combinatorial libraries: novel ligands for the SH3 domain of phosphatidylinositol 3-kinase". In: *J. Am. Chem. Soc.* (1993), pp. 12591–12592.

[58] S. Feng *et al.* "Two binding orientations for peptides to the Src SH3 domain: development of a general model for SH3-ligand interactions". In: *Science* (1994), pp. 1241–1247.

[59] S. Feng *et al.* "Specific interactions outside the proline-rich core of two classes of Src homology 3 ligands." In: *Proc. Natl. Acad. Sci. U. S. A.* (1995), pp. 12408–15.

[60] M. Lewitzky *et al.* "The C-terminal SH3 domain of the adapter protein Grb2 binds with high affinity to sequences in Gab1 and SLP-76 which lack the SH3-typical PxxP core motif." In: *Oncogene* (2001), pp. 1052–1062.

[61] J.-F. Trempe *et al.* "SH3 domains from a subset of BAR proteins define a Ubl-binding domain and implicate parkin in synaptic ubiquitination." In: *Mol. Cell* (2009), pp. 1–14.

[62] K. Murayama *et al.* "Crystal structure of the rac activator, Asef, reveals its autoinhibitory mechanism". In: *J. Biol. Chem.* (2007), pp. 4238–4242.

[63] K. Saksela and P. Permi. "SH3 domain ligand binding: What's the consensus and where's the specificity?" In: *FEBS Lett.* (2012), pp. 2609–14.

[64] K. Kami *et al.* "Diverse recognition of non-PxxP peptide ligands by the SH3 domains from p67phox, Grb2 and Pex13p". In: *EMBO J.* (2002), pp. 4268–4276.

[65] A. Stein and P. Aloy. "Contextual specificity in peptide-mediated protein interactions." In: *PLoS One* (2008), e2524–10.

[66] Y. Groemping *et al.* "Molecular basis of phosphorylation-induced activation of the NADPH oxidase." In: *Cell* (2003), pp. 343–55.

[67] F. Fazioli *et al.* "Eps15, a novel tyrosine kinase substrate, exhibits transforming activity." In: *Mol. Cell. Biol.* (1993), pp. 5814–5828.

[68] W. T. Wong *et al.* "A protein-binding domain, EH, identified in the receptor tyrosine kinase substrate Eps15 and conserved in evolution". In: *Proc. Natl. Acad. Sci. U. S. A.* (1995), pp. 9530–9534.

[69] S. Confalonieri and P. P. Di Fiore. "The Eps15 homology (EH) domain". In: *FEBS Lett.* (2002), pp. 24–29.

[70] A. E. Salcini *et al.* "Binding specificity and in vivo targets of the EH domain, a novel protein–protein interaction module". In: *Genes Dev.* (1997), pp. 2239–2249.

[71] E. Santolini *et al.* "The EH network". In: *Exp. Cell Res.* (1999), pp. 186–209.

[72] T. de Beer *et al.* "Molecular mechanism of NPF recognition by EH domains". In: *Nat. Struct. Mol. Biol.* (2000), pp. 1018–1022.

[73] R. H. Kretsinger *et al.* "The EF-hand, homologs and analogs". In: *Novel calcium-binding proteins*. Springer, 1991, pp. 17–37.

[74] S. Paoluzi *et al.* "Recognition specificity of individual EH domains of mammals and yeast". In: *EMBO J.* (1998), pp. 6541–6550.

[75] S. Kim *et al.* "Solution structure of the Reps1 EH domain and characterization of its binding to NPF target sequences". In: *Biochemistry* (2001), pp. 6776–6785.

[76] F. Kieken *et al.* "Mechanism for the selective interaction of C-terminal Eps15 homology domain proteins with specific Asn-Pro-Phe-containing partners." In: *J. Biol. Chem.* (2010), pp. 1–8.

[77] J. Rumpf *et al.* "1H, 13C, and 15N chemical shift assignments for the Eps15-EH2-stonin 2 complex." In: *Biomol. NMR Assignments* (2008), pp. 55–8.

[78] H. Fu, R. R. Subramanian and S. C. Masters. "14-3-3 proteins: structure, function, and regulation." In: *Annu. Rev. Pharmacol. Toxicol.* (2000), pp. 617–47.

[79] A. K. Gardino, S. J. Smerdon and M. B. Yaffe. "Structural determinants of 14-3-3 binding specificities and regulation of subcellular localization of 14-3-3-ligand complexes: a comparison of the X-ray crystal structures of all human 14-3-3 isoforms." In: *Semin. Cancer Biol.* (2006), pp. 173–82.

[80] M. B. Yaffe *et al.* "The structural basis for 14-3-3: phosphopeptide binding specificity". In: *Cell* (1997), pp. 961–971.

[81] C. Mackintosh. "Dynamic interactions between 14-3-3 proteins and phosphoproteins regulate diverse cellular processes". In: *Biochem. J.* (2004).

[82] N. Fukuhara *et al.* "SMG7 is a 14-3-3-like adaptor in the nonsense-mediated mRNA decay pathway". In: *Mol. Cell* (2005), pp. 537–547.

[83] A. J. Muslin *et al.* "Interaction of 14-3-3 with signaling proteins is mediated by the recognition of phosphoserine". In: *Cell* (1996), pp. 889–897.

[84] K. Rittinger *et al.* "Structural analysis of 14-3-3 phosphopeptide complexes identifies a dual role for the nuclear export signal of 14-3-3 in ligand binding". In: *Mol. Cell* (1999), pp. 153–166.

[85] C. Johnson *et al.* "Bioinformatic and experimental survey of 14-3-3-binding sites". In: *Biochem. J.* (2010), pp. 69–78.

[86] J. Jin *et al.* "Proteomic, functional, and domain-based analysis of in vivo 14-3-3 binding proteins involved in cytoskeletal regulation and cellular organization." In: *Curr. Biol.* (2004), pp. 1436–50.

[87] M. B. Yaffe. "How do 14-3-3 proteins work?–Gatekeeper phosphorylation and the molecular anvil hypothesis". In: *FEBS Lett.* (2002), pp. 53–57.

[88] J. M. Janz, T. P. Sakmar and K. C. Min. "A novel interaction between atrophin-interacting protein 4 and β-p21-activated kinase-interactive exchange factor is mediated by an SH3 domain". In: *J. Biol. Chem.* (2007), pp. 28893–28903.

[89] J. E. Harlan *et al.* "Pleckstrin homology domains bind to phosphatidylinositol-4, 5-bisphosphate." In: *Nature* (1994), pp. 168–170.

[90] M. L. Cheever *et al.* "Phox domain interaction with PtdIns (3) P targets the Vam7 t-SNARE to vacuole membranes". In: *Nature Cell Biol.* (2001), pp. 613–618.

[91] C. David, M. Solimena and P. De Camilli. "Autoimmunity in stiff-Man syndrome with breast cancer is targeted to the C-terminal region of human amphiphysin, a protein similar to the yeast proteins, Rvs167 and Rvs161". In: *FEBS Lett.* (1994), pp. 73–79.

[92] B. Qualmann, D. Koch and M. M. Kessels. "Let's go bananas: revisiting the endocytic BAR code." In: *EMBO J.* (2011), pp. 3501–15.

[93] A. Frost, V. M. Unger and P. De Camilli. "The BAR domain superfamily: membrane-molding macromolecules". In: *Cell* (2009), pp. 191–196.

[94] M. Masuda *et al.* "Endophilin BAR domain drives membrane curvature by two newly identified structure-based mechanisms". In: *EMBO J.* (2006), pp. 2889–2897.

[95] B. J. Peter *et al.* "BAR domains as sensors of membrane curvature: the amphiphysin BAR structure." In: *Science* (2004), pp. 495–9.

[96] J. L. Gallop *et al.* "Mechanism of endophilin N-BAR domain-mediated membrane curvature". In: *EMBO J.* (2006), pp. 2898–2910.

[97] A. Frost *et al.* "Structural basis of membrane invagination by F-BAR domains." In: *Cell* (2008), pp. 807–17.

[98] W. M. Henne *et al.* "Structure and analysis of FCHo2 F-BAR domain: a dimerizing and membrane recruitment module that effects membrane curvature." In: *Structure* (2007), pp. 1–14.

[99] Q. Wang *et al.* "Molecular mechanism of membrane constriction and tubulation mediated by the F-BAR protein Pacsin/Syndapin." In: *Proc. Natl. Acad. Sci. U. S. A.* (2009), pp. 12700–5.

[100] T. Itoh *et al.* "Dynamin and the actin cytoskeleton cooperatively regulate plasma membrane invagination by BAR and F-BAR proteins." In: *Dev. Cell* (2005), pp. 791–804.

[101] E. Dharmalingam *et al.* "F-BAR proteins of the syndapin family shape the plasma membrane and are crucial for neuromorphogenesis." In: *J. Neurosci.* (2009), pp. 13315–27.

[102] A. Pykäläinen *et al.* "Pinkbar is an epithelial-specific BAR domain protein that generates planar membrane structures." In: *Nat. Struct. Mol. Biol.* (2011), pp. 902–7.

[103] T. H. Millard *et al.* "Structural basis of filopodia formation induced by the IRSp53/MIM homology domain of human IRSp53". In: *EMBO J.* (2005), pp. 240–250.

[104] S. H. Lee *et al.* "Structural basis for the actin-binding function of missing-in-metastasis". In: *Structure* (2007), pp. 145–155.

[105] O. Pylypenko *et al.* "The PX-BAR membrane-remodeling unit of sorting nexin 9". In: *EMBO J.* (2007), pp. 4788–4800.

[106] J. Li *et al.* "Crystal structures of the BAR-PH and PTB domains of human APPL1". In: *Structure* (2007), pp. 525–533.

[107] M. M. Kozlov *et al.* "Mechanisms shaping cell membranes." In: *Curr. Opin. Cell Biol.* (2014), pp. 53–60.

[108] P. Janmey and P. Kinnunen. "Biophysical properties of lipids and dynamic membranes". In: *Trends Cell Biol.* (2006), pp. 538–546.

[109] A. Shimada *et al.* "Curved EFC/F-BAR-domain dimers are joined end to end into a filament for membrane invagination in endocytosis." In: *Cell* (2007), pp. 761–72.

[110] C. Mim *et al.* "Structural basis of membrane bending by the N-BAR protein endophilin." In: *Cell* (2012), pp. 1–9.

[111] E. Boucrot *et al.* "Membrane fission is promoted by insertion of amphipathic helices and is restricted by crescent BAR domains." In: *Cell* (2012), pp. 124–36.

[112] M. R. Ambroso, B. G. Hegde and R. Langen. "Endophilin A1 induces different membrane shapes using a conformational switch that is regulated by phosphorylation". In: *Proc. Natl. Acad. Sci. U. S. A.* (2014), pp. 6982–6987.

[113] S. Suetsugu *et al.* "The RAC binding domain/IRSp53-MIM homology domain of IRSp53 induces RAC-dependent membrane deformation". In: *J. Biol. Chem.* (2006), pp. 35347–35358.

[114] W. M. Henne *et al.* "FCHo proteins are nucleators of clathrin-mediated endocytosis." In: *Science* (2010), pp. 1281–4.

[115] G. Di Paolo and P. De Camilli. "Phosphoinositides in cell regulation and membrane dynamics". In: *Nature* (2006), pp. 651–657.

[116] M. J. Taylor, D. Perrais and C. J. Merrifield. "A high precision survey of the molecular dynamics of mammalian clathrin-mediated endocytosis". In: *PLoS Biol.* (2011), e1000604.

[117] I. Milosevic *et al.* "Recruitment of endophilin to clathrin-coated pit necks is required for efficient vesicle uncoating after fission." In: *Neuron* (2011), pp. 587–601.

[118] Y. Posor *et al.* "Spatiotemporal control of endocytosis by phosphatidylinositol-3,4-bisphosphate." In: *Nature* (2013), pp. 233–7.

[119] M. Meinecke *et al.* "Cooperative Recruitment of Dynamin and BIN/Amphiphysin/Rvs (BAR) Domain-containing Proteins Leads to GTP-dependent Membrane Scission." In: *J. Biol. Chem.* (2013), pp. 6651–61.

[120] S. J. Heasman and A. J. Ridley. "Mammalian Rho GTPases: new insights into their functions from in vivo studies." In: *Nat. Rev. Mol. Cell Biol.* (2008), pp. 690–701.

[121] P. Ji, S. R. Jayapal and H. F. Lodish. "Enucleation of cultured mouse fetal erythroblasts requires Rac GTPases and mDia2". In: *Nature Cell Biol.* (2008), pp. 314–321.

[122] K. Kobayashi *et al.* "p140Sra-1 (specifically Rac1-associated protein) is a novel specific target for Rac1 small GTPase." In: *J. Biol. Chem.* (1998), pp. 291–5.

[123] S. Eden *et al.* "Mechanism of regulation of WAVE1-induced actin nucleation by Rac1 and Nck". In: *Nature* (2002), pp. 790–793.

[124] L. M. Machesky and R. H. Insall. "Scar1 and the related Wiskott–Aldrich syndrome protein, WASP, regulate the actin cytoskeleton through the Arp2/3 complex". In: *Curr. Biol.* (1998), pp. 1347–1356.

[125] L. Blanchoin *et al.* "Direct observation of dendritic actin filament networks nucleated by Arp2/3 complex and WASP/Scar proteins". In: *Nature* (2000), pp. 1007–1011.

[126] L. A. Colgan and R. Yasuda. "Plasticity of dendritic spines: subcompartmentalization of signaling". In: *Annu. Rev. Physiol.* (2014), pp. 365–385.

[127] S. H. Soderling *et al.* "The WRP component of the WAVE-1 complex attenuates Rac-mediated signalling." In: *Nat. Cell Biol.* (2002), pp. 970–5.

[128] D. C. Edwards *et al.* "Activation of LIM-kinase by Pak1 couples Rac/Cdc42 GTPase signalling to actin cytoskeletal dynamics". In: *Nature Cell Biol.* (1999), pp. 253–259.

[129] A. Braun *et al.* "EHD proteins associate with syndapin I and II and such interactions play a crucial role in endosomal recycling." In: *Mol. Biol. Cell* (2005), pp. 3642–58.

[130] Y. Rao *et al.* "Molecular basis for SH3 domain regulation of F-BAR-mediated membrane deformation." In: *Proc. Natl. Acad. Sci. U. S. A.* (2010), pp. 8213–8.

[131] S. L. Goh *et al.* "Versatile membrane deformation potential of activated pacsin." In: *PLoS One* (2012), e51628–18.

[132] R. K. Saiki *et al.* "Primer-directed enzymatic amplification of DNA with a thermostable DNA polymerase". In: *Science* (1988), pp. 487–491.

[133] R. Don *et al.* "'Touchdown'PCR to circumvent spurious priming during gene amplification." In: *Nucleic Acids Res.* (1991), p. 4008.

[134] O. Edelheit, A. Hanukoglu and I. Hanukoglu. "Simple and efficient site-directed mutagenesis using two single-primer reactions in parallel to generate mutants for protein structure-function studies." In: *BMC Biotechnol.* (2009), p. 61.

[135] C. E. Seidman *et al.* "Introduction of plasmid DNA into cells". In: *Curr. Protoc. Mol. Biol.* (1997), pp. 1–8.

[136] R. B. DuBridge *et al.* "Analysis of mutation in human cells by using an Epstein-Barr virus shuttle system." In: *Mol. Cell. Biol.* (1987), pp. 379–387.

[137] O. Boussif *et al.* "A versatile vector for gene and oligonucleotide transfer into cells in culture and in vivo: polyethylenimine." In: *Proc. Natl. Acad. Sci. U. S. A.* (1995), pp. 7297–301.

[138] C. Ehrhardt *et al.* "Polyethylenimine, a cost-effective transfection reagent". In: *Signal Transduction* (2006), pp. 179–184.

[139] U. K. Laemmli. "Cleavage of structural proteins during the assembly of the head of bacteriophage T4." In: *Nature* (1970), pp. 680–685.

[140] S. M. Kelly, T. J. Jess and N. C. Price. "How to study proteins by circular dichroism." In: *Biochim. Biophys. Acta* (2005), pp. 119–39.

[141] T. Wiseman *et al.* "Rapid measurement of binding constants and heats of binding using a new titration calorimeter". In: *Anal. Biochem.* (1989), pp. 131–137.

[142] M. J. Todd and J. Gomez. "Enzyme kinetics determined using calorimetry: a general assay for enzyme activity?" In: *Anal. Biochem.* (2001), pp. 179–187.

[143] I. Jelesarov and H. R. Bosshard. "Isothermal titration calorimetry and differential scanning calorimetry as complementary tools to investigate the energetics of biomolecular recognition". In: *J. Mol. Recognit.* (1999), pp. 3–18.

[144] A. R. Ypsilanti, Y. Zagar and A. Chédotal. "Moving away from the midline: new developments for Slit and Robo". In: *Development* (2010), pp. 1939–1952.

[145] C. Bacon, V. Endris and G. A. Rappold. "The cellular function of srGAP3 and its role in neuronal morphogenesis." In: *Mech. Dev.* (2013), pp. 391–5.

[146] M. Seeger *et al.* "Mutations affecting growth cone guidance in Drosophila: genes necessary for guidance toward or away from the midline". In: *Neuron* (1993), pp. 409–426.

[147] J. M. Rothberg *et al.* "Slit: an extracellular protein necessary for development of midline glia and commissural axon pathways contains both EGF and LRR domains." In: *Genes Dev.* (1990), pp. 2169–2187.

[148] K. Brose *et al.* "Slit proteins bind Robo receptors and have an evolutionarily conserved role in repulsive axon guidance". In: *Cell* (1999), pp. 795–806.

[149] T. Kidd, K. S. Bland and C. S. Goodman. "Slit Is the Midline Repellent for the Robo Receptor in Drosophila". In: *Cell* (1999), pp. 785–794.

[150] T. Ringstedt *et al.* "Slit inhibition of retinal axon growth and its role in retinal axon pathfinding and innervation patterns in the diencephalon". In: *J. Neurosci.* (2000), pp. 4983–4991.

[151] K. Wong *et al.* "Signal transduction in neuronal migration: roles of GTPase activating proteins and the small GTPase Cdc42 in the Slit-Robo pathway." In: *Cell* (2001), pp. 209–21.

[152] C. Bacon *et al.* "Evidence for a role of srGAP3 in the positioning of commissural axons within the ventrolateral funiculus of the mouse spinal cord." In: *PLoS One* (2011), e19887.

[153] Y. Ma *et al.* "The inverse F-BAR domain protein srGAP2 acts through srGAP3 to modulate neuronal differentiation and neurite outgrowth of mouse neuroblastoma cells." In: *PLoS One* (2013), e57865.

[154] J. Coutinho-Budd *et al.* "The F-BAR domains from srGAP1, srGAP2, and srGAP3 differentially regulate membrane deformation." In: *J. Cell Sci.* (2012), pp. 3390–3401.

[155] C. Charrier *et al.* "Inhibition of SRGAP2 function by its human-specific paralogs induces neoteny during spine maturation." In: *Cell* (2012), pp. 923–35.

[156] S. Guerrier *et al.* "The F-BAR domain of srGAP2 induces membrane protrusions required for neuronal migration and morphogenesis." In: *Cell* (2009), pp. 990–1004.

[157] H. il Kim *et al.* "Disruption of Wave Associated Rac-GAP (Wrp) Leads to Abnormal Adult Neural Progenitor Migration Associated with Hydrocephalus." In: *J. Biol. Chem.* (2012), pp. 39263–39274.

[158] D. L. Vogt *et al.* "ARHGAP4 is a novel RhoGAP that mediates inhibition of cell motility and axon outgrowth." In: *Mol. Cell. Neurosci.* (2007), pp. 1–11.

[159] Q. Yao *et al.* "Regulated shuttling of Slit-Robo-GTPase activating proteins between nucleus and cytoplasm during brain development." In: *Cell. Mol. Neurobiol.* (2008), pp. 205–21.

[160] C. Bacon, V. Endris and G. Rappold. "Dynamic expression of the Slit-Robo GTPase activating protein genes during development of the murine nervous system." In: *J. Comp. Neurol.* (2009), pp. 224–36.

[161] V. Endris *et al.* "The novel Rho-GTPase activating gene MEGAP/srGAP3 has a putative role in severe mental retardation." In: *Proc. Natl. Acad. Sci. U. S. A.* (2002), pp. 11754–9.

[162] R. Waltereit *et al.* "Srgap3-/- mice present a neurodevelopmental disorder with schizophrenia-related intermediate phenotypes." In: *FASEB J.* (2012), pp. 1–11.

[163] B. R. Carlson *et al.* "WRP/srGAP3 facilitates the initiation of spine development by an inverse F-BAR domain, and its loss impairs long-term memory." In: *J. Neurosci.* (2011), pp. 2447–60.

[164] Y. Yang *et al.* "MEGAP impedes cell migration via regulating actin and microtubule dynamics and focal complex formation." In: *Exp. Cell Res.* (2006), pp. 2379–93.

[165] V. Endris *et al.* "SrGAP3 interacts with lamellipodin at the cell membrane and regulates Rac-dependent cellular protrusions." In: *J. Cell Sci.* (2011), pp. 3941–55.

[166] X. Li *et al.* "Structural basis of Robo proline-rich motif recognition by the srGAP1 Src homology 3 domain in the Slit-Robo signaling pathway." In: *J. Biol. Chem.* (2006), pp. 28430–7.

[167] S. F. Altschul *et al.* "Gapped BLAST and PSI-BLAST: a new generation of protein database search programs". In: *Nucleic Acids Res.* (1997), pp. 3389–3402.

[168] J. Söding *et al.* "HHsenser: exhaustive transitive profile search using HMM-HMM comparison." In: *Nucleic Acids Res.* (2006), W374–8.

[169] A. Biegert *et al.* "The MPI Bioinformatics Toolkit for protein sequence analysis." In: *Nucleic Acids Res.* (2006), W335–9.

[170] J. Söding, A. Biegert and A. N. Lupas. "The HHpred interactive server for protein homology detection and structure prediction". In: *Nucleic Acids Res.* (2005), W244–W248.

[171] L. J. McGuffin, K. Bryson and D. T. Jones. "The PSIPRED protein structure prediction server". In: *Bioinformatics* (2000), pp. 404–405.

[172] C. Cole, J. D. Barber and G. J. Barton. "The Jpred 3 secondary structure prediction server". In: *Nucleic Acids Res.* (2008), W197–W201.

[173] P. Rice, I. Longden and A. Bleasby. "EMBOSS: the European molecular biology open software suite". In: *Trends Genet.* (2000), pp. 276–277.

[174] M. Goujon *et al.* "A new bioinformatics analysis tools framework at EMBL–EBI". In: *Nucleic Acids Res.* (2010), W695–W699.

[175] H. McWilliam *et al.* "Analysis tool web services from the EMBL-EBI". In: *Nucleic Acids Res.* (2013), W597–W600.

[176] T. Frickey and A. Lupas. "CLANS: a Java application for visualizing protein families based on pairwise similarity". In: *Bioinformatics* (2004), pp. 3702–3704.

[177] S. F. Altschul *et al.* "Basic local alignment search tool". In: *J. Mol. Biol.* (1990), pp. 403–410.

[178] Y. Liu, B. Schmidt and D. L. Maskell. "MSAProbs: multiple sequence alignment based on pair hidden Markov models and partition function posterior probabilities". In: *Bioinformatics* (2010), pp. 1958–1964.

[179] R. C. Edgar. "MUSCLE: multiple sequence alignment with high accuracy and high throughput". In: *Nucleic Acids Res.* (2004), pp. 1792–1797.

[180] R. C. Edgar. "MUSCLE: a multiple sequence alignment method with reduced time and space complexity". In: *BMC bioinformatics* (2004), p. 113.

[181] C. Notredame, D. G. Higgins and J. Heringa. "T-Coffee: A novel method for fast and accurate multiple sequence alignment". In: *J. Mol. Biol.* (2000), pp. 205–217.

[182] M. E. Oates *et al.* "D2P2: database of disordered protein predictions". In: *Nucleic Acids Res.* (2013), pp. D508–D516.

[183] M. Sickmeier *et al.* "DisProt: the database of disordered proteins". In: *Nucleic Acids Res.* (2007), pp. D786–D793.

[184] F. M. Disfani *et al.* "MoRFpred, a computational tool for sequence-based prediction and characterization of short disorder-to-order transitioning binding regions in proteins". In: *Bioinformatics* (2012), pp. i75–i83.

[185] G. Yachdav *et al.* "PredictProtein—an open resource for online prediction of protein structural and functional features". In: *Nucleic Acids Res.* (2014), W337–W343.

[186] A. Lupas, M. Van Dyke and J. Stock. "Predicting coiled coils from protein sequences." In: *Science* (1991), pp. 1162–1164.

[187] M. Delorenzi and T. Speed. "An HMM model for coiled-coil domains and a comparison with PSSM-based predictions". In: *Bioinformatics* (2002), pp. 617–625.

[188] H. Dinkel *et al.* "ELM–the database of eukaryotic linear motifs." In: *Nucleic Acids Res.* (2012), pp. D242–51.

[189] H. Dinkel *et al.* "The eukaryotic linear motif resource ELM: 10 years and counting." In: *Nucleic Acids Res.* (2014), pp. D259–D266.

[190] J. C. Obenauer, L. C. Cantley and M. B. Yaffe. "Scansite 2.0: Proteome-wide prediction of cell signaling interactions using short sequence motifs". In: *Nucleic Acids Res.* (2003), pp. 3635–3641.

[191] M. B. Yaffe *et al.* "A motif-based profile scanning approach for genome-wide prediction of signaling pathways". In: *Nat. Biotechnol.* (2001), pp. 348–353.

[192] S. Zhou *et al.* "SH2 domains recognize specific phosphopeptide sequences". In: *Cell* (1993), pp. 767–778.

[193] Z. Songyang *et al.* "Recognition of unique carboxyl-terminal motifs by distinct PDZ domains". In: *Science* (1997), pp. 73–77.

[194] C. Mooney *et al.* "Prediction of short linear protein binding regions". In: *J. Mol. Biol.* (2012), pp. 193–204.

[195] P. V. Hornbeck *et al.* "PhosphoSite: A bioinformatics resource dedicated to physiological protein phosphorylation". In: *Proteomics* (2004), pp. 1551–1561.

[196] U. Rothbauer *et al.* "A versatile nanotrap for biochemical and functional studies with fluorescent fusion proteins." In: *Mol. Cell. Proteomics* (2008), pp. 282–9.

[197] D. Saerens *et al.* "Identification of a universal VHH framework to graft non-canonical antigen-binding loops of camel single-domain antibodies". In: *J. Mol. Biol.* (2005), pp. 597–607.

[198] M. H. Kubala *et al.* "Structural and thermodynamic analysis of the GFP:GFP-nanobody complex." In: *Protein Sci.* (2010), pp. 2389–401.

[199] A. Thain *et al.* "A method for the separation of GST fusion proteins from co-purifying GroEL". In: *Trends Genet.* (1996), pp. 209–210.

[200] A. C. Rufer *et al.* "Isoform-selective interaction of the adaptor protein Tks5/FISH with Sos1 and dynamins." In: *J. Mol. Biol.* (2009), pp. 939–50.

[201] J. Cox and M. Mann. "MaxQuant enables high peptide identification rates, individualized ppb-range mass accuracies and proteome-wide protein quantification". In: *Nat. Biotechnol.* (2008), pp. 1367–1372.

[202] J. Cox *et al.* "Andromeda: a peptide search engine integrated into the MaxQuant environment". In: *J. Proteome Res.* (2011), pp. 1794–1805.

[203] G. Pichler *et al.* "Versatile toolbox for high throughput biochemical and functional studies with fluorescent fusion proteins". In: *PLoS One* (2012), e36967.

[204] J. Schindelin *et al.* "Fiji: an open-source platform for biological-image analysis". In: *Nat. Methods* (2012), pp. 676–682.

[205] S. T. Gammon *et al.* "Spectral unmixing of multicolored bioluminescence emitted from heterogeneous biological sources." In: *Anal. Chem.* (2006), pp. 1520–7.

[206] K. Shalchian-Tabrizi *et al.* "Multigene phylogeny of choanozoa and the origin of animals". In: *PLoS One* (2008), e2098.

[207] I. Blasutig. "Phosphorylated Motif Recognition and Mechanisms of Cell Signaling in Actin-Cytoskeletal Regulation". PhD thesis. University of Toronto, 2008.

[208] A. M. A. Aguinaldo *et al.* "Evidence for a clade of nematodes, arthropods and other moulting animals". In: *Nature* (1997), pp. 489–493.

[209] K. M. Halanych *et al.* "Evidence from 18S ribosomal DNA that the lophophorates are protostome animals". In: *Science* (1995), pp. 1641–1643.

[210] C. W. Dunn *et al.* "Broad phylogenomic sampling improves resolution of the animal tree of life". In: *Nature* (2008), pp. 745–749.

[211] M. M. Babu *et al.* "Intrinsically disordered proteins: regulation and disease." In: *Curr. Opin. Struct. Biol.* (2011), pp. 432–40.

[212] H. Yu *et al.* "Structural basis for the binding of proline-rich peptides to SH3 domains." In: *Cell* (1994), pp. 933–45.

[213] X. Du, J. E. Fox and S. Pei. "Identification of a binding sequence for the 14-3-3 protein within the cytoplasmic domain of the adhesion receptor, platelet glycoprotein Ib". In: *J. Biol. Chem.* (1996), pp. 7362–7367.

[214] S.-H. Hu *et al.* "The Weak Complex between RhoGAP Protein ARHGAP22 and Signal Regulatory Protein 14-3-3 Has 1:2 Stoichiometry and a Single Peptide Binding Mode." In: *PLoS One* (2012), pp. 1–11.

[215] C. Ottmann *et al.* "Phosphorylation-independent interaction between 14-3-3 and exoenzyme S: from structure to pathogenesis". In: *EMBO J.* (2007), pp. 902–913.

[216] X. Yang *et al.* "Structural basis for protein–protein interactions in the 14-3-3 protein family". In: *Proc. Natl. Acad. Sci. U. S. A.* (2006), pp. 17237–17242.

[217] M. Fuxreiter, P. Tompa and I. Simon. "Local structural disorder imparts plasticity on linear motifs". In: *Bioinformatics* (2007), pp. 950–956.

[218] S. H. Soderling *et al.* "A WAVE-1 and WRP signaling complex regulates spine density, synaptic plasticity, and memory." In: *J. Neurosci.* (2007), pp. 355–65.

[219] Z.-B. Chen *et al.* "Slit-Robo GTPase-activating proteins are differentially expressed in murine dorsal root ganglia: modulation by peripheral nerve injury." In: *Anat. Rec.* (2012), pp. 652–60.

[220] L. Haussmann. "Identifizierung und Charakterisierung von MEGAP-Interaktionspartnern". PhD thesis. Ruprecht-Karls-Universität, Heidelberg, 2009.

[221] Y.-K. Dai *et al.* "A link between the nuclear-localized srGAP3 and the SWI/SNF chromatin remodeler Brg1." In: *Mol. Cell. Neurosci.* (2014), pp. 10–25.

[222] C. U. Stirnimann *et al.* "WD40 proteins propel cellular networks." In: *Trends Biochem. Sci.* (2010), pp. 565–74.

[223] G. J. Praefcke *et al.* "Evolving nature of the AP2 alpha-appendage hub during clathrin-coated vesicle endocytosis." In: *EMBO J.* (2004), pp. 4371–83.

[224] L. E. Olesen *et al.* "Solitary and repetitive binding motifs for the AP2 complex α-appendage in amphiphysin and other accessory proteins". In: *J. Biol. Chem.* (2008), pp. 5099–5109.

[225] K. C. Slep *et al.* "Structural determinants for EB1-mediated recruitment of APC and spectraplakins to the microtubule plus end". In: *J. Cell Biol.* (2005), pp. 587–598.

[226] C. Gorbea *et al.* "A protein interaction network for Ecm29 links the 26 S proteasome to molecular motors and endosomal components". In: *J. Biol. Chem.* (2010), pp. 31616–31633.

[227] M. E. Harbour *et al.* "The cargo-selective retromer complex is a recruiting hub for protein complexes that regulate endosomal tubule dynamics". In: *J. Cell Sci.* (2010), pp. 3703–3717.

[228] E. H. Michael, Y. B. Sophia and N. Matthew. "Recruitment of the endosomal WASH complex is mediated by the extended'tail'of Fam21 binding to the retromer protein Vps35". In: *Biochem. J.* (2012), pp. 209–220.

[229] E. Conti *et al.* "Crystallographic analysis of the recognition of a nuclear localization signal by the nuclear import factor karyopherin α". In: *Cell* (1998), pp. 193–204.

[230] M. A. Andrade *et al.* "Comparison of ARM and HEAT protein repeats". In: *J. Mol. Biol.* (2001), pp. 1–18.

[231] C. M. Waterman-Storer, S. Karki and E. Holzbaur. "The p150Glued component of the dynactin complex binds to both microtubules and the actin-related protein centractin (Arp-1)." In: *Proc. Natl. Acad. Sci. U. S. A.* (1995), pp. 1634–1638.

[232] E. A. Holleran *et al.* "βIII spectrin binds to the Arp1 subunit of dynactin". In: *J. Biol. Chem.* (2001), pp. 36598–36605.

[233] T. Köcher and G. Superti-Furga. "Mass spectrometry–based functional proteomics: from molecular machines to protein networks". In: *Nat. Methods* (2007), pp. 807–815.

[234] T. De Meyer, S. Muyldermans and A. Depicker. "Nanobody-based products as research and diagnostic tools". In: *Trends Biotechnol.* (2014), pp. 263–270.

[235] M. Lauwereys *et al.* "Potent enzyme inhibitors derived from dromedary heavy-chain antibodies". In: *EMBO J.* (1998), pp. 3512–3520.

[236] S. Muyldermans *et al.* "Camelid immunoglobulins and nanobody technology." In: *Vet. Immunol. Immunopathol.* (2009), pp. 1–6.

[237] D. C. Worth *et al.* "Drebrin contains a cryptic F-actin-bundling activity regulated by Cdk5 phosphorylation." In: *J. Cell Biol.* (2013), pp. 793–806.

[238] Y. K. Mok *et al.* "Dramatic stabilization of an SH3 domain by a single substitution: roles of the folded and unfolded states." In: *J. Mol. Biol.* (2001), pp. 913–28.

[239] D. Grabs *et al.* "The SH3 domain of amphiphysin binds the proline-rich domain of dynamin at a single site that defines a new SH3 binding consensus sequence". In: *J. Biol. Chem.* (1997), pp. 13419–13425.

[240] C. B. McDonald *et al.* "SH3 domains of Grb2 adaptor bind to PXψPXR motifs within the Sos1 nucleotide exchange factor in a discriminate manner". In: *Biochemistry (Mosc.)* (2009), pp. 4074–4085.

[241] B. A. Ballif *et al.* "Identification of 14-3-3epsilon substrates from embryonic murine brain." In: *J. Proteome Res.* (2006), pp. 2372–9.

[242] E. L. Huttlin *et al.* "A Tissue-Specific Atlas of Mouse Protein Phosphorylation and Expression". In: *Cell* (2010), pp. 1174–1189.

[243] A. Quan *et al.* "Phosphorylation of syndapin I F-BAR domain at two helix-capping motifs regulates membrane tubulation." In: *Proc. Natl. Acad. Sci. U. S. A.* (2012), pp. 3760–5.

[244] H. Saitsu *et al.* "Early infantile epileptic encephalopathy associated with the disrupted gene encoding Slit-Robo Rho GTPase activating protein 2 (SRGAP2)." In: *Am. J. Med. Genet. A.* (2011).

[245] S. Guo and S. Bao. "srGAP2 arginine methylation regulates cell migration and cell spreading through promoting dimerization." In: *J. Biol. Chem.* (2010), pp. 1–9.

[246] E. A. Golemis *et al.* "Interaction trap/two-hybrid system to identify interacting proteins". In: *Curr. Protoc. Cell Biol.* (1996), pp. 17–3.

[247] C. S. Goodyear and G. J. Silverman. "Phage-display methodology for the study of protein-protein interactions: Overview". In: *Cold Spring Harbor Prot.* (2008), pdb–top48.

[248] H. Okada *et al.* "SH3 domain-based phototrapping in living cells reveals Rho family GAP signaling complexes." In: *Sci. Signaling* (2011), rs13.

[249] W. Van Criekinge and R. Beyaert. "Yeast two-hybrid: state of the art". In: *Biol. Proced. Online* (1999), pp. 1–38.

[250] J. Torres and R. Pulido. "The tumor suppressor PTEN is phosphorylated by the protein kinase CK2 at its C terminus. Implications for PTEN stability to proteasome-mediated degradation." In: *J. Biol. Chem.* (2001), pp. 993–8.

[251] A. Brymora, V. A. Valova and P. J. Robinson. "Protein-Protein Interactions Identified by Pull-Down Experiments and Mass Spectrometry". In: *Curr. Protoc. Cell Biol.* (2004), pp. 17–5.

[252] D. Saerens *et al.* "Engineering camel single-domain antibodies and immobilization chemistry for human prostate-specific antigen sensing". In: *Anal. Chem.* (2005), pp. 7547–7555.

[253] D. Saerens *et al.* "Antibody fragments as probe in biosensor development". In: *Sensors* (2008), pp. 4669–4686.

[254] G.-L. Zhou *et al.* "Akt phosphorylation of serine 21 on Pak1 modulates Nck binding and cell migration". In: *Mol. Cell. Biol.* (2003), pp. 8058–8069.

[255] L. J. Jensen *et al.* "STRING 8–a global view on proteins and their functional interactions in 630 organisms". In: *Nucleic Acids Res.* (2009), pp. D412–D416.

[256] S. Leavitt and E. Freire. "Direct measurement of protein binding energetics by isothermal titration calorimetry." In: *Curr. Opin. Struct. Biol.* (2001), pp. 560–6.

[257] T. Kaneko, L. Li and S. S.-C. Li. "The SH3 domain–a family of versatile peptide- and protein-recognition module." In: *Front. Biosci.* (2008), pp. 1–15.

[258] T. Kaneko, S. S. Sidhu and S. S. Li. "Evolving specificity from variability for protein interaction domains." In: *Trends Biochem. Sci.* (2011), pp. 1–8.

[259] I. Nooren and J. M. Thornton. "Structural characterisation and functional significance of transient protein–protein interactions". In: *J. Mol. Biol.* (2003), pp. 991–1018.

[260] P. Chakrabarti and J. Janin. "Dissecting protein–protein recognition sites". In: *Proteins: Struct., Funct., Bioinf.* (2002), pp. 334–343.

[261] D. Owen *et al.* "Crystal structure of the amphiphysin-2 SH3 domain and its role in the prevention of dynamin ring formation". In: *EMBO J.* (1998), pp. 5273–5285.

[262] G. Cestra *et al.* "The SH3 domains of endophilin and amphiphysin bind to the proline-rich region of synaptojanin 1 at distinct sites that display an unconventional binding specificity." In: *J. Biol. Chem.* (1999), pp. 32001–7.

[263] W. Jockusch *et al.* "Clathrin-dependent and clathrin-independent retrieval of synaptic vesicles in retinal bipolar cells." In: *Neuron* (2005), pp. 869–78.

[264] N. Ringstad, Y. Nemoto and P. De Camilli. "Differential expression of endophilin 1 and 2 dimers at central nervous system synapses". In: *J. Biol. Chem.* (2001), pp. 40424–40430.

[265] P. J. Loll *et al.* "Structure of the SH3 domain of rat endophilin A2". In: *Acta Crystallograph. Sect. F Struct. Biol. Cryst. Commun.* (2008), pp. 243–246.

[266] J. A. Simon and S. L. Schreiber. "Grb2 SH3 binding to peptides from Sos: evaluation of a general model for SH3-ligand interactions." In: *Chem. Biol.* (1995), pp. 53–60.

[267] P. Chardin *et al.* "Human Sos1: a guanine nucleotide exchange factor for Ras that binds to GRB2". In: *Science* (1993), pp. 1338–1343.

[268] S. E. Egan *et al.* "Association of Sos Ras exchange protein with Grb2 is implicated in tyrosine kinase signal transduction and transformation". In: *Nature* (1993), pp. 45–51.

[269] N. a. Li *et al.* "Guanine-nucleotide-releasing factor hSos1 binds to Grb2 and links receptor tyrosine kinases to Ras signalling". In: *Nature* (1993), pp. 85–88.

[270] S. Maignan *et al.* "Crystal structure of the mammalian Grb2 adaptor." In: *Science* (1995), pp. 291–3.

[271] C. B. McDonald *et al.* "Grb2 adaptor undergoes conformational change upon dimerization". In: *Arch. Biochem. Biophys.* (2008), pp. 25–35.

[272] C. B. McDonald *et al.* "Bivalent binding drives the formation of the Grb2–Gab1 signaling complex in a noncooperative manner". In: *FEBS J.* (2012), pp. 2156–2173.

[273] D. M. Berry *et al.* "A High-Affinity Arg-X-X-Lys SH3 Binding Motif Confers Specificity for the Interaction between Gads and SLP-76 in T Cell Signaling". In: *Curr. Biol.* (2002), pp. 1336–1341.

[274] V. Neduva *et al.* "Systematic discovery of new recognition peptides mediating protein interaction networks". In: *PLoS Biol.* (2005), e405.

[275] M. Chaudhri, M. Scarabel and A. Aitken. "Mammalian and yeast 14-3-3 isoforms form distinct patterns of dimers in vivo". In: *Biochem. Biophys. Res. Commun.* (2003), pp. 679–685.

[276] J. Zha *et al.* "Serine Phosphorylation of Death Agonist BAD in Response to Survival Factor Results in Binding to 14-3-3 Not BCL-X_L". In: *Cell* (1996), pp. 619–628.

[277] G. Rena *et al.* "Roles of the forkhead in rhabdomyosarcoma (FKHR) phosphorylation sites in regulating 14-3-3 binding, transactivation and nuclear targetting." In: *Biochem J.* (2001), pp. 605–12.

[278] R. Y. Tweedie-Cullen, J. M. Reck and I. M. Mansuy. "Comprehensive mapping of post-translational modifications on synaptic, nuclear, and histone proteins in the adult mouse brain." In: *J. Proteome Res.* (2009), pp. 4966–82.

[279] B. D. Manning and L. C. Cantley. "Hitting the target: emerging technologies in the search for kinase substrates". In: *Sci. Signaling* (2002), pe49.

[280] N. Blom *et al.* "Prediction of post-translational glycosylation and phosphorylation of proteins from the amino acid sequence". In: *Proteomics* (2004), pp. 1633–1649.

[281] P. Riou *et al.* "14-3-3 proteins interact with a hybrid prenyl-phosphorylation motif to inhibit G proteins." In: *Cell* (2013), pp. 640–53.

[282] J. K. Campbell *et al.* "Activation of the 43 kDa inositol polyphosphate 5-phosphatase by 14-3-3ζ". In: *Biochemistry (Mosc.)* (1997), pp. 15363–15370.

[283] G. Zhang *et al.* "Overview of peptide and protein analysis by mass spectrometry". In: *Curr. Protoc. Prot. Sci.* (2010), pp. 16–1.

[284] M. Tinti *et al.* "Evolution of signal multiplexing by 14-3-3-binding 2R-ohnologue protein families in the vertebrates". In: *Open Biol.* (2012), pp. 120103–120103.

[285] K. Van Roey *et al.* "Short linear motifs: ubiquitous and functionally diverse protein interaction modules directing cell regulation". In: *Chem. Rev.* (2014), pp. 6733–6778.

[286] C. Tarricone *et al.* "The structural basis of Arfaptin-mediated cross-talk between Rac and Arf signalling pathways". In: *Nature* (2001), pp. 215–219.

[287] B. Xiao *et al.* "Structure of a 14-3-3 protein and implications for coordination of multiple signalling pathways". In: *Nature* (1995).

[288] C. Kintscher *et al.* "Autoinhibition of GEF activity in Intersectin 1 is mediated by the short SH3-DH domain linker." In: *Protein Sci.* (2010), pp. 1–11.

[289] E. M. Schmid and H. T. McMahon. "Integrating molecular and network biology to decode endocytosis". In: *Nature* (2007), p. 883.

[290] C. Chica, F. Diella and T. J. Gibson. "Evidence for the concerted evolution between short linear protein motifs and their flanking regions". In: *PLoS One* (2009), e6052.

[291] B. J. Schnapp. "Trafficking of signaling modules by kinesin motors". In: *J. Cell Sci.* (2003), pp. 2125–2135.

[292] H. Jung *et al.* "Remote Control of Gene Function by Local Translation". In: *Cell* (2014), pp. 26–40.

[293] P. Li *et al.* "Phase transitions in the assembly of multivalent signalling proteins". In: *Nature* (2012), pp. 336–340.

[294] A. Nag *et al.* "Aggregation of membrane proteins by cytosolic cross-linkers: theory and simulation of the LAT-Grb2-SOS1 system". In: *Biophys. J.* (2009), pp. 2604–2623.

[295] A. Nag *et al.* "Modeling and simulation of aggregation of membrane protein LAT with molecular variability in the number of binding sites for cytosolic Grb2-SOS1-Grb2". In: *PLoS One* (2012), e28758.

[296] S. Banjade, M. K. Rosen and A. A. Hyman. "Phase transitions of multivalent proteins can promote clustering of membrane receptors." In: *eLife* (2014).

[297] T. Pawson and J. D. Scott. "Signaling through scaffold, anchoring, and adaptor proteins". In: *Science* (1997), pp. 2075–2080.

[298] J. Liu, J. R. Faeder and C. J. Camacho. "Toward a quantitative theory of intrinsically disordered proteins and their function". In: *Proc. Natl. Acad. Sci. U. S. A.* (2009), pp. 19819–19823.

[299] K. Sugase, H. J. Dyson and P. E. Wright. "Mechanism of coupled folding and binding of an intrinsically disordered protein". In: *Nature* (2007), pp. 1021–1025.

[300] R. Mosca, R. A. Pache and P. Aloy. "The role of structural disorder in the rewiring of protein interactions through evolution." In: *Mol. Cell. Proteomics* (2012), p. M111.014969.

[301] T. Kaneko *et al.* "Superbinder SH2 Domains Act as Antagonists of Cell Signaling." In: *Sci. Signaling* (2012), pp. 1–11.

[302] H. Huang *et al.* "Defining the specificity space of the human SRC homology 2 domain". In: *Mol. Cell. Proteomics* (2008), pp. 768–784.

[303] N. J. Haslam and D. C. Shields. "Peptide-binding domains: are limp handshakes safest?" In: *Sci. Signaling* (2012), pp. 1–4.

[304] N. E. Davey, G. Travé and T. J. Gibson. "How viruses hijack cell regulation". In: *Trends Biochem. Sci.* (2011), pp. 159–169.

[305] P. Tompa *et al.* "A million peptide motifs for the molecular biologist". In: *Mol. Cell* (2014), pp. 161–169.

[306] X. Xin *et al.* "SH3 interactome conserves general function over specific form." In: *Mol. Syst. Biol.* (2013), p. 652.

[307] A. B. Huber *et al.* "Signaling at the growth cone: ligand-receptor complexes and the control of axon growth and guidance." In: *Annu. Rev. Neurosci.* (2003), pp. 509–63.

[308] F. M. Mason *et al.* "Bi-modal regulation of a formin by srGAP2." In: *J. Biol. Chem.* (2011), pp. 6577–86.

[309] M. J. Dayel *et al.* "Cell differentiation and morphogenesis in the colony-forming choanoflagellate Salpingoeca rosetta". In: *Dev. Biol.* (2011), pp. 73–82.

[310] A. Sebé-Pedrós *et al.* "Regulated aggregative multicellularity in a close unicellular relative of metazoa". In: *eLife* (2013).

[311] P. Burkhardt *et al.* "Evolutionary insights into premetazoan functions of the neuronal protein Homer". In: *Mol. Biol. Evol.* (2014), msu178.

[312] A. Sebé-Pedrós *et al.* "Insights into the origin of metazoan filopodia and microvilli". In: *Mol. Biol. Evol.* (2013).

[313] A. de Mendoza, H. Suga and I. Ruiz-Trillo. "Evolution of the MAGUK protein gene family in premetazoan lineages". In: *BMC Evol. Biol.* (2010), p. 93.

[314] S. R. Fairclough *et al.* "Premetazoan genome evolution and the regulation of cell differentiation in the choanoflagellate Salpingoeca rosetta". In: *Genome Biol.* (2013), R15.

[315] X. Cai. "Evolutionary genomics reveals the premetazoan origin of opposite gating polarity in animal-type voltage-gated ion channels". In: *Genomics* (2012), pp. 241–245.

[316] V. C. Foletta, F. D. Brown and W. S. 3rd. "Cloning of rat ARHGAP4/C1, a RhoGAP family member expressed in the nervous system that colocalizes with the Golgi complex and microtubules." In: *Brain Res. Mol. Brain Res.* (2002), pp. 1–15.

[317] C. David *et al.* "A role of amphiphysin in synaptic vesicle endocytosis suggested by its binding to dynamin in nerve terminals". In: *Proc. Natl. Acad. Sci. U. S. A.* (1996), pp. 331–335.

[318] P. Wigge, Y. Vallis and H. T. McMahon. "Inhibition of receptor-mediated endocytosis by the amphiphysin SH3 domain". In: *Curr. Biol.* (1997), pp. 554–560.

[319] Y. Chen *et al.* "Formation of an endophilin-Ca2+ channel complex is critical for clathrin-mediated synaptic vesicle endocytosis." In: *Cell* (2003), pp. 1–12.

[320] G. Zhang, T. A. Neubert and B. A. Jordan. "RNA binding proteins accumulate at the postsynaptic density with synaptic activity." In: *J. Neurosci.* (2012), pp. 1–11.

[321] S. Chowdhury *et al.* "Arc/Arg3.1 interacts with the endocytic machinery to regulate AMPA receptor trafficking." In: *Neuron* (2006), pp. 445–59.

[322] H.-Y. Man *et al.* "Regulation of AMPA receptor–mediated synaptic transmission by clathrin-dependent receptor internalization". In: *Neuron* (2000), pp. 649–662.

[323] E. Lowenstein *et al.* "The SH2 and SH3 domain-containing protein GRB2 links receptor tyrosine kinases to ras signaling". In: *Cell* (1992), pp. 431–442.

[324] J. I. MacDonald *et al.* "Direct binding of the signaling adapter protein Grb2 to the activation loop tyrosines on the nerve growth factor receptor tyrosine kinase, TrkA". In: *J. Biol. Chem.* (2000), pp. 18225–18233.

[325] M. Rozakis-Adcock *et al.* "Association of the Shc and Grb2/Sem5 SH2-containing proteins is implicated in activation of the Ras pathway by tyrosine kinases". In: *Nature* (1992), pp. 689–692.

[326] M. Rozakis-Adcock *et al.* "The SH2 and SH3 domains of mammalian Grb2 couple the EGF receptor to the Ras activator mSos1". In: *Nature* (1993), pp. 83–5.

[327] N. W. Gale *et al.* "Grb2 mediates the EGF-dependent activation of guanine nucleotide exchange on Ras". In: *Nature* (1993).

[328] Z. Wang and M. F. Moran. "Requirement for the adapter protein GRB2 in EGF receptor endocytosis". In: *Science* (1996), pp. 1935–1938.

[329] T. Yamazaki *et al.* "Role of Grb2 in EGF-stimulated EGFR internalization". In: *J. Cell Sci.* (2002), pp. 1791–1802.

[330] F. Huang and A. Sorkin. "Growth factor receptor binding protein 2-mediated recruitment of the RING domain of Cbl to the epidermal growth factor receptor is essential and sufficient to support receptor endocytosis". In: *Mol. Biol. Cell* (2005), pp. 1268–1281.

[331] L. Conti *et al.* "Expression and activation of SH2/PTB-containing ShcA adaptor protein reflects the pattern of neurogenesis in the mammalian brain". In: *Proc. Natl. Acad. Sci. U. S. A.* (1997), pp. 8185–8190.

[332] A. M. Cheng *et al.* "Mammalian Grb2 regulates multiple steps in embryonic development and malignant transformation". In: *Cell* (1998), pp. 793–803.

[333] L. Brodin, P. Löw and O. Shupliakov. "Sequential steps in clathrin-mediated synaptic vesicle endocytosis". In: *Curr. Opin. Neurobiol.* (2000), pp. 312–320.

[334] S. G. Penheiter *et al.* "Internalization-dependent and-independent requirements for transforming growth factor β receptor signaling via the Smad pathway". In: *Mol. Cell. Biol.* (2002), pp. 4750–4759.

[335] R. Irannejad *et al.* "Conformational biosensors reveal GPCR signalling from endosomes." In: *Nature* (2013), pp. 534–8.

[336] P. Billuart *et al.* "Oligophrenin-1 encodes a rhoGAP protein involved in X-linked mental retardation". In: *Nature* (1998), pp. 923–926.

[337] A. Nakano-Kobayashi *et al.* "The Rho-linked mental retardation protein OPHN1 controls synaptic vesicle endocytosis via endophilin A1." In: *Curr. Biol.* (2009), pp. 1133–9.

[338] N. N. Kasri, A. Nakano-Kobayashi and L. van Aelst. "Rapid synthesis of the X-linked mental retardation protein OPHN1 mediates mGluR-dependent LTD through interaction with the endocytic machinery." In: *Neuron* (2011), pp. 300–15.

[339] T. Kidd *et al.* "Roundabout controls axon crossing of the CNS midline and defines a novel subfamily of evolutionarily conserved guidance receptors". In: *Cell* (1998), pp. 205–215.

[340] H. Long *et al.* "Conserved roles for Slit and Robo proteins in midline commissural axon guidance". In: *Neuron* (2004), pp. 213–223.

[341] K. Keleman *et al.* "Comm sorts robo to control axon guidance at the Drosophila midline." In: *Cell* (2002), pp. 415–27.

[342] J. T. Kittler *et al.* "Constitutive endocytosis of GABAA receptors by an association with the adaptin AP2 complex modulates inhibitory synaptic currents in hippocampal neurons". In: *J. Neurosci.* (2000), pp. 7972–7977.

[343] L. Yang and G. J. Bashaw. "Son of sevenless directly links the Robo receptor to rac activation to control axon repulsion at the midline". In: *Neuron* (2006), pp. 595–607.

[344] R. Waltereit, S. Kautt and D. Bartsch. "Expression of MEGAP mRNA during embryonic development." In: *Gene Expression Patterns* (2008), pp. 307–10.

[345] T. Obsil *et al.* "Crystal Structure of the 14-3-3ζ:Serotonin N-Acetyltransferase Complex". In: *Cell* (2001), pp. 257–267.

[346] D. M. Bustos and A. A. Iglesias. "Intrinsic disorder is a key characteristic in partners that bind 14-3-3 proteins". In: *Proteins: Struct., Funct., Bioinf.* (2006), pp. 35–42.

[347] S. Ganguly, J. Weller and A. Ho. "Melatonin synthesis: 14-3-3-dependent activation and inhibition of arylalkylamine N-acetyltransferase mediated by phosphoserine-205". In: *Proc. Natl. Acad. Sci. U. S. A.* (2005).

[348] V. Cotelle *et al.* "14-3-3s regulate global cleavage of their diverse binding partners in sugar-starved Arabidopsis cells". In: *EMBO J.* (2000), pp. 2869–2876.

[349] P. Tompa *et al.* "Structural disorder serves as a weak signal for intracellular protein degradation". In: *Proteins: Struct., Funct., Bioinf.* (2008), pp. 903–909.

[350] S. Datta. "Akt Phosphorylation of BAD Couples Survival Signals to the Cell-Intrinsic Death Machinery". In: *Cell* (1997), pp. 231–241.

[351] T. Benzing *et al.* "14-3-3 Interacts with Regulator of G Protein Signaling Proteins and Modulates Their Activity". In: *J. Biol. Chem.* (2000), pp. 28167–28172.

[352] A. Brunet *et al.* "Akt Promotes Cell Survival by Phosphorylating and Inhibiting a Forkhead Transcription Factor". In: *Cell* (1999), pp. 857–868.

[353] S. Braselmann and F. McCormick. "Bcr and Raf form a complex in vivo via 14-3-3 proteins." In: *EMBO J.* (1995).

[354] C. Vincenz and V. Dixit. "14-3-3 proteins associate with A20 in an isoform-specific manner and function both as chaperone and adapter molecules". In: *J. Biol. Chem.* (1996).

[355] B. Schumacher *et al.* "Structure of the p53 C-terminus bound to 14-3-3: implications for stabilization of the p53 tetramer". In: *FEBS Lett.* (2010).

[356] C. Petosa *et al.* "14-3-3ζ binds a phosphorylated Raf peptide and an unphosphorylated peptide via its conserved amphipathic groove". In: *J. Biol. Chem.* (1998), pp. 16305–16310.

[357] B. Wang *et al.* "Isolation of high-affinity peptide antagonists of 14-3-3 proteins by phage display". In: *Biochemistry (Mosc.)* (1999), pp. 12499–12504.

[358] C. J. Brown *et al.* "Evolutionary rate heterogeneity in proteins with long disordered regions". In: *J. Mol. Evol.* (2002), pp. 104–110.

[359] Y.-S. Lin *et al.* "Proportion of solvent-exposed amino acids in a protein and rate of protein evolution". In: *Mol. Biol. Evol.* (2007), pp. 1005–1011.

[360] C. Chica *et al.* "A tree-based conservation scoring method for short linear motifs in multiple alignments of protein sequences". In: *BMC bioinformatics* (2008), p. 229.

[361] N. E. Davey, D. C. Shields and R. J. Edwards. "Masking residues using context-specific evolutionary conservation significantly improves short linear motif discovery". In: *Bioinformatics* (2009), pp. 443–450.

[362] D. P. Denning and M. F. Rexach. "Rapid evolution exposes the boundaries of domain structure and function in natively unfolded FG nucleoporins". In: *Mol. Cell. Proteomics* (2007), pp. 272–282.

[363] K. Linderstrøm-Lang. "Structure and enzymatic break-down of proteins". In: *Cold Spring Harbor Symp. Quant. Biol.* (1950), pp. 117–126.

[364] G. Markus. "Protein substrate conformation and proteolysis." In: *Proc. Natl. Acad. Sci. U. S. A.* (1965), p. 253.

[365] S. Hubbard, F. Eisenmenger and J. Thornton. "Modeling studies of the change in conformation required for cleavage of limited proteolytic sites". In: *Protein Sci.* (1994), pp. 757–768.

[366] J. Gsponer *et al.* "Tight regulation of unstructured proteins: from transcript synthesis to protein degradation." In: *Science* (2008), pp. 1365–8.

[367] U. B. Choi *et al.* "Beyond the random coil: stochastic conformational switching in intrinsically disordered proteins." In: *Structure* (2011), pp. 566–76.

[368] A. C. Ferreon *et al.* "Modulation of allostery by protein intrinsic disorder." In: *Nature* (2013), pp. 390–4.

[369] B. Qualmann *et al.* "Syndapin I, a synaptic dynamin-binding protein that associates with the neural Wiskott-Aldrich syndrome protein." In: *Mol. Biol. Cell* (1999), pp. 501–13.

[370] R. Fricke, C. Gohl and S. Bogdan. "The F-BAR protein family Actin' on the membrane". In: *Comm. Integr. Biol.* (2010), pp. 89–94.

[371] M. M. Kessels and B. Qualmann. “Syndapins integrate N-WASP in receptor-mediated endocytosis.” In: *EMBO J.* (2002), pp. 6083–94.

[372] M. Plomann *et al.* “PACSIN, a brain protein that is upregulated upon differentiation into neuronal cells.” In: *Eur. J. Biochem.* (1998), pp. 201–11.

[373] M. M. Kessels and B. Qualmann. “The syndapin protein family: linking membrane trafficking with the cytoskeleton.” In: *J. Cell Sci.* (2004), pp. 3077–86.

[374] B. Ritter *et al.* “PACSIN 2, a novel member of the PACSIN family of cytoplasmic adapter proteins”. In: *FEBS Lett.* (1999), pp. 356–362.

[375] B. Qualmann and R. B. Kelly. “Syndapin isoforms participate in receptor-mediated endocytosis and actin organization.” In: *J. Cell Biol.* (2000), pp. 1047–62.

[376] J. Modregger *et al.* “All three PACSIN isoforms bind to endocytic proteins and inhibit endocytosis.” In: *J. Cell Sci.* (2000), pp. 4511–21.

[377] F. Simpson *et al.* “SH3-domain-containing proteins function at distinct steps in clathrin-coated vesicle formation.” In: *Nat. Cell Biol.* (1999), pp. 119–24.

[378] A. Quan and P. Robinson. “Syndapin - a membrane remodelling and endocytic F-BAR protein.” In: *FEBS J.* (2013), pp. 1–15.

[379] E. L. Clayton *et al.* “The phospho-dependent dynamin–syndapin interaction triggers activity-dependent bulk endocytosis of synaptic vesicles”. In: *J. Neurosci.* (2009), pp. 7706–7717.

[380] L. Mintz *et al.* “EHD1–an EH-domain-containing protein with a specific expression pattern”. In: *Genomics* (1999), pp. 66–76.

[381] Y. Xu *et al.* “Mutually exclusive interactions of EHD1 with GS32 and syndapin II.” In: *Mol. Membr. Biol.* (2004), pp. 269–77.

[382] U. Pohl *et al.* “EHD2, EHD3, and EHD4 Encode Novel Members of a Highly Conserved Family of EH Domain-Containing Proteins”. In: *Genomics* (2000), pp. 255–262.

[383] B. Grant *et al.* “Evidence that RME-1, a conserved C. elegans EH-domain protein, functions in endocytic recycling.” In: *Nat. Cell Biol.* (2001), pp. 573–9.

[384] N. Naslavsky and S. Caplan. “EHD proteins: key conductors of endocytic transport.” In: *Trends Cell Biol.* (2011), pp. 122–31.

[385] D. Rapaport *et al.* “Recycling to the plasma membrane is delayed in EHD1 knockout mice”. In: *Traffic* (2006), pp. 52–60.

[386] S. X. Lin *et al.* "Rme-1 regulates the distribution and function of the endocytic recycling compartment in mammalian cells." In: *Nat. Cell Biol.* (2001), pp. 567–72.

[387] S. Caplan *et al.* "A tubular EHD1-containing compartment involved in the recycling of major histocompatibility complex class I molecules to the plasma membrane". In: *EMBO J.* (2002), pp. 2557–2567.

[388] C. C. C. Yap *et al.* "Alterations of EHD1/EHD4 protein levels interfere with L1/NgCAM endocytosis in neurons and disrupt axonal targeting." In: *J. Neurosci.* (2010), pp. 6646–57.

[389] Z. M. Lasiecka *et al.* "Neuronal early endosomes require EHD1 for L1/NgCAM trafficking." In: *J. Neurosci.* (2010), pp. 16485–97.

[390] O. Daumke *et al.* "Architectural and mechanistic insights into an EHD ATPase involved in membrane remodelling." In: *Nature* (2007), pp. 923–927.

[391] J. J. Blume *et al.* "EHD proteins are associated with tubular and vesicular compartments and interact with specific phospholipids." In: *Exp. Cell Res.* (2007), pp. 1–13.

[392] M. Sharma, N. Naslavsky and S. Caplan. "A role for EHD4 in the regulation of early endosomal transport". In: *Traffic* (2008), pp. 995–1018.

[393] C. Shah *et al.* "Structural Insights into Membrane Interaction and Caveolar Targeting of Dynamin-like EHD2." In: *Structure* (2014), pp. 1–12.

[394] B. Cai, S. Caplan and N. Naslavsky. "cPLA2α and EHD1 interact and regulate the vesiculation of cholesterol-rich, GPI-anchored, protein-containing endosomes." In: *Mol. Biol. Cell* (2012), pp. 1874–88.

[395] B. Cai *et al.* "Differential roles of C-terminal Eps15 homology domain proteins as vesiculators and tubulators of recycling endosomes." In: *J. Biol. Chem.* (2013), pp. 30172–80.

[396] A. Shi *et al.* "A Novel Requirement for C. elegans Alix/ALX-1 in RME-1-Mediated Membrane Transport". In: *Curr. Biol.* (2007), pp. 1913–1924.

[397] T. Takeda *et al.* "Drosophila F-BAR protein Syndapin contributes to coupling the plasma membrane and contractile ring in cytokinesis." In: *Open Biol.* (2013), p. 130081.

[398] L. Mayer *et al.* "Solute distributions and trapping efficiencies observed in freeze-thawed multilamellar vesicles". In: *Biochim. Biophys. Acta, Biomembr.* (1985), pp. 193–196.

[399] U. Pick. "Liposomes with a large trapping capacity prepared by freezing and thawing of sonicated phospholipid mixtures". In: *Arch. Biochem. Biophys.* (1981), pp. 186–194.

[400] M. M. Kessels and B. Qualmann. "Syndapin oligomers interconnect the machineries for endocytic vesicle formation and actin polymerization." In: *J. Biol. Chem.* (2006), pp. 13285–99.

[401] K. Sarfo, G. B. Moorhead and R. J. Turner. "A novel procedure for separating small peptides on polyacrylamide gels". In: *Lett. Pept. Sci.* (2003), pp. 127–133.

[402] S. Schael *et al.* "Casein Kinase 2 Phosphorylation of PACSIN 1 Regulates Neuronal Spine Formation." In: *J. Biol. Chem.* (2013), pp. 1–18.

[403] M. Jović *et al.* "Eps15 homology domain 1-associated tubules contain phosphatidylinositol-4-phosphate and phosphatidylinositol-(4, 5)-bisphosphate and are required for efficient recycling". In: *Mol. Biol. Cell* (2009), pp. 2731–2743.

[404] F. D. Brown *et al.* "Phosphatidylinositol 4, 5-bisphosphate and Arf6-regulated membrane traffic". In: *J. Cell Biol.* (2001), pp. 1007–1018.

[405] D.-w. Lee *et al.* "ATP binding regulates oligomerization and endosome association of RME-1 family proteins." In: *J. Biol. Chem.* (2005), pp. 17213–20.

[406] S. S. Giridharan *et al.* "Cooperation of MICAL-L1, Syndapin2 and Phosphatidic Acid in Tubular Recycling Endosome Biogenesis." In: *Mol. Biol. Cell* (2013), pp. 1–15.

[407] B. Morén *et al.* "EHD2 regulates caveolar dynamics via ATP-driven targeting and oligomerization." In: *Mol. Biol. Cell* (2012), pp. 1–14.

[408] N. Naslavsky *et al.* "EHD1 and Eps15 interact with phosphatidylinositols via their Eps15 homology domains." In: *J. Biol. Chem.* (2007), pp. 16612–22.

[409] J. Folch. "Brain diphosphoinositide, a new phosphatide having inositol metadiphosphate as a constituent". In: *J. Biol. Chem.* (1949), pp. 505–519.

[410] H. Brockerhoff and C. E. Ballou. "The structure of the phosphoinositide complex of beef brain". In: *J. Biol. Chem.* (1961), pp. 1907–1911.

[411] M. Plomann, J. G. Wittmann and M. G. Rudolph. "A hinge in the distal end of the PACSIN 2 F-BAR domain may contribute to membrane-curvature sensing." In: *J. Mol. Biol.* (2010), pp. 1–8.

[412] X. Bai and X. Zheng. "Tip-to-tip interaction in the crystal packing of PACSIN 2 is important in regulating tubulation activity." In: *Protein and Cell* (2013), pp. 1–7.

[413] D. Yarar, C. M. Waterman-Storer and S. L. Schmid. "SNX9 couples actin assembly to phosphoinositide signals and is required for membrane remodeling during endocytosis". In: *Dev. Cell* (2007), pp. 43–56.

[414] J. C. Stachowiak, C. C. Hayden and D. Y. Sasaki. "Steric confinement of proteins on lipid membranes can drive curvature and tubulation." In: *Proc. Natl. Acad. Sci. U. S. A.* (2010), pp. 7781–6.

[415] T. Trudeau *et al.* "Structure and Intrinsic Disorder in Protein Autoinhibition." In: *Structure* (2013), pp. 1–10.

[416] R. Rohatgi *et al.* "The interaction between N-WASP and the Arp2/3 complex links Cdc42-dependent signals to actin assembly". In: *Cell* (1999), pp. 221–231.

[417] R. Zaidel-Bar *et al.* "The F-BAR domain of SRGP-1 facilitates cell-cell adhesion during C. elegans morphogenesis." In: *J. Cell Biol.* (2010), pp. 1–9.

A. General Supporting Information

Table A.1.: Genotypes of *Escherichia coli* strains.

Strain	Genotype
TOP10 (Invitrogen)	F$^-$ *mcrA* Δ(*mrr-hsd*RMS-*mcr*BC) Φ80*lacZ*ΔM15 Δ *lac*X74 *rec*A1 *ara*D139 Δ(*araleu*)7697 *gal*U *gal*K *rps*L (StrR) *end*A1 *nup*G
Bl21(DE3) Gold	Hte F$^-$ *lon ompT hsdS*$_B$(r$_B^-$ m$_B^-$) *gal dcm*+ λ(DE3) *endA* Tet^R
Rosetta 2 (DE3)pLysS (Novagen)	F$^-$ *ompT hsdS*$_B$(r$_B^-$ m$_B^-$) *gal dcm* λ(DE3) pLysSRARE2 (Cam^R)

B. Supporting Information srGAP3

Table B.1.: Clones obtained from other groups for subcloning.

Insert	Organism[a]	Vector	Comment
14-3-3β	Hs	pGEX4T1	from S. Beer-Hammer, Tübingen
14-3-3γ	Rn	pGEX4T1	from S. Beer-Hammer, Tübingen
14-3-3ϵ	Rn	pGEX4T1	from S. Beer-Hammer, Tübingen
14-3-3ζ	Hs	pGEX4T1	from S. Beer-Hammer, Tübingen
14-3-3η	Hs	pGEX2TK	from S. Beer-Hammer, Tübingen
14-3-3θ/τ	Hs	pGEX4T1	from S. Beer-Hammer, Tübingen
Amphiphysin	Rn	pGEX	from H. T. McMahon, Cambridge
AP2 α2 (701-938)	Mm	pGEX4T1	from H. T. McMahon, Cambridge
α-Cop	Mm	pCR-Blunt	from F. Wieland, Heidelberg
Drebrin	Hs	pOTB7	Biocat[b] Clone ID 3343626
EB1	Hs	pDEST/N1GFP	Addgene[b] clone 27382
Endophilin-A1	Hs	pGEX	from H. T. McMahon, Cambridge, clone E85001
Endophilin-A2	Hs	pGEX	from H. T. McMahon, Cambridge, clone E135000
mCherry		199_UAS_ERT2crep	from A. Mongera, Tübingen
myc-Vps26	Hs	pCIm	from J. Bonifacino, Bethesda
myc-Vps35	Hs	pCIm	from J. Bonifacino, Bethesda
Neurochondrin	Hs	pcMVSport6	Biocat Clone ID 3914058
srGAP3	Hs	pcDNA3.1	from G. Rappold, Heidelberg
Strap	Hs	pOTB7	Biocat[b] Clone ID 3349549
α-Centractin	Hs	pCDNA3	from E. Holzbaur, Philadelphia

[a] Hs, *Homo sapiens*; Rn, *Rattus norvegicus*; Mm, *Mus musculus*
[b] Biocat GmbH, Heidelberg; addgene, https://www.addgene.org/

Table B.2.: Generated vectors.

Name	Insert	Backbone[a]	Res. Sites[a]	Primer (5′ → 3′)[a]
pEGFPC23C_fr1	3C site of pGEX6P1[b]	pEGFPC2	BsrGI-BglII	GGCTGTACAAATCGGATCTGGAAGTTC
				CATTAGATCTCAGGGGCCCCTGGAAC
pEGFPC23C_fr2	3C site of pGEX6P1	pEGFPC2	BsrGI-BglII	GGCTGTACAAATCGGATCTGGAAGTTC
				CATTAGATCTCCAGGGGCCCCTGGAAC
pEGFPC23C_fr3	3C site of pGEX6P1	pEGFPC2	BsrGI-BglII	GGCTGTACAAATCGGATCTGGAAGTTC
				CATTAGATCTCCCAGGGGCCCCTGGAAC
pmCherryC2	mCherry	pEGFPC2	AgeI-BsrGI	CTACCGGTCGCCACCATGGTGAGCAAGGGC
				CGTACTTGTACAGCTCGTCCATG
pmCherryC23C_fr1	3C site of pGEX6P1	pmCherryC2	BsrGI-BglII	cut from pEGFPC23C_fr1
pmCherryC23C_fr2	3C site of pGEX6P1	pmCherryC2	BsrGI-BglII	cut from pEGFPC23C_fr2
pmCherryC23C_fr3	3C site of pGEX6P1	pmCherryC2	BsrGI-BglII	cut from pEGFPC23C_fr3

[a] Backbone: source vector, Res. Sites: restriction site used for cloning, Primer: forward/reverse.
[b] PreScission Protease (GE Healthcare) cleavage site.

Table B.3.: DNA constructs and primers for srGAP3.

Insert	Organism[a]	Residues	GI Number[a]	Vector	Res. Sites[a]	Primer (5′ → 3′)[a]	Comment
srGAP3 constructs							
srGAP3	Hs	1-1099	24307967	pEGFPC23C_fr2	EcoRI-XbaI	cut from pcDNA3.1_srGAP3	
srGAP3	Hs	1-1099	24307967	pmCherryC23C_fr2	EcoRI-XbaI	cut from pcDNA3.1_srGAP3	
srGAP3 S858A	Hs	1-1099	24307967	pEGFPC23C_fr2	EcoRI-XbaI	GTGCGGTTACGAGCTGATGGAGCAG	phosphorylation-incompetent
						CTGCTCCATCAGCTCGTAACCGCAC	
srGAP3 S895A	Hs	1-1099	24307967	pEGFPC23C_fr2	EcoRI-XbaI	CTGCCTGCCCCAGCGCCCCCCACAAAATC	phosphorylation-incompetent
						GATTTTGTGGGGGGCGCTGGGGCAGGCAG	
srGAP3 S919A	Hs	1-1099	24307967	pEGFPC23C_fr2	EcoRI-XbaI	GATGGCGACGTTCGGGGCCGCTGGCAGCATCAAC	phosphorylation-incompetent
						GTTGATGCTGCCAGCGGCCCCGAACGTCGCCATC	
srGAP3 S858A S919A	Hs	1-1099	24307967	pEGFPC23C_fr2	EcoRI-XbaI	as before	phosphorylation-incompetent
srGAP3 CTR[b]	Hs	810-1099	24307967	pETGST1c[b]	NcoI-NotI	CATGCCATGGGAAGCCTGAGCCAGAAGGCTGACAG	
						ATAGTTTAGCGGCCGCTCACATGGTGCCCGACTTGTCCGCTGAG	
srGAP3 PxxP-fragment	Hs	CY+1047-1079	24307967	pGEX6P1	BamHI-XhoI	CGCGGATCCTGTTACCTGGCTGGCGCCCAGCTC	
						CCGCTCGAGTCACGGGCTGCCCACG	
srGAP3 AxxA-fragment (P1056A/P1059A)	Hs	CY+1047-1079	24307967	pGEX6P1	BamHI-AgeI	GATCCTGTTACCTGGCTGGCGCCCAGCTCCGCCCG	SH3-binding mutant[c]
						CCCGCCATGCGGGCCGTGCGGCCGGTGGTCCAGCA	
						CCGGTGCTGGACCACCGGCCGCAC	
						GGCCCGCATGGCGGGCGGGCGGAGCTGGGCGCCAGCCAGGTAACAG	
srGAP3 linker	Hs	470-508	24307967	pGEX6P1	EcoRI-NotI	CGGAATTCGAAAGAGCAGAATGCGGCACCACC	
						ATAGTTTAGCGGCCGCTCACATACTGCCGTTAAAGAGTTTATGG	
Binding partner constructs							
14-3-3β	Hs	2-246	4507949	pmCherryC23C_fr1	BamHI-EcoRI	cut from template	ligated into BglII-EcoRI
14-3-3γ	Rn	1-247	9507245	pmCherryC23C_fr2	EcoRI-XhoI	cut from template	ligated into EcoRI-SalI
14-3-3ϵ	Rn	1-255	13928824	pmCherryC23C_fr1	BamHI-SalI	cut from template	ligated into BglII-SalI
14-3-3ζ	Hs	1-245	208973238	pmCherryC23C_fr2	SacI-BamHI	CGCGAGCTCATGGATAAAAATGAGC	
						GCAGGATCCTTAATTTTCCCCTCCTTC	
14-3-3η	Hs	2-246	4507951	pmCherryC23C_fr1	BamHI-EcoRI	cut from template	ligated into BglII-EcoRI
14-3-3θ/τ	Hs	1-245+V	5803227	pmCherryC23C_fr1	BglII - HindIII	GGAAGATCTATGGAGAAGACTGAGCTGATCCAGAAG	
						CCCAAGCTTTTAAACGTTTTCAGCCCCTTCTGCCGCATCAC	

continued on next page

(continued)

Insert	Organism[a]	Residues	GI Number[a]	Vector	Res. Sites[a]	Primer (5′ → 3′)[a]	Comment
Amphiphysin	Rn	1-683	11560002	pmCherryC23C_fr2	EcoRI-XhoI	CGGAATTCATGGCCGACATCAAGACACG	
						CCGCTCGAGCTATTCTAGGTGTCGTGTGAAGTTCTC	
Ap2 α2[d]	Mm	701-938	163644277	pmCherryC2	EcoRI-XhoI	cut from template	ligated into EcoRI-SalI
α-Cop	Mm	1-1224	226823359	pmCherryC23C_fr2	EcoRI-SacII	GCGGCGAATTCATGCTAACCAAATTCGAG	
						ATCCGCGGTTAGCGAAACTGAAGAGG	
Drebrin	Hs	1-649	18426915	pmCherryC23C_fr1	BglII-SacII	GCCAGATCTATGGCCGGCGTCAGCTTC	
						CATCCGCGGCTAATCACCACCCTCGAAG	
EB1	Hs	1-268	6912494	pmCherryN1	AgeI-BsrGI	cut from template	mCherry from pmCherryC2 inserted into pDEST/N1GFP_EB1
Endophilin-A1	Hs	1-352	4506931	pmCherryC23C_fr2	EcoRI-KpnI	GCGGCGAATTCATGTCGGTGGCCGGCCTCAAG	
						CTTGGTACCTCAATGGGGCAGGGCAACCAGAATTTC	
Endophilin-A2	Hs	1-368	4506929	pmCherryC23C_fr2	EcoRI-SalI	GCGGCGAATTCATGTCGGTGGCGGGGCTGAAG	
						ACGCGTCGACTCACTGCGGCAGGGGCACAAG	
Grb2	Hs	1-217	4504111	pmCherryC23C_fr3	SacI-KpnI	GATCGAGCTCATGGAAGCCATCGCCAAATATG	
						CTTGGTACCTTAGACGTTCCGGTTCACGGG	
GST		1-221	pGEX6P1	pmCherryC23C_fr3	SacI-KpnI	GGCGAGCTCATGTCCCCTATACTAGG	
						CAGGTACCTCACAGATCCGATTTTGGAGG	
Neurochondrin	Hs	1-729	62526029	pmCherryC23C_fr1	BglII-SacII	GCCAGATCTATGTCGTGTTGTGACCTGGC	
						CATCCGCGGTCAGGGCTCTGACAGGC	
Strap	Hs	1-350	148727341	pmCherryC2	BglII-KpnI	GCCAGATCTATGGCAATGAGACAGACGCCG	
						CATCCGCGGTCAGGCCTTAACATCAGGAG	
Vps26A	Hs	L+2-327	17978519	pmCherryC23C_fr1	BamHI-EcoRI	cut from template	ligated into BglII-EcoRI
Vps35	Hs	1-796	17999541	pmCherryC23C_fr3	SacI-BamHI	CTAGAGCTCATGCCTACAACACAGCAG	
						CGGGATCCTTAAAGGATGAGACCTTCATAAATTGG	
α-Centractin	Hs	1-376	5031569	pmCherryC23C_fr2	HindIII-XhoI	cut from template	ligated into HindIII-SalI mutation Y4H
SH3 domain constructs							
Amphiphysin SH3	Rn	610-683	11560002	pGEX6P1	EcoRI/SalI	CGGGAATTCGGCTTTCTCTACAAGGTG	
						GCGTCGACCTATTCTAGGTGTCGTGTG	

continued on next page

(continued)

Insert	Organism[a]	Residues	GI Number[a]	Vector	Res. Sites[a]	Primer (5′ → 3′)[a]	Comment
Endophilin-A1 SH3	Hs	209-349	4506931	pGEX6P1	EcoRI-XhoI	CTAGAATTCATGGATCAGCCCTGCTGC	
						CGCCTCGAGCTAGGCAACCAGAATTTC	
Endophilin-A2 SH3	Hs	301-368	4506929	pGEX6P1	EcoRI-SalI	CTAGAATTCAGCATGCCGCCCCTG	
						ATTGTCGACTCACTGCGGCAGGG	
Grb2	Hs	1-217	4504111	pET 19b TEV	NdeI - XhoI	GGAATTCCATATGGAAGCCATCGCCAAATATGACTTCAAAGC	
						GCGCTCGAGTTAGACGTTCCGGTTCACG	
Grb2 SH3C	Hs	156-214	4504111	pGEX6P1	EcoRI-SalI	CTAGAATTCCAGCAGCCGACATACGTC	
						ATTGTCGACCTAGTTCACGGGGGTGAC	
Grb2 SH3N	Hs	1-56	4504111	pGEX6P1	EcoRI-SalI	CTAGAATTCATGGAAGCCATCGCC	
						ATTGTCGACCTATTTCATTTCTATGTAGTTC	

[a] Organism: Hs, *Homo sapiens*; Rn, *Rattus norvegicus*; Mm, *Mus musculus*. GI number: sequence identifier from http://www.ncbi.nlm.nih.gov/. Res. Sites: restriction sites. Primer: forward/reverse

[b] CTR, C-terminal region; pETGST1c from Gunter Stier: http://babel.ucmp.umu.se/cpep/web_content/Pages/CPEP_09_vectors.html

[c] Insert constructed by primer phosphorylation and ligation

[d] Appendage domain only

C. Supporting Information Syndapin1

Table C.1.: DNA constructs and primers for Syndapin1 and EHD1.

Insert	Organism[a]	Residues	GI Number[a]	Vector	Res. Sites[a]	Primer (5′ → 3′)[a]	Comment
Syndapin1 constructs							
Syndapin1	Mm	1-441	557948024	pGEX6P1	BamHI-XhoI	CGCGGATCCATGTCTGGCTCCTACGATGAG	
						CCGCTCGAGTCATATAGCCTCAACGTAGTTGGCAGGATAG	
Syndapin1 F-BAR[b]	Mm	1-326	557948024	pGEX4T1	BamHI-XhoI	CACCCTGTGAAATGCCACTGGGGCTCTAGAATCCACATC	stop codon at residue 326 inserted
						GATGTGGATTCTAGAGCCCCAGTGGCATTTCACAGGGTG	
Syndapin1 Linker	Mm	327-384	557948024	pGEX4T1	BamHI-XhoI	CGCGGATCCAATGCCACTGGGGCTGTAGAATCC	
						CCGCTCGAGTCATCCCTTGGCATCATCCTCGAAG	
Syndapin1 ΔSH3[b]	Mm	1-384	557948024	pGEX4T1	BamHI-XhoI	CGCGGATCCATGTCTGGCTCCTACGATGAG	
						CCGCTCGAGTCATCCCTTGGCATCATCCTCGAAG	
Syndapin1 *mNPF*[b]	Mm	1-441	557948024	pGEX6P1	BamHI-XhoI	CAGACGATGAGAGCGGAGCCGCCGCGGGGGGCAATGAGGCCAATG	NPF motifs mutated to AAA
						CATTGGCCTCATTGCCCCCCGCGGCGGCTCCGCTCTCATCGTCTG	
						GAGGCCAATGGTGGCGCCGCCGCGGCCGAGGATGATGCCAAGGGAG	
						CTCCCTTGGCATCATCCTCGGCCGCGGCGGCGCCACCATTGGCCTC	
EHD1 constructs							
EHD1	Hs	1-534	540344515	pET_Trx_1b[b]	NcoI-XhoI	GGACATGCCATGGTCAGCTGGGTCAGCAAGGATG	carries F2V mutation
						CCGCTCGAGTCACTCATGTCTGCGCTTGGAGG	
EHD1 W485A	Hs	1-534	540344515	pET_Trx_1b	NcoI-XhoI	CTAGGGAAGATCGCGAAGCTGGCCGACGTCGACAAGGACG	carries F2V mutation, inactivated EH domain
						CGTCCTTGTCGACGTCGGCCAGCTTCGCGATCTTCCCTAG	
EHD1 EH[b]	Mm	438-534	7106303	pGEX6P1	BamHI-XhoI	CGCGGATCCGAGTGGGTGGTGGGCAAGGACAAG	
						CCGCTCGAGTCACTCATGTCTGCGCTTGGAGG	

[a] Organism: Mm, *Mus musculus*; Hs, *Homo sapiens*. GI number: sequence identifier from http://www.ncbi.nlm.nih.gov/. Res. Sites: restriction sites. Primer: forward/reverse

[b] F-BAR, Fes-Cip4-homology Bin-Amphiphysin-Rvs domain; SH3, Src-homology 3 domain; NPF, linear peptide motif consisting of Asn-Pro-Phe; EH, Eps15-homology domain; Pet_Trx_1b from Gunter Stier: http://babel.ucmp.umu.se/cpep/web_content/Pages/CPEP_09_vectors.html